Ice-flow patterns in Boknafjorden and the deglaciation history of the Espedalen-Høgsfjorden region in Forsand, Rogaland

Master's thesis in Earth Science

Quaternary Geology and Paleoclimate

Talin Tuestad

Department of Earth Science

University of Bergen

June 2019

Abstract

Over 1000 glacial striation observations have been collected from various published and unpublished sources and compiled in a GIS striations database for Rogaland. An interpretation of the major flowsets represented by the collected striae is presented and compared with the existing knowledge of the deglaciation history in the Boknafjord region. Four major flowsets from the early deglaciation Boknafjorden have been identified. The oldest relative flow is represented by northerly striae along the outmost coast attributed to the northerly flowing Norwegian Channel Ice Stream (NCIS) that was active near the end of the Last Glacial Maximum. Following the collapse of the NCIS, striae show that ice flowed towards the west, which was followed by a distinct southwesterly flow out of Boknafjorden. A younger southerly flow along northern Boknafjorden reflects the development of a calving ice margin in the large and wide fjord.

This thesis then focuses on the Espedalen-Høgsfjorden region in Forsand to the southeast of Boknafjorden, where ^{10}Be surface exposure dating was combined with LiDAR-based geomorphological mapping and field observations of sediment sections exposed in a gravel pit at Nedre Espedal to investigate the deglaciation history of the region. Observations indicate that Espedalen and the adjacent higher elevation Lauvvatnet region were both occupied by ice-dammed lakes at an early phase during deglaciation. The subsequent drainage of these lakes reflects the gradual thinning and ultimate retreat of the damming ice-lobe in Høgsfjorden-Frafjorden.

Two ice margins are located in Espedalen distal to the Younger Dryas ice sheet margin mapped by Andersen (1954). Although a proper chronology has not yet been established, the older ice margin is an ice-contact delta that corresponds with the oldest ice-dammed lake phase in Espedalen and is believed to represent standstill during the net ice retreat. A relatively younger ice front at Øvre Espedal may belong to a regional readvance that corresponds to the Older Dryas period. Further studies are necessary to constrain the deglacial chronology for the Espedalen-Høgsfjorden region. The resulting ^{10}Be ages from two summits in Forsand exhibit a large spread in ages from ~13 to ~18 ka and thus are inconclusive. By comparing the most reliable ages with other nearby ^{10}Be ages in Forsand, a deglaciation age of around 15 ka is suggested.

Acknowledgements

I am incredibly grateful for all the help I have received from a number of people over the course of this project. I would first like to thank my supervisor, professor John Inge Svendsen for his constructive input, ideas, and enthusiasm over these past two years, and also for always being available for discussion and support. Many thanks to my co-supervisor Anna Hughes for her patience and valued assistance with ArcGIS, working with LiDAR data and map construction. I am also very grateful for the guidance and consideration I received from my co-supervisor associate professor Henriette Linge, who provided invaluable assistance, particularly with the exposure dating section of this project. I would also like to thank Lars Evje for his time, care and effort in processing and preparing my samples for ^{10}Be analysis. Additional thanks to professor emeritus Jan Mangerud for his occasional helpful feedback and assistance, and to Carl Regnéll for providing feedback and support with my LiDAR mapping endeavors.

Finally, I want to express my eternal gratitude to my parents, Sigurd and Salpi, for their unwavering love and support, and for travelling to Norway to join me in my fieldwork as fantastic field assistants.

Bergen, 31 May 2019

Talin Tuestad

Table of Contents

1. Introduction 1

1.1 Motivation 2

1.2 Research questions 2

1.3 Study area 3

1.4 Previous studies from the Boknafjord and Forsand-Lysefjord regions 6

2. Geological and glacial history of southwestern Norway 8

2.1 Bedrock geology 8

2.2 Ice-flow indicators 10

2.2.1 Glacial striations 11

2.2.2 Other small-scale erosional forms 11

2.2.3 Streamlined bedforms: drumlins & mega-flutings 11

2.3 Glacial history 12

2.3.1 The Weichselian glaciation 12

2.3.2 Norwegian Channel Ice Stream 15

2.4 Deglaciation history 17

2.4.1 Younger Dryas 19

2.5 Post-glacial uplift and relative sea level 21

3. Methods 22

3.1 Field methods 22

3.1.1 Glacial striae measurements 22

3.1.2 ^{10}Be surface exposure sampling 22

3.1.3 Field observations in Espedalen 23

3.2 Glacial striae 23

3.2.1 Collection of data from other published/unpublished sources 23

3.2.2 Striation database 24

3.2.3 Creating maps with ArcGIS 27

3.2.4 Reconstructing ice retreat patterns using striations 27

3.3 Surface exposure dating using cosmogenic nuclides 30

3.3.1 Method background 30

3.3.2 Mineral separation and sample preparation for ^{10}Be analysis 33

3.3.3 Age calculations 34

3.3.4 Comparisons with preliminary ^{10}Be ages provided from Uburen 35

3.4 LiDAR 36

3.4.1 LiDAR: How it works 36
3.4.2 LiDAR applications in geologic mapping 37
3.4.3 LiDAR mapping of geomorphological features in ArcMap 38

4. Results 40
4.1 Overview of striations & their orientations 40
4.2 Field observations: striae and other ice flow indicators 44
4.3 Streamlined terrain 48
4.4. Geomorphological and sedimentological observations in Nedre Espedal 51
4.4.1. Ice-marginal features at Løland/Nedre Espedal 51
4.4.2. Løland gravel pit sections 53
4.4.3 Depositional environments of gravel pit sediments 65
4.5 Terraces in Espedalen 67
4.6 Other LiDAR observations in Espedalen 71
4.6.1 Lateral moraine in Øvre Espedal 71
4.6.2 Outwash Fan in Nedre Espedal 73
4.6.3 Ancient lake shorelines Lauvvatnet region 75
4.7. ^{10}Be surface exposure dating results 78
4.7.1 Site and sample description 78
4.7.2 ^{10}Be exposure age results 80
4.7.3 Exposure age distributions & camel plots 84

5. Interpretation and discussion of ice flow patterns in Boknafjorden 87
5.1 Overview of flow sets over Boknafjord region 87
5.1.1 Flowset 1: North 92
5.1.2 Flowset 2: West 92
5.1.3 Flowset 3: Southwest 93
5.1.4 Flowset 4: South 94
5.2 Ice flow in Boknafjord after the breakup of the NCIS 96
5.2.1 Striae evidence and streamlined terrain comparisons 96
5.2.2 Drumlins on Karmøy 96
5.2.3 Comparison of ice flow evidence with modeled 18 ka flowlines 97
5.3 Ice margin stability in Boknafjorden during deglaciation 99

6. Interpretation and discussion of ^{10}Be ages 100
6.1 ^{10}Be production rate discussion 100
6.1.1 ^{10}Be production rate choice 100
6.1.2 ^{10}Be production rate uncertainty 100
6.2 ^{10}Be ages on Bergfjellet 101

6.3 ^{10}Be ages on Husafjellet 102
6.3.1 Potential causes of young apparent ^{10}Be ages..... 103
6.4. Comparisons with Uburen ^{10}Be ages 104
6.5 Comparisons with other ^{10}Be ages from the Boknafjord region..... 104
7. Deglaciation history of Espedalen and the Høgsfjorden-Frafjorden region 105
7.1 Oldest deglacial environments in Espedalen 105
7.1.1 Ice-contact glaciolacustrine delta at Nedre Espedal 105
7.1.2 Formation of 126 m a.s.l. glaciofluvial terrace at Løland..... 106
7.2 Ice-dammed lake in the Lauvvatnet region 107
7.3 Development of glaciofluvial/fluvial terraces 111
7.4 Environmental development of Espedalen during deglaciation 114
7.5 Ice-margin fluctuations in Espedalen-Vinddalen..... 117
7.6 Evidence of Older Dryas ice advance in the Lysefjord region..... 119
8. Conclusions 123
References..... 125
Appendix..... 133

1. Introduction

The last ~2.6 million years of Earth's history, known as the Quaternary period, is characterized by climatic cycles oscillating between cold glacial conditions and warmer interglacial periods. Over time, repeated glacial-interglacial cycles created the dramatic fjord-and-mountain landscape of western Norway. Glacial imprints can be studied to reconstruct past ice sheets, ice flow patterns and deglaciation history, which can ultimately be used to better understand ice sheets in the present as well in the future. During the Last Glacial Maximum (LGM), the entirety of Scandinavia was covered by an ice sheet that also extended over the UK, Northern Europe, Russia and Svalbard (Hughes et al., 2016). The LGM was followed by deglaciation initially triggered by the collapse of the Norwegian Channel Ice Stream around 18.5 ka (Sejrup et al., 2018), followed by the landward retreat of ice sheet (Mangerud et al., 2011, Svendsen et al., 2015; Briner et al., 2014; Gump et al., 2017). A collection of over a thousand glacial striae sourced from several published and unpublished sources has been gathered in a database for Rogaland and used to reconstruct ice flow changes from the LGM and the subsequent deglaciation over the Boknafjord region (Figure 1.1). This project then focuses on the region around Espedalen, located just south of Lysefjorden, where ^{10}Be surface exposure dating is combined with geomorphological and sedimentological observations to reconstruct the deglaciation history of the area (Figure 1.2).

1.1 Motivation

This master's thesis is a part of an effort to learn more about the early deglaciation history in southwestern Norway and its relationship to climatic changes. The investigation falls under the purview of a larger interdisciplinary project Eurasian Ice Sheet and Climate Interactions (EISCLIM), whose objective is to gain new knowledge of ice sheet growth and decay over the last glacial cycle. This thesis is comprised of several components. The first component is the compilation of a glacial striations database for Rogaland, which is part of an effort to fill in gaps of the Norwegian Geological Survey's (NGU) collection of glacial striae in Norway. This section of the project is an extension of a striations database for Hordaland, complied in a previous master's thesis (Sæle, 2017), which is now part of a new publication concerning the deglaciation history in the area (Mangerud et al., 2019). The compiled striations are then displayed on a GIS-based map to allow for flow pattern analysis. The results are used to enhance the existing knowledge of ice sheet retreat patterns over the Boknafjord region and adjacent areas. The second component of this thesis involves the reconstruction of depositional environments around Espedalen, near Forsand and the mouth of Lysefjorden (Figure 1.2), in order to learn more about the deglacial history in that particular area. Finally, ^{10}Be exposure ages are presented from the Forsand area to improve chronological constraints on the deglaciation of the Lysefjord/Forsand region in southwest Norway.

1.2 Research questions

- What are the major ice flow directions in the Boknafjord region that can be distinguished from glacial striae?
- How did the direction of ice flow change as the ice sheet became thinner and the ice margin retreated? How do these flow patterns compare with prior knowledge of the deglaciation of Boknafjorden?
- How did the depositional environments in Espedalen and the adjacent Høgsfjorden-Frafjorden region evolve during the last deglaciation? What information does it provide about the deglaciation history of the area?
- When did the mountaintops in Forsand become ice-free? How do the ^{10}Be exposure dates from Forsand compare to other exposure dates from the region?

1.3 Study area

Boknafjorden is a fjord in southwestern Norway located between Haugesund and Stavanger in the county of Rogaland (Figure 1.1). It is characterized by its broad width and deep trough, in contrast to the other narrower fjords in western Norway such as Hardangerfjorden and Sognefjorden. The large fjord is about 96 kilometers long from its mouth to its innermost towards the mainland, and around 20 kilometers wide from the southern tip of Karmøy to the northern tip of the Stavanger Peninsula. Moving towards the mainland, Boknafjorden branches off into numerous smaller fjords (Figure 1.1). To the southeast of Boknafjorden, Lysefjorden and Frafjorden branch out from NW-SE-oriented Høgsfjorden (Figure 1.2). The study area of Forsand is located just south of the mouth of Lysefjorden (Figure 1.2). Several mountain summits are found in the area of Forsand including Bergfjellet and Uburen, as well as Husafjellet further south near Espedalen. Glacial erratics from Bergfjellet and Husafjellet were sampled for ^{10}Be exposure dating (Figure 1.2).

Espedalen is a ~10 km long valley located just south of the village of Forsand and oriented perpendicular to Høgsfjorden (Figure 1.2). The valley is divided into Nedre (lower) and Øvre (upper) Espedal, which are separated by the lake Espedalsvatnet (108 m a.s.l.) that has a maximum depth of 60 meters (NVE, 2015). The river Espedalsåna flows from Espedalsvatnet along the base of Nedre Espedalen and drains into Høgsfjorden at the mouth of the valley. Two gravel pits are located in the inner part of Nedre Espedalen near the southern edge of Espedalsvatnet. Observations of the stratigraphy and sedimentology of the sediment in the valley were concentrated in the Løland gravel pit along the northern slope of Espedalen (Figure 1.2), as it provided more access to clear sediment sections.

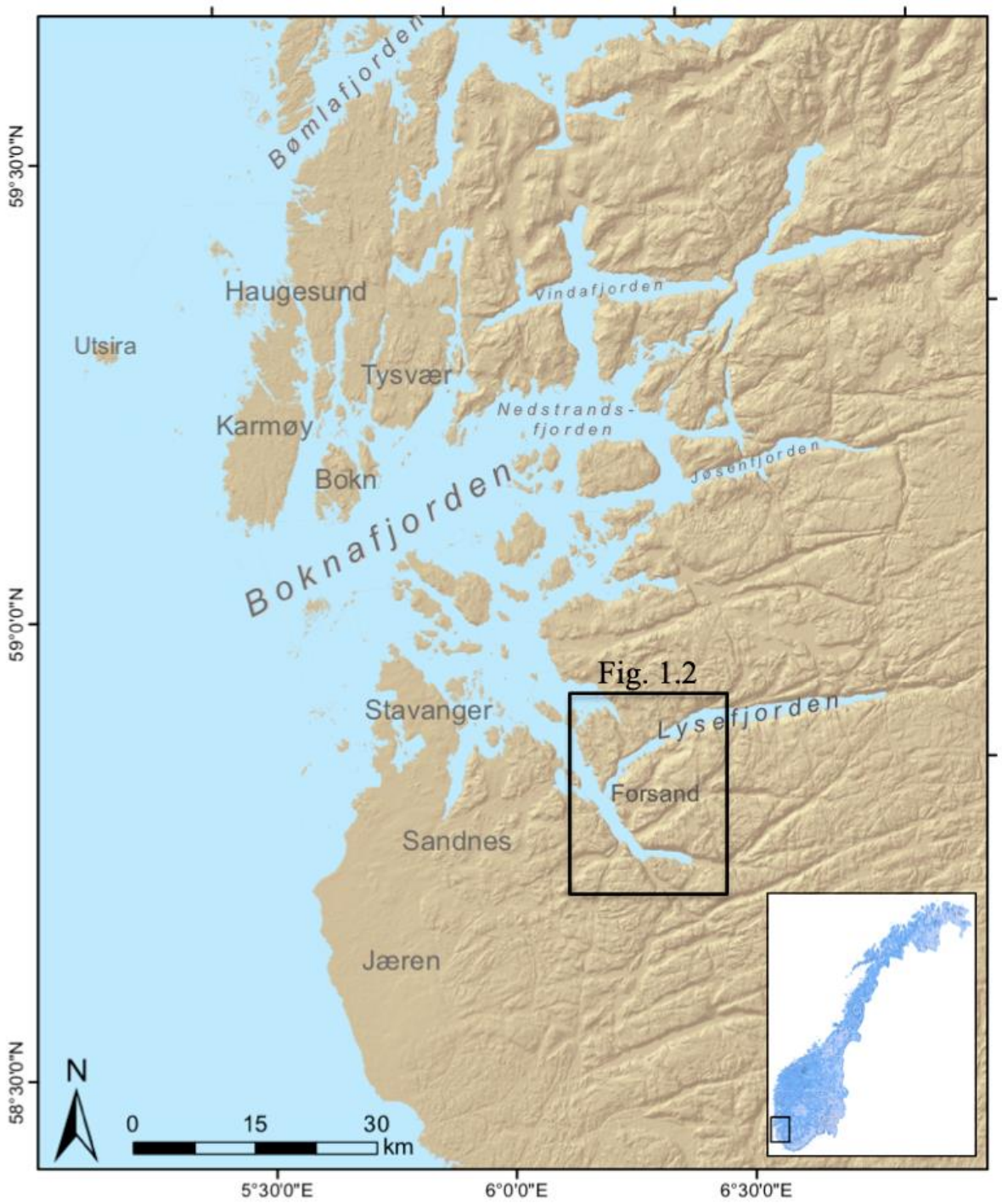

Figure 1.1. Map of Boknafjorden in southwestern Norway. Location of Figure 1.2 is shown by the black box.

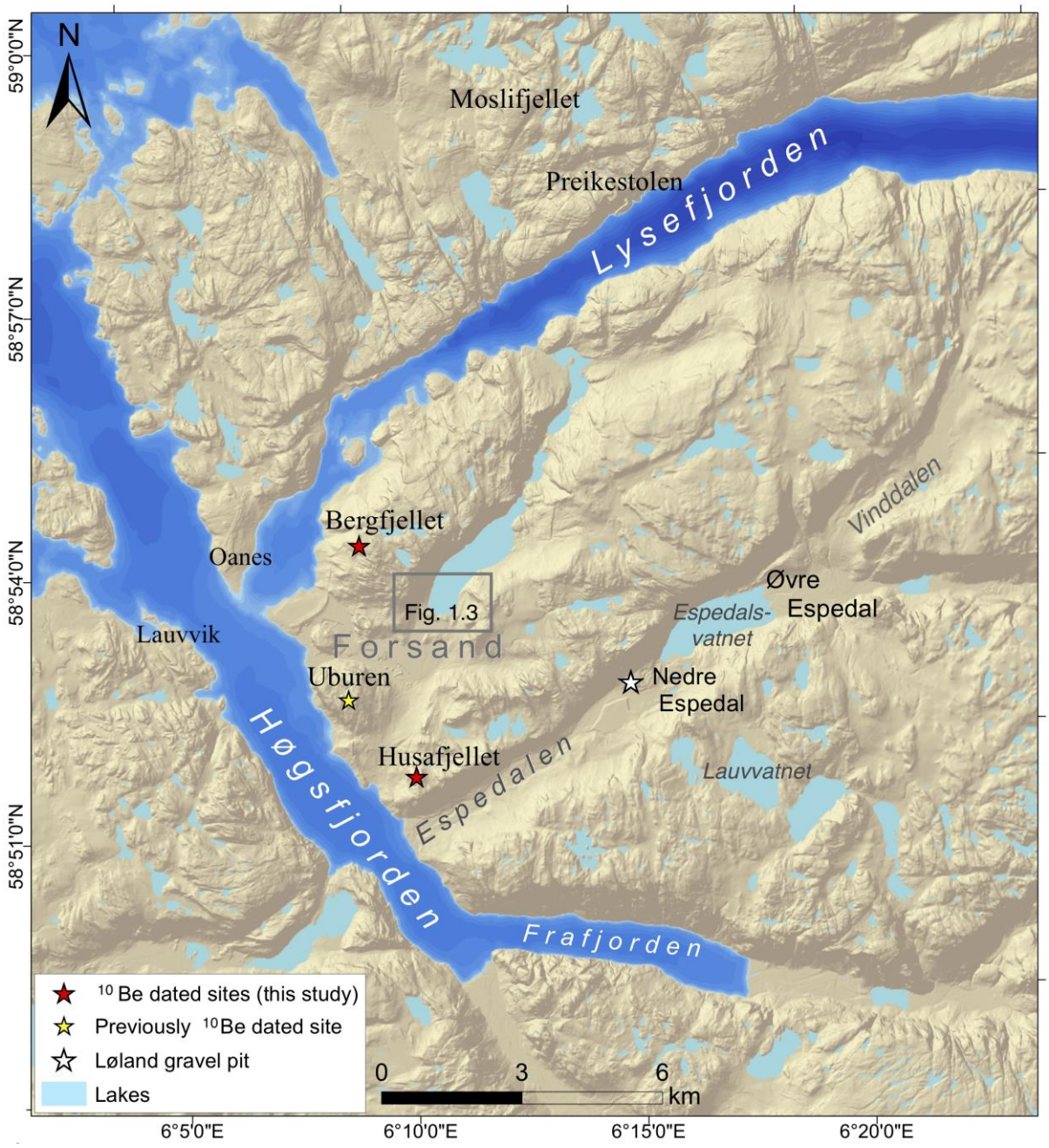

Figure 1.2. Map of the study area in Forsand and Espedalen in the region between Lysefjorden and Høgsfjorden-Frafjorden. Sites that were sampled for ^{10}Be dating are shown by a red star. Location of preliminary ^{10}Be dates from Uburen is also shown by the yellow star (J.I. Svendsen, pers. comm. 2019) White star shows the location of the Løland gravel pit at Nedre Espedal that is further discussed in the following chapters.

1.4 Previous studies from the Boknafjord and Forsand-Lysefjord regions

The deglaciation history of the Boknafjord region has previously been investigated by numerous studies. The earliest studies in the region generally involved radiocarbon dating of lake basin sediments (Anundsen, 1977, 1985; Paus 1988). Regional studies are also presented by Økland (1947), Rønnevik (1971), as well as Anundsen (1972), which discusses the late glacial history using ice-terminal deposits around the inner regions of Boknafjorden. In the more recent years, several papers have presented a series of ^{10}Be exposure ages from the Boknafjord region in an effort to further constrain the deglaciation history. ^{10}Be ages from Utsira and Karmøy presented by Svendsen et al. (2015) suggest that the islands might have been ice-free soon after the LGM. Gump et al. (2017) built on the work done by Svendsen et al. (2015) by providing additional ^{10}Be exposure ages from several more localities in the region. Further inland, ^{10}Be ages from the Lysefjord region presented by Briner et al. (2014) help constrain late deglacial events in the region after the Bølling interstadial.

In southwestern Norway, the Younger Dryas ice margin is clearly delineated by a moraine complex that been comprehensively mapped throughout the region (Andersen, 1954; Anundsen, 1972; Briner et al., 2014). The moraine system can be traced over the Lysefjord region, with several prominent moraine ridges found near Forsand (Figure 1.2). The most historically significant moraine in Forsand is Esmark's moraine at Haukelivatnet (Figure 1.3). The moraine is named after the geologist Jens Esmark, who in 1823 developed the theory of past large-scale glaciations in Norway that reached sea-level after comparing observations of the moraine at Haukalivatnet with modern ice-terminal deposits near Jostedalsbreen (Hestmark, 2018).

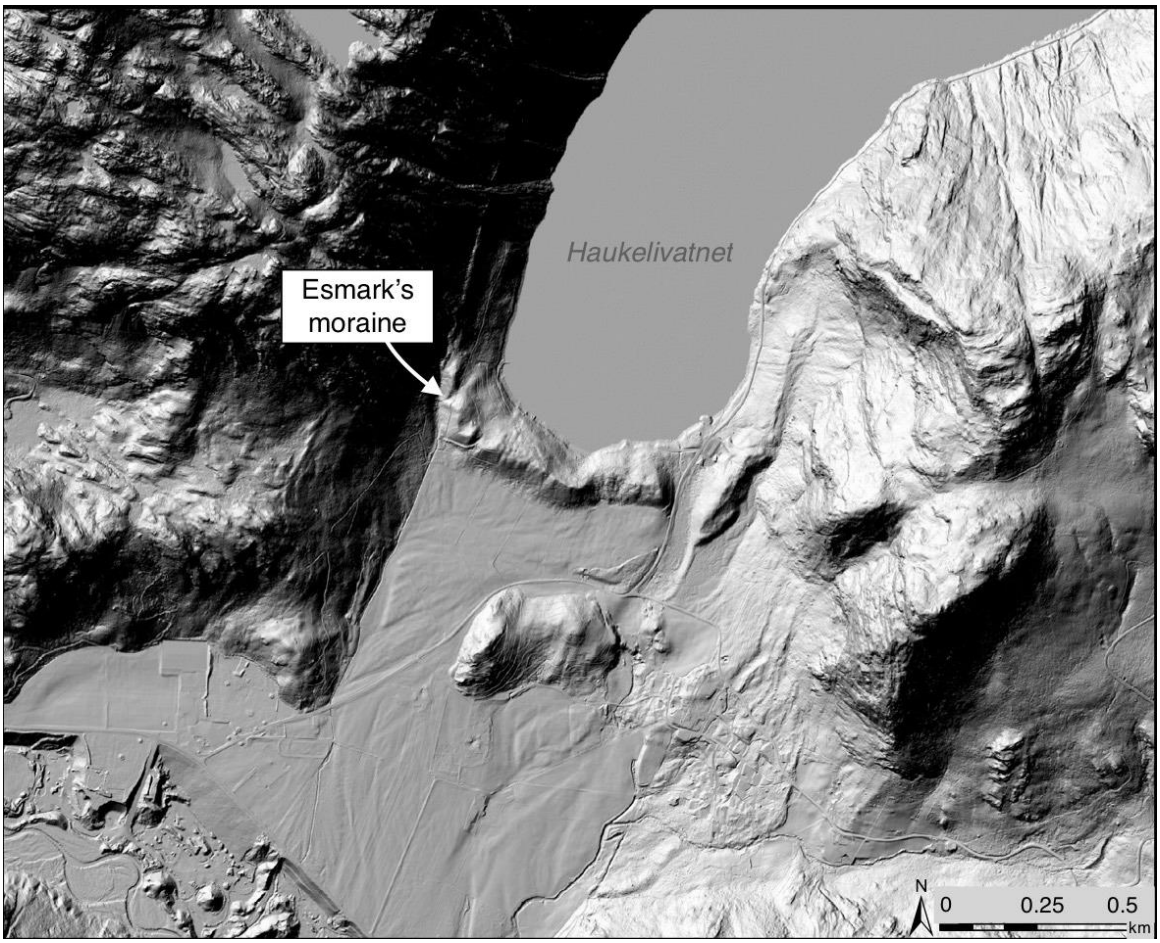

Figure 1.3. LiDAR image of Esmark's moraine in Forsand. Location of image is shown in Figure 1.2.

.

2. Geological and glacial history of southwestern Norway

2.1 Bedrock geology

The Boknafjord region is characterized by a series of Caledonian nappes and thrust sheets formed around 400 million years ago that are underlain by autochthonous basement rock (Rønning et al., 2006). The Precambrian basement in the Boknafjord region is composed of granitic to dioritic gneiss and the lowermost Caledonian allochthonous units include the Ryfylke schist (Cambrian to Ordovician schist/phyllite) and the Storheia nappe (Precambrian crystalline gneiss) (Figure 2.1; Rønning et al., 2006). The uppermost nappe in the region is the Hardanger nappe that is composed of the Torvastad Group (greenstone and volcanic sediments) and the Karmøy ophiolite (mafic to ultramafics) (Figure 2.1; Rønning et al., 2006).

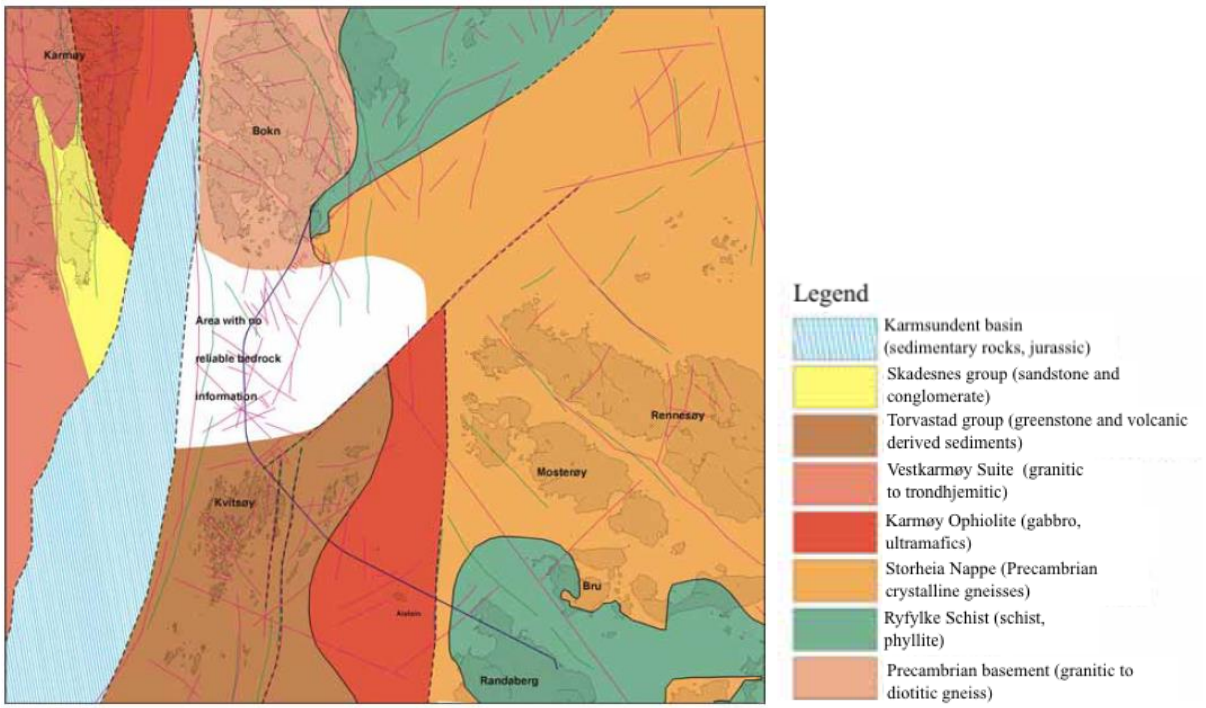

Figure 2.1. Bedrock geology and tectonic map over the Boknafjord region. (Rønning et al., 2006)

The bedrock of the Lysefjord region is largely dominated by Augen gneiss, granite and foliated granites, while the area of Forsand and Espedalen is composed of dioritic to granitic gneiss and migmatite (Figure 2.2; NGU, 2019). Additionally, bands of amphibolite, hornblende, and mica-rich gneiss are also found among the more dominant lithologies in the region (Figure 2.2; NGU, 2019).

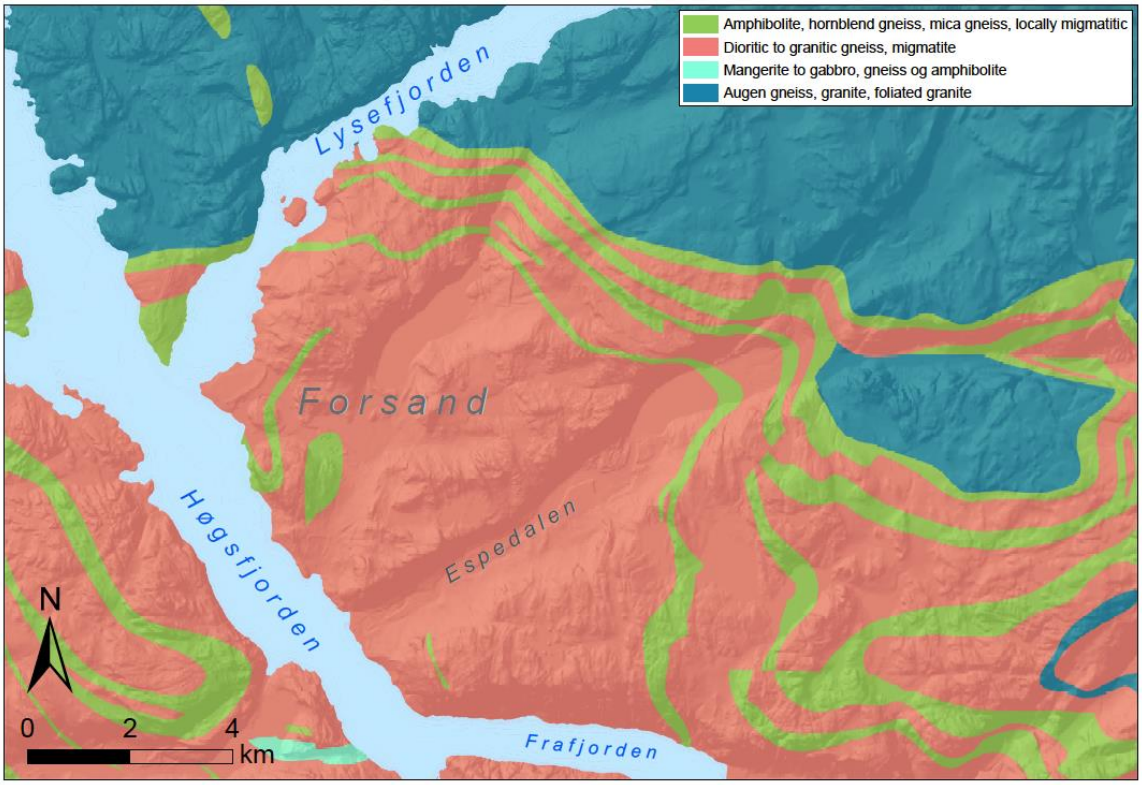

Figure 2.2. Bedrock geology of the Lysefjord-Forsand region (NGU, 2019).

2.2 Ice-flow indicators

Subglacial processes can form various erosional and depositional features in terrain that can provide information about the ice flow direction of a past ice sheet or glacier. Several relevant examples of these ice-flow indicators are discussed below.

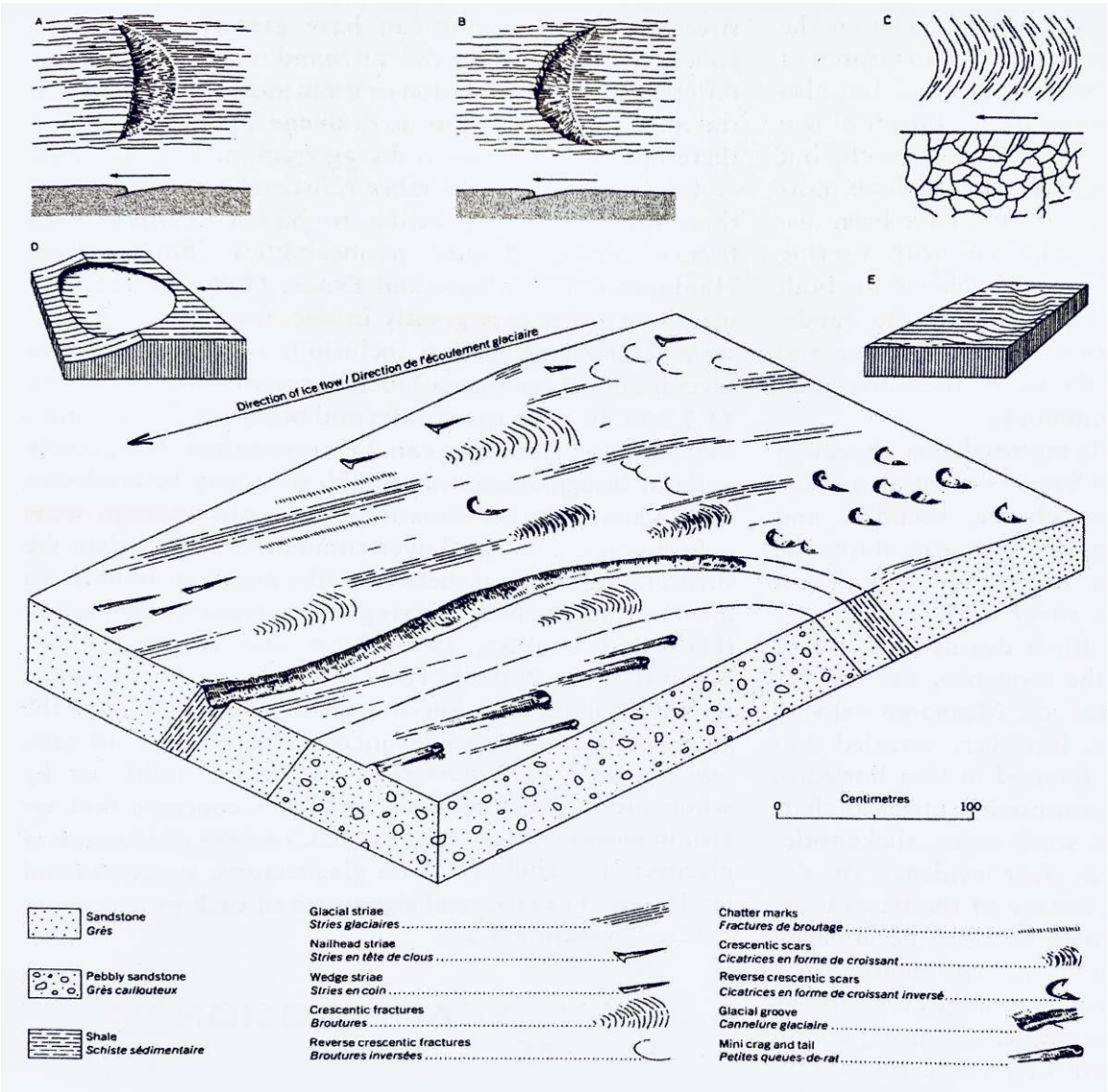

Figure 2.3. Illustration of various examples of small-scale glacial erosion (Benn and Evans, 2010).

2.2.1 Glacial striations

Glacial striations are typical examples of small-scale subglacial erosion. Striations are thin grooves in bedrock that are formed when rocks or sediment in ice scour the underlying bedrock along the base of a flowing glacier. They can range in scale, from larger, coarse striae that are visible to the naked eye to micro-scale striae that are generally exhibited on well-preserved glacially polished surfaces. Glacial striae are believed to form along the base of an erosive, warm-based ice sheet and are oriented perpendicular to the ice margin (Figure 2.3, 3.3) (Chamberlin, 1883; Hoppe, 1948; Iverson, 1991).

2.2.2 Other small-scale erosional forms

Other examples of erosional ice flow indicators can include chatter marks, crescentic gouges and fractures in bedrock. Chatter marks are centimeter-scale, crescent-shaped series of fractures in bedrock whose concave sides point in the direction of ice flow (Figure 2.3). Crescentic gouges are crescent-shaped scours in bedrock with their convex sides pointing towards ice flow direction, while crescentic fractures' convex sides point in the up-ice direction (Figure 2.3). A summary of various additional small-scale glacial erosional features is illustrated in Figure 2.3.

2.2.3 Streamlined bedforms: drumlins & mega-flutings

Drumlins and flutings are streamlined subglacial landforms whose longer axes are oriented parallel to ice flow direction. Drumlins are generally defined as oval-shaped mounds of glacial sediment with a steeper, stoss-side and a gently sloping lee side, the latter of which point towards the direction of ice flow (Menzies 1979). Drumlins can also have varied morphologies that cover a spectrum of drumlinoid forms, as well as different elongation ratios. Particularly elongated drumlinoid ridges can be referred to as mega-flutings or flutes (Benn and Evans, 2010). The subglacial formation and evolution of these streamlined glacial landforms is still relatively enigmatic, as there are still many questions about where and when these ridges form at the base of an ice sheet (Benn and Evans, 2010). Large drumlins fields and mega-flutings may have been formed under past fast-flowing ice streams or glacial lobes, and are frequently observed in low elevation areas and broad valleys (Patterson and Hooke, 1996).

2.3 Glacial history

The Quaternary period covers the last ~2.6 million years of the Cenozoic era in Earth's history and is further subdivided into the Pleistocene and Holocene epochs. The Pleistocene is characterized by repeated glacial-interglacial climate cycles that lasted from ~2.6 mya to ~11.7 kya. The Pleistocene was followed by the onset of the Holocene around 11.7 ka and spans to the present. The variations in Earth's climate during the Quaternary are associated with the Milankovitch cycles that affect the amount of solar insolation the Earth receives from the sun (Imbrie et al., 1992, 1993). The resulting growth and decay of large-scale ice sheets is recorded in the oxygen isotope ratios ($^{16}O/\ ^{18}O$, $\delta^{18}O$) of benthic foraminifera in deep-sea sediment cores. $\delta^{18}O$ values have been used to develop the marine isotope stage (MIS) timescale that assigned a stage to each glacial and interglacial period (Figure 2.4). $\delta^{18}O$ of deep-sea sediments have also been correlated with oxygen isotopes from ice core records, for example, from the North Greenland Ice Core Project (NGRIP; NGRIP members, 2004).

2.3.1 The Weichselian glaciation

In northern Europe, the last glacial period of the Pleistocene is referred to as the Weichselian glaciation, which corresponds with MIS 5d to MIS 2 (Figure 2.4). The Weichselian started at the end of the Eemian, the previous interglacial that corresponds to MIS 5e (Figure 2.4). In general, there is a lack of evidence from the early Weichselian, as most of it has eroded away by the Late Weichselian ice sheet during the last glacial maximum (LGM). However, early, middle to late Weichselian deposits have been found at several key sites along the west coast of Norway, notably at Fjøsanger, Karmøy, Skjonghelleren, and on Jæren, which overall demonstrate significant ice-margin fluctuations throughout the Weichselian (Figure 2.4; e.g. Mangerud et al., 1981; Andersen et al., 1983; Sejrup, 1987; Raunholm et al., 2004; Mangerud et al., 2010).

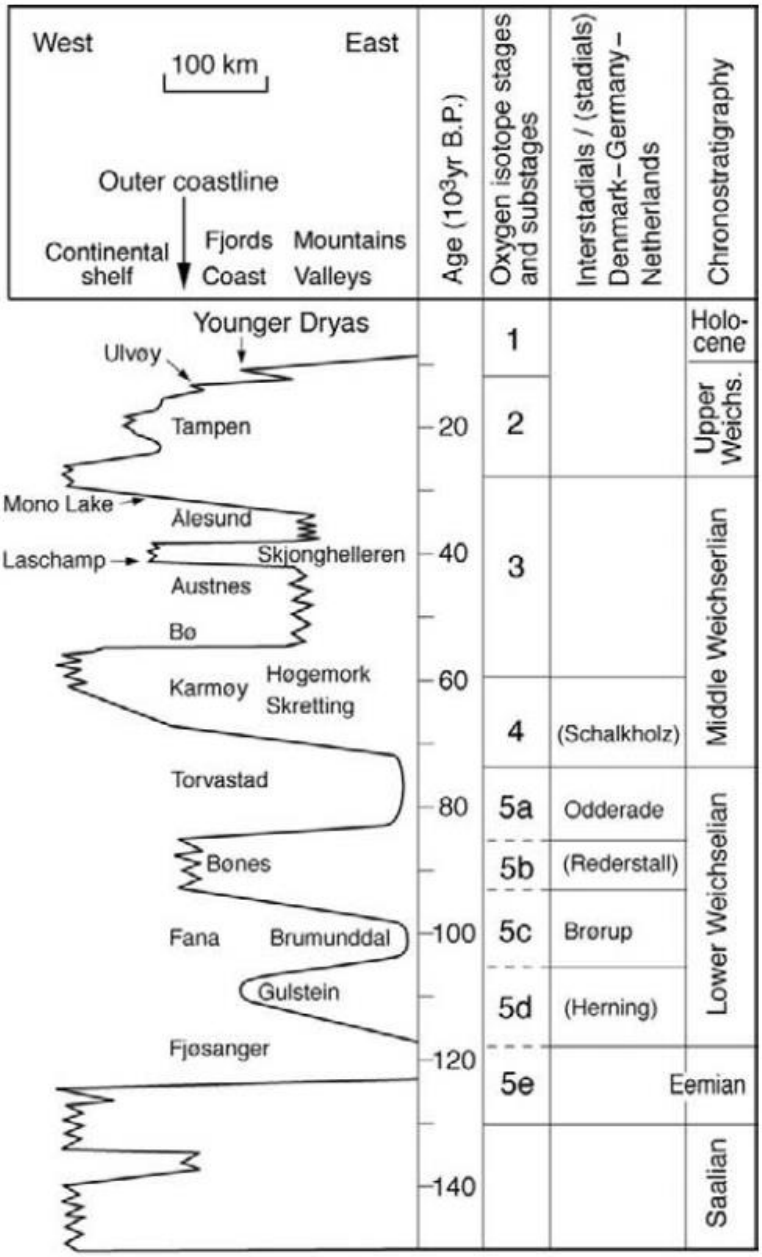

Figure 2.4. Time-distance diagram demonstrating the ice sheet fluctuations in the southwest region of the Scandinavian ice sheet during the Weichselian glaciation (from Mangerud et al., 2011).

The most recent late Weichselian glacial period is referred to as the Last Glacial Maximum (LGM; MIS 2: Figure 2.4). During the LGM, the Scandinavian ice sheet merged with the British-Irish ice sheet and the Barents-Kara and Svalbard ice sheets, forming a joint ice sheet complex known as the Eurasian ice sheet (Svendsen et al., 2004; Hughes et al., 2016). At its maximum extent, the LGM Eurasian ice sheet reached over Britain and Ireland, Scandinavia, northern Europe, Russia, Nova Zemlya and Svalbard (Figure 2.5; Svendsen et al., 2004; Sejrup et al., 2005; Hughes et al., 2016). Nevertheless, the timing of the maximum ice extent was not simultaneous for all areas of the ice sheet (Hughes et al., 2016).

Figure 2.5. Map showing the maximum extent of the Eurasian ice sheet during the LGM. Dashed white lines represent the approximate boundaries between the three separate ice sheets that coalesced to form the LGM Eurasian ice sheet: the Svalbard-Barents-Kara ice sheet (SBKIS), the British-Irish ice sheet (BIIS), and the Scandinavian ice sheet (SIS). Areas shaded in orange show the distribution of trough-mouth fans that were deposited by the continental shelf-edge glaciation during the LGM (Hughes et al., 2016).

A variety of glacial geomorphologic features such as moraine ridges and mega-scale glacial lineations (MSGL) have been mapped on the continental shelf off western Norway, providing strong evidence of a marine-terminating ice front that reached the shelf edge during the LGM (e.g. Ottesen et al., 2005; Sejrup et al. 2005, 2009, 2016). Evidence from the continental shelf, such as cross-shelf troughs, MSGLs, grounding-zone wedges, and trough-mouth fans (Figure 2.5), also indicates that there were numerous ice streams flowing over the shelf during the shelf-edge glaciation (Sejrup et al., 2003, 2005; Ottesen et al., 2005, 2016). Ice streams are fast-flowing channels of ice that flow more rapidly than the ice along the channel margins (Patterson, 1994). Although the impact of paleo-ice streams has yet to be fully understood, ice streams have been shown to have a profound effect on the dynamics, stability and configuration of an ice sheet (Bentley, 1987; Stokes and Clark, 2001).

2.3.2 Norwegian Channel Ice Stream

The Norwegian Channel Ice Stream (NCIS) was a major ice stream that drained large volumes of ice from the southern region of the Fennoscandian ice sheet and had been periodically active over the past 1.1 Ma (Figure 2.6; Sejrup et al., 2000, 2003; Nygård et al., 2005; Hjelstuen et al., 2012). Glacigenic debris flow evidence from the mouth of the Norwegian Channel indicates that the NCIS did not flow continually throughout the LGM, but rather was active during periodic episodes, the last of which was between 20 to 19 ka (Nygård et al., 2007).

N-NW oriented glacial striations have been found on the coast of Jæren, as well as on the island of Utsira (Figure 2.6; Undås, 1948; Andersen et al., 1987; Larsen et al., 2000), indicating that those regions had been inundated by the northerly-flowing NCIS. Several NW-SE trending ridges on the low coastal regions of Lågjæren have been interpreted as drumlins (Sejrup et al., 1998), and till fabric measurements from southern Jæren also indicate northerly ice flow that predates the W-SW ice flow over the region (Andersen et al., 1987; Jonsdottir et al., 1999). On Jæren, the easternmost boundary of the NCIS is delineated by an escarpment that separates the lowland region of Lågjæren and the upland region of Høgjæren, as no northerly trending features are found east of the escarpment (Sejrup et al., 1998).

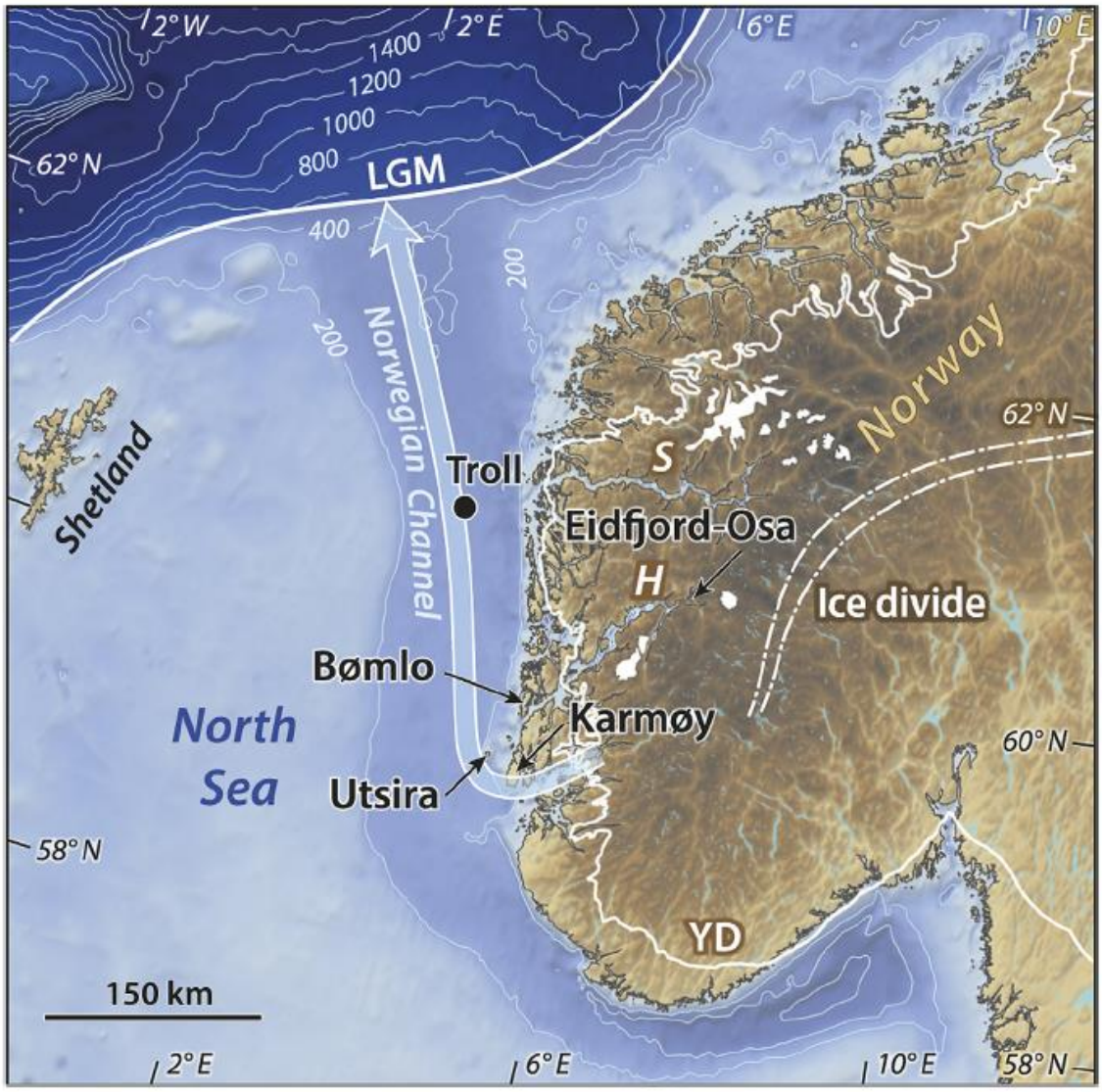

Figure 2.6. Map of southern Norway showing the LGM ice extent. The Norwegian Channel ice stream (NCIS) flowed during late stages of the LGM,is shown, as well as the ice flow out of Boknafjorden shown merging with the northward flow of the NCIS. Location of the Troll core site is shown, .. S = Sognefjord, H =Hardangerfjord. (from Svendsen et al., 2015)

2.4 Deglaciation history

The onset of the last deglaciation in southwestern Norway is marked by the collapse of the NCIS (Sejrup et al., 2016). The retreat of the NCIS is initially shown by the cessation of glacigenic debris flows at the mouth of the Norwegian Channel around 19 ka, marking the retreat of its grounding line (Nygård et al., 2007; Morén et al., 2018). Radiocarbon dates from the Troll core (Figure 2.6) indicate that the NCIS had retreated southwards past the core site by 18.5 cal. ka (Sejrup et al., 1994, 2009). The deglaciation age from the Troll core is corroborated by radiocarbon dates of basal marine sediments from isolation basins on Karmøy that suggest ice-free conditions by 18 cal. ka BP (Svean, 2016; Vasskog et al., in press). ^{10}Be ages from the island of Utsira, located around 175 km south of the Troll core site, initially yielded a deglaciation age as early as 20.3 ± 0.1 ka (Figure 2.7; Svendsen et al., 2015). Subsequent work by Briner et al. (2016) suggests that deep subsurface ^{10}Be accumulation during ice-free periods may have affected ^{10}Be ages on Utsira, resulting in ages that are too old. Therefore, Utsira and southern Karmøy were likely deglaciated between ~18.5 and ~18 ka (Briner et al., 2016), which is in good agreement with the offshore records (Morén et al., 2018). Later ^{10}Be ages presented by Gump et al. (2017) suggest that southeastern Karmøy had deglaciated around 16 ka, and the ice margin had retreated past Bokn by ~15 ka (Figure 2.7). Several studies have yielded radiocarbon dates for the deglaciation of Bokn (Johnsen, 2017; Hernar, 2017; Strømsnes, 2018), the most recent of which suggest that Bokn became ice-free by 15.4 cal ka BP (Strømsnes, 2018). On the mainland, radiocarbon ages from Jæren indicate that the coastal lowland became ice free sometime between 17 and 16 cal ka BP (Knudsen, 2006).

The ^{10}Be chronology of Boknafjorden shows that the mouth of the fjord started to deglaciate around 16 ka, which is well before the Bølling warming and more than a thousand years earlier than the deglaciation of other fjords in southwestern Norway, such as Bømlafjorden and Hardangerfjorden (Figure 2.8; Mangerud et al., 2013, 2016b; Svendsen et al., 2015; Gump et al., 2017). Radiocarbon ages from southern Bømlo are supported by ^{10}Be ages from the mouth of Bømlofjorden, indicating that the fjord started to deglaciated around ~15 ka (Karlsen, 2009; Mangerud et al., 2013; Gump et al., 2017).

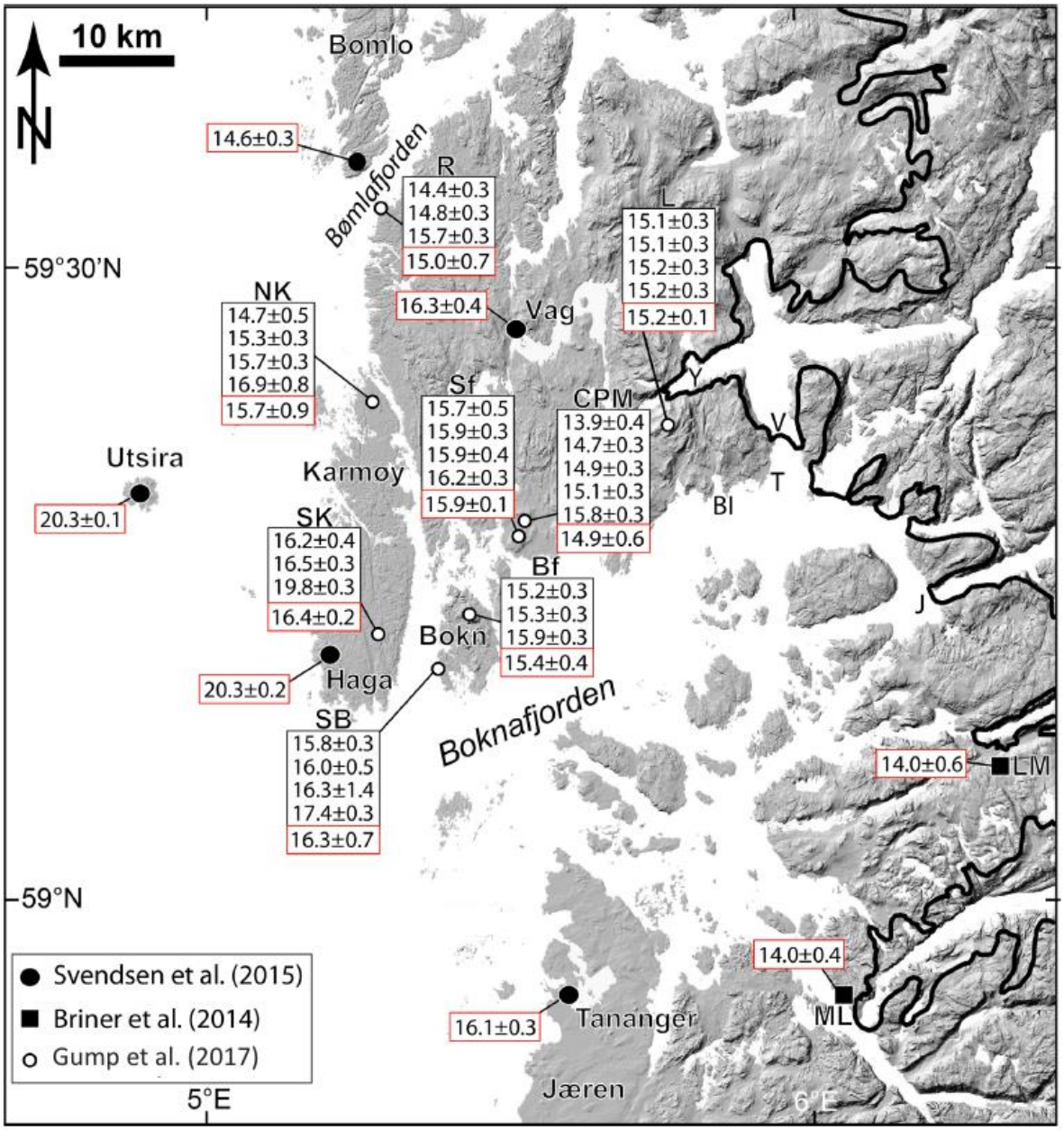

Figure 2.7. Map of Boknafjorden showing the locations of published ^{10}Be exposure ages from Gump et al. (2017), Svendsen et al. (2015) and Briner et al. (2014). Locations with ^{x}Be ages are: northern Karmøy (NK), southern Karmøy (SK), Ryvarden (R), southern Bokn (SB), Boknafjellet (Bf), Sandviksfjellet (Sf), Cleng Peerson Moraine (CPM), Lammanuten (L), Leiken moraine (LM), and mouth of Lysefjorden (ML). Radiocarbon dated sites are also depicted (Y = Yrkefjorden, V = Vindafjorden, J = Jøsenfjorden, BI = Borgøy island, T = Tveit). Black line represents the Younger Dryas ice extent. (modified from Gump et al., 2017)

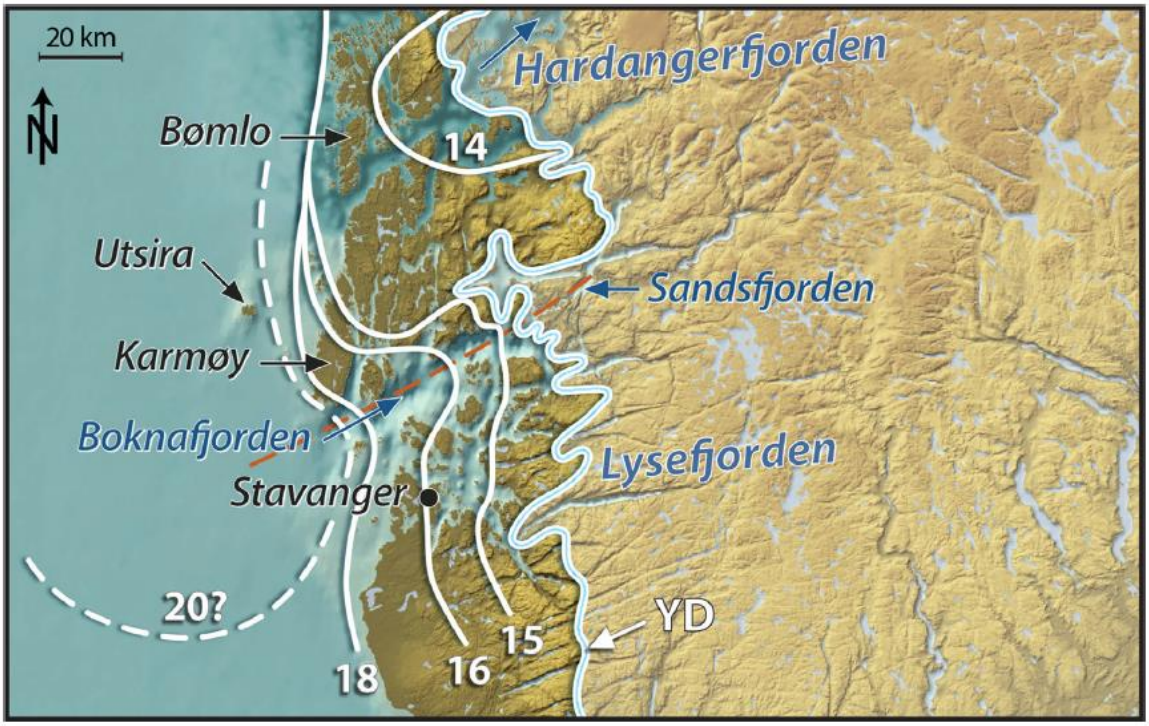

Figure 2.8. Deglaciation history of southwestern Norway reconstructed from published ^{10}Be exposure ages from the region (Figure 2.7) (Gump et al., 2017).

2.4.1 Younger Dryas

The net ice margin retreat that occurred during the first phase of the last deglaciation was followed by the Younger Dryas (YD) cold period. In Greenland ice core records, Greenland Stadial 1 corresponds to the YD and is defined as the period from 12.8 ka to 11.7 ka (Rasmussen et al., 2006). The YD has also been defined by radiocarbon ages of lake sediments from western Norway as the period from 12.7 to 11.5 cal ka BP (Lohne et al., 2013, 2014). In southwestern Norway, the ice margin underwent a re-advance during the YD after having retreated to a relatively unknown extent during the preceding Allerød interstadial (Mangerud et al., 2016a; Hughes et al., 2016). The YD maximum ice extent is outlined by a complex of moraines that can be mapped almost continuously throughout Norway, as well as the rest of Scandinavia (Mangerud et al., 2011). In the inner part of Boknafjorden, the YD moraine belt can be found along the mouths of the inner tributary fjords (Figure 2.8; Andersen et al., 1954).

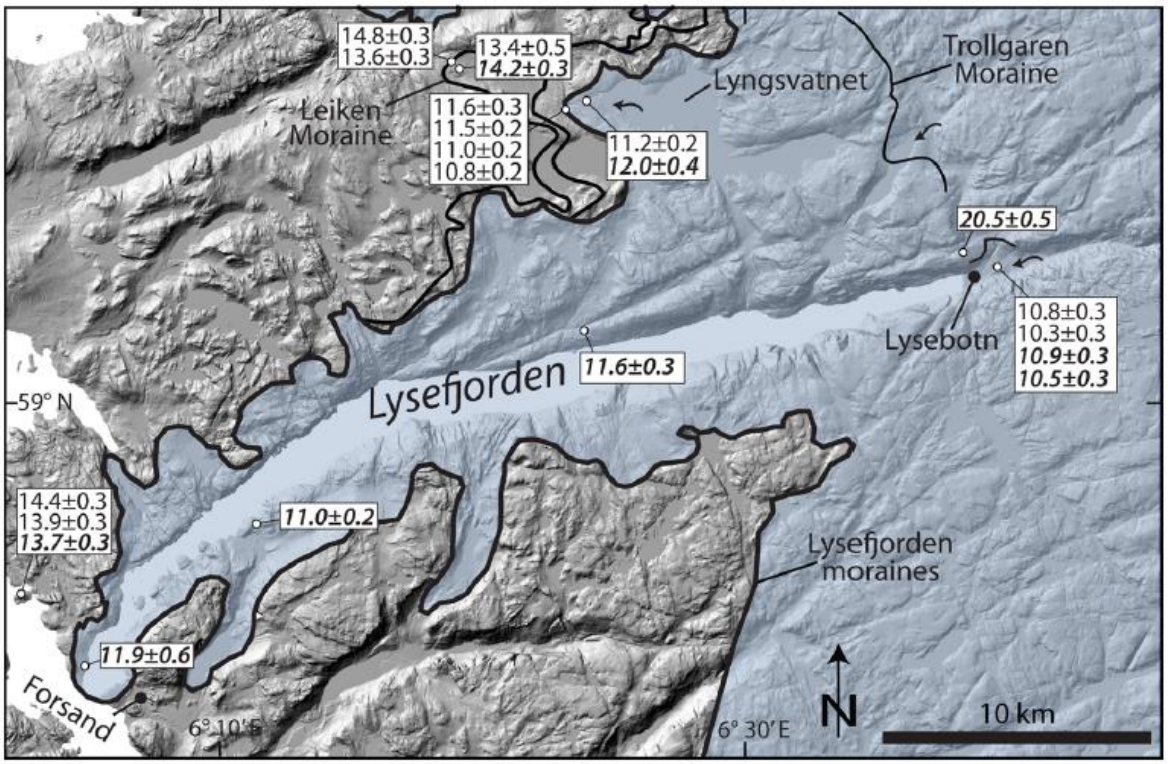

Figure 2.9. Map showing the Younger Dryas ice cover over the Lysefjord region. Locations of ^{10}Be ages and the Leiken moraine are also shown. The distribution of the Lysefjord (thick black line) and Trollgaren moraines (thin black lines) are outlined, which were originally mapped by Andersen (1954) (from Briner et al., 2014).

In the Lysefjord region, the Lysefjord moraine system has for the most part been ^{10}Be-dated to belong to the YD (Figure 2.9; Briner et al., 2014). Just north of Lysefjorden, the moraine belt splits into three separate ridges, of which the outmost yielded ^{10}Be ages of ~14 ka that evidently corresponds to the Older Dryas (OD) (Figure 2.9; Briner et al., 2014). This older moraine is referred to as the Leiken Moraine and is thus believed to represent an Older Dryas re-advance between the Bølling and Allerød warm periods (Briner et al., 2014). Ice advance corresponding to this time period has also been documented in other areas along the western coast of Norway (Anundsen, 1972; Blystad and Anundsen, 1983; Mangerud et al., 2011, 2016a).

After the Younger Dryas, the ice sheet underwent relatively rapid retreat in the fjords at the onset of the Holocene. The ice margin reached the Trollgaren moraines near the head of Lysefjord (Figure 2.9) by ~11.3 ka, reflecting rapid retreat within Lysefjord in a relatively short amount of time. Over the course of the next thousand years or so, the Scandinavian ice sheet retreated and eventually disappeared into the Holocene.

2.5 Post-glacial uplift and relative sea level

A consequence of deglaciation is the isostatic uplift of the crust that had previously been depressed by the weight of an overlying ice sheet. At the peak of the LGM, large volumes of water were trapped within vast ice sheets, resulting in a eustatic (global) sea level that was about 125 meters below present (Lambeck et al., 2014). During deglaciation, melting ice sheets lead to a significant rise eustatic sea level. However, the relative sea level experienced in formerly glaciated regions like Scandinavia is highly influenced by the regional isostatic uplift. Thus, significant post-glacial uplift outpaced the rise in eustatic sea level during the last deglaciation, resulting in a net fall of relative sea level in many parts of Scandinavia. The relative sea level (RSL) history varies from area to area based on differing degrees of isostatic uplift, with the greatest uplift occurring in the region that was covered by the thickest ice.

The post-glacial RSL history of western Norway is reasonably well established through radiocarbon dates from isolation basins (e.g. Anundsen, 1985; Lohne et al., 2007, Helle et al., 2007; Vasskog et al., in press). Regional RSL history in SW Norway demonstrates an initial drop in RSL caused by the glacio-isotatic uplift as a result of the deglaciation that reaches a lowstand around the Bølling-Allerød warm period, which was followed by a regional transgression of ~10 m that culminated during the late Younger Dryas (Helle et al., 2007; Lohne et al., 2007). The YD sea level transgression is a reflection of a break in glacio-isostatic uplift caused by the renewed growth of the ice sheet in southwest region of Norway, but since the transgression may have started as early as the mid-Allerød, the YD ice sheet readvance is believed to have actually commenced before the onset of the YD (Lohne et al., 2007).

3. Methods

3.1 Field methods

Fieldwork for this project was done over the course of three trips to the Forsand-Lysefjord region. The aims of fieldwork included measuring glacial striae, collecting erratic boulder samples for ^{10}Be surface exposure dating, and making sedimentological and geomorphological observations in Espedalen to investigate the deglaciation history of the region.

3.1.1 Glacial striae measurements

Glacial striation orientations were measured at a variety of localities around the mouth of Lysefjorden, both within and outside the Younger Dryas ice sheet margin. Striations were measured with a Suunto MC-2G mirror compass, and coordinates and elevations of each locality were determined with a hand-held GPS. The orientation of striations was measured by aligning the compass edge along the striation and rotating the degree wheel to align it with the north arrow. The orientation was read to the nearest degree and recorded. Generally, the more measurements taken at a single locality, the better the average orientation at a locality is represented. Furthermore, striations essentially give the orientation of ice movement, but not necessarily the direction of ice movement. Other erosional ice flow indicators such as crescentic gouges and chatter marks, if present, can be used in conjunction with striations to indicate the direction of ice flow.

3.1.2 ^{10}Be surface exposure sampling

During a fieldwork trip to Forsand in October 2018, a total of seven erratic boulders on bedrock were sampled for ^{10}Be surface exposure dating. Three samples were taken from erratics at the peak of Bergfjellet, and four samples were taken from erratics at the peak of Husafjellet (Figure 1.2). All samples were taken above the local marine limit. Samples were collected from the top 1-2 cm of each boulder from flat surfaces and away from boulder edges wherever possible. A rock saw was used to saw a grid on the top of each boulder, then rock samples were removed with a hammer and chisel. A clinometer (Suunto MC-2G) was used to measure the topographic shielding and a handheld GPS was used to determine sample

coordinates and elevation. Sample elevations were verified using a 1-meter contoured topographic map from www.norgeskart.no. The samples were subsequently transported back to the University of Bergen, where they were processed for ^{10}Be analysis.

3.1.3 Field observations in Espedalen

Sedimentological and geomorphological observations were made in the valley of Espedalen, located immediately to the south of Forsand (Figure 1.2). Of the two large gravel pits at Nedre Espedalen, observations were focused in the Løland gravel pit along the northern slope (Figure 1.2), since it exhibited more intact sediment sections and is more accessible than the one along the southern slope.

3.2 Glacial striae

The glacial striation database portion of this master's project expands on the work done by Sæle (2017) and Mangerud et al. (2019), who present a striations database for the county of Hordaland, in which glacial striations from published and unpublished literature were collected in order to reconstruct ice flow and retreat patterns. This project utilizes a similar database structure to assemble striations from Rogaland, with a particular focus on the Boknafjord region.

3.2.1 Collection of data from other published/unpublished sources

The majority of glacial striations assembled in this project were collected from previously published literature (Anundsen, 1977; Andersen et al. 1987; Anundsen, 1990), as well as several older unpublished theses (Økland, 1947; Rønnevik, 1971; Ringen, 1974;). Several unpublished observations spanning from 2014 to 2016 were also recorded from field notes provided by Jan Mangerud. Nonetheless, the majority of the sources used date back to the 1940s to 1990s. Moreover, striations in these older papers are only included as symbols on geologic maps rather than a table format with corresponding coordinates and elevations. After scanning and enlarging the maps, the orientation of each striation was measured with a Suunto MC-2G mirror compass using the map border outlines as references. Next, the coordinates and elevations of each measurement were determined from topographic maps with 1-meter

contours (provided by www.norgeskart.no) by identifying the corresponding location of each striation as accurately as possible. Nevertheless, the scale of the original maps greatly affected the precision of each geographic location; thus the geographic precision of each entry is also noted.

3.2.2 Striation database

All striation measurements were entered into database for Rogaland using Microsoft Excel, which is provided as a table in Appendix A and available digitally in Appendix B. The general structure of the database is adapted from a similar database developed by Sæle (2017) and subsequently published by Mangerud et al., (2019). In the database, all striation observations are numbered, with each row representing one striation observation. In many instances, there are several striation observations at a single locality, and so they are given the same locality number accordingly. Table 3.1 provides a description of each column included in the database.

Table 3.1. Description of columns in the striation database (Appendix A). Adapted from database presented in Sæle (2017) and Mangerud et al. (2019).

Column #	*Title*	*Description*
1	StriaeNo	*Striae number*. Database number of the striation.
2	Loc.No	*Location/site number*. There can be several striations on one location.
3	County	*County*. This database mainly refers to striations in Rogaland. However, it could be useful if striations from different counties are used.
4	Placename	*Place.* Name of the location/site to quickly identify the locality on the map.
5	Lat.N	*Coordinates*, latitude (N). Latitude is given with 5 decimals. For striations recorded during new fieldwork, GPS coordinates are given. Locations from other authors are taken from "norgeskart.no" (Kartverket), after identification of the localities. Coordinates used; EU89-geografiske grader.
6	Long.E	*Coordinates*, longitude (E). Longitude is given with a precision of maximum 4 decimals. For striations recorded during new fieldwork, GPS coordinates are given. Locations from other authors are taken from "norgeskart.no" (Kartverket), after identification of the localities. Coordinates used; EU89-geografiske grader.

7	Precision	*Precision.* Precision for the geographical stating, rated from 1-4 based on how precise the coordinates are considered to be. How the scale is defined: 1. Very precise. Only used for coordinates taken from GPS. 2. Precise. The locality is given on a map where it is easy to recognize a point in the topography, like an island. We consider the margin of error to be <50 m. 3. Less precise. Used if the original map has a scale 1:50 000 or 1:100 000. Consider the margin of error to be <500 m. 4. Not precise. The locality is given on small maps in publications. The margin of error may be several km. These are only used if the orientation is significant for the glaciological interpretation.
8	Elev_masl	*Altitude,* m a.s.l. Height for own field observations are from maps combined with GPS. Altitude from other authors is from "norgeskart.no", if the height is not referred to in a table.
9	Midpoint	*Midpoint*. For some of the striations a sector is recorded. This column is used if the sector is <10°. If the sector is from 0°-10°, then 5° is the value.
10	Plus_Minus	±. If the sector is >10° this column is used. An example: the striations are from 0°-30°, then 15 is the midpoint to be put in column 8, and the ± value is 15.
11	Youngest	*Youngest.* The orientations of the youngest striae is given in this column. If there is only one direction mentioned in the table, this number is also given here. Relative age 1.
12	Older	*Older*. This column is used to record the orientation of the next oldest striations. Relative age 2.
13	Even_Older	*Even older*. Even older striations than that in Column 12 are given here. Relative age 3.
14	Even_Older2	Even older than that in Column 13. Relative age 4.
15	Oldest	*Oldest.* The oldest striations are given in this column. Relative age 5.
16	Unknown_rel_age	*Undetermined relative age*. This column is used for striations with an undetermined relative age. There may be two striations at one location that are undetermined relative age. There may be two striations at one location that are indeterminable. Even at some locations, there may be one striae that is the youngest and one that are undetermined.
17	Quality	*Quality*. Quality of the striations is defined in a scale of 1-3: 1. Polished surface. Newly revealed surface that appears totally polished and the smallest striations are preserved. It may also exist between high and low water. 2. A surface that is almost unweathered. Such surfaces may also contain finer striations. 3. Weathered surface. The orientation is clear, but the finer striations may be lost.
18	Source	*References.* The reference for the striations.

19	Code_symbol	*Code symbol*. This column is useful for the mapping program (ArcMap). The codes are used to identify the correct symbology for the striations on the map. The codes are the same used by the Norwegian Geological Survey "Norges geologiske undersøkelse" (NGU). The legend for relative age symbology is shown in Figure 3.2. 212: striation with two possible ice flow directions. 213: striation where the relative age is not determined. 214: striation within a sector. 215: cross-cutting striation, relative age 1 (youngest) 216: cross-cutting striation, relative age 2 217: cross-cutting striation, relative age 3 218: cross-cutting striation, relative age 4 219: cross-cutting striation, relative age 5 (oldest)
20	All_orientations	*All orientations*. All the striations are assembled in this column independent of relative age or sector. This is also used with respect for ArcMap.
21	Comments	*Comments*. This column is used when there are some relevant comments. For example, if the location of the striae is leeward.
22	ErosionalMarks	*Erosional mark*s. Erosional marks like chatter marks or crescentic fractures are used to support the direction of ice movement.

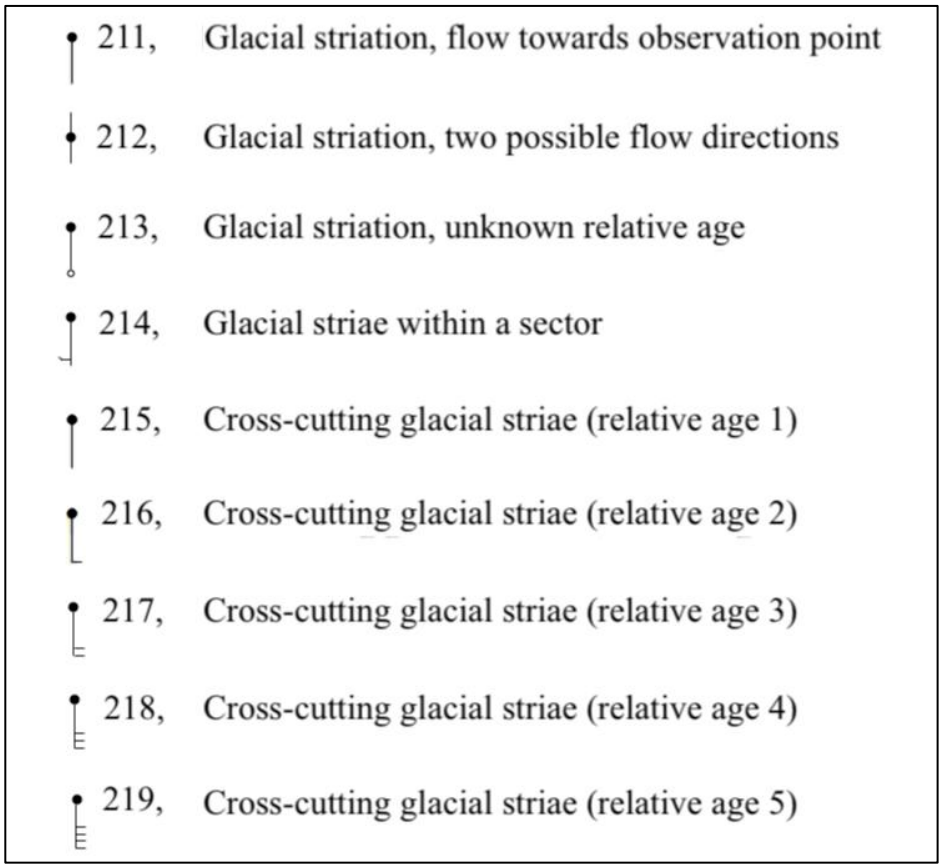

Figure 3.2. The legend used to describe the NGU symbology for striations with relative age. The codes are used for ArcMap to produce the correct orientation of the striations on the map. The symbols in the legend describe all striae observations shown on the maps included in this thesis.

3.2.3 Creating maps with ArcGIS

The mapping software ArcMap 10.6 was used to produce a map of the striations. The striation database in Excel was converted to a shapefile in ArcMap and then displayed with a background map of the study area to produce an overview map of all the striation orientations assembled in the database. This process helps illustrate and visualize patterns in the data that would not be discernable simply by studying the database alone. Striations are displayed with the same symbology used by the NGU (Figure 3.2).

3.2.4 Reconstructing ice retreat patterns using striations

Glacial striae have historically been a valuable tool for the reconstruction of former ice sheet flow patterns. They are particularly useful in areas lacking extensive sediment coverage, like the southwestern coast of Norway. Glacial striae are believed to form below a warm-based ice sheet, especially underneath the flanks of the ice sheet during periods of deglaciation and they are oriented perpendicular to the ice margin (Figure 3.3) (Chamberlin, 1883; Hoppe, 1948; Iverson, 1991). Consequentially, glacial striae are time-transgressive, meaning that they may represent a continuous flow of ice through time as the direction changes rather than a single flow event (Kleman, 1990; Smith and Knight, 2011). As a retreating warm-based ice sheet continuously creates striae at its margins, the oldest striae will be located near the maximum extent of the ice sheet and will be increasingly younger towards the ice-divide (Kleman, 1990). Furthermore, since striae represent the laminar flow of ice, the presence of striae with significantly different orientations at a particular outcrop indicates different generations of ice flows (Figure 3.3; Kleman, 1990).

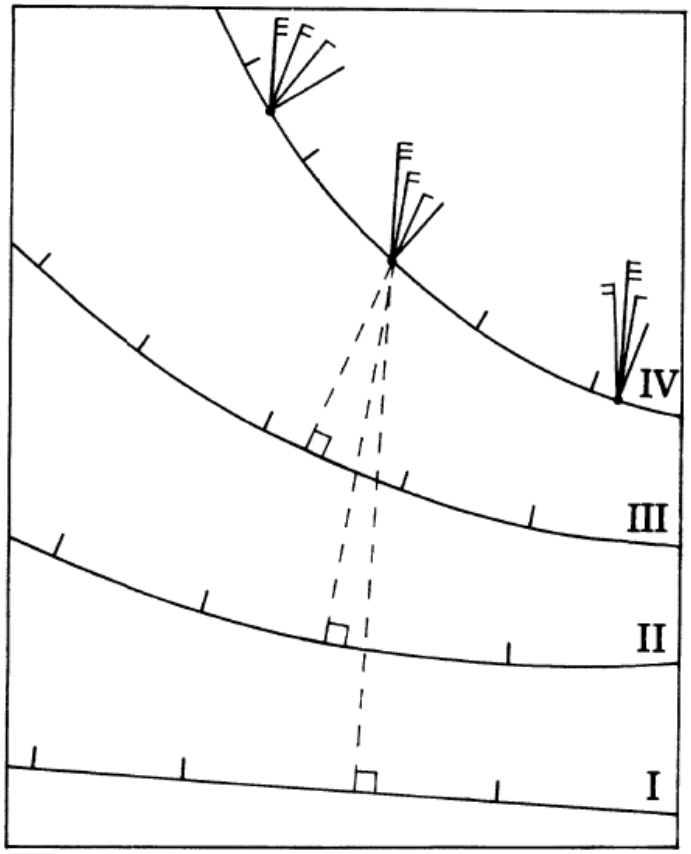

Figure 3.3. Sketch showing the changing orientation of striae formed at the margin of a warm-based ice sheet during retreat (from Kleman, 1990).

The relative age of differently oriented striae can be determined in areas when they exhibit cross-cutting relationships, where younger striae cut over older, preexisting striae. Additionally, the following criteria was used by Jansson et al. (2002) to determine the relative ages of striae (Figure 3.4):

- Striae found on the lee-side of an outcrop are older
- Striae found on crests between grooves are younger
- Striae that cut into other striae are younger

Moreover, since striae only provide the orientation of ice flow, and not necessarily the direction, other criteria are necessary to determine the ice-flow direction. Such criteria can include rat-tails, stoss- and lee-side topography, crescentic gouges and fractures, and striae deflection caused by topography (Figure 3.4; Jansson et al. 2002).

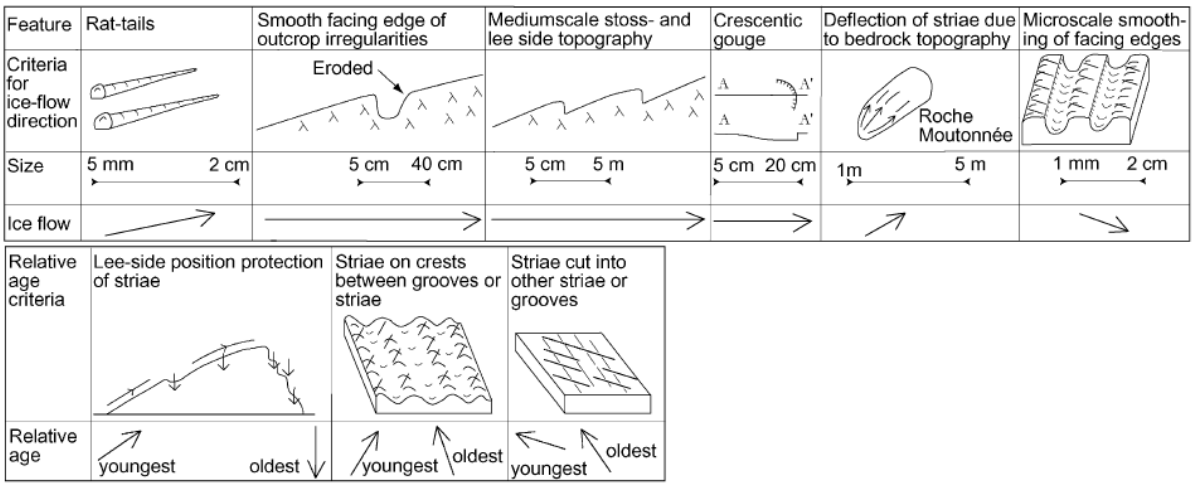

Figure 3.4. Criteria used in determining ice-flow direction and the relative ages of different striae. (from Jansson et al. 2002).

In this study, the striae observations assembled in the database are used to develop a general interpretation of the oldest flowsets. Relative ages of ice flows are determined primarily from cross-cutting relationships among the striae. Most, if not all striae in the database are assumed to belong to the last glacial maximum and subsequent deglaciation. These flowsets are then compared and contrasted to existing knowledge about the position of the ice front and changes in flow patterns during the last deglaciation. Since only a general overview of ice flow patterns is presented here, this database can be utilized in the future for a more exhaustive analysis of ice front geometry during the last deglaciation.

3.3 Surface exposure dating using cosmogenic nuclides

3.3.1 Method background

Surface exposure dating with *in situ* cosmogenic nuclides is based on the accumulation of cosmogenic nuclides in minerals at the Earth's surface that are exposed to cosmic radiation, which can be used to calculate the exposure age of a particular surface since the resulting nuclide concentration within a mineral is direct measure of time (Lal, 1991; Dorn and Phillips, 1991; Gosse and Phillips, 2001). Primary cosmogenic nuclides are high-energy charged particles that collide with particles within the Earth's atmosphere, which causes a cascade of secondary particles over the Earth's surface (Figure 3.5). This cosmic ray flux increases with higher altitudes and latitudes, and can vary temporally as a result of variations in solar wind and Earth's magnetic field (Gosse and Phillips, 2001).

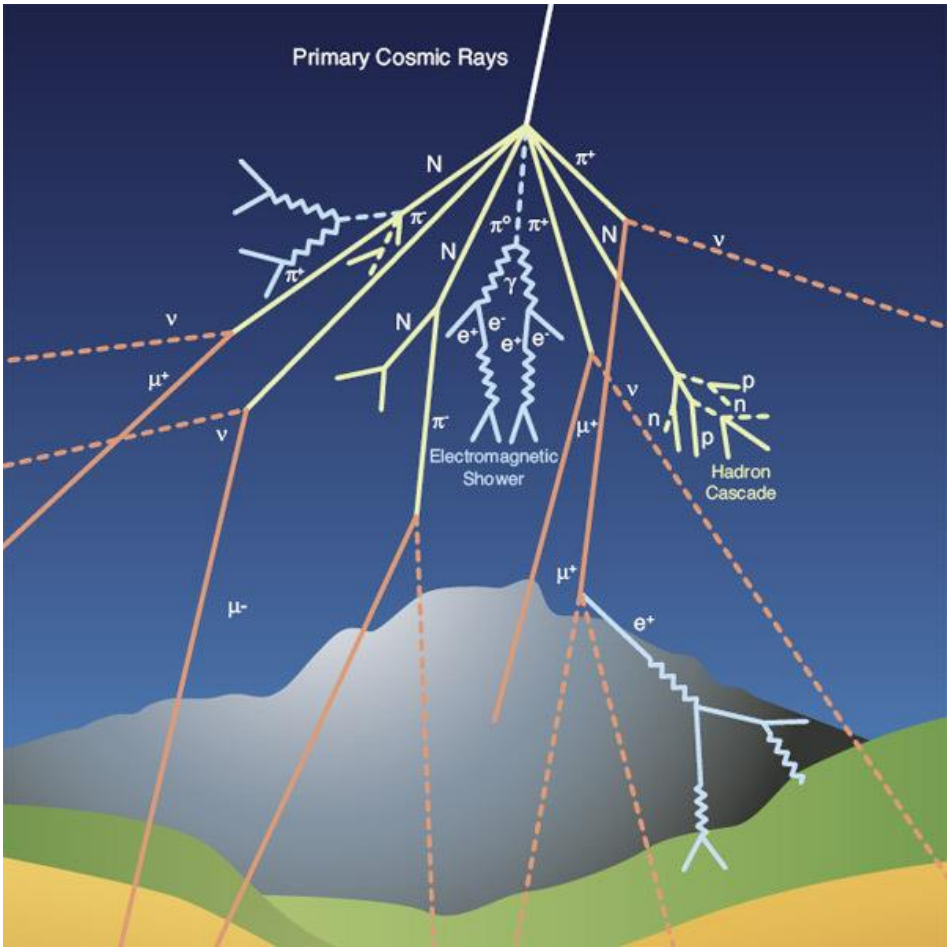

Figure 3.5. Schematic illustrating the cosmic ray cascade over the Earth's surface. Primary particles convert to a shower of secondary particles after colliding with nuclei in the Earth's atmosphere (CERN, 2019).

Cosmogenic nuclides are produced in minerals by three mechanisms: high-energy spallation, negative-muon capture, and low-energy neutron capture (Lal and Peters, 1967). The effect these mechanisms have on nuclide production varies with surface depth, lithology, and density (Lal, 1991). Cumulatively, the nuclide production rate decreases with depth from the exposed surface (Nishiizumi et al., 1993). Nuclide production rates may also be influenced by topography and the geometry of exposure, as well as the lithology and density of the exposed rock/mineral (Nishiizumi et al., 1993). Such factors should therefore be considered when scaling site-specific production rates and reference production rates. A scaling scheme defines the production rate as it varies with time, latitude, and altitude, while the reference production rate is based on the rate at a specific time, location and elevation (Balco et al., 2008). There are several scaling schemes available for scaling production rates (e.g. Lal, 1991; Stone, 2000), which generally differ on the degree to which past magnetic field variations are taken into account and the method used to determine cosmic flux variations (Balco et al., 2008).

The dating range of surface exposure dating with cosmogenic nuclides can range from several hundred years up to millions of years, a range that can be affected by factors such as the nuclide decay constant, topographic shielding, surface erosion rate and the overall degradation of the surface (Ivy-Ochs and Kober, 2008). Exposure dating of a rock surface has several underlying assumptions about the past conditions of the dated surface: the surface has undergone only one exposure episode, it has experienced uninterrupted exposure, and its position has not changed since the start of the exposure (Gosse and Phillips 2001; Ivy-Ochs and Kober, 2007). Another assumption is that the rock surfaces are closed systems, where there has been no loss or contamination of nuclides since the start of the exposure (Nishiizumi et al., 1993).

In an ideal case where all the above assumptions are true, a rock surface can be dated using this method. In most cases however, it is difficult to be completely certain about a rock surface's exposure history. Consequentially, factors such as the degradation of surfaces and nuclide inheritance from earlier exposure events can add a large degree of uncertainty to the accuracy of the method; the former resulting in "too young" exposure ages and the latter resulting in "too old" ages (Figure 3.6; Ivy-Ochs et al., 2007). Young apparent ages can also be obtained if a surface has been shielded from exposure to cosmic rays by snow cover, sediment cover or inundation by water (Benson et al., 2004). Furthermore, exposure ages using cosmogenic nuclides tend to have uncertainties around 10%, which is relatively high

compared to other dating methods such as radiocarbon dating (Ben and Evans, 2010). For these reasons, results should be compared to and corroborated by independent ages using other dating methods whenever possible.

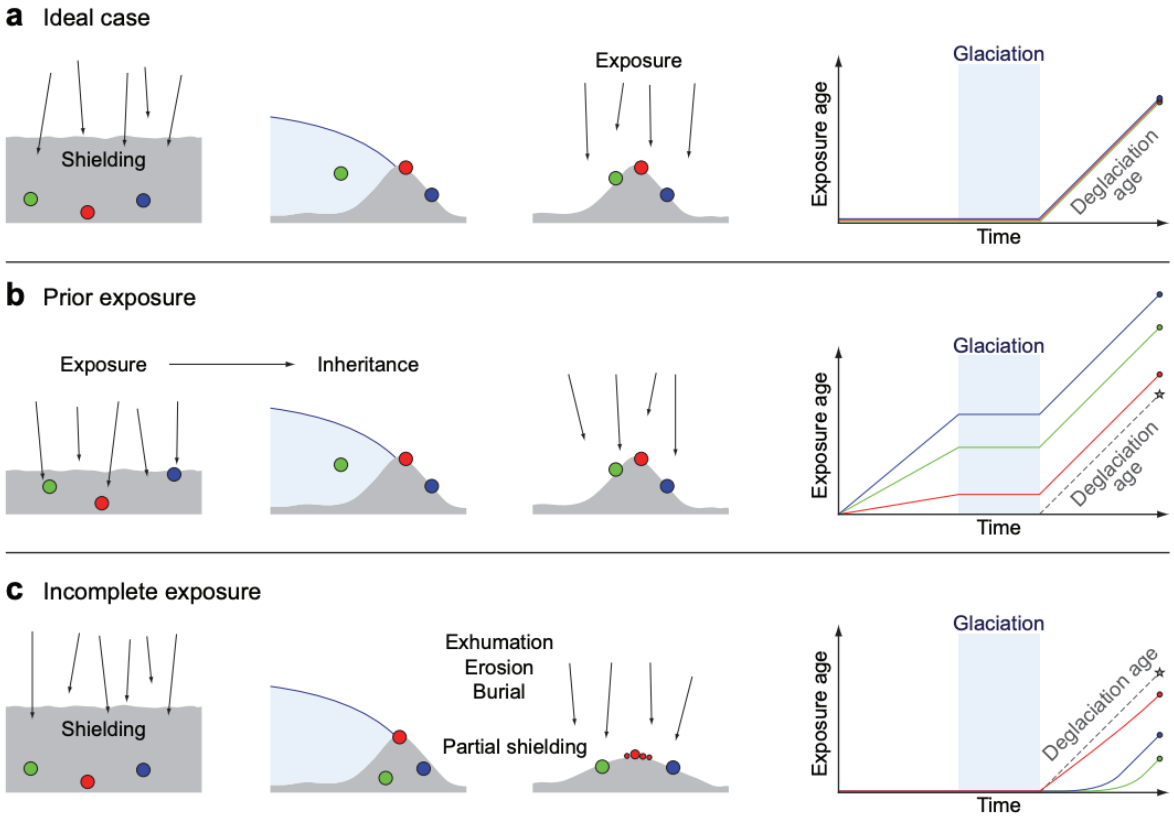

Figure 3.6. Illustration depicting various exposure scenarios and the corresponding effects on resulting exposure ages. (a) the ideal case for exposure dating where the sample has had no exposure prior to deglaciation and has been continuously exposed after deglaciation. (b) Sample has been exposed prior to glaciation, then is continuously exposed after deglaciation. The resulting age will be older than the true age of deglaciation. (c) Sample has had no exposure prior to glaciation, then experiences incomplete exposure following deglaciation due to partial shielding of the surface. The resulting age will be younger than the true age of deglaciation (Heyman et al., 2011).

A distinguishing factor of surface exposure dating using cosmogenic nuclides is the variety of nuclides that can be analyzed (i.e ^{10}Be, ^{14}C, ^{36}Cl, ^{26}Al, etc.), making it possible to date most lithologies and multitude of surfaces and landforms (Ivy-Ochs and Kober, 2008). Quartz is the predominant mineral used for many nuclide analyses, including ^{10}Be, due to its abundance in nature, resistivity to weathering, and ease of preparation. Additionally, the production rate of ^{10}Be is best known for quartz, in comparison to other potential minerals like feldspar. In

glacial landscapes, ^{10}Be dating can be used to date landforms such as moraines, as well as providing exposure ages of erratic boulders or bedrock surfaces, which can provide insight into the deglaciation history of an ice sheet. This master's thesis uses ^{10}Be surface exposure dating of erratic boulders from mountain summits in Forsand to investigate when the sample sites became ice-free during the last deglaciation, allowing for the accumulation of ^{10}Be in the boulder surfaces.

3.3.2 Mineral separation and sample preparation for ^{10}Be analysis

The rock samples from Husafjellet and Bergfjellet were processed by Lars Evje at the University of Bergen's cosmogenic nuclide preparation facility. A comprehensive description of the lab procedures is provided by Grant (2016). As such, only a general overview of the procedure is included here.

The samples were crushed and pulverized to grain sizes of 250-500 μm, after which they were treated with an AqR solution (HNO_3/HCl 1:3) to remove metals, carbonates and micas. Samples underwent floatation to separate the quartz from the feldspar, followed by magnetic separation to further refine the quartz by removing any remaining micas and heavy minerals. The samples then went through a heated ultrasound leaching process to further purify the quartz and remove the meteoric ^{10}Be. The purity of the quartz is checked using ICP-OES. Once the quartz samples were purified of other minerals, metals and meteoric ^{10}Be, they were digested in an HF solution to start the process of beryllium extraction. The digested quartz samples were spiked with ~254 μm of ^{9}Be carrier. The sample batch contained one process blank (UiB 1902) with a ^{10}Be/^{9}Be ratio of (9.03 ± 2.88) x 10^{-16} that corresponds a background correction of 0.45% the sample total. To extract the beryllium fraction, the samples went through chlorine conversion, anion exchange chromatography, sulphate conversion, and finally, cation exchange chromatography. The beryllium fraction was precipitated and dried, then oxidized, mixed with Nb, and pressed into cathodes. The cathodes were sent to the Aarhus AMS Centre where the beryllium ratios were measured by accelerator mass spectrometry (AMS). Samples were normalized to standard 07KNSTD with a ratio of 2.85 x 10^{-12} (Nishiizumi et al., 2007).

3.3.3 Age calculations

Exposure ages were calculated using the CRONUS-Earth online exposure age calculator, version 3, which makes corrections for latitude, longitude, elevation, erosion rate, topographic shielding, sample thickness, and density (Balco et al., 2008; hess.ess.washington.edu). A regional production rate for western Norway was used (Goehring et al., 2012a, b) with the Lm scaling scheme (Balco et al., 2008). In addition, ages calculated with the Scandinavian production rate (Table 3.2; Stroeven et al., 2015) are also presented for the ease of comparison. Since the previously published ^{10}Be ages from the Lysefjord and Boknafjord region are calculated with the western Norway production rate, the ages presented in this thesis are also calculated with the same production rate to allow for comparisons among the ages. The production rate choice is further discussed in Chapter 6.

Table 3.2. Production rates of the Western Norway and Scandinavian datasets and the time ranges that they represent.

Data set	Production rate (atoms g^{-1} a^{-1}) (Lm scaling)	Time range (ka cal before sampling)	Reference
Western Norway	4.15 ± 0.15	~11.6 to ~6.1	Goehring et al. (2012a, b)
Scandinavian	4.13 ± 0.11	~11.6 to ~6.1	Stroeven et al. (2015)

An Lm scaling scheme is chosen since the ^{10}Be production rate is believed to be minimally influenced by the Earth's magnetic field at high latitudes (Gosse and Phillips, 2001; Briner et al., 2014). All previously presented ^{10}Be ages from the region (Briner et al., 2014; Svendsen et al., 2015; Gump et al., 2017) did not make corrections for postglacial erosion and weathering due to the relatively erosion-resistant lithology in region and numerous glacial striae observations. Following the same reasoning and for the sake of comparison, no corrections for post-glacial erosion are made here as well. Isostatic uplift corrections of sample elevations are also not made, since the shoreline displacement is relatively minimal and the marine limit (~34 m a.s.l; Anundsen, 1985) most likely represents the maximum level of the Younger Dryas transgression (Karlsen, 2016). Corrections for such a low degree of isostatic uplift would result in ages about less than one percent older, and thus does not significantly change the resulting chronology. Furthermore, the effect of minor isostatic uplift

on the ^{10}Be ages may be counterbalanced by the effect of unknown atmospheric pressure changes since deglaciation (Staiger et al., 2007; Briner et al., 2014, Svendsen et al., 2015).
The ^{10}Be ages are presented only with their internal uncertainty, based on a 1-sigma internal AMS analytical uncertainty. The uncertainty of average ages for each site is based on the standard deviation of the group of individual ^{10}Be ages at each site. Outliers (greater than 2 sigma from other ages) and vastly imprecise ages are not included in the calculations for average ages.

3.3.4 Comparisons with preliminary ^{10}Be ages provided from Uburen

The ^{10}Be ages from this thesis have been compared with preliminary ages from glacial erratics on Uburen, a mountain in Forsand located in the same vicinity as Husafjellet and Bergfjellet. The Uburen ^{10}Be ages have been provided by John Inge Svendsen (pers. comm. 2019) and the samples were processed at the University of Buffalo Cosmogenic Nuclide Laboratory under the guidance of Jason Briner following similar procedures and age calculations outlined in Briner et al. (2014) and Gump et al. (2017). The ^{10}Be/^{9}Be ratios were measured by AMS at the Center for Mass Spectrometry Lawrence Livermore National Laboratory.

3.4 LiDAR

3.4.1 LiDAR: How it works

Light detection and ranging technology, commonly referred to as LiDAR, is a type of airborne laser scanning that can produce high-resolution digital elevation models of the Earth's surface, which has a multitude of implementations in Quaternary geology. In principle, airborne LiDAR data is collected from an aircraft that essentially scans the earth's surface by emitting high energy laser pulses and measuring the time elapsed until the return of the backscattered pulse after it hits the Earth's surface (Figure 3.7; Dowman, 2004). This measured travel time is used to calculate the range, or distance between the airborne laser scanner and particular points on the earth's surface, which translates into the elevation of those points (Glennie *et al.*, 2013).

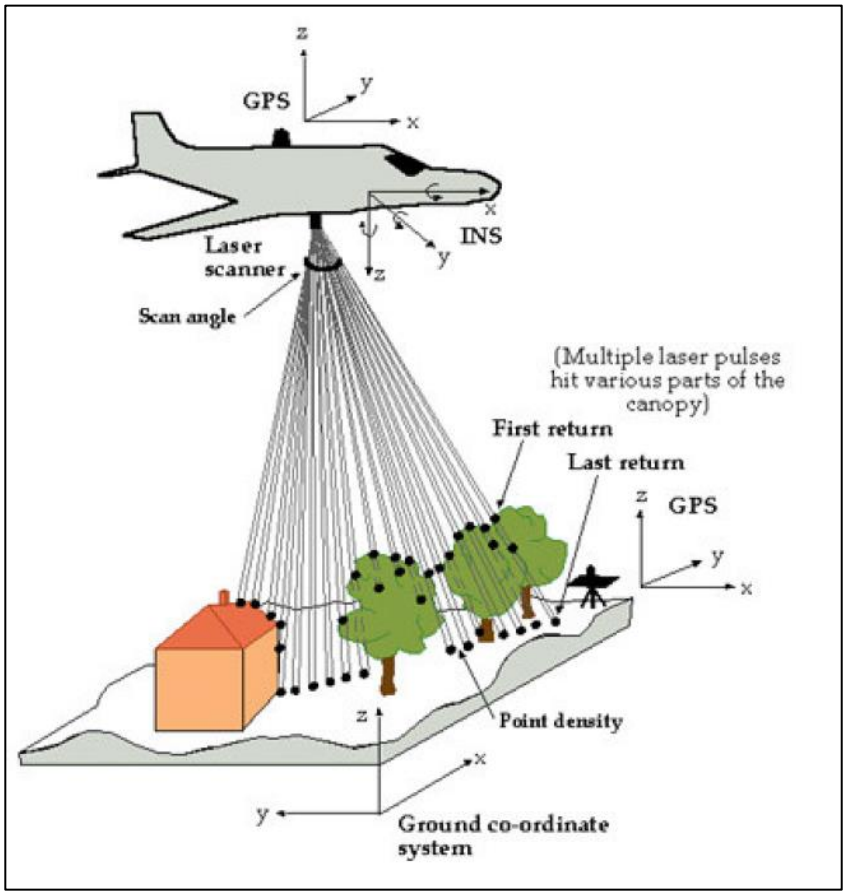

Figure 3.7. Schematic representation of airborne LiDAR summarizing the key concepts and components involved (Dowman, 2004).

Since the laser-scanning unit in airborne LiDAR is continually in 3D motion through space, a position and orientation system is necessary to estimate the scanner's position within 3D space (Wehr & Lohr, 1999). Thus, the laser scanner's georeferencing data is combined with the distance to target data to create a three-dimensional point cloud of the Earth's surface, which effectively encompasses the coordinates and elevation (X, Y, Z) of densely spaced points on the earth's surface (Glennie *et al*., 2013). Finally, these point clouds are used to develop digital surface models, or DSMs.

LiDAR data is distinctly advantageous due to the ability to 'remove' the vegetation signals from DSMs to produce digital terrain models of the bare ground. When an emitted laser makes contact with multiple objects on its path to the bare surface, multiple returns of the laser pulse are recorded, the last of which represents the true bare-ground signal (Figure 3.7; Dowman, 2004). All but the last return signal can be filtered out from DSMs to produce a digital terrain model (DTM), essentially removing the vegetation from terrain (Dowman, 2004). Thus LiDAR data of areas with vegetated terrain can be particularly advantageous to geological investigations as it allows researchers to observe subtle features in the terrain that would otherwise be obscured by vegetation.

3.4.2 LiDAR applications in geologic mapping

LiDAR-derived DTMs have been used to identify a variety of landforms, such as moraines, raised beach ridges, shorelines, glaciofluvial and fluvial terraces, meltwater channels, and post-glacial scarps (i.e Ojala *et al.*, 2013, 2015; Möller & Dowling, 2015; Eilertsen *et al*., 2015). LiDAR DTMs can be used to identify small to mid-scale landforms that might otherwise be difficult to distinguish in the field, on aerial photos, or on topographic maps (Johnson et al., 2015). Nevertheless, some landforms and deposits may not be decisively identified though LiDAR data alone. For example, bedrock exposures, boulders, discontinuous till-covered areas and organic soil cover may be difficult to distinguished from one another (Sarala *et al*., 2015). Similarly, it can sometimes be difficult to distinguished till from slope deposits (Johnson *et al*., 2015). Thus, field-checking may still be necessary in many cases.

Furthermore, the LiDAR coverage of an area can vary and may be an issue in regions where the coverage is patchy, particularly at higher elevations. Most of the region of interest to this thesis has LiDAR coverage, but there are certain higher elevation areas where there is no 1-meter resolution (DTM1) data available. Nevertheless, there is 10-meter resolution (DTM10) data available that covers the entire region, which was used in the following chapters to display hillshaded terrain base maps.

3.4.3 LiDAR mapping of geomorphological features in ArcMap

For this project, LiDAR-derived Digital Terrain Models (DTM) provided by the Norwegian Mapping Authority (Kartverket) were used to map certain geomorphological features, such as marginal moraines, lineated terrain, fluvial and glaciofluvial terraces, and ice-dammed lake shorelines. These features were mapped and analyzed to assist with the identification of past ice flow directions over the region, as well as reconstructing the depositional environments around Espedalen during the last deglaciation.

LiDAR DTMs covering most of Norway are available for download in 1-meter, 10-meter and 50-meter resolutions (https://hoydedata.no/LaserInnsyn/). LiDAR data with 1-meter resolution (DTM1) was added to the mapping program ArcMap 10.6 to produce LiDAR-derived hillshade models for identifying and mapping the geomorphological features of interest. Hillshades display DTM data in the form of shaded relief produced by an illumination source. Parameters such as illumination azimuth, altitude of illumination, and Z-factor (vertical exaggeration) can be adjusted to produce hillshades that emphasize various terrain characteristics to meet the demands of the task at hand. The azimuth refers to the direction from which the sun is illuminating the terrain and is expressed in degree from 0 to 360. The altitude refers to the angle of the illumination source above the horizon, and is expressed in degrees from 0 to 90. For this thesis, three hillshades (Figure 3.8) were generated with varying illumination azimuths and altitudes to produce various shadings of the terrain for best identifying different landforms. The presented LiDAR hillshade maps and figures are displayed with a z-factor of 2. Identified features were mapped on separate layers using the polygon, line and multipoint editing tools. All presented maps are shown with an ETRS 1989 UTM Zone 33N projection.

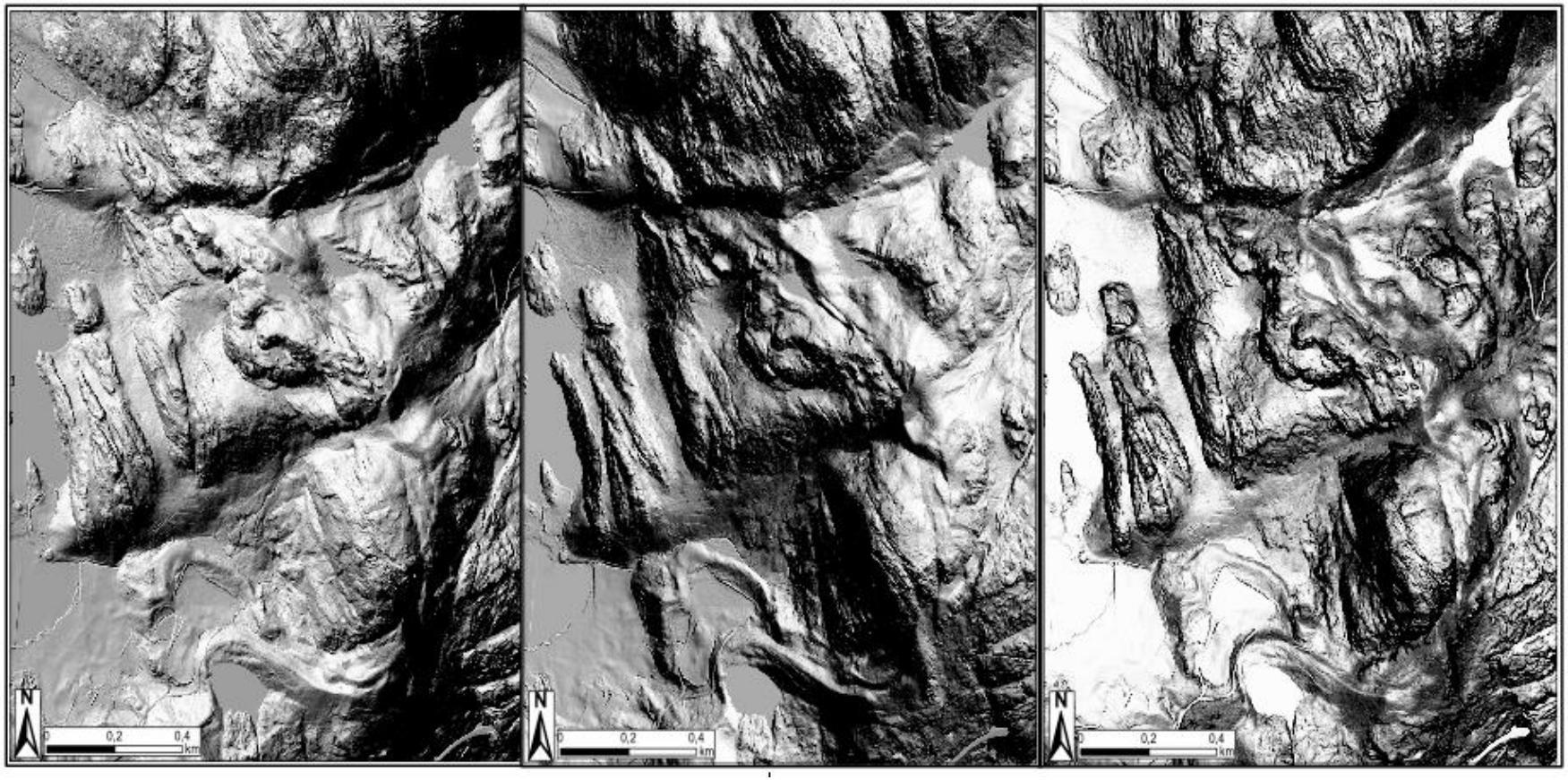

Figure 3.8. Three different LiDAR DTM1 hillshades of the same terrain. Each hillshade emphasizes different features of the terrain. (a) Hillshade with 315° azimuth, 45° illumination altitude and a Z-factor of 2. (b) Hillshade with 45° azimuth, 45° illumination altitude, and a Z-factor of 2. (c) Hillshade with 315° azimuth, 90° illumination altitude, and a Z-factor of 2.

4. Results

4.1 Overview of striations & their orientations

An overview map of all the collected striations is presented in Figure 4.1. Table 4.1 shows a breakdown of all the striations and their sources. Since several of these sources built upon one another in the presentation of their striations, it is possible that there may be duplicates of the same striae within the database. The database has been examined for these potential duplicates, but it is still possible that some may have gone unnoticed. The database itself is provided as a table in Appendix A and is also available digitally (Appendix B).

The database striations are predominantly located in the county of Rogaland in the region surrounding Boknafjorden, though several measurements along the southern border of Hordaland are also included. Although the striae orientations can vary within 180° to 270°, they exhibit a clear general trend towards the W-SW (Figure 4.2). About three quarters of the striae are located outside the YD ice sheet margin, with orientations that trend towards the WSW, within 225° and 270° (Figure 4.3). Around a quarter of the striations are located inside the YD ice margin. Compared to those outside the YD margin, the majority of the proximal striae have orientations within 180° and 315° (Figure 4.4).

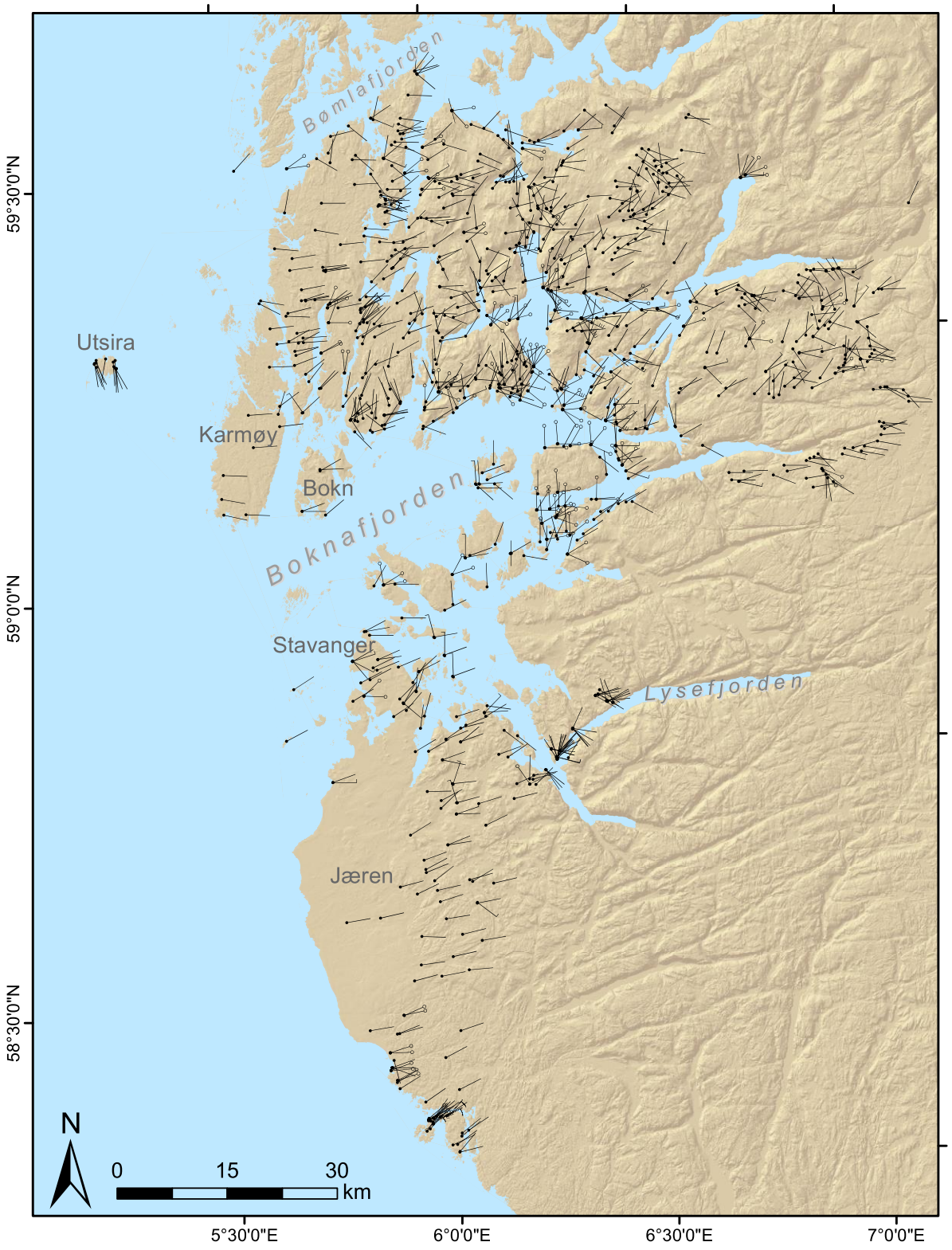

Figure 4.1. An overview map of the Boknafjord region showing all 1073 striae included in the database. Striae are displayed on a DTM10 hillshade base map, illumination from NW (data downloaded from kartverket.no).

Table 4.1. Overview of all collected striations in the database.

Source	Year	Total striae	Area
Undås	1948	8	Utsira
Økland	1947	21	Tysvær, Haugesund, Karmøy, Sveio
Rønnevik	1971	77	Sveio, Haugesund, Tysvær, Karmøy
Ringen	1974	13	Karmøy
Garnes	1976	25	Eigerøy
Anundsen	1977	464	Tysvær, Vindafjord, Sveio, Suldal, Etne
Andersen *et al.*	1987	106	Stavanger, Randaberg, Sola, Sandnes, Jæren
Anundsen	1990	296	Stavanger, Randaberg, Sola, Finnøy, Hjelmeland, Suldal, Sauda, Sveio, Tysvær, Karmøy
Mangerud	2014 - 2016	12	Utsira, Bokn, Tysvær
Tuestad	2019	51	Forsand, Oanes, Lauvvik, Preikestolen, Moslifjellet
	Total	**1073**	

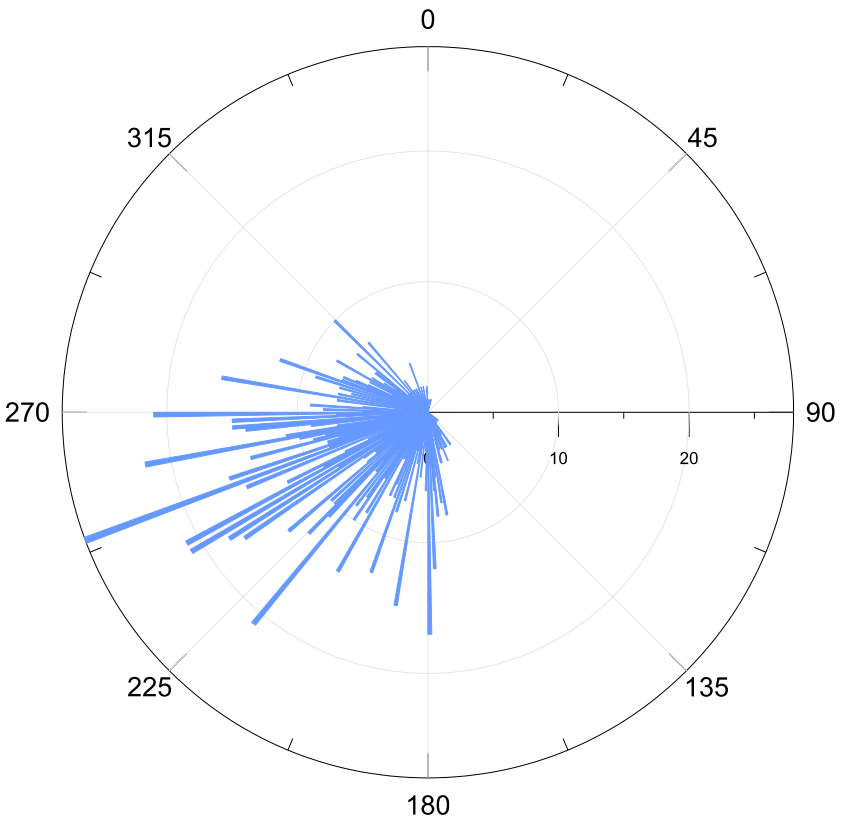

Figure 4.2. Rose diagram showing the orientations of all the striations in the database. The predominant orientation of the striations is towards the WSW, within 180° and 315°. Diagram represents 1073 striation measurements and there is a maximum of 28 striae with the same orientation.

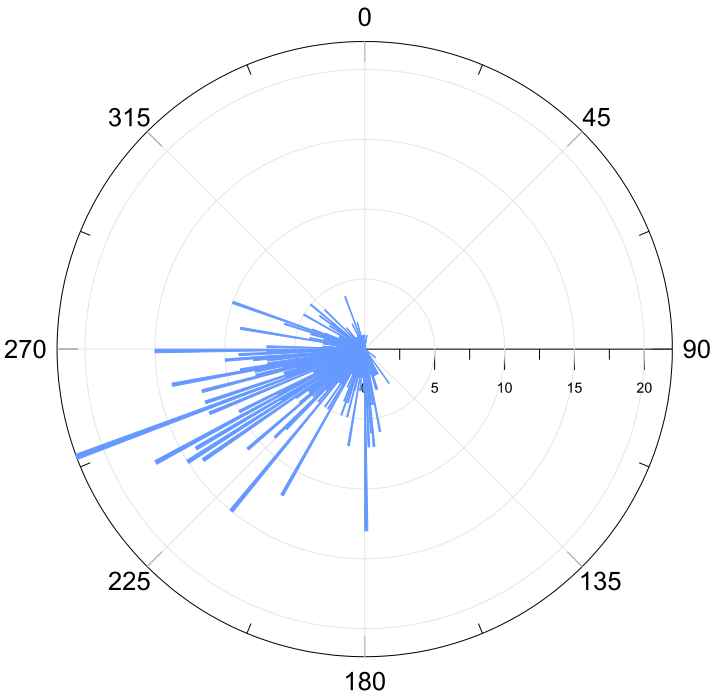

Figure 4.3. Rose diagram showing the orientations of all striations located outside the Younger Dryas ice margin. The predominant orientation of these striae is towards the WSW, within 225° and 270°. There are a total of 701 striae represented in diagram and there are up to 22 striae with the same orientation.

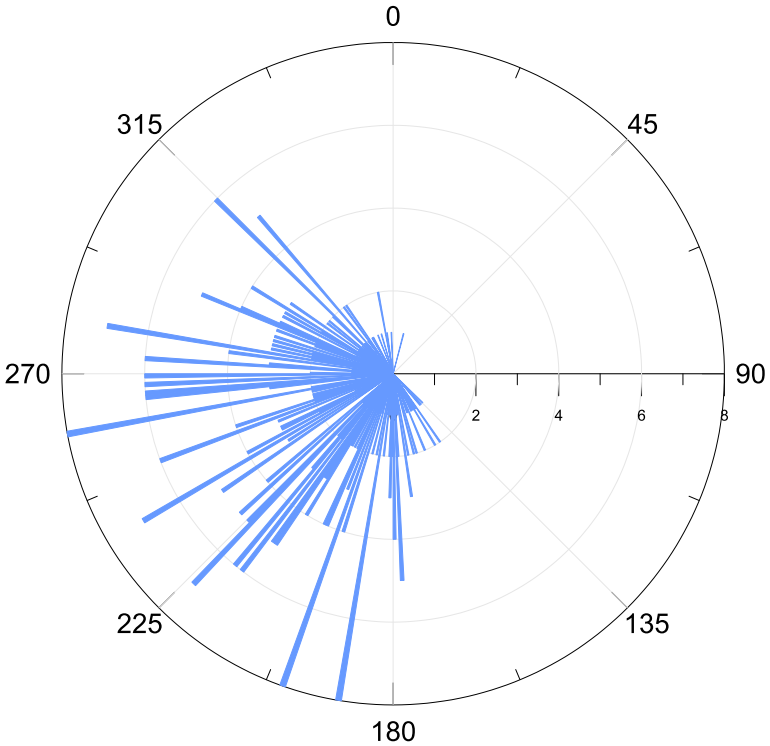

Figure 4.4. Rose diagram showing the orientations of all striations located inside the Younger Dryas ice margin. Most of these striae have orientations scattered from 135° to 315°, with a slight peak towards the south. There are a total of 372 striae represented in the diagram and there is a maximum of 8 striae with the same orientation.

4.2 Field observations: striae and other ice flow indicators

A total of 51 striation measurements were collected from the Lysefjord-Forsand area. Along the main hiking trail to Preikestolen, numerous striations were observed on bedrock exposures, which range from glacially polished to moderately weathered. Other ice flow indicators like crescentic gouges and fractures were also present and relatively abundant at several localities that complement the striation measurements by demonstrating the direction of ice flow (Figure 4.5, 4.6; Table 4.2),. Striae were found immediately proximal to the Younger Dryas margin (Figure 4.9), which is marked by a prominent moraine that crosses the main hiking path to Preikestolen (Figure 4.7). There are several SW-oriented striae within the YD margin, as well as several SSE-oriented striae whose orientations were confirmed by similarly oriented crescentic gouges (Figure 4.5c). Striae from Moslifjellet distal to the YD margin indicate two different flow directions of unknown relative age: WNW and SW (Figure 4.9). Crescentic gouges demonstrating a WNW-flow direction were also observed near the WNW-oriented striae (Figure 4.6b).

In general, the bedrock exposures at the highest elevations around Preikestolen and Moslifjellet have a higher degree of weathering and thus well-preserved striae were difficult to find at these elevations. The best-preserved striae were observed on bedrock exposures along hiking trails recently cleared of sediment and vegetation. Similarly, the bedrock on Bergfjellet and Husafjellet is also quite weathered; hence few to no striations were discernable. Well-preserved striae were found at localities around Oanes and Forsand (Figure 4.9), predominantly on roadside bedrock exposures at lower elevations (<35m a.s.l). The striae at Oanes near the mouth of Lysefjorden demonstrate two main ice flow directions: to the SW parallel to Lysefjorden, and to the WNW (Figure 4.9). Crosscutting relationships indicate that the SW fjord-parallel striae are younger than the WNW striae. A couple of SSE-oriented striae that tilt towards Lysefjorden were also observed. Several striae were also observed along Høgsfjorden near the Lauvvik ferry port (Figure 4.8, 4.9), which demonstrate a NW flow direction parallel to the fjord.

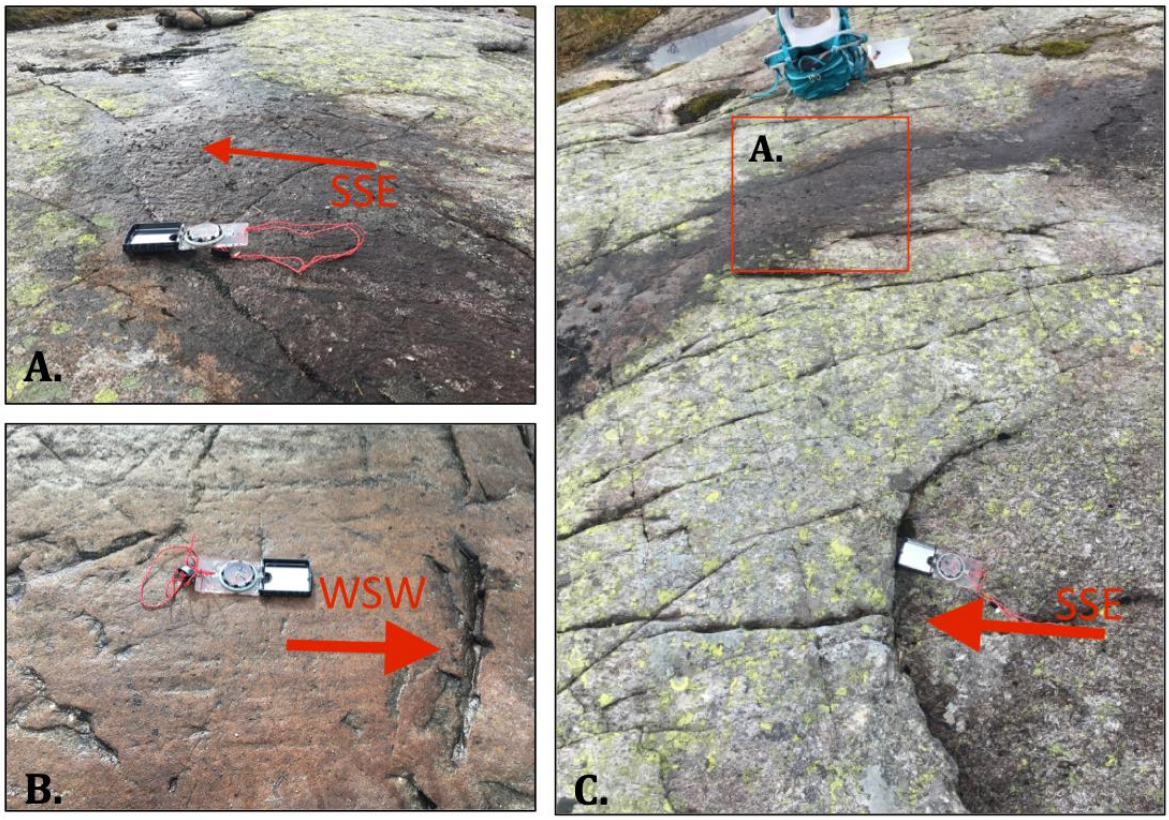

Figure 4.5. (A) & (B) Glacial striae on a bedrock exposure off hiking path to Preikestolen. (B) Striae & crescentic gouge are oriented towards the WSW, (C) SSE-oriented crescentic gouge and striae found ~1 m away, shown up close in (A). Location of (A) is denoted by the red box in (C). *Photo: T. Tuestad*

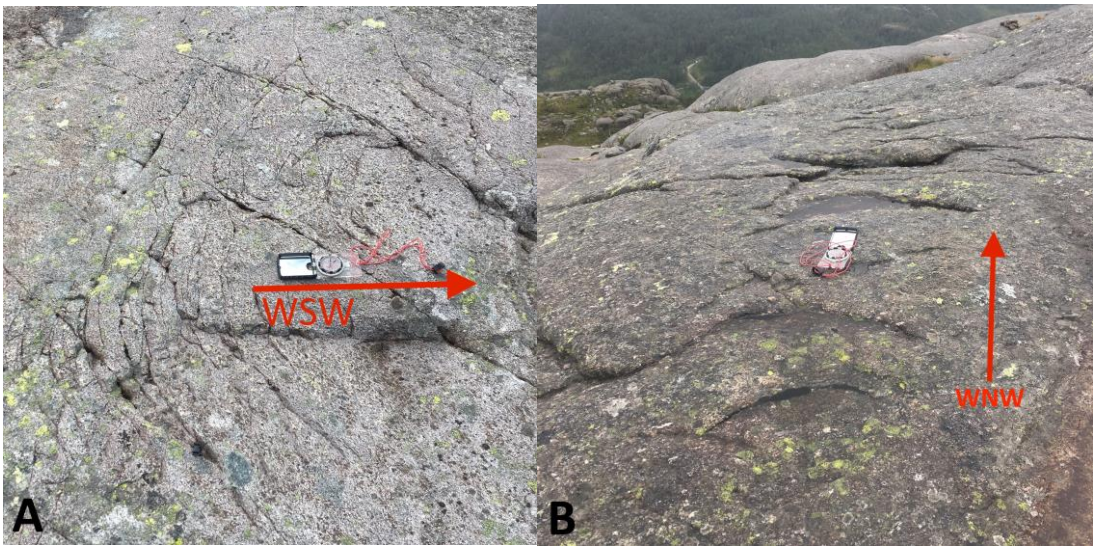

Figure 4.6. (A) Crescentic fractures indicating ice flow towards the WSW on Preikestolen, and (B) crescentic gouges oriented towards WNW on Moslifjellet. *Photos: T. Tuestad*.

Table 4.2. Other ice flow direction indicators found in the Preikestolen-Moslifjellet area.

Location	Latitude (N)	Longitude (E)	Elevation (m a.s.l)	Type	Orientation (°)
Moslifjellet	58.993400	6.1484675	528	Crescentic gouge	300
Preikestolen	58.988334	6.1756646	546	Crescentic gouge	268
Preikestolen	58.988323	6.1756946	546	Crescentic gouge	270
Preikestolen	58.988290	6.1757805	546	Crescentic gouge	180
Preikestolen	58.988353	6.1756192	546	Crescentic gouge	244
Preikestolen	58.988296	6.1757777	546	Crescentic gouge	156
Preikestolen	58.988300	6.1755123	544	Crescentic fracture	254
Preikestolen	58.988300	6.1749635	557	Crescentic gouge	158
Preikestolen	58.989000	6.1795244	544	Crescentic fracture	240

Figure 4.7. Photo of the Younger Dryas moraine located along the hiking trail to Preikestolen. Hikers along the trail on the left provide scale. *Photo: T. Tuestad.*

Figure 4.8. NW-oriented coarse striae at Lauvvik, showing ice flow parallel to Høgsfjorden. *Photo: T. Tuestad.*

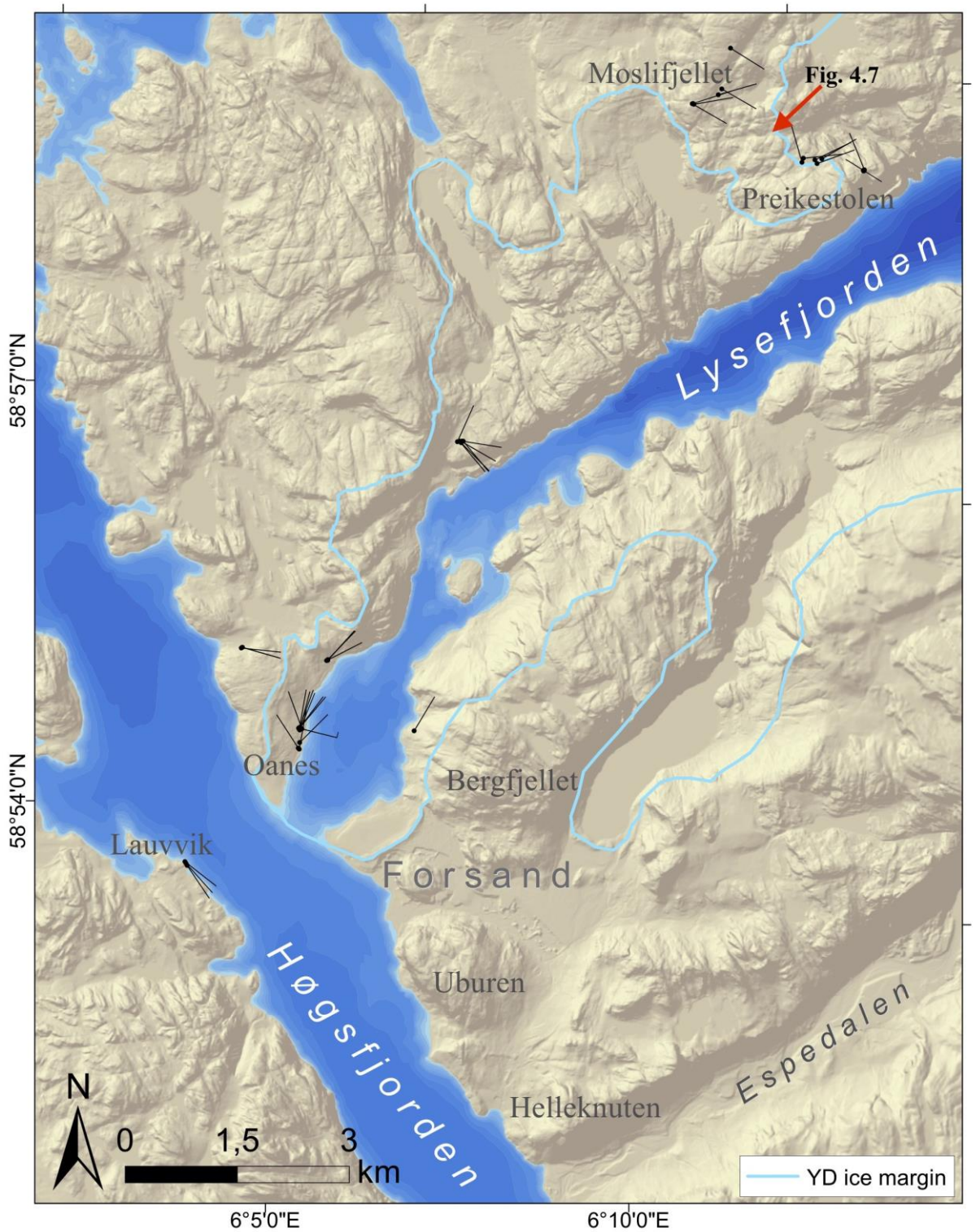

Figure 4.9. Map of the Lysefjord-Forsand study area showing striae measurements taken during fieldwork. The YD ice margin is outlined in blue, according to Andersen (1954). Red arrow shows location of YD moraine in Figure 4.7.

4.3 Streamlined terrain

Distinctive streamlined terrain is visible on LiDAR throughout the Boknafjord region, hence the orientation and distribution of these features has been mapped (Figure 4.11). The majority of these features are streamlined sediment forms such as drumlins and flutings, but some lineated features in bedrock are also included as well, to a lesser extent. SW-oriented drumlinoid ridges and mega-scale flutings are particularly pronounced around the Stavanger peninsula (Figure 4.10), but they can also be traced further south on Jæren as well as over many islands throughout the inner Boknafjord region. Additionally, several distinct W-oriented drumlin-like ridges are clearly visible on the island of Karmøy, in an area otherwise devoid of sediment cover. These ridges have also been previously mentioned and discussed in earlier literature (e.g. Ringen, 1964; Andersen et al., 1983).

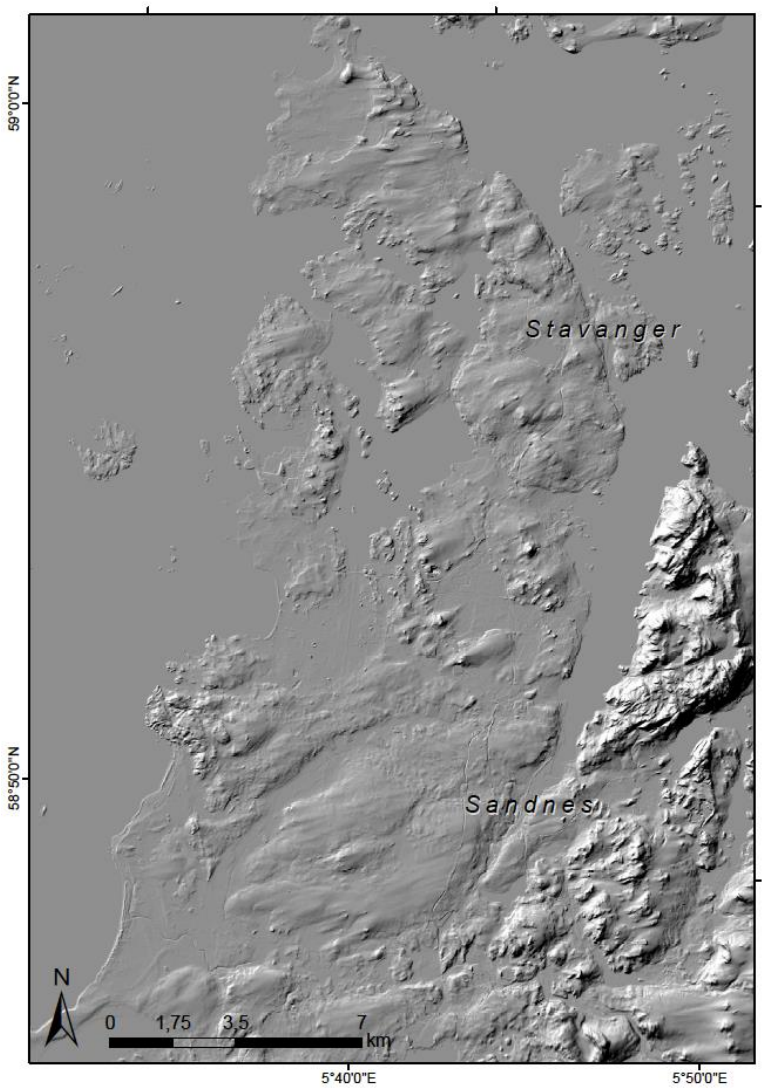

Figure 4.10. Streamlined terrain characterized by elongated drumlinoid ridges and flutings shown on LiDAR hillshade of the Stavanger peninsula. Location shown in Figure 4.12.

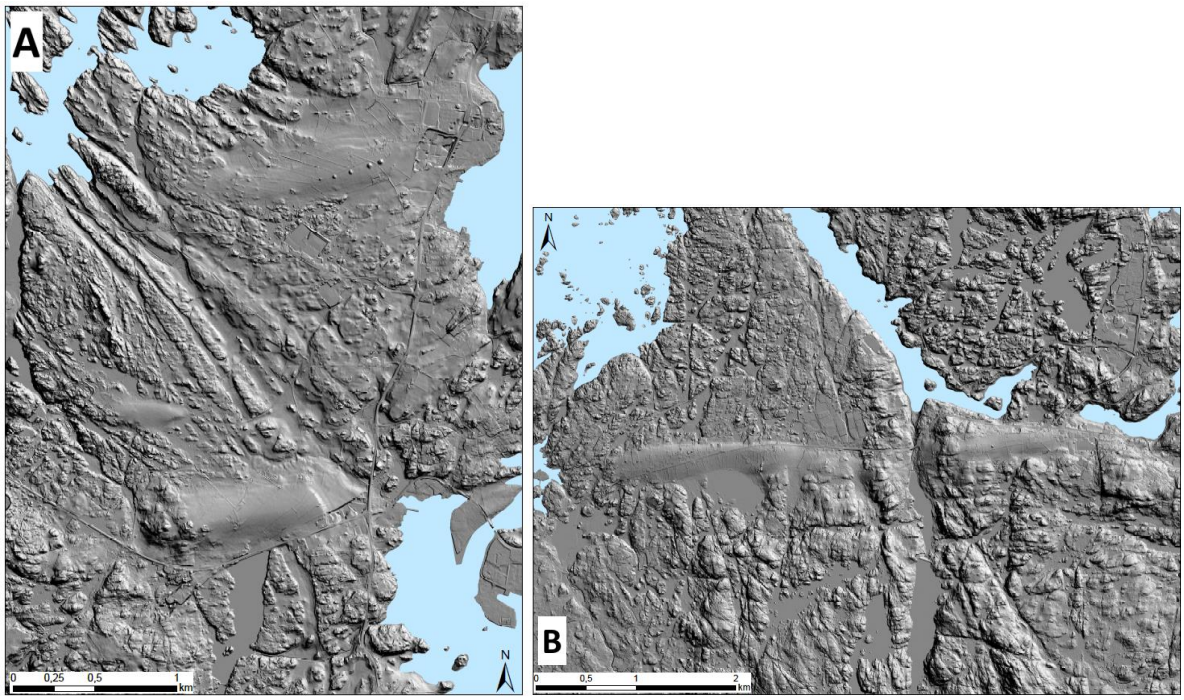

Figure 4.11. LiDAR hillshade of drumlins on Karmøy. Locations are shown in Figure 4.12.

The vast majority of the streamlined features around the mouth of Boknafjorden are oriented towards the W and SW. Moving further east towards the inner fjords, there is a slight shift in orientation from W-SW to W. There are also several localities at the mouth of Høgsfjorden and Idsefjorden where flutings are oriented towards the NW. The streamlined terrain is assumed to represent the most recent ice flow over a particular region, which is based on the reasoning that older subglacial depositional landforms like flutings or drumlins would have been eroded by subsequent ice flows. Therefore, there should be agreement between orientation of the youngest striae and ice-flow indicators like flutings and drumlins in close proximity to one another if they both correspond to the youngest ice flow over the region. As shown in Figure 4.12, there is a reasonable similarity between the striae and the proximate streamlined terrain, particularly in areas such as Stavanger, Jæren, and Karmøy.

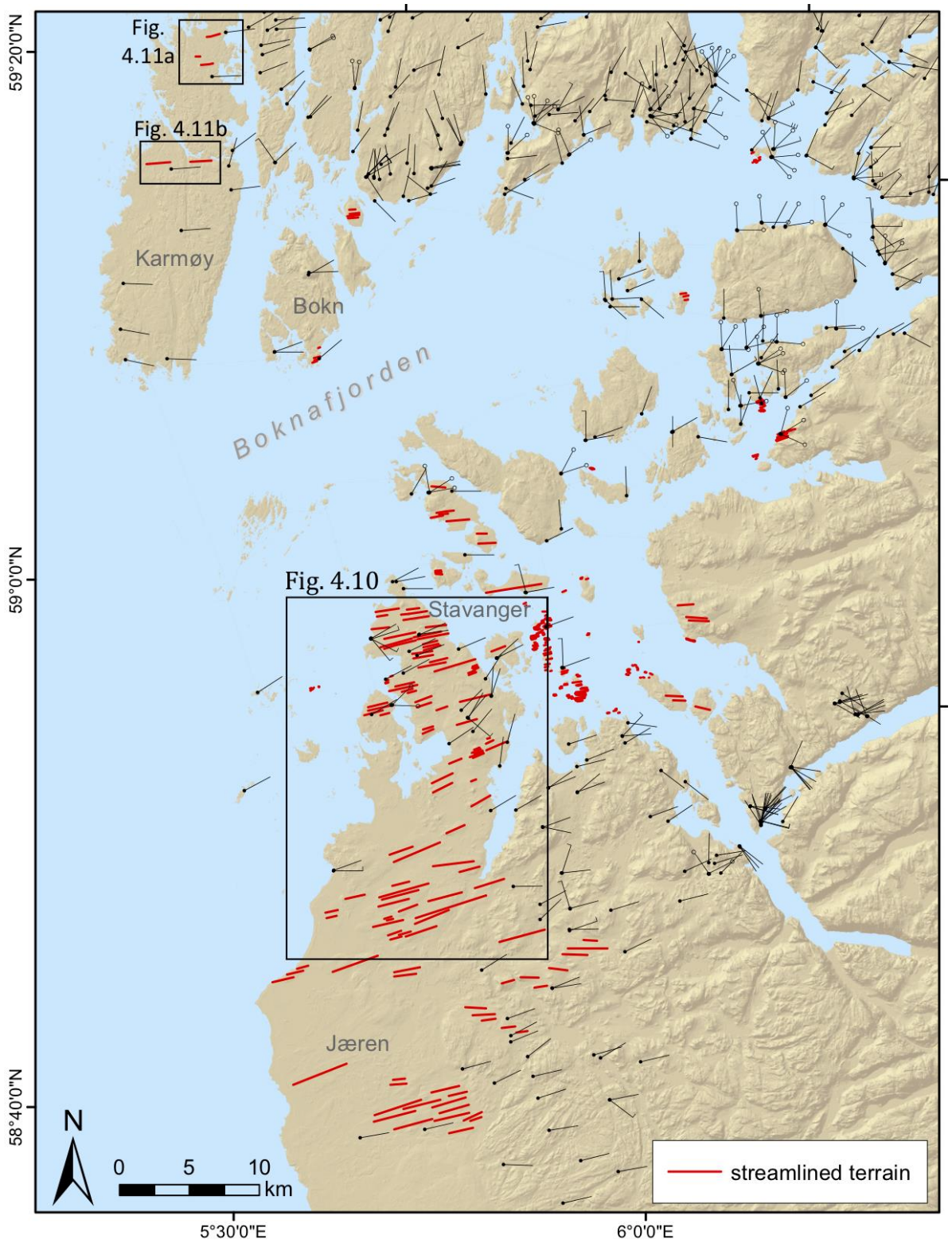

Figure 4.12. Map of striae showing the distribution of streamlined terrain (i.e. drumlins, flutings, bedrock lineations) over the Boknafjord region. Locations of Figure 4.10 and 4.11 on Karmøy are shown in by the black boxes.

4.4. Geomorphological and sedimentological observations in Nedre Espedal

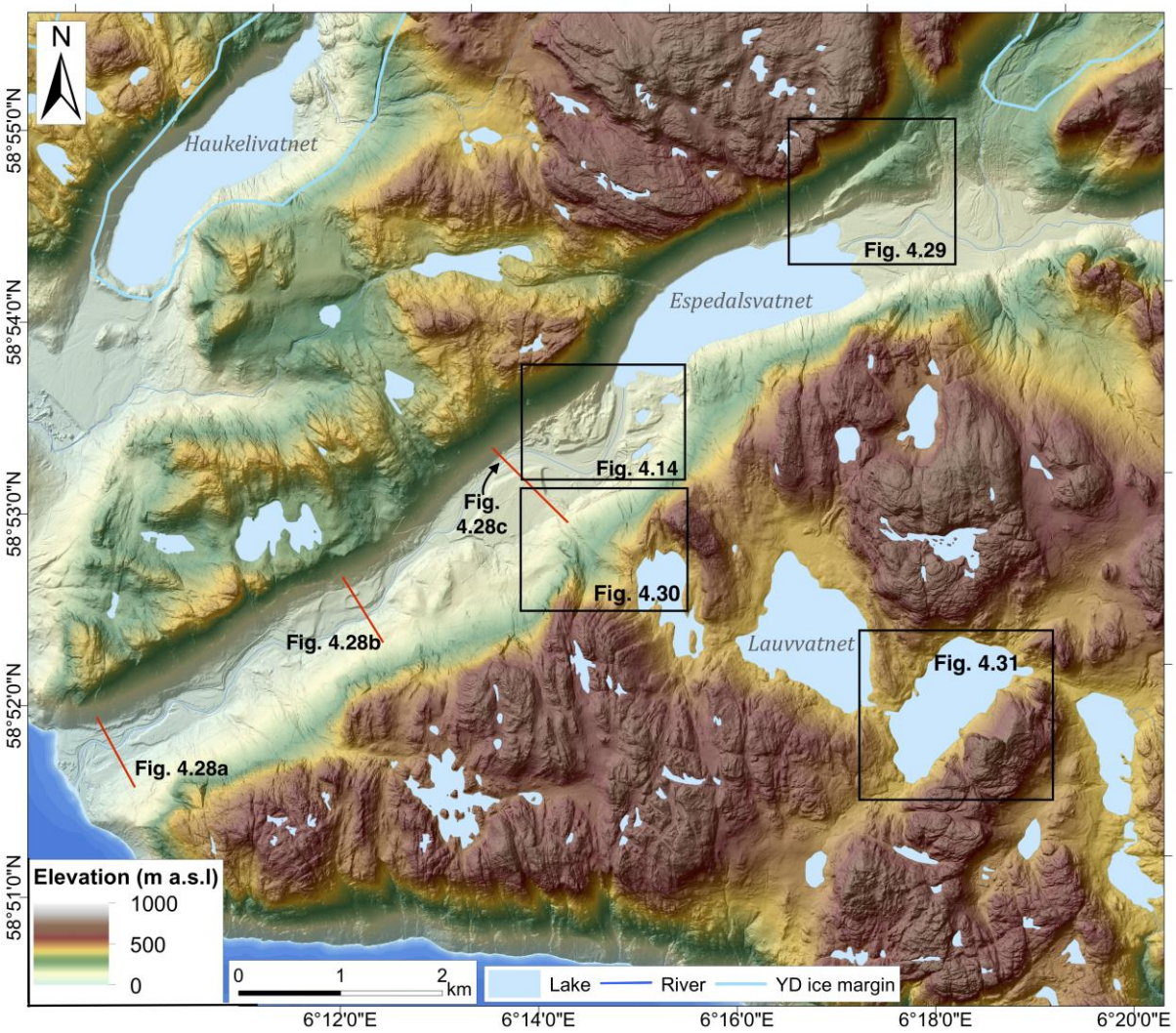

Figure 4.13. Overview hillshade map of Espedalen and the surrounding region. Black boxes show the locations of Figures 4.14, 4.29, 4.30 and 4.31. Transects of elevation profiles in Figure 4.28 are shown by the red lines.

4.4.1. Ice-marginal features at Løland/Nedre Espedal

The inner portion of Nedre Espedal near the outlet of Espedalsvatnet is characterized by distinct hummocky terrain, which is found adjacent to two terraces at Løland (Figure 4.13, 4.14). Various geomorphological observations were made primarily based on the LiDAR DTM1 elevation data and hillshades of the terrain. For example, the relatively flat surface of a 157 m a.s.l terrace is clearly juxtaposed with the bordering uneven, hummocky terrain (Figure 4.14b). Moreover, a series of ridges are distributed within the hummocky terrain (Figure 4.15). The distribution and morphology of the ridges quite resembles that of ice-marginal

moraine ridges, hence they are interpreted as ice-marginal features deposited at a retreating ice-front. Moreover, several kettle hole lakes are observed on the opposite side of Espedalsåna, indicating the former presence of buried ice (Figure 4.14a). Thus, the geomorphological observations on LiDAR of the terrain along the southern outlet of Espedalsvatnet provide compelling evidence of a former ice margin positioned at Løland/Nedre Espedalen.

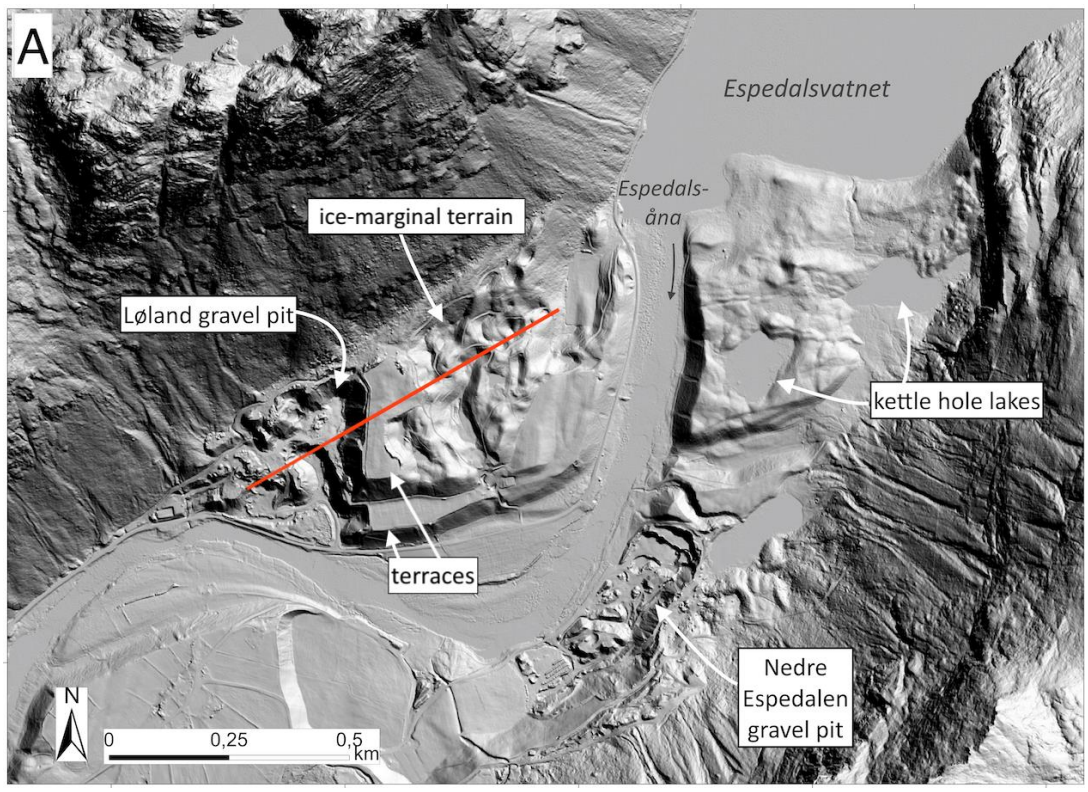

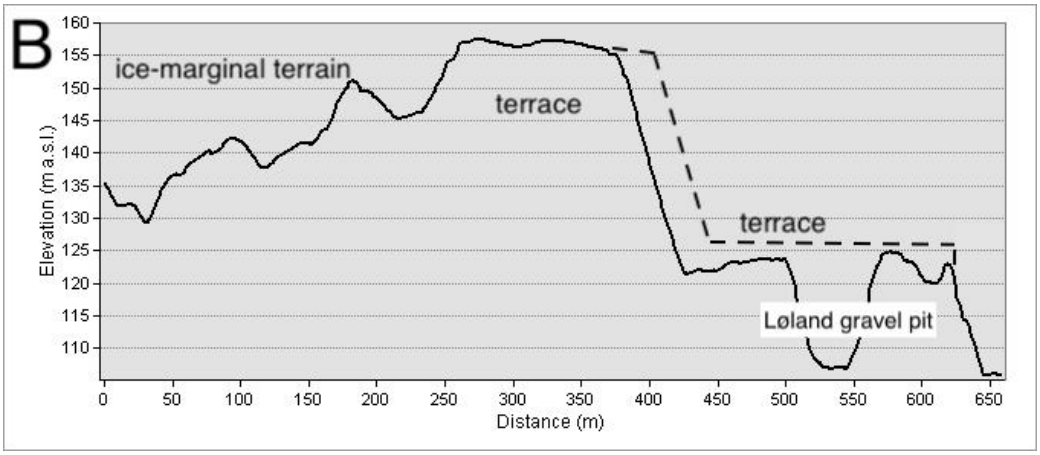

Figure 4.14. (A) Ice-marginal terrain at Løland and Nedre Espedalen, marked by hummocky terrain and kettle hole lakes. Gravel pits are dug into the terraces. (B) Elevation profile showing the hummocky ice-marginal terrain, the adjacent 157 m terrace and the lower 125 m terrace. Location of transect in (B) is shown by the red line in (A).

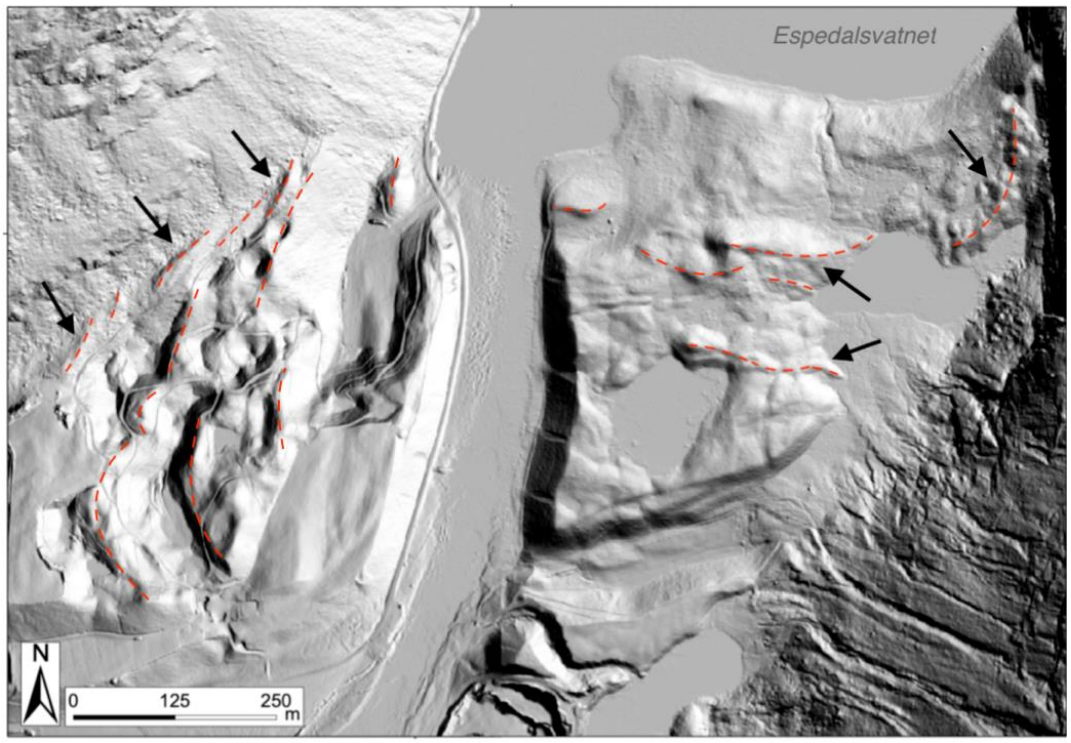

Figure 4.15. LiDAR hillshade of ice-marginal terrain near the outlet of Espedalsvatnet. The observed ridges bordering the hummocky terrain on the west side of Espedalsåna, as well as among the kettle hole lakes on the east side of the river. Ridges are interpreted as ice-marginal deposits, but field checking is necessary to confirm. Red-dashed lines trace the long-axis of the ridges. Left half of the hillshade is illuminated from the east, and the right half is illuminated from the northeast.

4.4.2. Løland gravel pit sections

Two distinct terraces are found at the Løland site in Nedre Espedalen. The upper terrace bordering the ice-marginal terrain has a surface elevation of around 157 m a.s.l., which is about 50 meters higher than Espedalsvatnet (Figure 4.14 a, b). The lower terrace has a surface elevation of about 126 m a.s.l. The Løland gravel pit has been dug into the two terraces, and provides several well-exposed sediment sections of the lower terrace (Figure 4.16). No detailed observations of the higher terrace (157 m a.s.l) sediments were possible, as most of the slope is obscured by slope debris. However, the surface of the 157 m terrace seems to be underlain by a several-meter thick coarse sediment unit that contains some larger boulders. The lower section of the 157 m terrace is not exposed, but seems to be composed of much finer sediment than the terrace surface, such as sand and gravel. The surface of the lower terrace is draped with coarse sediment mostly consisting of cobbles and boulders, some of which have a volume up to 1 m^3. The source of these cobble and boulders is not clear, as they

are not believed to be *in situ*. At some sections, it is difficult to distinguish between the *in* situ terrace deposits and the overlying cobbles/boulders draped over the surface.

The following section is a preliminary overview of the main sediment facies that are exposed in the lower terrace (112 to 122 m a.s.l) of the gravel pit at Løland (Figure 4.16). Various sediment facies are observed in each sediment section, a summary of which is presented in Table 4.3.

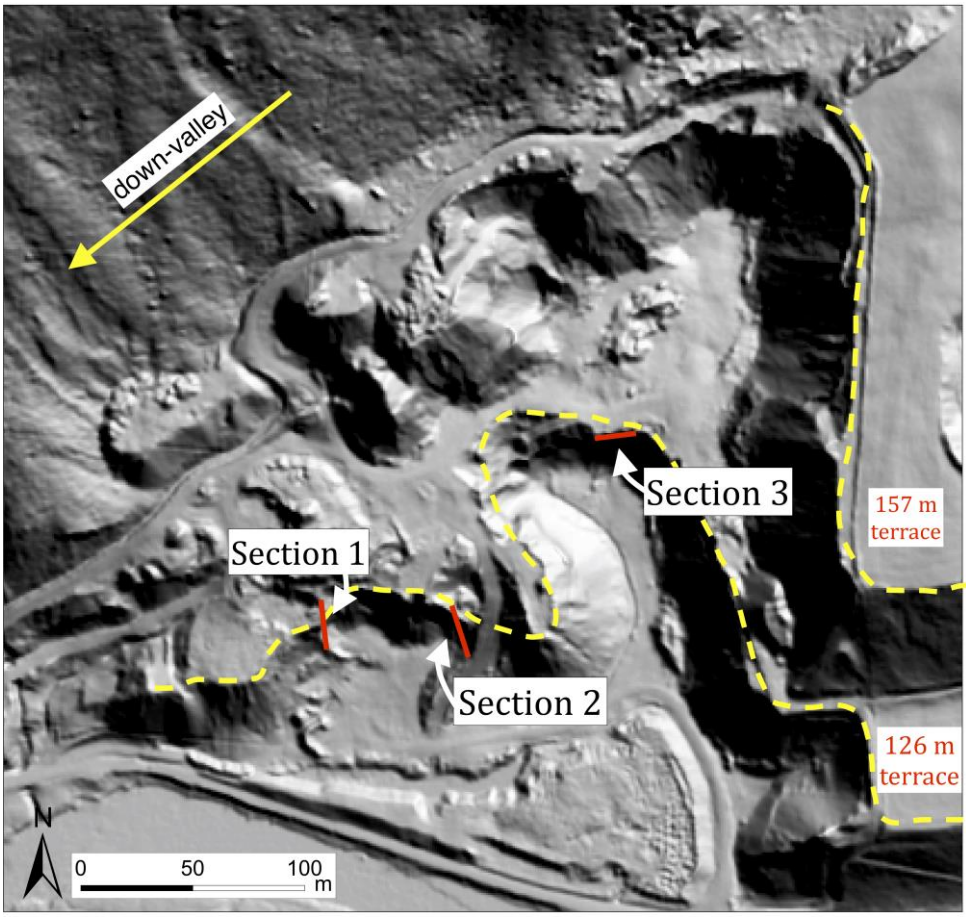

Figure 4.16. Close-up LiDAR view of the Løland gravel pit, showing the locations and transects of the three sediment sections discussed in the text. Yellow dashed line delineates the margins of the two terraces (126 m a.s.l. and 157 m a.s.l.) into which the gravel pit has been dug. Down-valley direction is indicated by the yellow arrow.

Section 1

Section 1 is about 6 meters high, from around 112 m a.s.l at its base up to 118 m a.s.l at the top (Figure 4.17, 4.18). A ~0.5 meter-thick bed of sigmoidally stratified medium to coarse sand (facies B) is found at the top of Section 1 at an elevation of about 118 m a.s.l. This sandy bed can be traced up to ~9 meters, after which it pinches off laterally. A ~1 meter unit of

alternating beds of stratified fine-medium sand, silt and clay (facies A) is found below facies B from ~115 to 117 m a.s.l. Lenticular beds of massive coarse sand and gravel (facies H) are found throughout facies A, as well as isolated outsized gravel to cobble sized clasts that distort underlying laminations. Facies A is interbedded with several beds of sub-angular to sub-rounded gravelly sand (facies C). The gravelly sand beds can be traced laterally up to 7-8 meters, beyond which they pinch off into the overlying and underlying beds. Several beds of sigmoidally cross-stratified laminated fine to medium sand (facies B) are also present in the middle portion of Section 1 at ~114 to ~115 m a.s.l. These sand beds vary in thickness (2 cm to 30 cm), pinching off laterally in some areas then thickening again in other areas. Some of the beds of facies B can be traced laterally up to several meters. Beds of hummocky, sinusoidally stratified gravelly medium to coarse sand (facies F) are also present in conjunction with facies B. Locally, sigmoidal cross-stratification can flatten to subhorizontal laminae (facies E). Gravel to cobble-size outsized clasts occur within the sandy facies B, F and E, distorting the underlying beds. A local lenticular scour infilled with massive sand and gravelly sand (Facies D) is observed with an erosional base cutting into the sigmoidally stratified sand. The bottom ~2 m of Section 1 (~112 to 114 m a.s.l.) is composed of several meters of facies A (Figure 4.17). Beds of massive coarse sand up to several cm thick are interbedded with the finer, laminated sediment. Lenses of unsorted, angular to sub-rounded, massive coarse sand, gravel and pebbles truncate into the underlying laminae (facies H). These lenses range from mm to several cm thick, and can be up to 15 to 20 cm laterally. Isolated gravel to cobble-size, angular to sub-rounded outsized clasts are dispersed throughout the laminated unit and distort the underlying laminae.

Interpretation: Facies A is interpreted as suspension deposits from turbiditic flow on a distal deltaic slope (Lønne, 1993). Lenticular beds of facies H are interpreted as ice-rafted debris, and isolated outsized clasts interpreted as dropstones (Thomas and Connell, 1985). Sigmoidally stratified sand (facies B) is commonly associated with sinusoidally stratified sand (facies F) and sub-horizontally stratified sand (facies E), which are interpreted as humpback dune, aggregating antidune, and migrating antidune deposits, respectively (Lang et al., 2017). Local scours infilled with facies D are interpreted as diamicton deposited by cohesive debris flows, likely from the ice ablation or flow till (McCabe and Eyles, 1988; Winsemann et al., 2009). The massive gravelly sediment of facies C is interpreted as non-cohesive debris flow deposits (Winsemann et al., 2009).

Figure 4.17. Lower unit of section 1 showing stratified beds of sand, silt and clay with dispersed outsize clasts and lenses of coarse sand and gravel (facies A). 1-meter stick for scale. *Photo: T.Tuestad* .

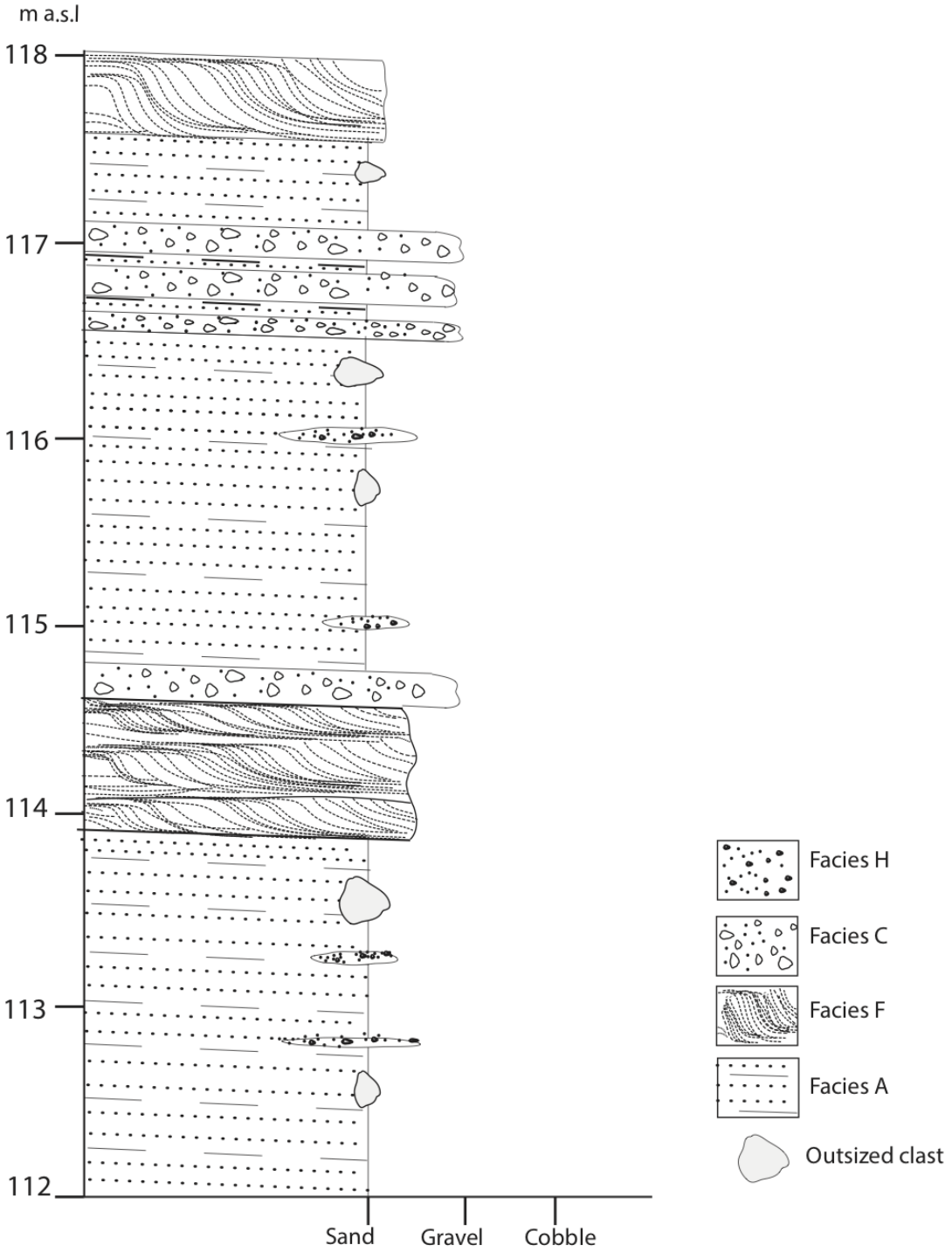

Figure 4.18. Sediment log for Section 1 at the Løland gravel pit. Section 1 is exposed from an elevation of 112 m a.s.l up to 118 m a.s.l and exhibits four observed facies.

Section 2

Section 2 is a 13-meter high sediment section that reaches up around 122 m a.s.l. (Figure 4.19). About 8 meters of sediment is clearly exposed in this section. The uppermost ~6 meters (~116 to 122 m a.s.l.) are largely characterized by horizontal to sub horizontal stratified sand with dispersed gravels and cobbles (facies E). Some areas of facies E exhibit low-angle cross-stratification and truncations of the strata are distinctly visible. Facies E may transition into sigmoidally and sinusoidally stratified sand (facies B & F).

Numerous lenticular scours infilled with massive, poorly sorted, matrix-supported gravel, sand and cobbles are observed within the stratified sand facies (facies D) (Figure 4.19, 4.21). The lenticular scours can be up to 1 m thick and range from a meter to several meters laterally in length. The lowermost unit of section 2 (~114 to 116 m a.s.l) is composed of stratified, moderately sorted gravel and medium to coarse sand with occasional cobble-sized clasts (facies G) (Figure 4.20). Bedding is dipping (15-20°) towards the west-southwest (~250°). Facies G has a seemingly erosive contact with the underlying beds.

Interpretation: The sub-horizontal, cross-stratified sand of facies E is interpreted as migrating antidune deposits, likely in a glaciolacustrine setting (Lang et al., 2017). The lenticular scours within facies E are infilled with facies D, interpreted as cohesive debris flows (Winsemann et al., 2009). At the base of the section, Facies F is interpreted as gravelly sand foresets, possibly deposited in high-velocity turbulent flows (Winsemann et al., 2009).

Figure 4.19. Panoramic view of section 2 with a N-S orientation, facing the up-valley direction. The upper sediment section exposed in the left side of the photo corresponds to facies B. Black dashed lines outline scours infilled with diamicton (facies D) interpreted as debris flows. The lower sediment unit exposed at the lower right side of the photo corresponds to facies F. A down-valley profile view of facies F in section 2 is shown in Figure 4.20. *Photo: T. Tuestad.*

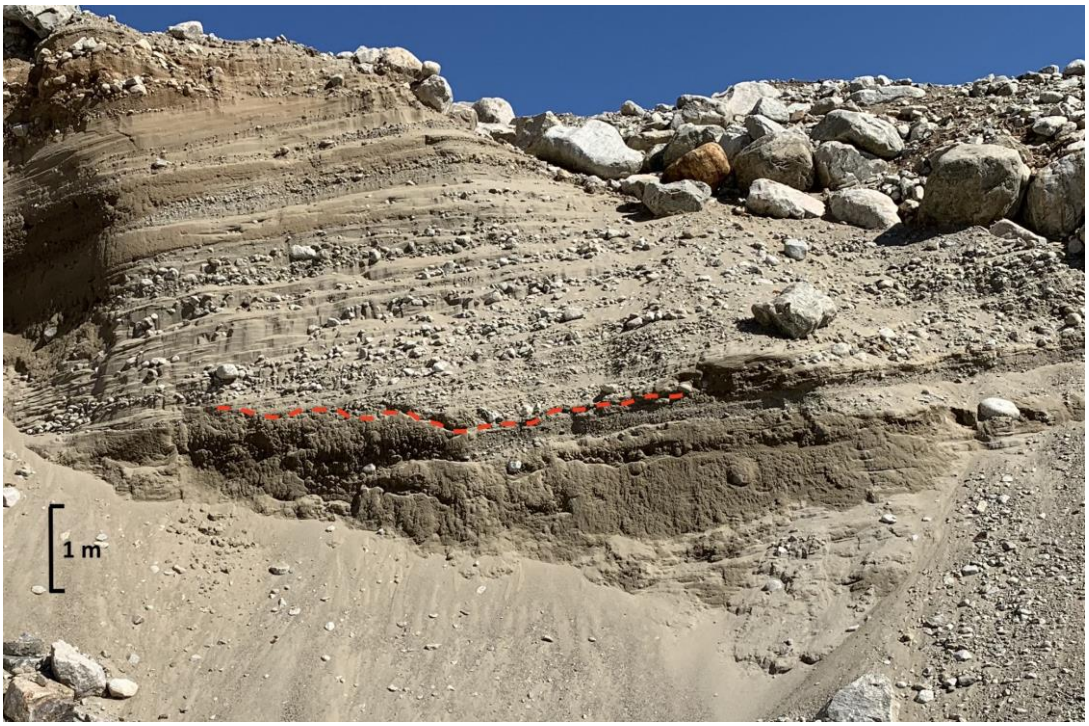

Figure 4.20. Side profile of facies F in section 2 showing down-valley dipping foresets. Red dashed line outlines the erosive contact with the underlying beds. *Photo: T. Tuestad*

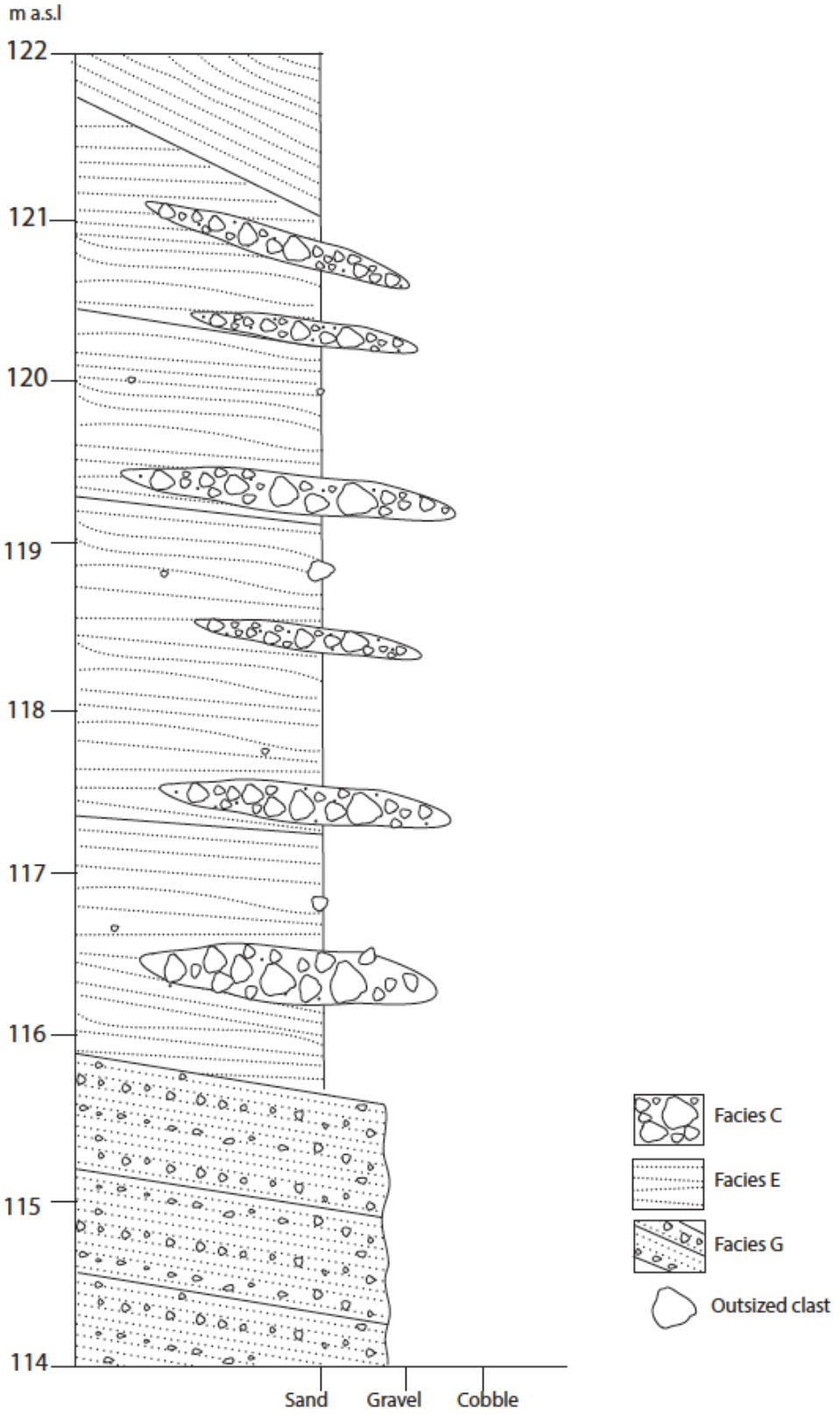

Figure 4.21. Sediment log for Section 2 at the Løland gravel pit. Section 2 is exposed at elevations from 114 m a.s.l. up to 122 m a.s.l. and exhibits three predominant observed facies.

Section 3

Section 3 shows about 3 meters of sediment at elevations around 117 to 121 m a.s.l (Figure 4.22, 4.23). The upper ~1 m of Section 3 is composed of moderately sorted, massive, clast-supported, angular to sub-rounded gravel (facies I). In section 3, it is difficult to distinguish the overlying in-situ facies I deposits from the cobbles and boulder draped over the top of the section. Nonetheless, remnants of facies I are well exposed at similar elevations elsewhere in the gravel pit where the surface of the terrace is still relatively intact (Figure 4.24). Facies I has an erosive, unconformable contact with the underlying beds.

In Section 3, facies I is underlain by subhorizontally stratified medium to coarse sand (facies E) around 120 m a.s.l. The sand beds of facies E are dipping (5-15 °) towards the southeast (~250°), and locally exhibit low-angle cross-stratification, climbing ripples, and some truncated strata. Isolated outsized clasts of gravel to cobble size also occur within the sand beds. A 4-m long, 0.5-m thick lenticular bed of unsorted, massive sandy gravel, cobbles and boulders (facies D) is found near the base of facies E with an erosive base contact.

At the base of Section 3 is a ~2 meter thick unit of stratified gravelly medium to coarse sand with dispersed cobbles (Facies G) with beds that are dipping (15-20°) towards the west-southwest (~250°) (Figure 4.22). There is a sharp, potentially erosive contact between Unit 2 and the underlying beds. It is difficult to determine the nature of contact between facies G and E since the contact between the two facies is largely obscured by slope debris.

Interpretation: The sedimentary facies observed in Section 3 are likely an upslope extension of those in Section 2. Dipping gravelly beds (facies G) are interpreted as gravelly foresets that are overlain by migrating antidune deposits (facies E), with a local scour infilled by a debris-flow diamicton (facies D). Facies I is interpreted as glaciofluvial gravel deposited near the surface of the 126 m Løland terrace, which implies a glaciofluvial origin of the terrace.

Figure 4.22. Photo of sediment section 3 at the Løland gravel pit. Lenticular bed of debris-flow deposits (red dashed line) found within the dipping beds of facies F, which is draped by a unit of facies E. Sharp contact of facies F with the bed below (black dashed line). *Photo: T. Tuestad*

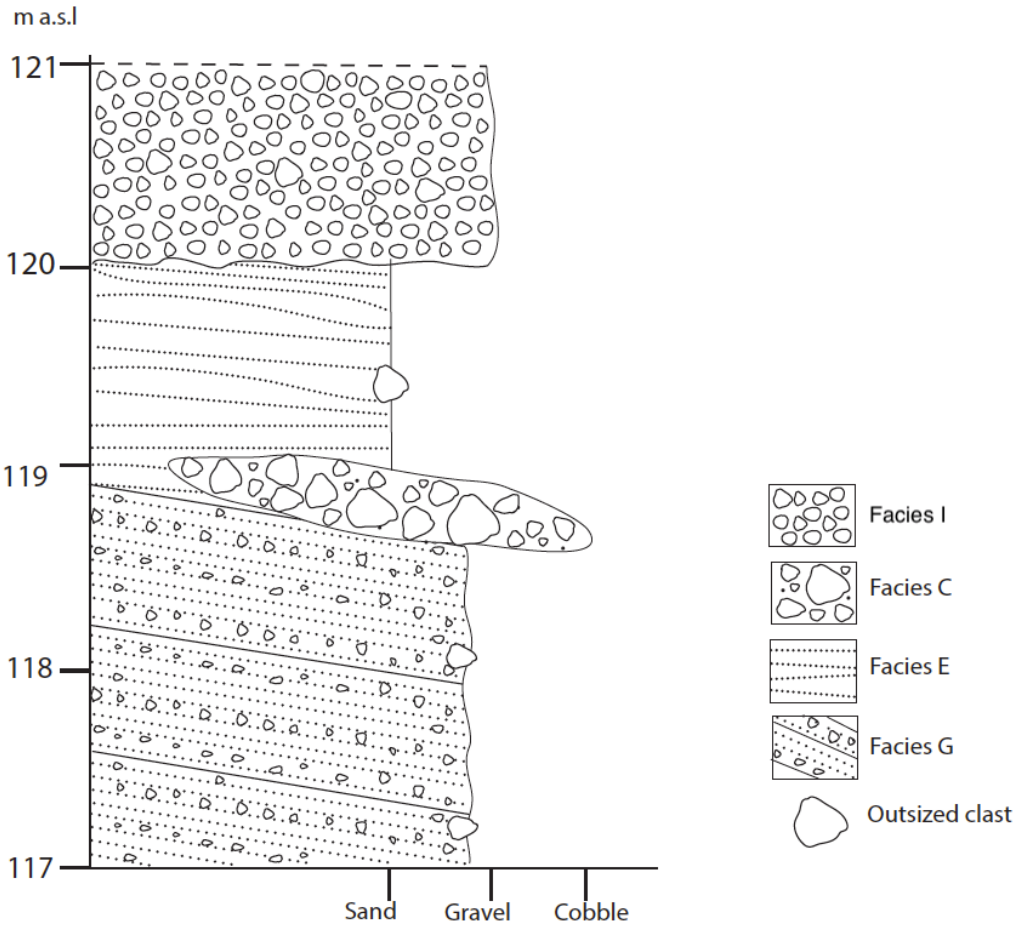

Figure 4.23. Sediment log for Section 3 at the Løland gravel pit. Section 3 is exposed at elevations from 117 m a.s.l. to 121 m a.s.l. and exhibits four predominant observed facies (C, E, G, I).

4.24. Exposures of glaciofluvial gravel bed (facies I) found at the surface of the ~126 m Løland terrace. Gravel bed has an erosive contact with the underlying older ice-contact deltaic strata (further described in text). *Photos: T. Tuestad.*

Table 4.3. Summary of facies observed in the Løland gravel pit, including facies descriptions, interpretations, and the sections where each facies are observed.

Facies	Description	Interpretation	Sections
A	Stratified fine-medium sand beds interbedded with silt and clay. Some beds of massive coarse sand up to several cm thick are present and may pinch out laterally. Isolated gravel to cobble-size, angular to sub-rounded clasts are dispersed throughout the finer sediment and distort the underlying beds.	Deposition by turbiditic suspension on a distal deltaic slope (Lønne, 1993). Dropstones deposited by ice-rafting (Thomas and Connell, 1985).	1
B	Sigmoidally laminated fine to medium sand interbedded with coarse sand. Outsized clasts gravel to cobble-size common and distort underlying beds.	Humpback dune deposits (Lang et al., 2017)	1, 2, 3
C	Massive matrix-supported sand, gravel and cobbles. Matrix is composed of fine to medium sand.	Non-cohesive debris flows (Winsemann et al., 2009)	1
D	Diamicton. Massive, matrix-supported, poorly sorted sand, gravel and cobbles with a fine-grained matrix.	Cohesive debris flows from ablation or flow till (McCabe and Eyles, 1988; Winsemann et al., 2009)	1, 2, 3
E	Horizontal to sub horizontal stratified sand with dispersed gravels and cobbles. Some low-angle cross-stratification, internally truncations, and scour and fill features occur.	Migrating antidune deposits (Lang et al., 2017) with chute fill deposits in the mid-deltaic slope (Lønne, 1993).	1, 2, 3
F	Sinusoidally stratified gravelly medium to coarse sand.	Aggregating antidunes (Lang et al., 2017)	1, 2, 3
G	Stratified medium to coarse sand beds with occasional gravely beds. Gravel-size clasts may show inverse grading within the stratified sand beds. High-angle beds are dipping ~15-20° towards WSW (~250°). Erosive contact with underlying bed.	Gravelly foresets prograding over a preformed scoured base (Lang et al., 2017), or deposition by high-velocity turbulent flows in preformed scours (Winsemann et al., 2009).	2, 3
H	Lenticular beds of unsorted, angular to sub-rounded, massive coarse sand, gravel and pebbles. Lenses disturb underlying beds.	Ice-rafted debris (Thomas and Connell, 1985).	1
I	Moderately sorted, massive, clast-supported, gravel. Clasts can range from angular to sub-rounded, but most are angular to sub-angular. Largest clasts can range up to cobble-size. Matrix is predominantly composed of medium to coarse sand.	Glaciofluvial gravel sheet deposits (Miall, 1977)	3

4.4.3 Depositional environments of gravel pit sediments

The majority of the sediment sections at the Løland gravel pit exhibit facies that are commonly associated with ice-contact deltaic environments (Løhne, 1993; Winsemann et al., 2009; Lang et al., 2017). Since the gravel pit is located significantly higher than the local marine limit (~34 m a.s.l.; Anundsen, 1985), the ice-contact delta had to have been deposited within a rather deep lake occupying the valley. Stratified sand deposited by turbuditic suspension with dropstones and ice-rafted debris likely represents a distal deltaic slope in a glaciolacustrine environment that was in contact with an ice-margin (Lønne, 1993). Infilled scours of debris-flow diamicton are also characteristic of an ice-contact delta (McCabe and Eyles, 1988). Since the deltaic sediments within the 126 m a.s.l. terrace are unconformably overlain by glaciofluvial gravels, the contact between the two probably represents a hiatus within the sediment succession. Thus, the surface of the adjacent, 157 m a.s.l. terrace is interpreted to be the deltaic surface, composed of coarser sediment that could potentially be representative of the deltaic topsets (Figure 4.25), hough further investigation is necessary to confirm the presence of topsets. In sum, the Løland gravel pit sediments are believed to represent an ice-contact glaciolacustrine delta with a surface elevation of ~157 m.a.s.l., which was subsequently incised by glaciofluvial processes that formed the 125 m a.s.l glaciofluvial terrace with younger glaciofluvial gravel deposits overlying the older deltaic sediments (Figure 4.25).

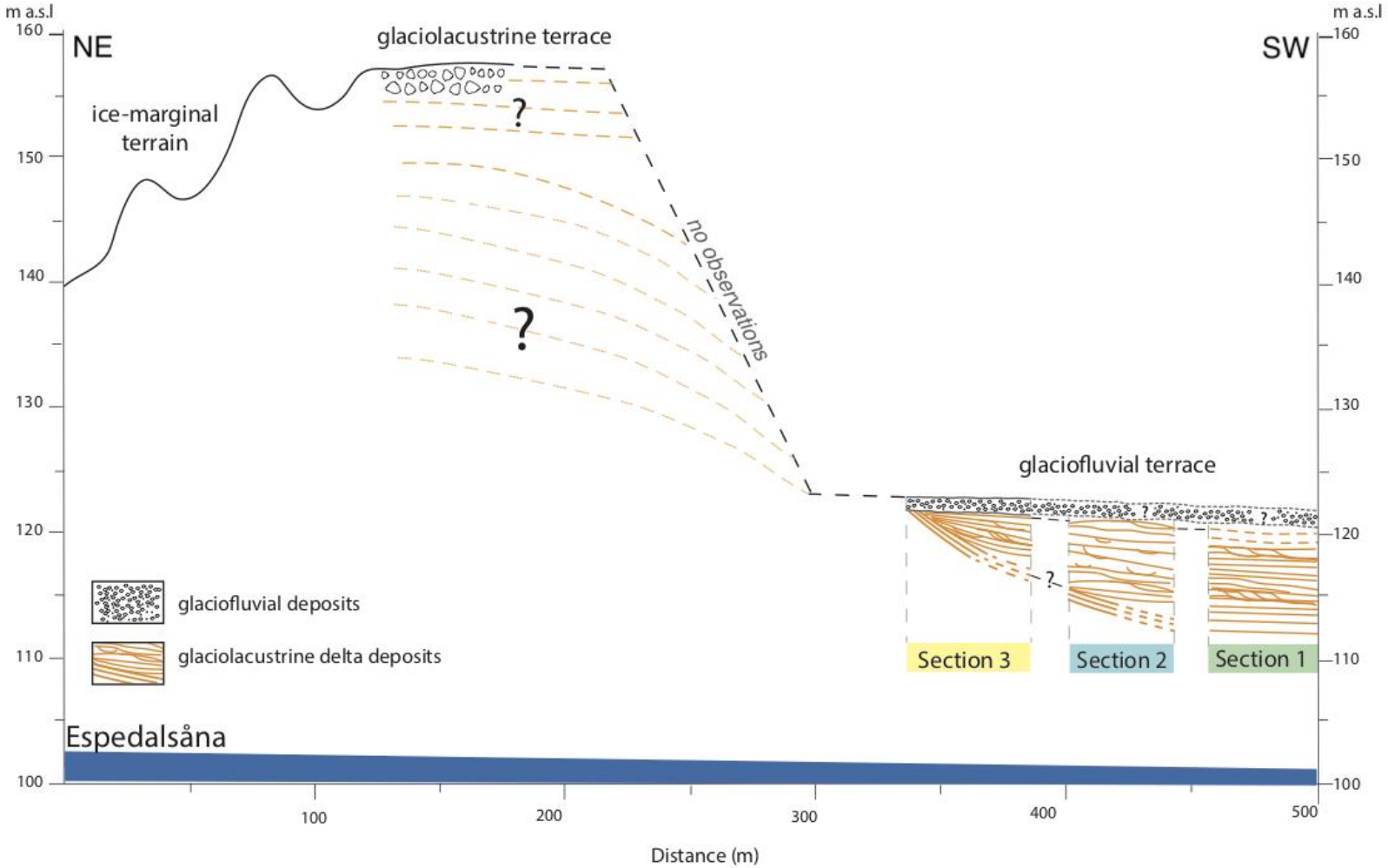

Figure 4.25. A cross-section overview of the observed gravel pit sections in relation to the terrace surfaces and the ice-proximal terrain, as well as the modern river Espedalsåna.

4.5 Terraces in Espedalen

Numerous terraces are observed along the northern and southern slopes in Espedalen (Figure 4.27, 4.28). The terraces have been plotted along a longitudinal cross-section of Espedalen, showing the distribution, gradient and elevation of the highest terraces (Figure 4.27). The 157 m a.s.l terrace at Løland is the highest elevation terrace in Nedre Espedalen and has a relatively flat surface, while the lower Løland terrace (~126 m a.s.l) has a relatively steeper surface gradient that follows the slope of the modern-day river Espedalsåna. Based on the gravel pit sediment sections and terrace morphology, the 126 m terrace is interpreted as a glaciofluvial terrace that incised into the older 157 m glaciolacustrine terrace.

Additionally, a series of terraces are found down-valley from Løland that are interpreted as fluvial/glaciofluvial given their down-valley sloping surfaces and relatively continuous gradation (Figure 4.27). Some of these terraces exhibit remnants of ancient channels on their surface, and so they are interpreted glaciofluvial terraces (Figure 4.26; Eilertsen et al., 2015). Since further field observations are necessary to categorize the majority of these terraces as fluvial or glaciofluvial, they will collectively be referred to as fluvial/glaciofluvial, aside from the few that have been observationally confirmed as glaciofluvial.

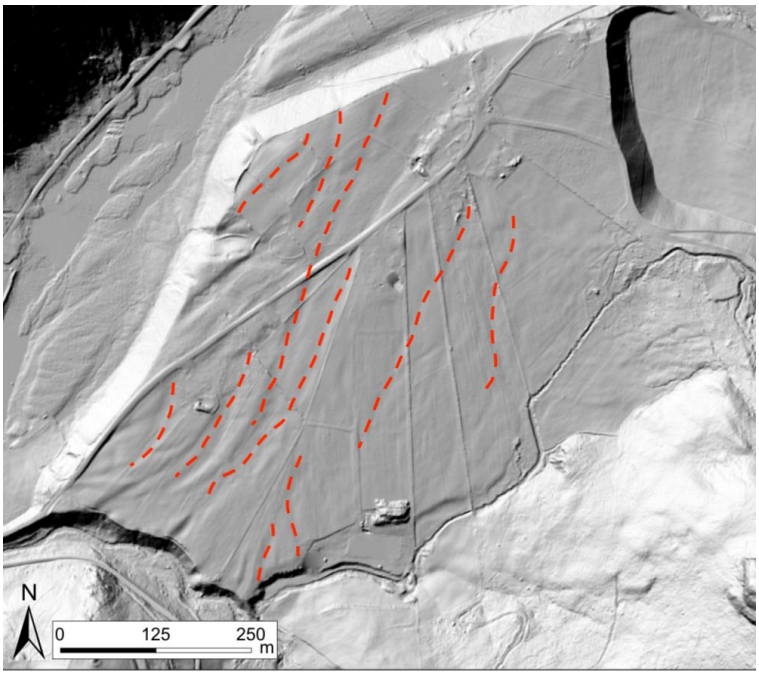

Figure 4.26. LiDAR hillshade of a glaciofluvial terraces with relict channels on the terrace surface (red dashed lines). A corresponding cross-section of the terrace is shown in Figure 4.28c.

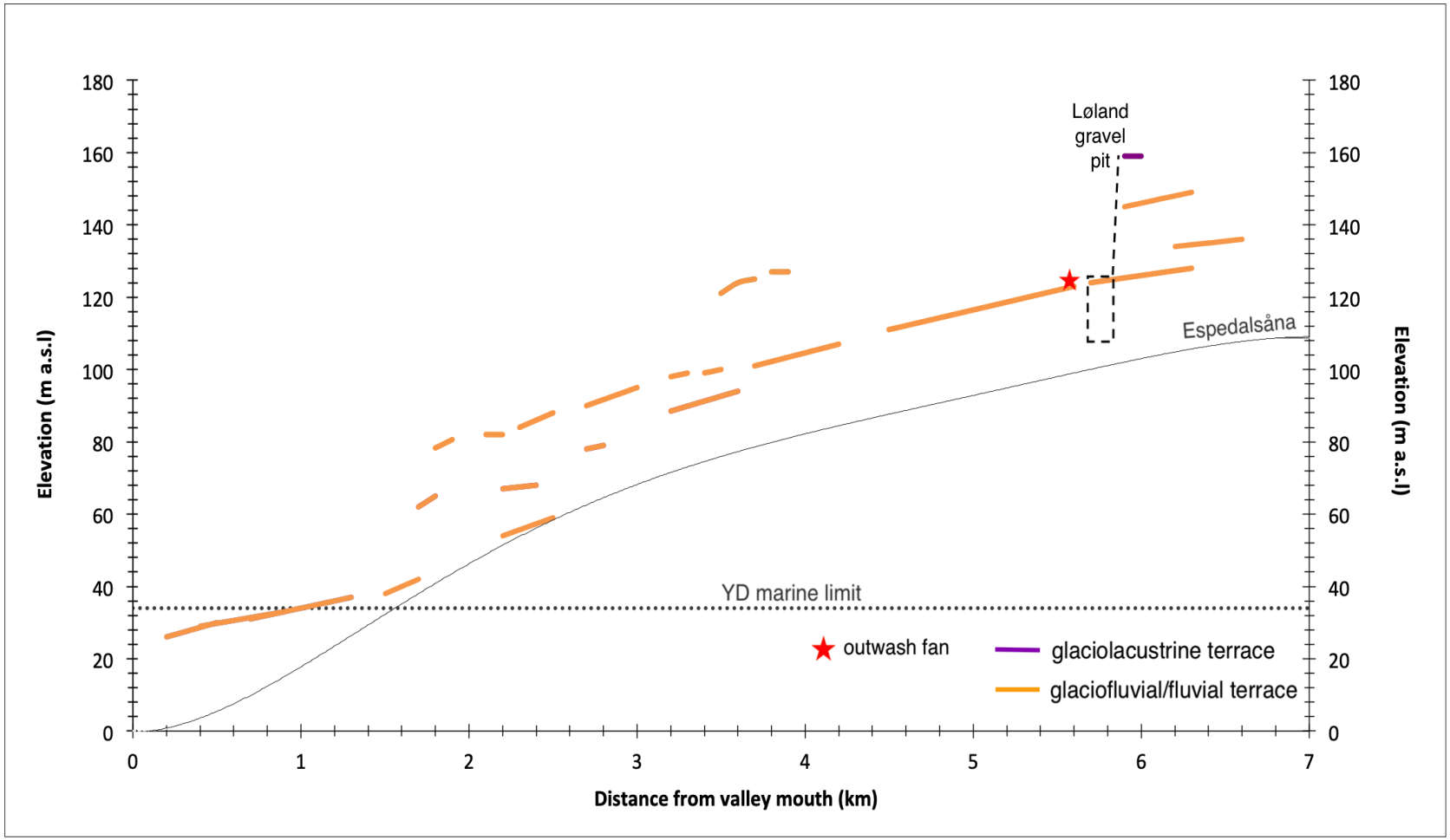

Figure 4.27. Terraces in Espedalen plotted along the long-valley axis based on elevation and distance from the valley mouth. The modern river, Espedalsåna that flows along the base of the valley. The location and depth of the Løland gravel pit is shown in relation the other terraces in the valley. The outwash fan deposited on the glaciofluvial terrace at ~120 m a.s.l. is denoted by a red star.

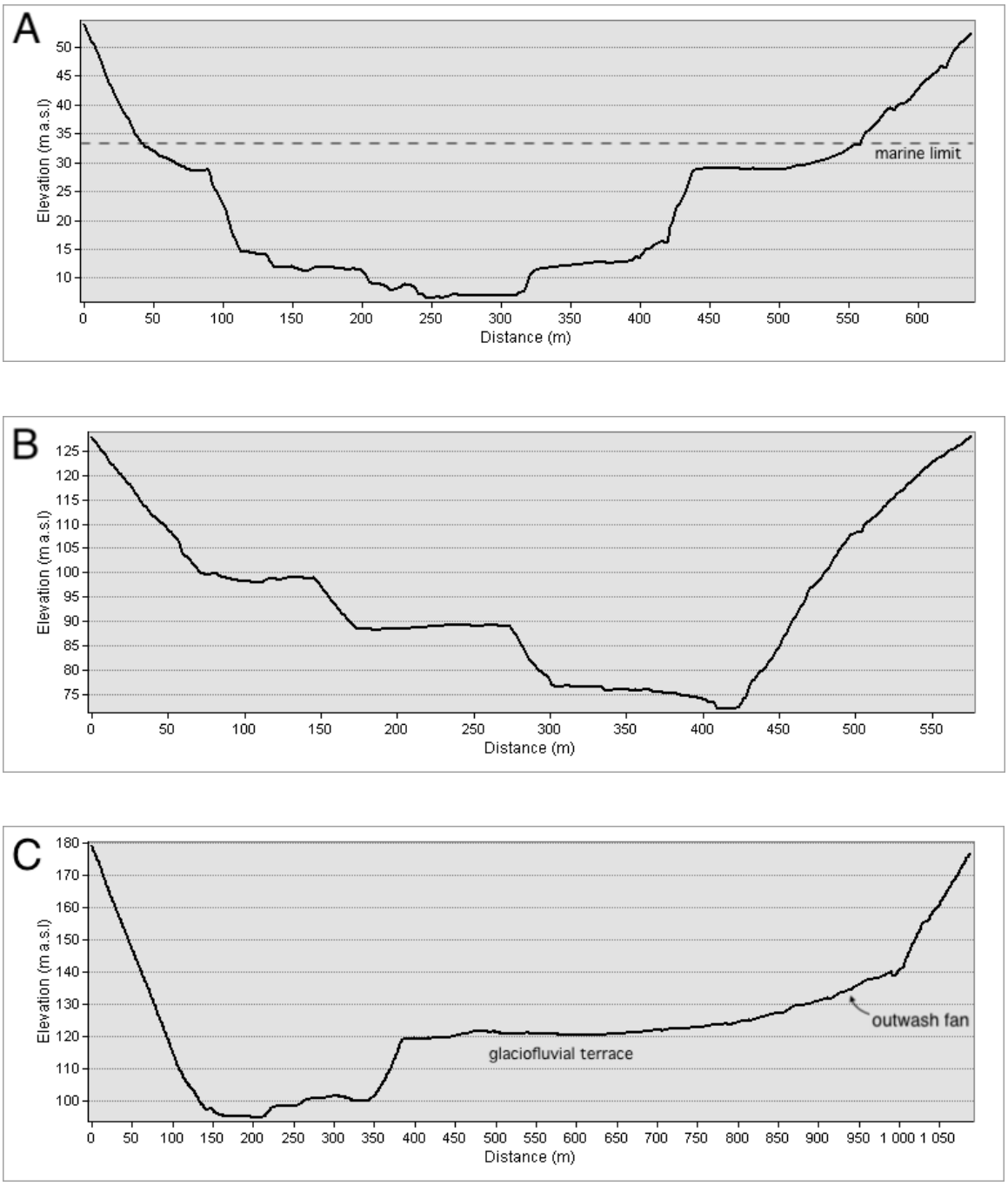

Figure 4.28. Espedalen cross-valley elevation profiles of fluvial/glaciofluvial terraces near the valley mouth (A), mid-valley (B), and inner valley (C). Locations of transects for each profile are outlined in Figure 4.13. The highest terraces in profile (A) grades to and just below the Younger Dryas marine limit. LiDAR and field photos of the glaciofluvial terrace and outwash fan in (C) are shown in Figure 4.30.

The fluvial/glaciofluvial terraces seem to belong to several generations, which form a relatively continuous gradation down the valley before leveling off and abruptly terminating at particular elevations (Figure 4.27). For example, one set terminates about 1.8 km from the valley-mouth at an elevation of around 80 m a.s.l. A subsequent generation levels off and terminates about 1.6 km from the valley mouth at an elevation of about 60 m a.s.l. after which there is an abrupt drop in terrace elevations. The lowest set of high-lying terraces appears ~1.4 km from the valley mouth at an elevation of ~40 m a.s.l, which then grades down to and just below the marine limit (~34 m a.s.l) that formed during the Younger Dryas transgression (Anundsen, 1985; Lohne et al., 2007). These latter terraces are around 20 meters lower in elevation than the previous set of terraces that terminate at about 60 m a.s.l. (Figure 4.27). Hence, it seems clear that the river that formed the higher terraces (> 60 m a.s.l.) was not grading towards a contemporaneous sea level as the lower terraces (~40 m a.s.l.).

4.6 Other LiDAR observations in Espedalen

4.6.1 Lateral moraine in Øvre Espedal

A ~10-15 m high ridge is located along the northern slope of Øvre Espedalen with an orientation parallel to the long axis of the valley (Figure 4.29). It is has an elevation of ~230 m a.s.l. at its highest point and an elevation of ~180 m a.s.l. at its lowest. The ridge's long-axis is dipping down valley with a gradient of ~100 m/km and can be traced laterally for about 320 meters. It is composed of mainly poorly sorted, massive, angular to sub-rounded gravels, cobble and boulders with a fine-grained matrix. The ridge is draped with large highly angular cobbles and large boulders, assumed to be rock fall debris from the adjacent slope.

Interpretation: The morphology of the ridge is very similar to other marginal moraine ridges in the region, such as Esmark's moraine (Figure 1.3), and is therefore interpreted as a lateral moraine. The relatively low elevation of the moraine within the valley signifies a very proximal ice front, and since the moraine curves in towards Espedalsvatnet, the corresponding ice front was probably located within the northeastern part of the lake. The moraine corresponds to an ice margin included in the "Glacial Map of Norway" by Holtedahl and Andersen (1960). It is found distal to the Younger Dryas ice margin mapped by Andersen (1954), which is located further up valley from Øvre Espedalen. If the YD margin is correct, this lateral moraine was deposited by an older glacial lobe that extended to the northeastern edge of Espedalsvatnet. Moreover, one would expect to find corresponding ice-marginal features on the opposite slope given the rather large size of the moraine on the northern slope in Øvre Espedalen. However, such moraines are not evidently visible on the southern slope of the valley, potentially due to a steeper slope.

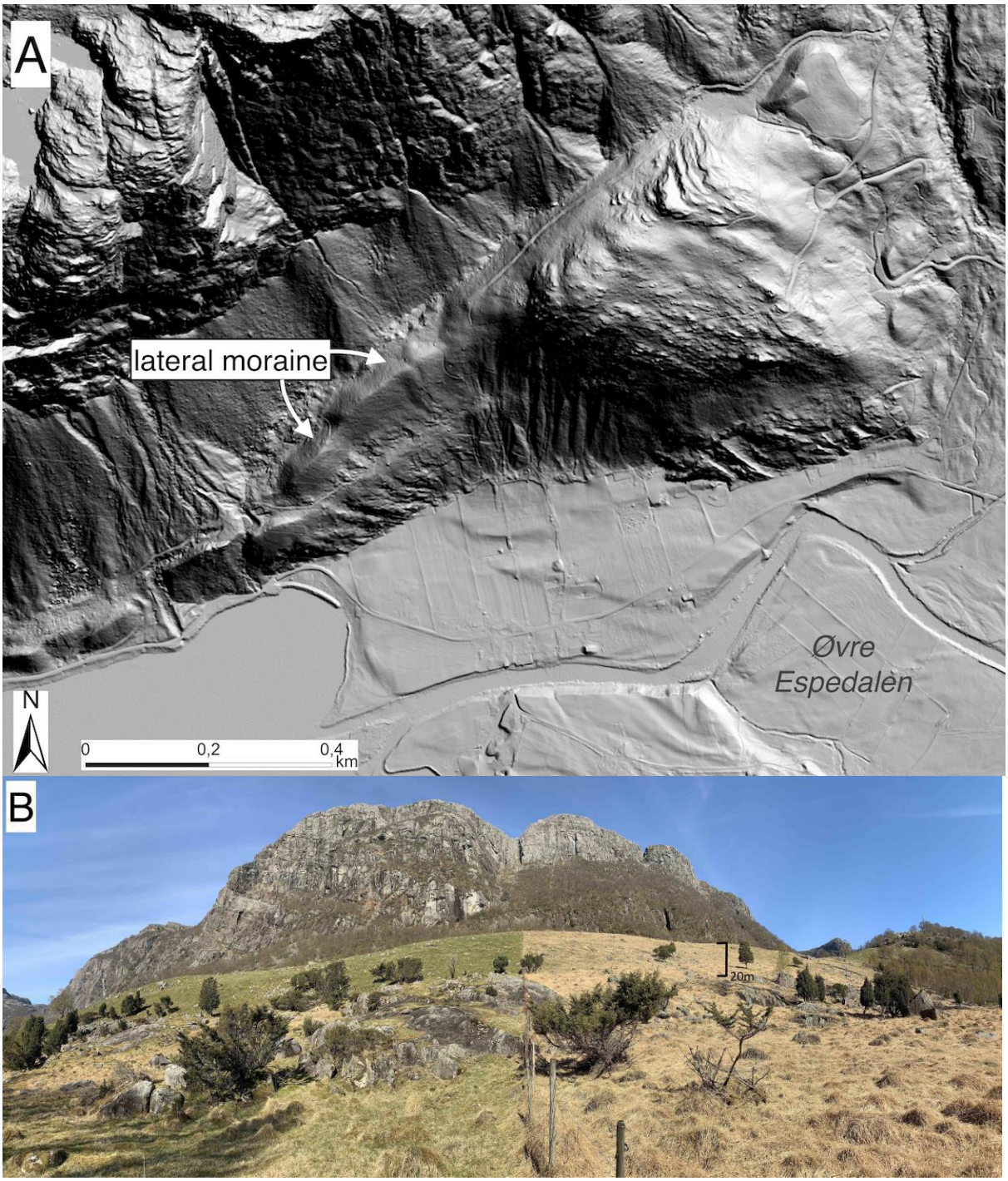

Figure 4.29. (A) Lateral moraine along the northern slope in Øvre Espedalen shown on a LiDAR hillshade. Location is shown in Figure 4.23. (B) Panoramic photo of the lateral moraine in Øvre Espedalen. Bedrock exposures are found along the base of the ridge. Ridge is about 15-20 meters high, and photo covers about 430 meters in length. *Photo: T. Tuestad*

4.6.2 Outwash Fan in Nedre Espedal

A distinct, fan-shaped landform is observed on LiDAR on top of a glaciofluvial terrace in Nedre Espedalen (Figure 4.30a, b). The underlying terrace has a surface elevation of ~120 m a.s.l. and exhibits relict channels (Figure 4.26), hence is characterized as glaciofluvial. The surface of the fan is up to 15 meters higher than the underlying terrace surface, covering an area of around 42,200 m^2. Numerous partially buried boulders are present throughout the surface of the fan. Some boulders are quite large and can be up to several meters wide (Figure 4.30b). The fan is located at the base of a canyon along the southern slope of Nedre Espedalen that acts as an outlet for the higher-elevation lake Brekkevatnet (Figure 4.30a, b). A small modern tributary streams run along the canyon and across the fan at its base, eventually joining with Espedalsåna further down-valley. A cross-section of the Brekkevatnet outlet shows that it has been incised down from about 522 m a.s.l. to 516 m a.s.l. (Figure 4.30c).

Interpretation: The fan has clear indications of subaerial channels on its surface, and is therefore interpreted as an outwash fan. The significant thickness and area covered by the fan, as well as the sizably large boulders buried within the deposits indicate that it was formed by rather substantial discharge of water flowing out of the Brekkevatnet outlet. Given the relatively small dimensions of the modern-day stream that runs along the canyon, it is probably not capable of forming a feature as extensive as the outwash fan with such large boulders. Moreover, given the elevation of the underlying glaciofluvial terrace surface (~120 m a.s.l; Figure 4.25), this terrace, as well as the overlying fan, is younger than the oldest lake phase in Espedalen (157 m a.s.l; see Section 4.4.3).

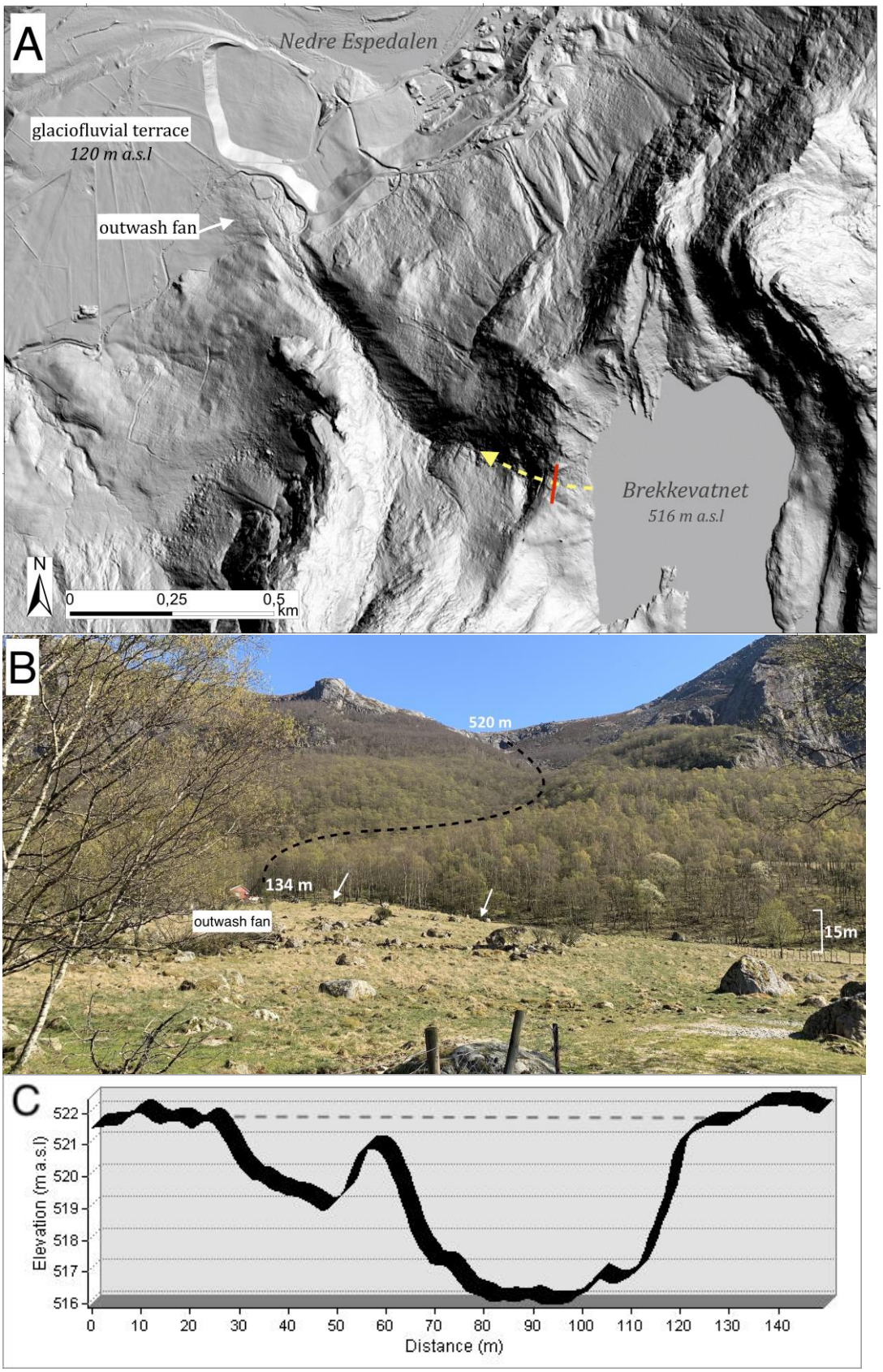

Figure 4.30. (A) LiDAR hillshade of outwash fan deposited on a glaciofluvial terrace in Nedre Espedalen, formed at the base of the outlet from Brekkevatnet. Lake outlet is outlined by the yellow arrow. (B) Field photo of an outwash fan in Nedre Espedalen. Black dashed line represents the canyon cut by the flow of the Brekkevatnet outlet. *Photo: T. Tuestad.* (C) Cross-section of Brekkevatnet's outlet showing the outlet has been eroded down into bedrock from around 521 m a.s.l. Location of transect is shown by red line in (A).

4.6.3 Ancient lake shorelines Lauvvatnet region

A complex of five modern lakes is located in the mountainous region between Espedalen and Frafjorden (Figure 4.32). These lakes are found at elevations ranging from 480 to 516 m a.s.l, with decreasing elevations moving from west to east. Of the five modern lakes, Stølsvatnet has the lowest elevation (480 m a.s.l), and has an outlet that flows south through Norddalen into inner Frafjorden (Figure 4.32). Brekkevatnet (516 m a.s.l) has the highest elevation and has an outlet that drains northwest into Nedre Espedal with the previously described outwash fan deposited its base.

LiDAR mapping of the region around the five lakes revealed a series of well-preserved terrace-like features along the lake margins (Figure 4.31). These terraces have flat surfaces, with elevations ranging from 520 m a.s.l up to 524 m a.s.l rising slightly towards the east. Terraces have widths ranging 10 and 35 meters. The longest terraces can be traced laterally up to 750 meters, while shortest can only be traced to about 35 meters. Finally, the terraces are located 4 meters above modern-day Brekkevatnet (516 m a.s.l) up to 46 meters above modern day Stølsvatnet (480 m a.s.l.) (Figure 4.32).

Interpretation: Based on their relatively flat surfaces and their distribution following the lake margins, the terraces are interpreted as former lake shorelines. The elevation difference between the modern-day lakes and older shorelines indicates that the water levels of the five lakes were once 4 to 46 meters higher. The fact that the former shorelines are distributed around all five lakes and are at similar elevations, with a slight difference accounting for the difference in terrain relief, indicates that the 5 modern-day lakes were likely connected, forming one large lake with a 522 ± 2 m a.s.l shoreline. Moreover, the ancient shoreline elevations are significantly higher (>40 meters) than the primary outlet out of Stølsvatnet (480 m a.s.l) that drains into the inner part of Frafjorden (Figure 4.31). Hence the Stølsvatnet outlet would have had to be dammed for the formation of a lake level over 40 meters higher than the outlet, which is most easily by the presence of an ice lobe in Frafjorden damming the lake outlet. Therefore, these higher shorelines are believed to belong to an ancient ice-dammed lake that was formed over this area during the deglaciation.

A cross-section of the secondary Brekkevatnet outlet (516 m a.s.l) shows that the bedrock was initially down-cut from about 522 m a.s.l (Figure 4.30c), which is an elevation that closely corresponds to those of the ice-dammed lake shorelines (Figure 4.32). Thus, this outlet may have been likely formed contemporaneously to the higher ice-dammed lake shorelines when the primary Stølsvatnet outlet was theoretically dammed by ice.

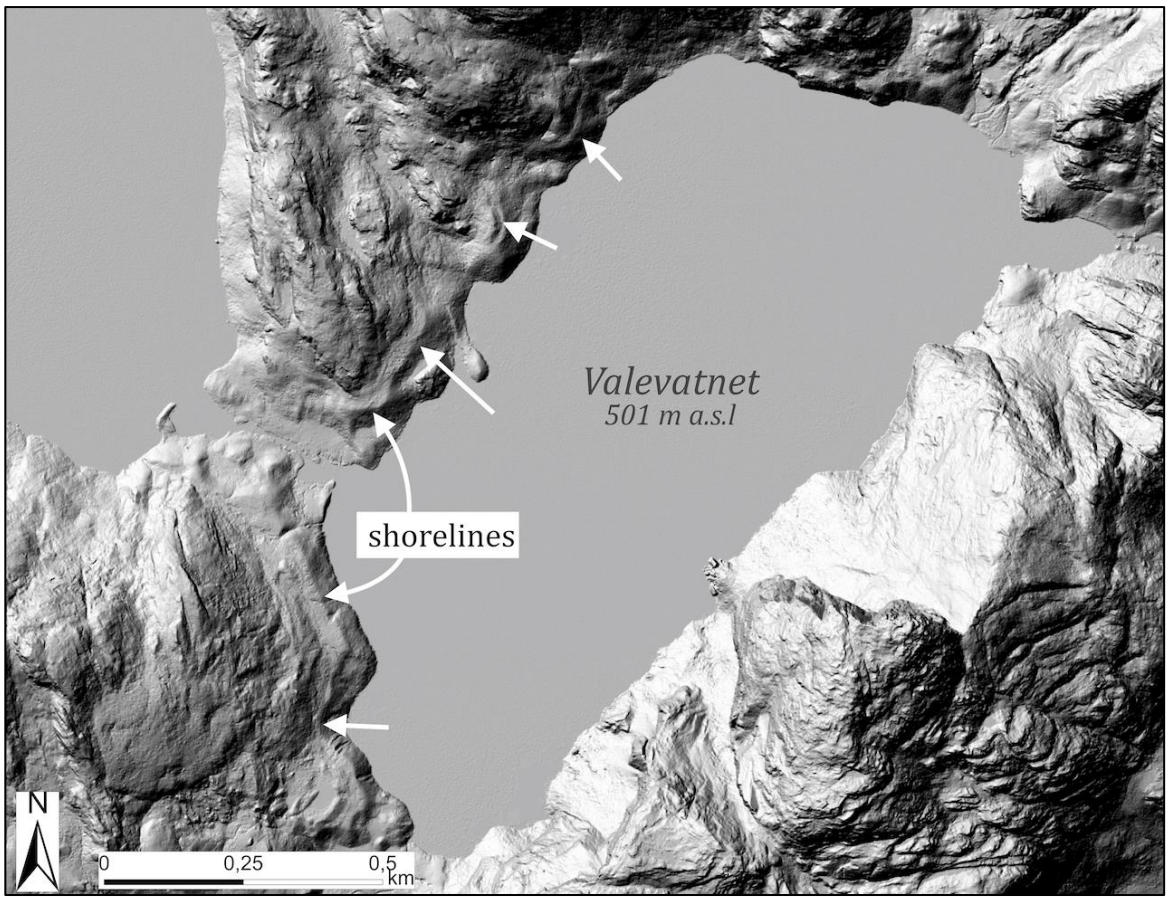

Figure 4.31. Ancient shorelines (arrows) around Valevatnet with an elevation of ~521 m a.s.l, which is ~20 meters higher than the present day lake level. Location is shown in Figure 4.13.

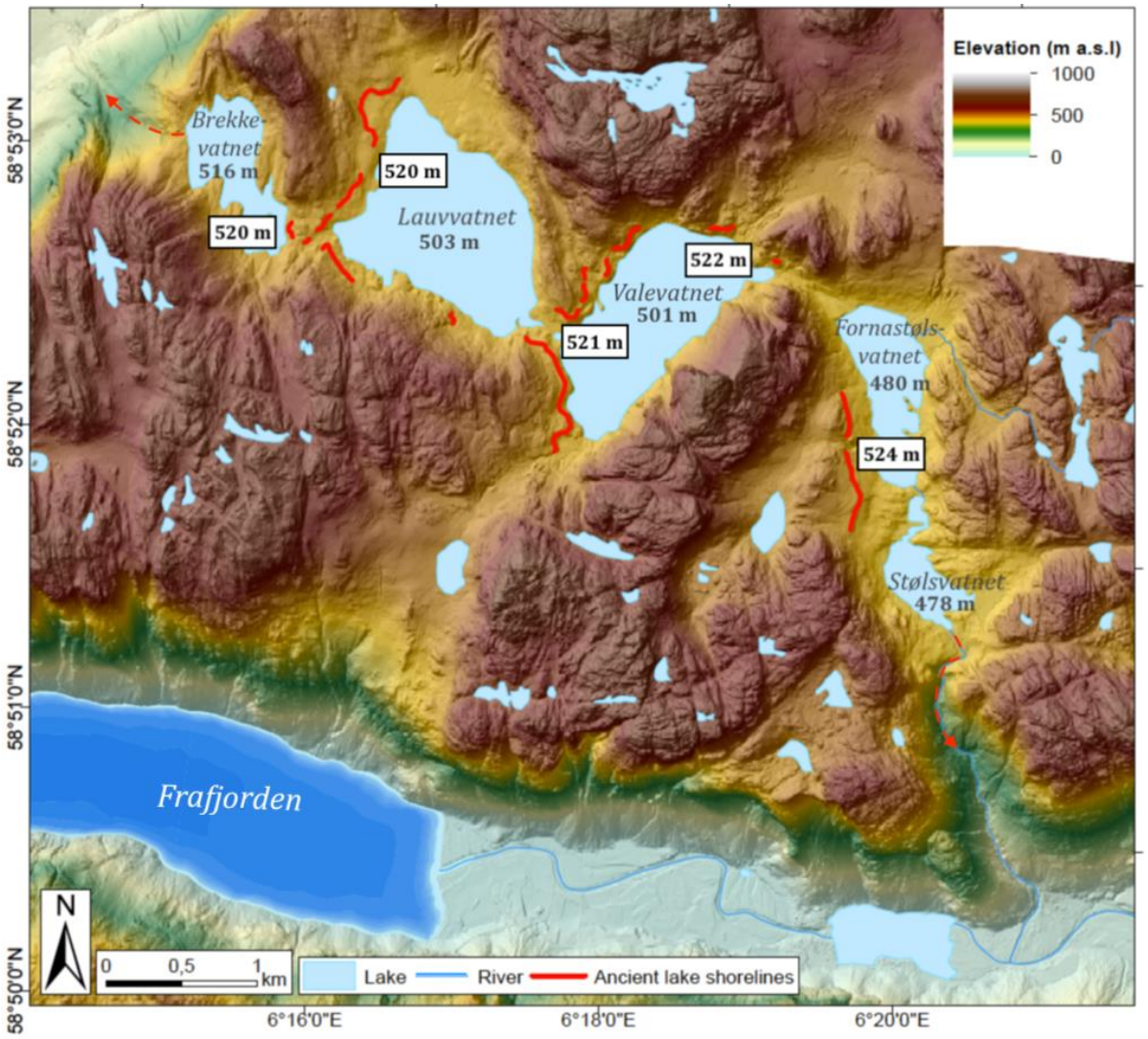

Figure 4.32. Hillshaded map of the lakes southeast of Espedalen, showing mapped ancient lake shorelines. Elevations of the higher shorelines are shown in the white boxes, which increase in elevation towards the east from 520 to 524 m a.s.l. There are two lake outlets (red dashed arrows): the primary outlet flows south out of Stølsvatnet (480m a.s.l) into inner Frafjorden, the secondary outlet flows out of Brekkevatnet (516 m a.s.l) into Nedre Espedalen.

4.7. ^{10}Be surface exposure dating results

4.7.1 Site and sample description

Bergfjellet

Three boulders resting on bedrock were sampled near the summit of Bergfjellet, B-1, B-2, and B-3. The sampled boulder B-1 measures about 110 x 120 x 100 cm, and is located at 614 m a.s.l. B-2 and B-3 were sampled from relatively smaller boulders (104 x 70 x 80 cm and 60 x 90 x 100 cm, respectively) in close proximity (~3 meters) to one another (Figure 4.33). B-2 has an elevation of 620 m a.s.l. and B-3 has an elevation of 619 m a.s.l. All boulders on Bergfjellet have moderate lichen coverage, have a low to moderate degree of weathering, and experience very low, virtually negligible topographic shielding. Aside from the three sampled boulders, there are relatively few erratic boulders found around the summit of Bergfjellet.

Husafjellet

In contrast to Bergfjellet, Husafjellet has numerous erratic boulders at its summit. Four boulders sitting on bedrock were sampled on Husafjellet (H-1, H-2, H-3 and H-4). H-1 is a large boulder perched along the margins of the summit at 472 m a.s.l with dimension of 130 x 150 x 230 cm (Figure 4.33). The upper surface of H-1 has large extent of lichen coverage and exhibits a moderately weathered surface. H-2 and H-3 were both sampled from boulders from the highest elevations on Husafjellet. H-2 (468 m a.s.l) has dimensions of 115 x 150 x 150 cm with a moderately weathered surface and limited to moderate lichen coverage. H-3 (470 m a.s.l.) has dimensions of 105 x 163 x 100 cm with a rough, relatively high degree of weathering compared to H-1 and H-2, as well as extensive lichen coverage. H-4 (463 m a.s.l.) was sampled from a boulder resting along the southwestern margin of the Husafjellet summit with dimensions of 120 x 190 x 124 cm. The surface of H-4 has extensive lichen coverage, as well as a moderate to fairly high degree of weathering.

Figure 4.33. Erratic boulders sampled for surface exposure dating. B-1 to B-3 are at the summit of Bergfjellet. H-1 to H-4 are at the summit of Husafjellet. Person for scale has a height of 185 cm. Site locations are shown in Figure 1.2.

4.7.2 ^{10}Be exposure age results

The resulting ^{10}Be ages from Bergfjellet and Husafjellet are distributed over a large range from 18.56 ± 0.67 to 12.73 ± 0.67 ka (Table 4.4, 4.5; Figure 4.34). From Bergfjellet, B-1, B-2 and B-3 yielded an ages of 15.36 ± 1.94 ka, 17.50 ± 0.80 ka and 18.56 ± 0.67 ka respectively, with an average of 18.00 ± 0.77 ka. The AMS analysis of B-1 ran with a very low ^{9}Be current, hence resulting in a large uncertainty of the ^{10}Be/^{9}Be ratio (Table 4.4). B-1 is therefore excluded from the average age calculation. From Husafjellet, H-1, H-2, H-3 and H-4 yielded ages of 16.64 ± 0.58 ka, 15.20 ± 0.55 ka, 12.73 ± 0.67 ka and 14.39 ±0.58 ka respectively, with an average of 14.74 ± 1.63 ka. Samples H-2 and H-3 had a high native ^{9}Be content, therefore additional ICP measurements were made to constrain the results.

Table 4.4. ^{10}Be surface sample field data, lab data, and AMS results from Bergfjellet (B-1 to B-3) and Husafjellet (H-1 to H-4).

	Field data							Lab data			AMS results	
Sample ID	**Lithology**	**Elevation (m a.s.l)**	**Latitude (degrees)**	**Longitude (degrees)**	**Shielding factor**	**Sample thickness (cm)**	**Sample weight (g)**	**Be carrier added (g)**	**Be spike (µg)**	**Uncertainty**	**^{10}Be / ^{9}Be (x 10^{-12})**	**Uncertainty (x 10^{-12})**
B-1	Gneiss	614	58.912902	6.123106	0.9968	1.5	24.59041	0.78947	254.35	2.01	0.1798	0.0225
B-2	Gneiss	620	58.912898	6.122902	0.9989	1.5	24.71241	0.78880	254.14	2.01	0.2072	0.0093
B-3	Gneiss	619	58.912899	6.123004	0.9989	1.5	24.29181	0.78885	254.15	2.01	0.2161	0.0075
H-1	Gneiss	472	58.872298	6.150706	0.9997	1.0	24.83955	0.78837	254.00	2.01	0.1743	0.0059
H-2	Granite	468	58.872808	6.149345	1.0000	1.5	20.87725	0.78903	254.21	2.01	0.1309	0.0046
H-3	Granite	470	58.872899	6.149406	1.0000	1.0	20.93446	0.78918	254.26	2.01	0.1101	0.0056
H-4	Gneiss	463	58.871698	6.149802	0.9986	1.0	24.66146	0.78930	254.30	2.01	0.1482	0.0058

Table 4.5. ^{10}Be sample data and calculated ages from Bergfjellet and Husafjellet. Preliminary ages from Uburen (J.I. Svendsen, pers. comm. 2019) are also shown for comparison.

Sample ID	Elevation (m a.s.l.)	Lat (°N)	Long (°E)	Top. shield. factor	^{10}Be concentration	^{10}Be age (ka)*	^{10}Be age (ka) (Scandinavian)**
B-1	614	58.912902	6.123106	0.9968	123672 ± 15593	15.36 ± 1.94	15.96 ± 2.00
B-2	620	58.912898	6.122902	0.9989	141747 ± 6486	17.50 ± 0.80	18.15 ± 0.83
B-3	619	58.912899	6.123004	0.9989	150417 ± 5370	18.56 ± 0.67	19.28 ± 0.69
					Average	**18.00 ± 0.77**	**18.72 ± 0.80**
H-1	472	58.872298	6.150706	0.9997	118508 4131	16.64 ± 0.58	17.29 ± 0.61
H-2	468	58.872808	6.149345	1	105733 ± 3817	15.20 ± 0.55	15.79 ± 0.57
H-3	470	58.872899	6.149406	1	88631 ± 4643	12.73 ± 0.67	13.23 ± 0.70
H-4	463	58.871698	6.149802	0.9986	101593 ± 4101	14.39 ± 0.58	14.95 ± 0.61
					Average	**15.40 ± 1.12**	**15.93 ± 1.22**

Uburen, Forsand (J.I. Svendsen, pers. comm. 2019)

Sample ID	Elevation (m a.s.l.)	Lat (°N)	Long (°E)	Top. shield. factor	^{10}Be age (ka)*
F-26	435	58.88571	6.12279	1	15.34 ± 0.29
F-27	440	58.88591	6.12222	1	14.60 ± 0.30
F-28	433	58.88617	6.12072	1	15.48 ± 0.30
F-29	429	58.88545	6.12067	1	28.31 ± 0.54
F-30	428	58.88545	6.12067	1	15.78 ± 0.30
				Average	**15.30 ± 0.53**

* Western Norway production rate (Goehring et al., 2012a, b).
**Scandinavian production rate (Stroeven et al., 2015)

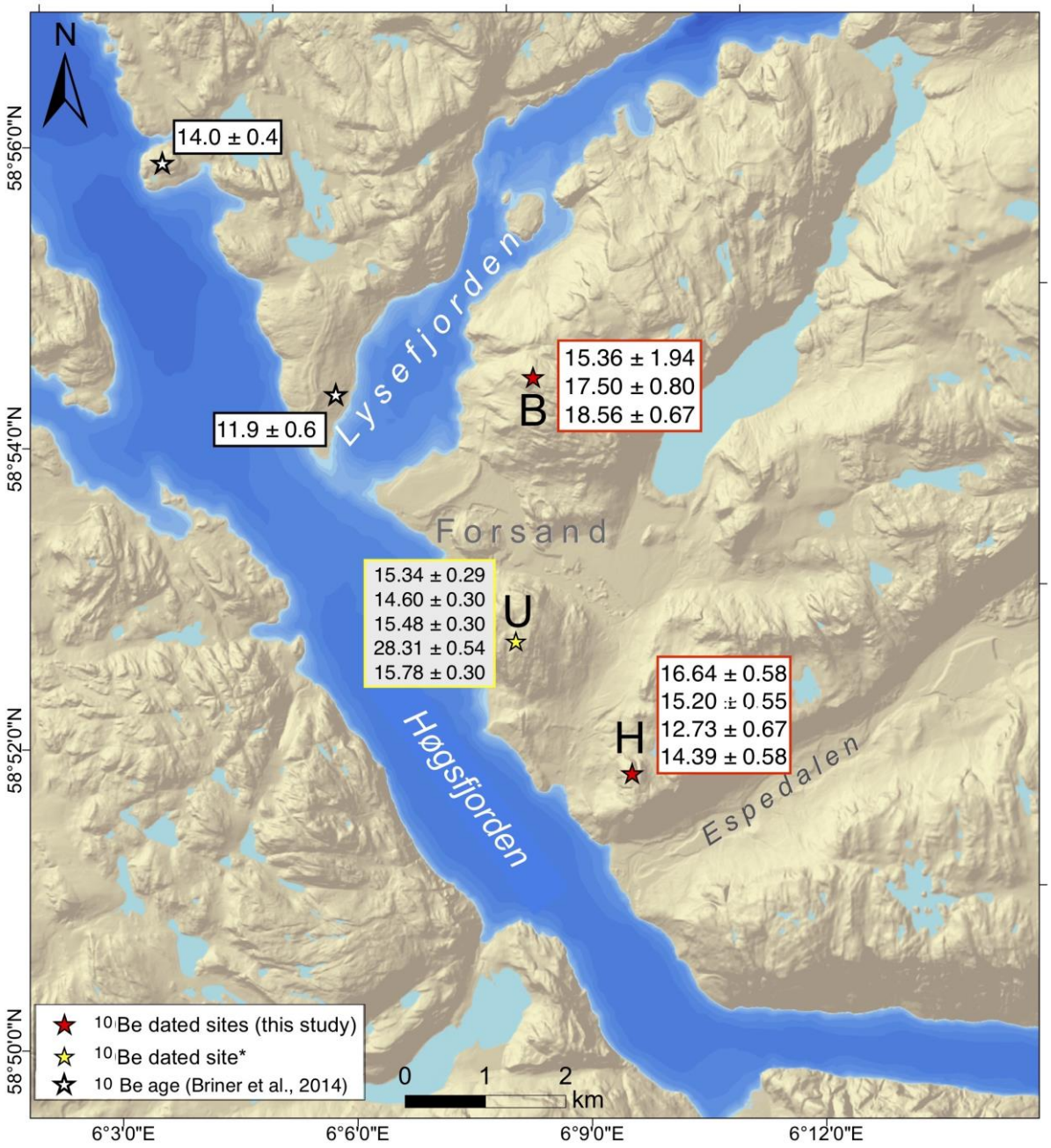

Figure 4.34. ^{10}Be ages from the Forsand-Lysefjord region. Ages yielded by this study are displayed in conjunction with other existing ages from the area (Briner et al., 2014; J.I Svendsen, pers. comm. 2019). U, Uburen; B, Bergfjellet; H, Husafjellet. * J. I. Svendsen, pers. comm., 2019.

4.7.3 Exposure age distributions & camel plots

Camel plot diagrams represent the distribution of several age measurements with individual Gaussian uncertainties (Balco, 2011). Each measurement is plotted as a curve based on its mean and the AMS analytical uncertainty, which allows for the visual analysis of overlap between measurements by taking into account their uncertainties (Balco, 2011). A camel plot also displays a summary curve that represents the sum frequency distribution of individual collected measurements. A single peak in a summary curve suggests that there is a high likelihood that the individual age measurements are dating the same event, with some inaccuracy due to analytical uncertainties (Balco, 2011). On the other hand, multiple prominent or subtle peaks suggests that the individual age measurements don't effectively represent the same event, which can be visually evident as a lack of overlap in their individual curves (Balco, 2011). Several camel plots are presented here for a general analysis of the exposure age distributions. All camel plots were created using a MATLAB code provided by Balco (2001).

The exposure ages from Bergfjellet are displayed in two plots: one showing all the resulting ages (Figure 4.35a), and one showing the all ages excluding B-1 due to its imprecision (Figure 4.35b). With the exclusion of B-1, the Bergfjellet ages have a large degree of statistical overlap and their summed curve has a single distinct peak.

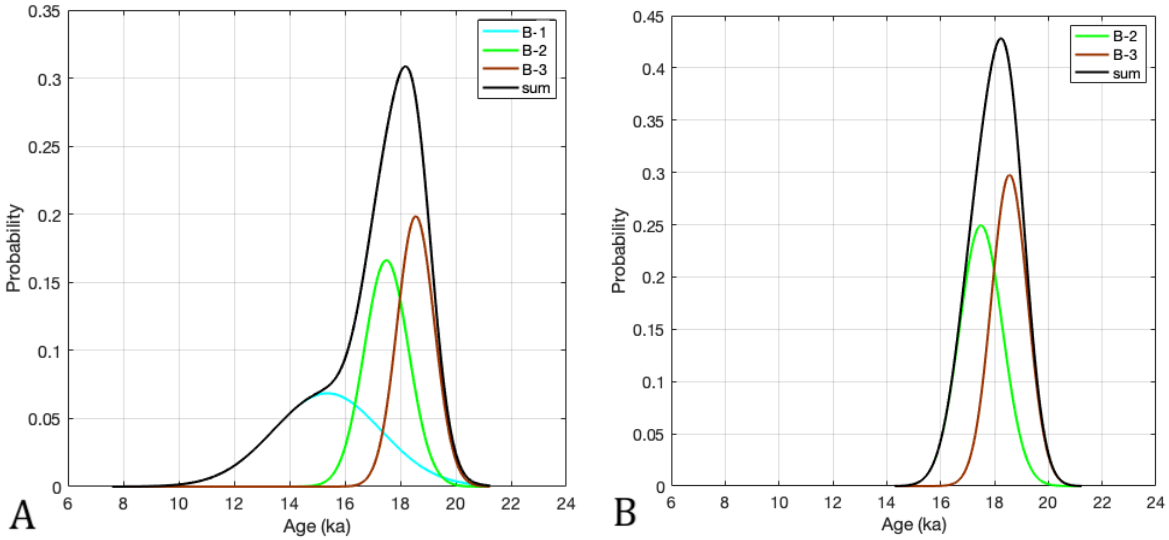

Figure 4.35. Camel plots of ^{10}Be age populations from Bergfjellet. (A) All ^{10}Be age populations, (B) ^{10}Be age populations excluding vastly imprecise ages (B-1). Black line represents the sum of individual frequency distributions.

The ages on Husafjellet are also represented in a similar format: one plot showing all resulting ages (Figure 4.36a), and another that excludes the too young (H-3) and too old (H-1) ages (Figure 4.36b). The summed curve for all Husafjellet ages exhibits one major peak and two lesser peaks, indicating that the true age being dated by these measurements is not well-represented by this dataset. The most overlap among these ages occurs between H-2 (15.20 ± 0.55 ka) and H-4 (14.39 ±0.58 ka), denoted by largest peak in the summed frequency distribution curve (Figure 4.35b). There is also a lack of overlap between H-1 (16.64 ± 0.58 ka) with H-2 or H-4, which suggests that H-1 may not correspond to the same "true age" as H-2 and H-4. Interestingly enough, H-1 has a larger degree of overlap with the Bergfjellet ages, than with the other Husafjellet ages (Figure 4.37).

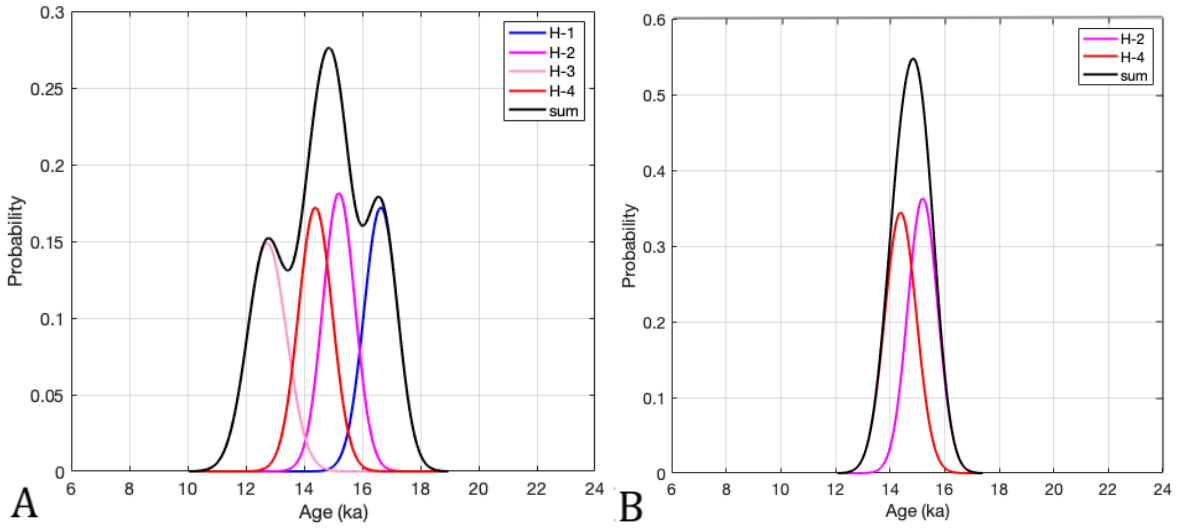

Figure 4.36. Camel plots of ^{10}Be age populations from Husafjellet. (A) All ^{10}Be age populations, (B) ^{10}Be age populations excluding too young or too old ages (H-1, H-3). Black line represents the sum of individual frequency distributions.

Comprehensive camel plots that represent all exposure ages from both Bergfjellet and Husafjellet are similarly presented as well (Figure 4.37a, b). With the exclusion of B-1, H-1, and H-3, the ages tend to fall into two inexplicit age populations roughly based on site: an overall older population from Bergfjellet, and a relatively younger population from Husafjellet (Figure 4.37). The older populations from Bergfjellet are probably older than the true age of deglaciation, most likely due to inheritance. The younger ages on Husafjellet are probably closer to the true deglaciation age, but the spread in the ages is too large to conclusively determine the deglaciation age based solely on the exposure ages alone. Additional information about the deglaciation history of the area could provide some context for interpretation of the ^{10}Be ages, which is further discussed in Chapter 6.

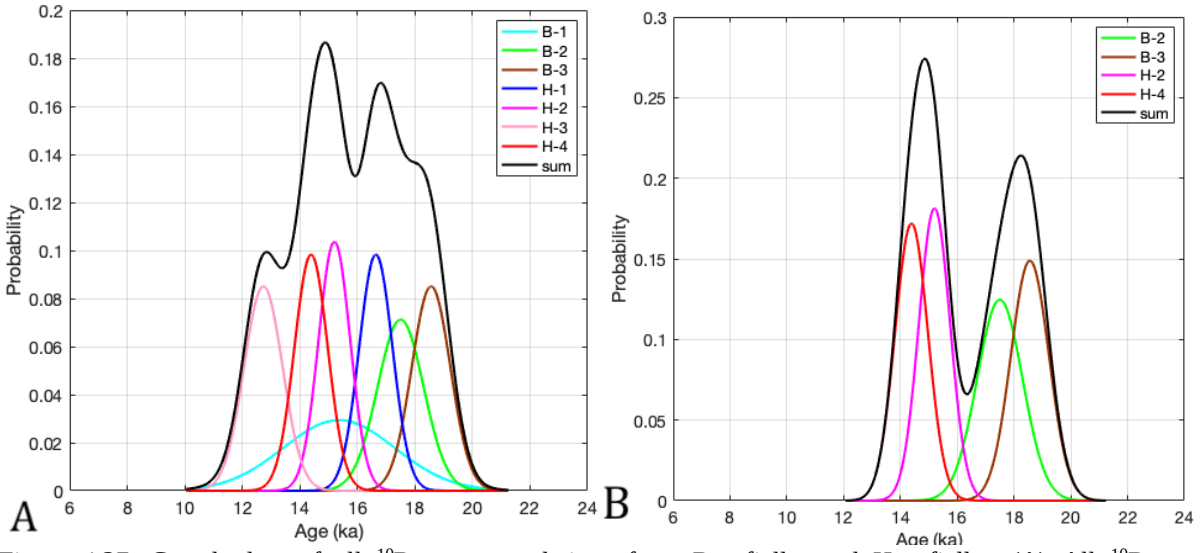

Figure 4.37. Camel plots of all ^{10}Be age populations from Bergfjellet and Husafjellet. (A) All ^{10}Be age populations, including outliers and vastly imprecise ages. (B) all ^{10}Be age populations, excluding old/young apparent ages (H-1, H-3) and vastly imprecise ages (B-1). Black line represents the sum of individual frequency distributions.

5. Interpretation and discussion of ice flow patterns in Boknafjorden

5.1 Overview of flow sets over Boknafjord region

Although it has been demonstrated that some striae older than the LGM may have been preserved in the western Norwegian landscape (Mangerud et al., 2019), the striae shown in Figure 4.1 are, for the most part, assumed to have formed during the LGM and the last deglaciation of the region. In order to determine the major flowsets over the region, crosscutting relationships in the striae data were consulted wherever available as they reflect changes in ice flow direction over a specific area. One general assumption is that striae reflect progressively younger ice flows moving west to east, towards the Younger Dryas ice margin, corresponding to the general inland direction of ice retreat. Another assumption is that striae found in close proximity are likely of similar age. Nevertheless, one cannot rule out the possibility that pre-LGM striae may have been preserved particularly in the areas of higher elevation further inland, as is the case further north in Hordaland (Mangerud et al., 2019). While there are some striae that don't appear to follow the local topography at higher elevations furthest inland in the region (Figure 4.1), these striae have very poor geographic precision, and hence are not reliable enough to be considered as evidence of older preserved striae.

The majority of the striae measurements included in the database are found distal to the Younger Dryas ice margin. By combining the striae observations with the known deglacial history of the region, four ice flowsets are identified that reflect changes in ice flow direction in the early part of the deglaciation. Flowset 1 is based on the striae found on Utsira, as well several on the coast of Jæren that represent a N-NW flow (Figure 5.1). Set 2 is oriented towards the west, and is based on striae found mainly on Karmøy (Figure 5.2). Set 3 is oriented towards the southwest, and is well represented by striae from around Boknafjorden (Figure 5.3). And lastly, set 4 flows towards the south, and is concentrated in the northern coastal areas of Boknafjorden (Figure 5.4). Flowsets 1 to 4 are visually compiled in Figure 5.5.

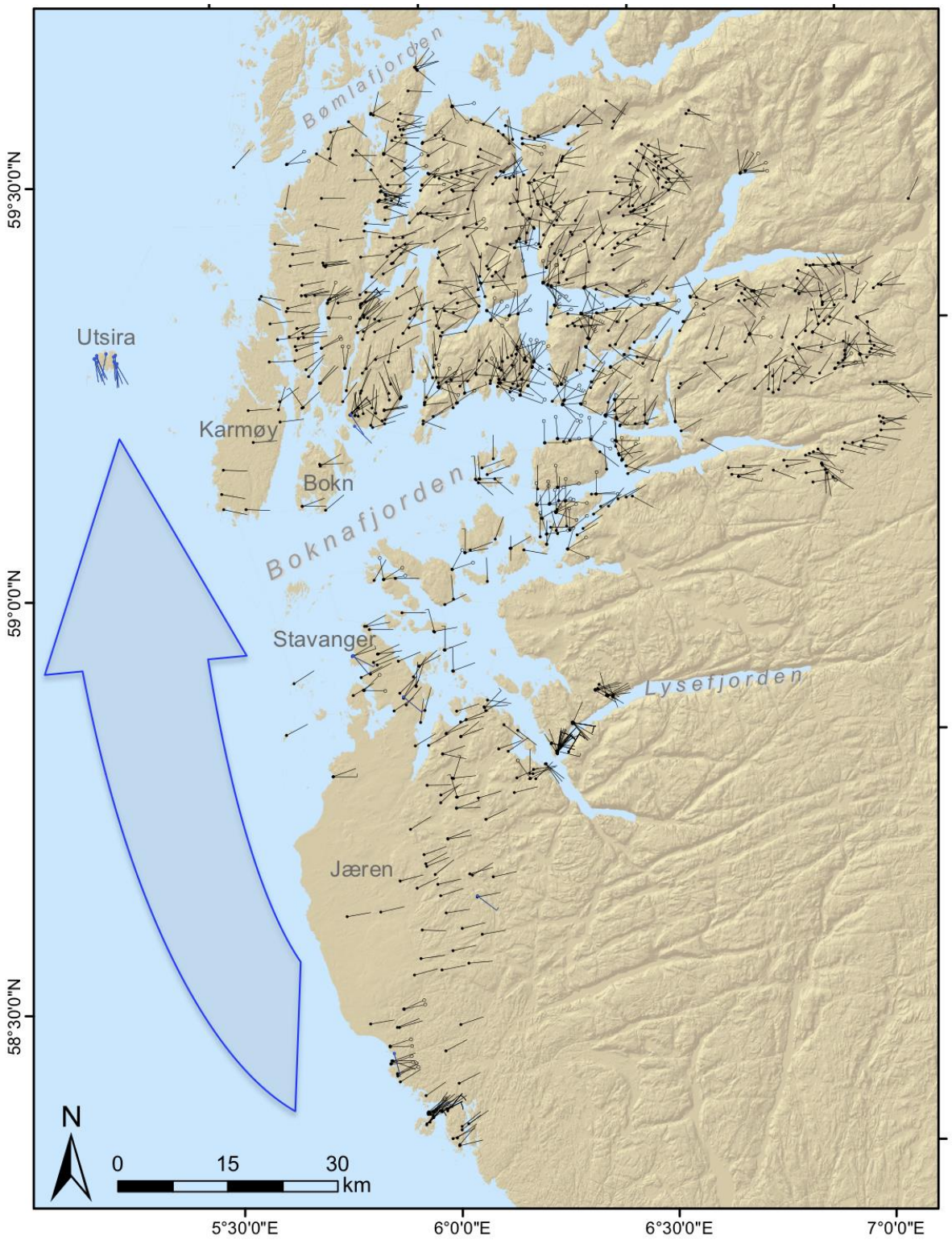

Figure 5.1. Map of striae depicting the flow of flowset 1 towards the N-NW during an active NCIS. Striae associated with flowset 1 are shown in blue.

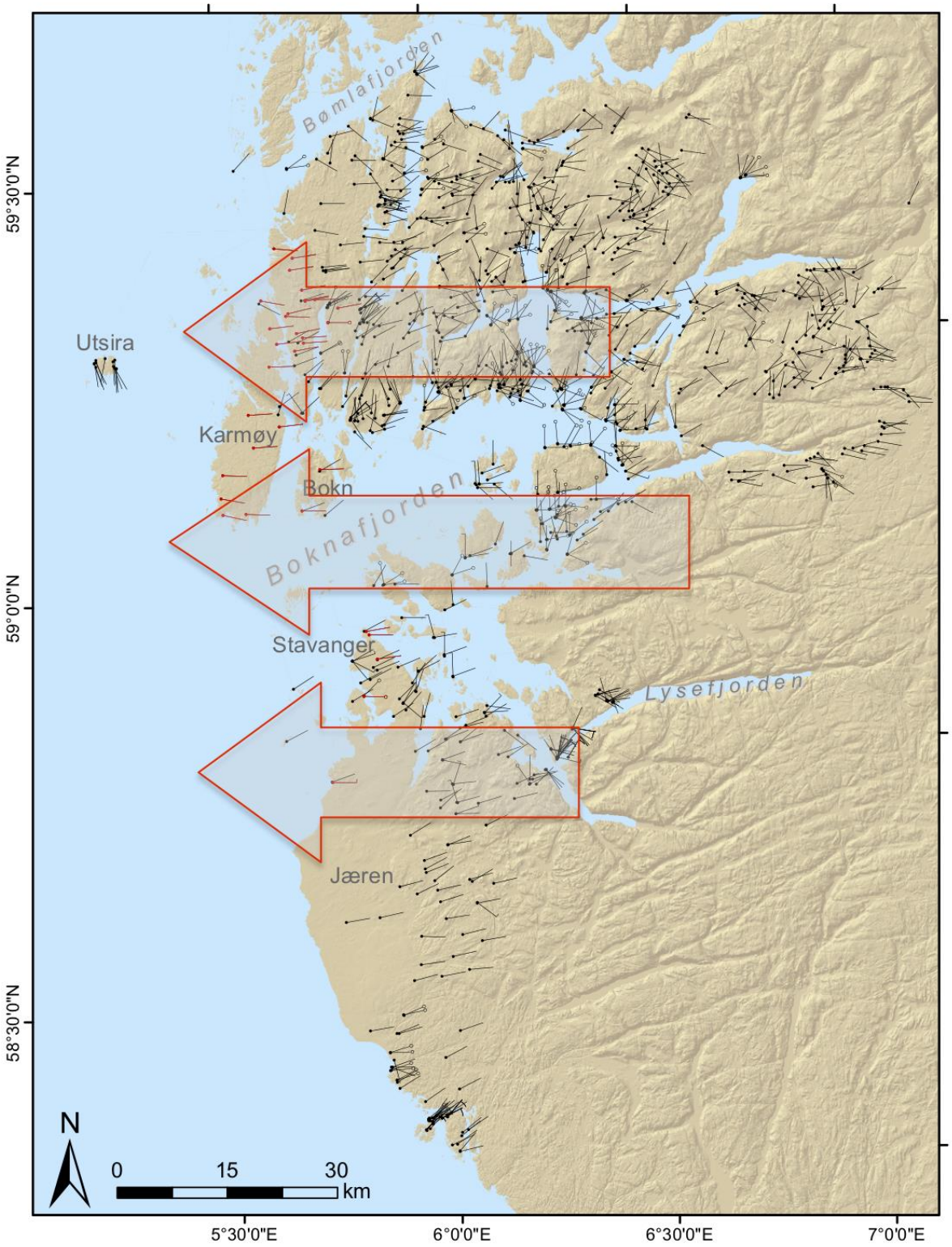

Figure 5.2. Map of striae showing the flow of flowset 2. The striae representing flowset 2 are shown in red.

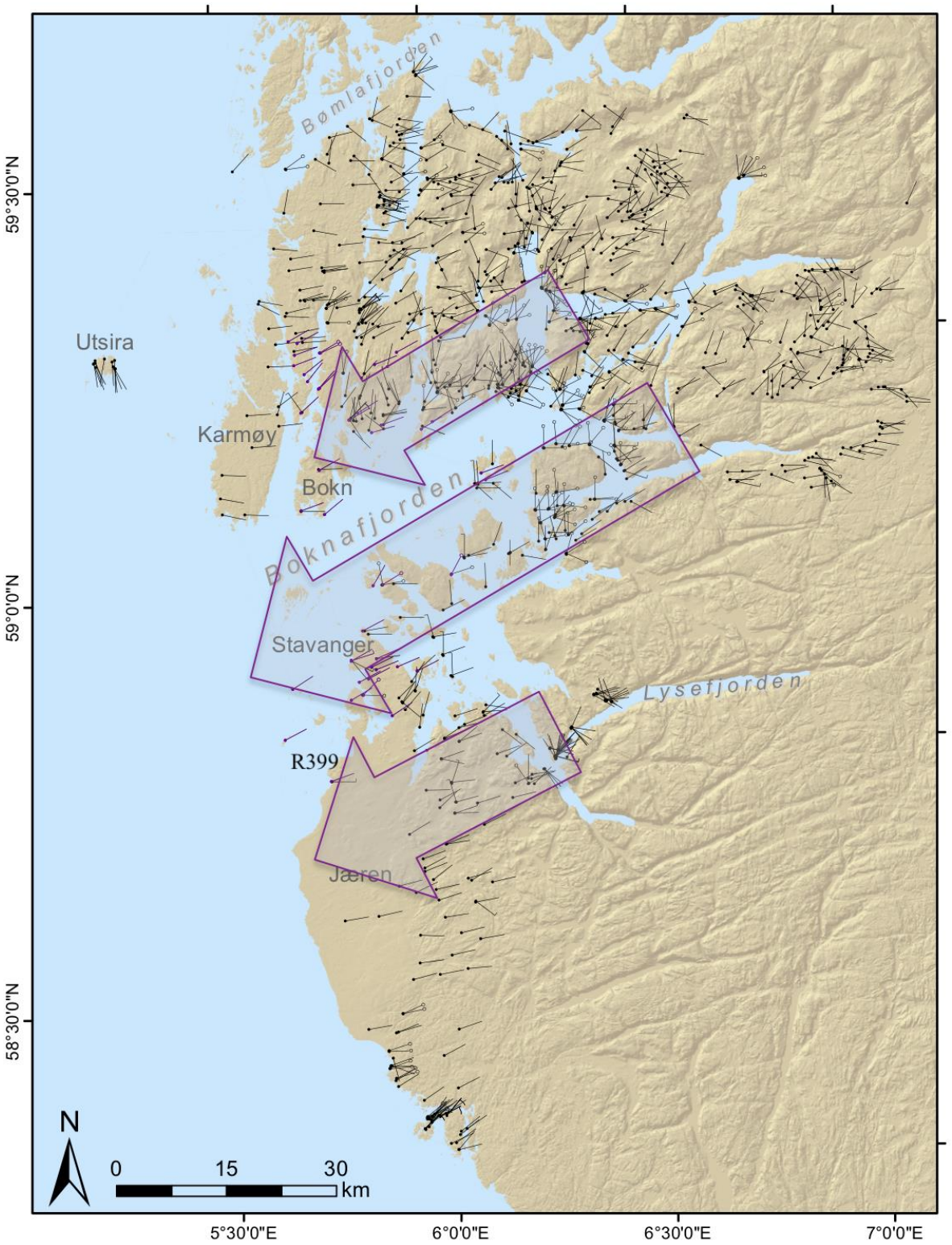

Figure 5.3. Map of striae showing the flow of flowset 3. The striae representing flowset 3 are shown in purple.

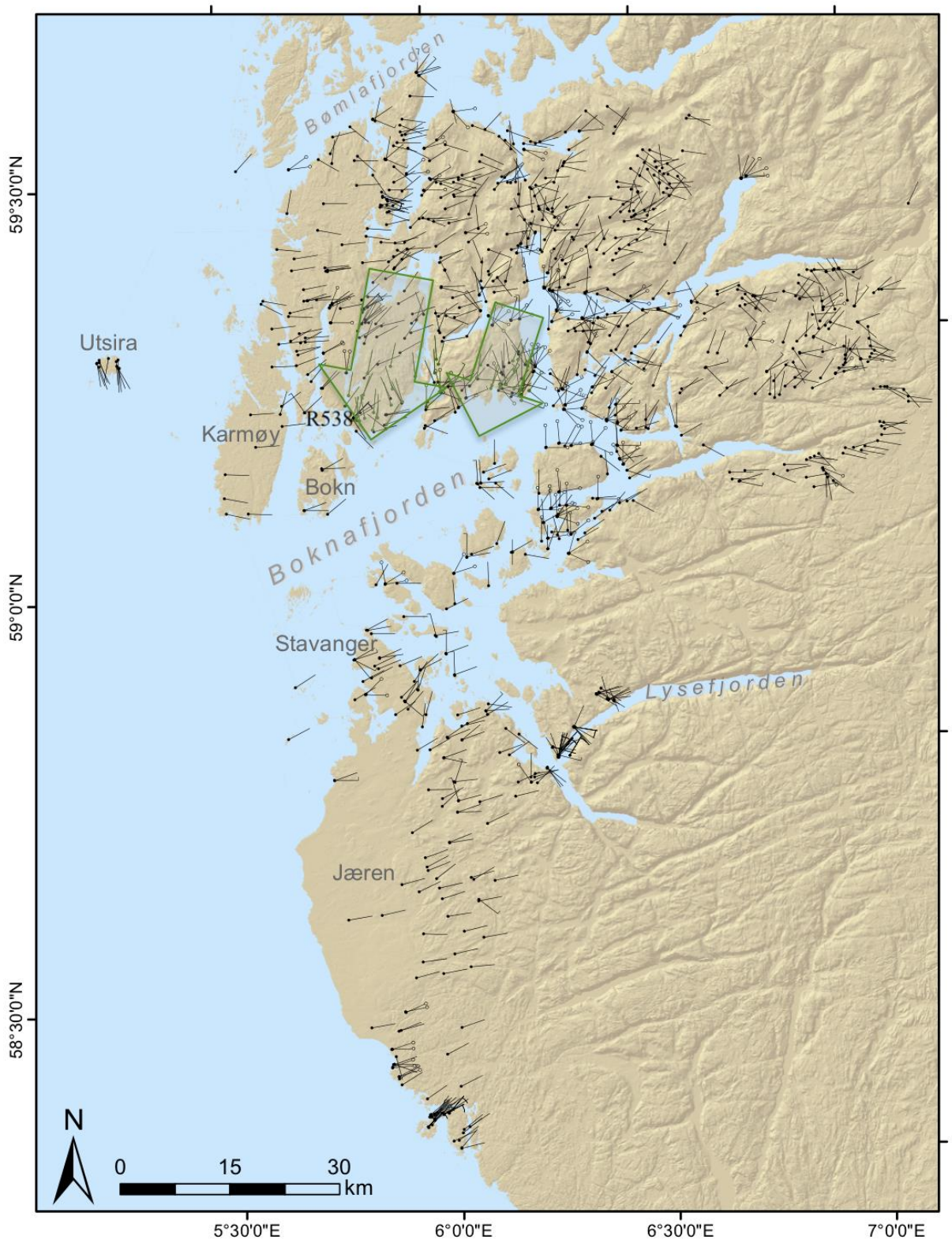

Figure 5.4. Map of striae showing the flow of flowset 4 over the region just north of Bokanfjorden. Striae representing flowset 4 are shown in green.

5.1.1 Flowset 1: North

With the initial collapse of the Norwegian Channel ice stream around 19 ka and its retreat past the Troll core site by 18.5 ka (Figure 2.6; Sejrup et al., 1994, 2009; Morén et al., 2018), the island of Utsira became ice-free relatively early during the deglaciation (Svendsen et al., 2015; Briner et al., 2016). Therefore, the striae associated with the oldest ice flow just prior to deglaciation should be found on Utsira as it is also the westernmost locality in the study area. Utsira is unique in this particular region because it is the only place where only N-oriented striae have been found (Undås 1948; Svendsen et al. 2015). Since Utsira is believed to be the first deglaciated area in the study region, the northerly striae are considered to represent the oldest ice flow (flowset 1). This northerly ice flow over Utsira has been attributed to the northerly flow of the NCIS, which overrode Utsira before its collapse starting around 19 ka (Undås, 1948; Svendsen et al., 2015; Morén et al., 2018). Previous studies on Jæren also have concluded that the lower elevation area known as Lågjæren was overrun by the NW-flowing NCIS, creating an erosional escarpment between Lågjæren and the higher elevations of Høgjæren (Sejrup et al., 1998, Larsen et al., 2000). Observations of N-S trending drumlins and till fabric measurements indicate that an older NW flow overrode the coast of Jæren prior to a subsequent W-SW inland ice flow (Andersen et al., 1987; Sejrup et al., 1998; Jonsdottir et al., 1999). Taking these facts into consideration, N/NW-oriented striae on Utsira and along the coast of Jæren are attributed to flowset 1, which may correspond to the time period when the NCIS was active flowing between 20 and 19 ka (Nygard et al., 2007).

5.1.2 Flowset 2: West

Flowset 2 primarily corresponds with W-oriented on Karmøy, but is also found at several other localities as well (Figure 5.2). Since southern Karmøy was the first area to become deglaciated subsequent to Utsira around 18 ka (Vasskog et al., in press.), the W-oriented striae found on Karmøy are considered to be the next oldest striae in flowset 2. There is a stark difference between the W-oriented striae on Karmøy and the N-oriented striae on Utsira about 20 km to the west. The authors of Svendsen et al. (2015) led a thorough search for any westerly flow indicators on Utsira, but similar the findings of Undås (1947), only N-oriented striae were found. Based on these findings, Svendsen et al (2015) concluded that the westerly ice flow found on Karmøy did not reach Utsira, suggesting that the ice margin during flowset 2 had to have been located somewhere between the two islands.

In the Jæren area, the margin between the NCIS and the inland ice was located east from the present-day coastline when the NCIS was active (Sejrup et al 1998). After the NCIS collapsed, the inland ice margin reconfigured towards the west, past the present-day coastline, demonstrating a westerly ice flow (Sejrup et al 1998, 2018; Raunholm et al., 2003). Therefore, set 2 is believed to represent a similar reconfiguration of inland ice flow towards the west that occurred when it was debuttressed by the retreat of the NCIS (Sejrup et al., 2016). This ice flow direction is perpendicular to the deep, N-S oriented Karmsundet sound that separates Karmøy from the mainland, demonstrating that the ice sheet was thick enough to ignore the underlying topography.

5.1.3 Flowset 3: Southwest

Flow set 3 is composed of SW-oriented striae and is younger than the westerly ice flow shown by cross cutting striae at locality 399 (Figure 5.3). A SW flow is well-represented by the striae around Boknafjorden (Figure 5.3). The SW flow of ice indicated by the striae in set 3 demonstrates that the ice in Boknafjorden did not immediately retreat following the collapse of the NCIS, but rather that there was a period of actively flowing ice in the fjord following the westerly flow of flowset 2. The database striae show only westerly flow over Karmøy, while just to its east, both westerly and southwesterly striae are found on Bokn (Figure 5.3), suggesting that the southwest flow did not reach Karmøy, which remained ice-free following flowset 2. Just to the south, SW-oriented striae associated with flowset 3 are even found on several islands off the west coast of the Stavanger Peninsula (Figure 5.3). While flowset 3 appears to largely ignore the underlying topography of smaller fjords, it evidently follows the orientation of the Boknafjord trough, which may imply that there was a certain degree of topographical influence on flow of the ice sheet.

5.1.4 Flowset 4: South

Along the northern coasts of Boknafjorden and Nedstrandsfjorden, there are a multitude of striae oriented towards the south (Figure 5.4) (Rønnevik, 1971). These southerly striae are attributed to flowset 4, which represent a local shift in ice flow direction from the SW towards the south. This change in flow direction is exhibited by cross-cutting striae at locality R538 that show that the southerly flow is younger than the SW flow represented by flowset 3 (Figure 5.4). The shift of ice flow towards the south in this area has been explained by the opening of a calving bay in Boknafjorden, reflecting faster rate of ice retreat in the fjord compared to the mainland to the north (Rønnevik, 1971; Gump et al., 2017). Calving bays are a concave form of a marine-terminating, calving ice front. Since striae are believed to form perpendicular to the ice front, a concave, calving ice front can form striae that are tilted in towards a fjord (Strömberg, 1981). Hence southerly striae in the northern area of Boknafjorden indicate the presence of a calving bay in Boknafjorden, reflecting the change in flow direction towards the rapidly deglaciating fjord.

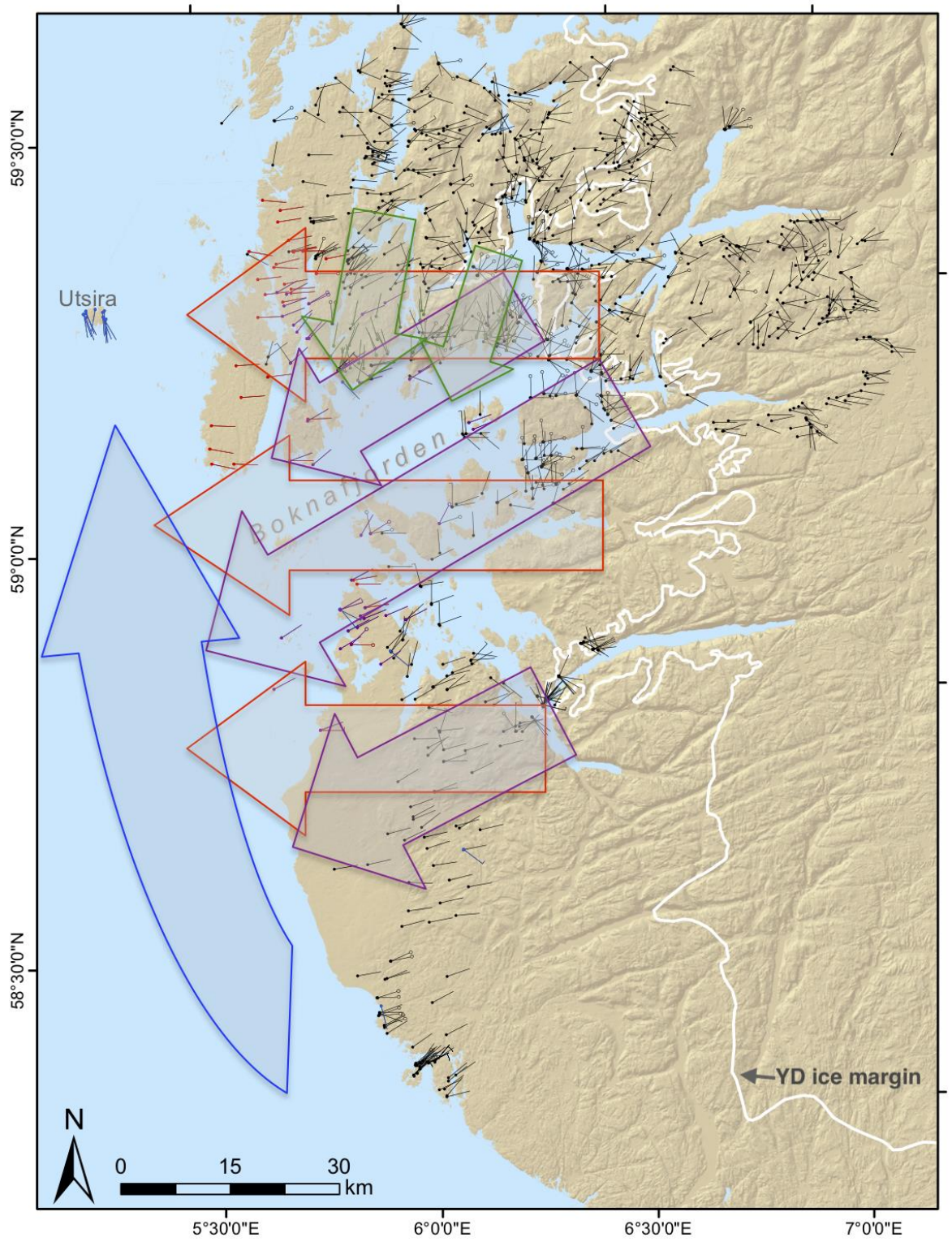

Figure 5.5. All flowsets described in Table 5.1. Blue arrow corresponds to flowset 1, red arrows and striae correspond to flowset 2, purple arrows and striae correspond to flowset 3, and green arrows and striae correspond to flowset 4. White line represents the Younger Dryas ice extent, after Anundsen (1972) and Andersen (1954).

5.2 Ice flow in Boknafjord after the breakup of the NCIS

5.2.1 Striae evidence and streamlined terrain comparisons

Since streamlined terrain, in addition to striae, provides information about the direction of ice flows, there is value in comparing and contrasting the striae evidence and the observed streamlined terrain over the region. Striae evidence suggests that there was a prominent ice flow out of the fjord towards the SW that is attributed to flowset 3 prior to Boknafjorden becoming ice-free (Figure 5.3). There is a striking similarity between the orientation of these striae and the orientation of drumlinoid ridges from the Stavanger peninsula and Jæren observed on LiDAR (Figure 4.10). The streamlined features are particularly well expressed in the southern Boknafjorden area compared to the rest of the region, which may be explained by its flat topography and relatively continuous sediment cover. Similar to the striae, the streamlined bedforms are assumed to have formed during the most recent ice flow over this region shortly before deglaciation. Many of the elongated ridges have been previously mapped and interpreted as drumlins, some of which are evidently associated with bedrock knobs, while others are not (Andersen et al. 1987; Garnes 1976). The fact that the striae evidence from bedrock is supported by streamlined bedforms provides further support for a significant ice flow to the SW prior to deglaciation, particularly since bedforms like drumlins and mega-flutings may indicate the presence of a past fast-flowing glacier lobe or ice stream (Patterson and Hooke, 1996). A ice flow direction is demonstrated by till fabric analyses on Jæren, which are also roughly parallel to the SW glacial striae in the area (Andersen et al. 1987). A slight difference in orientation is noted however between northern and southern Jæren, with a more westerly flow over the latter and a southwesterly flow over the former (Andersen et al. 1987). Andersen et al. (1987) interpreted this regional difference as an indication of a strong, dominant flow of ice coming out Boknafjorden that forced the ice flow over northern Jæren towards the SW.

5.2.2 Drumlins on Karmøy

Moving further north to the island of Karmøy, the W-oriented striae are complemented by several drumlinoid ridges that also have a W-E orientation (Figure 4.11; Ringen, 1964). Ringen (1964) concluded that these ridges are likely drumlins, rather than terminal moraines. Subsequent studies indicate that the drumlin at the Bø site is underlain by Eemian marine

sediments (Figure 5.6b; Andersen et al., 1983; Miller et al., 1983, Sejrup, 1987). On LiDAR, the drumlins on Karmøy (Figure 4.11) have a passing resemblance to the streamlined terrain further south around the Stavanger peninsula (Figure 4.10). But further south on Eigerøy, several drumlins on the leeside of bedrock knobs have been described on an island that otherwise lacks sediment cover (Garnes, 1976). The morphology of these drumlins is strikingly similar to that of the ridges described on Karmøy, and they are parallel to the glacial striae in the area as well. The stratigraphy of these drumlins reveals a lower unit of beach sediments overlain by mid-Weichselian marine sediments, which are topped by till (Garnes, 1976). The drumlins are therefore believed to have been formed by glacial erosion rather than deposition, as the late Weichselian ice sheet eroded into the underlying mid-Weichselian marine sediments and produced the elongated ridges (Garnes, 1976). Given the similarity in morphology and stratigraphy of the drumlinoid ridges on Karmøy and on Eigerøy, it is reasonable to postulate that both sets of landforms could have been formed by a similar erosional process during the last deglaciation. Assuming that the interpretation of these ridges is accurate, they do indeed have an orientation parallel to ice flow. Therefore, the Karmøy drumlins provide further evidence that the last ice flow on Karmøy was towards the west, supporting the relative age of flowset 2. Hence the drumlins on Karmøy (flowset 2) are postulated to be relatively older than the drumlins and flutings in the Stavanger area to the south that correspond to the SW flow of flowset 3.

5.2.3 Comparison of ice flow evidence with modeled 18 ka flowlines

Åkesson et al. (2017) presents insights into the deglaciation of the marine-based ice sheet in southwest Norway from 18 ka to 11 ka through the use of a high-resolution, 2D ice sheet model that incorporates grounding line dynamics. An 18 ka velocity field and flowline model (Figure 5.6) shows a clear westward ice flow across Karmøy as well as further south over Stavanger and Jæren. These modeled flowlines fit well with the striae and drumlin evidence on Karmøy, which are also oriented towards the west and are attributed to flowset 2 (Figure 4.12; 5.2). As a result, this overlap could tentatively suggest that flowset 2 could correspond to around 18 ka, which is also supported by offshore records indicating that the NCIS has retreated past the Troll core site around 18.5 ka (Sejrup et al., 1994, 2009). Radiocarbon dates from southern Karmøy that indicate it became ice-free around 18 ka (Vasskog et al., in press).

Conversely, striae evidence and streamlined terrain around the Stavanger peninsula clearly show ice flow towards the southwest (i.e. Andersen et al. 1987; Figure 4.12), and not to the west as shown by the model. On one hand, this discrepancy could indicate that the southwest flow is younger than the westerly flow in the southern Boknafjord region. Since the SW flow is postulated to belong to flowset 3, one could suggest that the SW flow is younger than 18 ka, assuming the model is accurate. On the other hand, Åkesson et al. (2017) suggests that the local discrepancy implies that their model underestimates the ice thickness along the coast, producing ice flows that are more sensitive to topography. This suspicion is supported by the fact that the 18 ka model considers several mountain summits as nunataks, but ^{10}Be exposure dates (Gump et al. 2017; Svendsen et al., 2015) indicate that those peaks were still covered by ice at this time (Åkesson et al., 2017). This explanation would suggest that a SW ice flow requires slightly thicker ice to ignore underlying topography, while thinner ice would flow closer to due west with higher topographical influence.

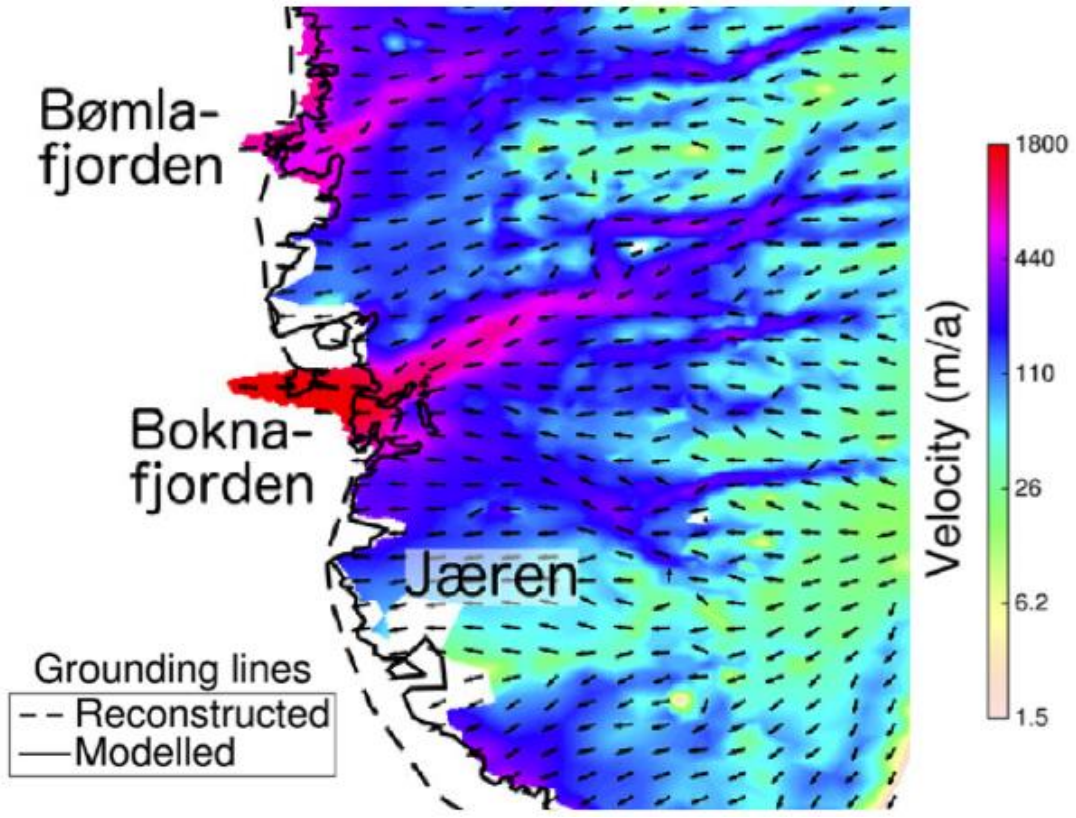

Figure 5.6. 18 ka steady-state velocity field modeled by Åkesson et al. (2017), showing modeled/reconstructed ice sheet grounding lines, ice velocities and flowlines directions (modified from Åkesson et al. 2017).

5.3 Ice margin stability in Boknafjorden during deglaciation

Thick glaciomarine sediment sequences up to 250 meters-thick have been found in the Karmsundet sound near the mouth of Boknafjorden that have a minimum age of ~13 cal ka BP (Bøe et al., 2000), which have been suggested to reflect a period of ice margin stability or even a re-advance (Svendsen et al., 2015). ^{10}Be ages from Tananger, Våg, Bokn and Sandviksfjellet all indicate that they became ice-free around 16 ka (Figure 2.7; Gump et al., 2017; Svendsen et al., 2015), which is around 2000 years after southern Karmøy was deglaciated around 18 ka (Vasskog et al., in press). Given that the ice margin retreated a relatively short distance from 18 ka to 16 ka, the margin may have been stable for a significant period of time within this time span (Svendsen et al., 2015). Following a period of ice-stability, the fjord subsequently underwent a renewed phase of deglaciation starting from ~16 ka (Gump et al., 2017).

The widespread imprint of SW ice flow (flowset 3) in the form of striae and streamlined terrain implies that Boknafjorden did not deglaciate immediately after the collapse of the NCIS, but rather, that there was a period of stable, actively flowing ice that preceded the development of a calving ice front in the fjord. The striae evidence is therefore consistent with previous evidence of a prolonged period of ice margin stability in Boknafjorden. Flowset 3 is thus proposed to have occurred sometime between ~18 ka and ~16 ka. Flowset 4 would accordingly have occurred after ~16 ka, marking the re-initiation of ice retreat and the formation of a calving bay in Boknafjorden.

Additionally, the presence of SW striae (flowset 3) on islands west of the Stavanger peninsula indicates that the ice margin may have extended beyond the coastline in the southern Boknafjord area during flowset 3, an extent that may even be indicative of an ice advance. The lack of SW striae on Karmøy suggests that it was not overridden by ice after flowset 2 and its deglaciation around ~18 ka. Conversely, both westerly (flowset 2) and southwesterly (flowset 3) striae are found on Bokn, located just east of Karmøy, which suggests that the ice margin in northern Boknafjorden during flowset 3 was located somewhere between southern Karmøy and Vestre Bokn.

6. Interpretation and discussion of ^{10}Be ages

6.1 ^{10}Be production rate discussion

6.1.1 ^{10}Be production rate choice

The ^{10}Be ages were calculated using the western Norway regional production rate that is based two calibration sites: a rock avalanche in Oldedalen with ^{14}C dates from wood, as well as a well-dated Younger Dryas moraine on Halsnøy (Goehring et al., 2012a, b). However, a Scandinavian production rate has also been presented by Stroeven et al. (2015) that uses a dataset from the drainage of the Baltic ice lake in southern Sweden to recalibrate three sites in Norway (including Oldedalen and Halsnøy), combining them to create a reference ^{10}Be production rate for Scandinavia. Nonetheless, the western Norway and Scandinavian production rates are similar enough that the ages calculated by the two production rates have a high degree of statistical overlap. Consequentially, choosing one production rate over the other does not significantly change the time range represented by the resulting ages and their uncertainties.

6.1.2 ^{10}Be production rate uncertainty

The western Norway production rate is calibrated using the ^{14}C ages of around 11.65 ± 0.10 cal ka before 2008 (Halsnøy) and 6.07 ± 0.11 cal ka before 2008 (Oldedalen) (Goehring et al., 2012a,b). Since the surfaces dated in this study are at least several thousand years older than the time range represented by the western Norway production rate, there is an inherent production rate uncertainty involved in the age calculations due to potential production rate variations through time. The ^{10}Be ages are presented here with only their internal/analytical uncertainties, and hence do not reflect the production rate uncertainty. The Scandinavian production rate (Stroeven et al., 2015) is calibrated using ^{14}C ages of a similar time span as those used to calibrate the western Norway production rate, and so both production rates represent a time range that is younger than the dated boulder surfaces. Hence, the production rate used to calculate the ^{10}Be ages for Bergfjellet and Husafjellet is a significant source of

uncertainty that cannot be ameliorated given the younger time range of the regional production rates presently available for the region.

6.2 ^{10}Be ages on Bergfjellet

Two of the three ^{10}Be ages on Bergfjellet, B-2 (17.50 ± 0.80 ka) and B-3 (18.56 ± 0.67 ka) suggest a deglaciation age that is older than what would have been otherwise expected for the area near the mouth of Lysefjorden. The apparent ages of B-2 and B-3 would suggest that Bergfjellet became ice free around the same time as southern Karmøy around 18 k cal a BP (Vasskog et al., in press), which is highly improbable given how much further east Bergfjellet is located relative to Karmøy.

Anomalously old exposure ages from bedrock in the inner Lysefjord region may help explain the older ages yielded from boulders on Bergfjellet. Several ^{10}Be exposure ages from Lysebotn, located near the head of Lysefjorden, are presented by Briner et al (2014). Boulders and bedrock sampled at relatively low elevations (<100 m a.s.l) near the valley base yielded similar ages with an average of ~10.6 ka, while bedrock surface sampled at a higher elevation (405 m a.s.l) yielded a significantly older age of ~20 ka (Figure 2.9; Briner et al. 2014). Thus it was concluded that the bedrock at higher elevations exhibits inheritance, indicating that the lower elevations were more effectively eroded by ice than higher elevations, which were not sufficiently eroded during the last glaciation to fully remove nuclides from previous exposures (Briner et al., 2014).

Furthermore, an investigation into the rates and patterns of glacial erosion in a mountain plateau south of Lysebotn yielded ^{10}Be ages of mostly bedrock surfaces ranging between 8.9 ± 1.1 ka and 37.9 ± 0.6 ka (Egholm et al., 2018; Brække, in prep). Corresponding measurements of ^{26}Al allowed for the analysis of ^{26}Al/^{10}Be ratios for the sampled surfaces, which confirm the complex exposure histories in the region (Brække, in prep.). The sampled surfaces have elevations between 428 and 1102 m a.s.l., but the ^{10}Be ages do not show a trend in regards to elevation (Brække, in prep.). Nonetheless, relatively old apparent ages of bedrock up to ~40 ka indicates that it was not sufficiently eroded by ice during the last glaciation, resulting in inherited ^{10}Be concentrations. If the sampled boulders B-2 and B-3 were plucked by ice from bedrock that had been eroded less than 2 meters during the last glaciation, the boulders may yield apparent ages that are too old (Goehring et al., 2008).

Since the data and observations presented from the inner Lysefjord area may be representative of the larger surrounding regions, including the source areas of the boulders in this study with old apparent ages, it is possible that the boulder in question were plucked from such bedrock with nuclide inheritance, then were transported and deposited near the mouth of the Lysefjord.

Given the prevalent issue of inheritance in the Lysefjord region, the apparent ^{10}Be ages of B-2 and B-3 are concluded to be older than the true deglaciation age of Bergfjellet. Sample B-1 (15.36 ± 1.94 ka) could potentially have yielded a more accurate deglaciation age if its AMS analysis ran with a stronger ^{9}Be current and produced a smaller analytical uncertainty. In spite of having a median age of 15.36 ka, an uncertainty of almost 2000 years is too broad to provide any useful indication of when Bergfjellet became ice-free.

6.3 ^{10}Be ages on Husafjellet

The resulting ^{10}Be ages from Husafjellet are generally younger than those from Bergfjellet, but also exhibit a large age spread (1σ = ~1600 yrs), which makes it difficult to produce a reliable estimate for the deglaciation age based solely on the ^{10}Be ages. Nevertheless, prior knowledge of the deglaciation history and the geological context of the surrounding region provide clues that may assist in the interpretation of the apparent ^{10}Be ages on Husafjellet.

Husafjellet is located outside the Younger Dryas ice sheet extent, which is clearly delineated in the area by the quintessential terminal moraines found around Forsand such as Esmark's moraine (Andersen, 1954; Briner et al., 2014). It can therefore almost certainly be concluded that Husafjellet became ice-free prior to the Younger Dryas, which immediately casts doubt upon the ^{10}Be age of 12.73 ± 0.67 ka yielded by the sample H-3. As a result, the apparent age of H-3 very likely underestimates the true age of deglaciation. Nevertheless, the exclusion of H-3 still leaves three remaining ^{10}Be ages that range over 3000 years, hence it becomes a question of whether the two older or two younger ages have the higher probability of accuracy. Husafjellet was likely ice-free prior to the Older Dryas as well, since the Older Dryas ice extent has been demonstrated to be similar to that of the Younger Dryas in the Lysefjord-Forsand region (Section 7.6; Briner et al., 2014; Karlsen, 2016). Accordingly, H-4 with an apparent age of 14.39 ± 0.58 ka may be a borderline younger age, but could still be a valid estimate when its uncertainty is taken into account. Moreover, the camel plot of the

Husafjellet ^{10}Be ages (Figure 4.36) illustrates that the two younger samples, H-4 (14.39 ± 0.58 ka) and H-2 (15.20 ± 0.55 ka) have higher statistical overlap than the two older samples H-2 and H-1 (16.64 ± 0.58 ka), resulting in a higher probability that the two younger ages represent the true deglaciation age. Furthermore, considering that the older apparent ^{10}Be ages on Bergfjellet demonstrate the issue of inheritance in this area, it is logical to place more certainty on the younger ages. Thus, sample H-1 may demonstrate a certain degree of inheritance, similar to samples B-2 and B-3. Interestingly enough, the apparent ^{10}Be age of H-1 has a higher degree of overlap with those of B-2 and B-3 than with the other Husafjellet samples (Figure 4.35a), which further strengthens the argument that these three oldest samples all likely have some degree of inheritance. Accordingly, H-2 and H-4 with respective ages of 15.20 ± 0.55 ka and 14.39 ± 0.58 ka may be the closest to the true age of deglaciation of all seven presented ^{10}Be ages. Nonetheless, as previously stated, the large degree of spread among the ^{10}Be ages is problematic for determining a definitive age of deglaciation at this time.

6.3.1 Potential causes of young apparent ^{10}Be ages

While the older apparent ages of B2, B-3 and H-1 can essentially be explained by inheritance, it is slightly more problematic to pinpoint the causes of the younger age yielded by H-3. The boulder H-3 did not show any indications of being moved or turned since its initial deposition by ice, as all the sampled boulders rested on stable, relatively flat surfaces with no nearby slopes from which to potentially roll down. Post-glacial weathering on boulder surfaces could yield younger apparent ages, and can vary from boulder to boulder. It may be possible that the boulder H-3 has been weathered to a higher degree than the other sampled boulders, but the degree of erosion is difficult to quantify without erosional indicators such as protruding quartz veins. Besides, all sampled boulders have similar lithologies and were essentially concentrated in the same area at the summit of Husafjellet, as such one would expect that they all experienced similar degrees of post-glacial weathering. Another potential cause is seasonal snow shielding, but the boulder with a younger apparent age does not exhibit characteristics that would suggest they would be more susceptible to snow shielding than the other adjacent Husafjellet boulders. Consequently, it is evidently difficult to identify a single, obvious cause for the young apparent ^{10}Be age of H-3.

6.4. Comparisons with Uburen ^{10}Be ages

The preliminary ^{10}Be ages from Uburen (J.I. Svendsen, pers. comm., 2019) are overall more consistent than the ^{10}Be ages from Husafjellet and Bergfjellet (Table 4.4). With the exception of one significantly older age (F-29, 28.31 ± 0.54 ka), the Uburen samples have an average age of 15.30 ± 0.53 ka. Thus, more confidence can be placed on the Uburen ages as closer representations of when the mountaintops in Forsand started to deglaciate than the ^{10}Be ages on Husafjellet and Bergfjellet. A deglaciation age of ~15.3 ka on Uburen also supports the conclusion that samples H-2 and H-4 are the most reliable of the Husafjellet samples, due to the similar elevation and relative proximity between Uburen and Husafjellet. Moreover, this ~15.3 ka deglaciation age fits with the known late deglacial history of Forsand, which is further discussed in the Chapter 7.

6.5 Comparisons with other ^{10}Be ages from the Boknafjord region

A deglaciation age of around ~15.3 ka of Uburen/Husafjellet in Forsand overlaps with several other ^{10}Be dated sites around Boknafjorden such as Lammanuten (15.2 ± 0.1 ka), Ryvarden (15.0 ± 0.7 ka) and Boknafjellet (15.4 ± 0.4 ka) and northern Karmøy (15.7 ±0.9 ka) (Gump et al., 2017; Figure 2.7). Thus, the mountaintops in Forsand started to become ice-free after the majority of Boknafjorden has already deglaciated. Previous studies have demonstrated that the deglaciation of Boknafjorden commenced significantly before the deglaciation of Bømlafjorden-Hardangerfjorden further to the north, the latter of which is closer associated with the Bølling warming (Mangerud et al, 2013; Svendsen et al., 2015: Gump et al., 2017). Furthermore, ^{10}Be ages as well as radiocarbon ages indicate that the mouth of Bømlafjorden deglaciated just after ~15 ka (Karlsen, 2009; Mangerud et al., 2013; Gump et al., 2017), which suggests that Uburen/Husafjellet may have become ice free around the same time as, or just prior to the start of ice retreat further north in Bømlafjorden. Yet ^{10}Be ages from ~100 m a.s.l. at the mouth of Lysefjorden, just outside the YD moraine yield a final deglaciation age of 14.0 ± 0.4 ka, which also corresponds to the Older Dryas (Briner et al., 2014; Figure 2.7, 2.9). Hence the Forsand-Lysefjord region may still have been periodically glaciated for for at least 1000 years after the Forsand summits became ice-free.

7. Deglaciation history of Espedalen and the Høgsfjorden-Frafjorden region

7.1 Oldest deglacial environments in Espedalen

7.1.1 Ice-contact glaciolacustrine delta at Nedre Espedal

The sediment sections at Løland present persuasive evidence of a glacial lake occupying the inner region of Espedalen for a certain duration during the last deglaciation. The presence of debris flow diamicton within sediment facies associated with foresets, antidunes and humpback dunes suggest that the sediments were deposited in an ice-contact deltaic environment. Moreover, since most ice-contact deltas initiate as ice-contact fans that build up to the water surface (Powell, 1990; Benn and Evans, 2010), it is possible that there may be subaqueous fan deposits at the core of the deltaic terrace at Løland. With a relatively stationary ice margin and high-enough sedimentation rate, a subaqueous ice-contact fan can aggregate up to the water surface to form an ice-contact delta (Powell, 1990). Nonetheless, further analysis would be necessary to investigate whether or not the ice-contact delta emerged from a subaqueous fan. Regardless, the environmental implication of an ice-contact glaciolacustrine setting is evident.

The ice-contact glaciolacustrine delta interpretation is supported by the ice-marginal terrain located just adjacent to the Løland gravel pit. It is therefore concluded that the ice-margin in contact with the delta was situated precisely at Løland/Nedre Espedalen, delineated by the distinct contact between the flat 157 m a.s.l. glaciolacustrine terrace and the adjacent hummocky/ice-marginal terrain. Conclusively, the Løland ice-contact delta corresponds to a previously mapped ice margin included in the “Glacial Map of Norway” by Holtedahl and Andersen (1960). The presence of an ice-proximal delta at elevations significantly higher than the marine limit (~34 m a.s.l. in Forsand; Anundsen, 1985) indicates that it was likely formed in a lake that was dammed down-valley, potentially by ice occupying Høgsfjorden, which is oriented perpendicular to Espedalen. Furthermore, the elevation of the lake surface is denoted by the 157 m a.s.l. surface of the relict Løland ice-proximal delta. Since the water level in an ice-dammed lake provides a minimum thickness of the ice-dam, it seems that the surface of

the ice in Høgsfjorden was at least 157 m a.s.l. during the oldest/highest lake phase. Assuming that the ice was grounded within the fjord that has a maximum depth of 170 m, the Høgsfjord ice lobe would have had a minimum thickness of ~300 meters at the mouth of Espedalen.

In sum, the overall environmental implication of the oldest Løland gravel pit sediments is that a glacial lake in Espedalen was dammed by ice in Høgsfjorden at the valley mouth, and was in contact with proximal ice margin at Nedre Espedalen (Figure 7.1). This scenario suggests that a portion of lower Espedalen was ice-free while upper Espedalen and Høgsfjorden were still occupied by ice. The presented geomorphological evidence observed on LiDAR and in the field supports this scenario and indicates that it is pre-dates the Younger Dryas, assuming the YD margin mapped by Andersen (1954) further up-valley in Vinddalen is accurate (Figure 7.3). Finally, striations found at Lauvvik along the western margin of Høgsfjorden (Figure 4.9) demonstrate that the youngest ice flow was parallel to the fjord, which is consistent with a topographically-steered ice lobe in Høgsfjorden. Thus the striae evidence points to a scenario that is consistent with the conclusions drawn from the other regional observations discussed here.

7.1.2 Formation of 126 m a.s.l. glaciofluvial terrace at Løland

The stratigraphy of the 126 m a.s.l. glaciofluvial terrace at Løland indicates a shift from a glaciolacustrine to a glaciofluvial depositional environment at Nedre Espedal, which can mostly simply be explained by the regression of the lake-level. It is unclear where the corresponding ice margin was located when the meltwater flows incised into the glaciolacustrine deposits and deposited the glaciofluvial gravels found at the surface of the 126 m a.s.l. Løland terrace. However, it stands to reason that if the ice margin retreated towards Øvre Espedal, the majority of the glaciofluvial sediment from the meltwater flows would be trapped in Espedalsvatnet. Hence, the ice margin may have persisted in the vicinity of Nedre Espedal for certain duration as the lake drained for the deposition of glaciofluvial sediment at Løland/Nedre Espedal. With the eventual retreat of the ice margin, the glaciofluvial depositional processes presumably transitioned to and were eventually replaced by fluvial processes over time.

7.2 Ice-dammed lake in the Lauvvatnet region

Given that the ancient shorelines mapped in the Lauvvatnet region have significantly higher elevations (>40 m higher) than the Stølsvatnet outlet (480 m a.s.l.), the outlet would have had to be dammed for the lake level to reach 520 m a.s.l. (Figure 7.1). An ice-dammed lake in the Lauvvatnet region strongly suggests that inner Frafjorden was occupied by at least 520 m-thick ice at some point during the deglaciation prior to the YD, which is significant because Frafjorden is an up-fjord extension of Høgsfjorden. Thus, if Frafjorden was occupied by >520 meter-thick ice, it is reasonable to postulate that this ice lobe extended further down into Høgsfjorden damming Espedalen as well. Consequentially, the presence of the higher-elevation ice-dammed lake shorelines provides additional support for the hypothesis that suggests a lake in Espedalen was dammed by ice in Høgsfjorden.

The secondary outlet out of Brekkevatnet with an initial elevation that corresponds to the higher shorelines probably formed as a result of the higher ice-dammed lake levels. As meltwater accumulated in this higher elevation ice-dammed lake, an additional outlet started flowing out of Brekkevatnet down into Nedre Espedal (Figure 7.1). Over time, the outlet flow eroded down into bedrock, forming a canyon with an outwash fan at its base. The Brekkevatnet outlet is particularly noteworthy because the corresponding outwash fan was deposited on a 120 m a.s.l. glaciofluvial terrace in Nedre Espedal that exhibits relict subaerial channels on its surface. Since the glaciofluvial terraces formed after the ice-dammed lake drained from Nedre Espedal, the outwash fan must also be younger than oldest lake phase in Espedalen. As a result, a relative chronology can be established between the Lauvvatnet and Espedalen ice-dammed lakes. It is postulated that both lakes likely existed contemporaneously as the Høgsfjorden-Frafjorden ice lobe dammed both their outlets, during which there may have been active flow from the higher lake into the lower Espedalen lake through the Brekkevatnet outlet (Figure 7.1). The two ice-dammed lakes provide minimum estimates for the surface elevation of both an up-fjord and down-fjord location (>520 m a.s.l and >150 m a.s.l., respectively) of the Høgsfjorden-Frafjorden ice lobe, yielding a tentative ice-surface gradient estimate of 27 m/km.

Active discharge from the Brekkevatnet outlet demonstrated by the outwash fan deposition after the oldest Espedalen ice-dammed lake phase simply implies that the higher lake was still dammed after Nedre Espedal was drained (Figure 7.2).

Such a scenario is logical, given Espedalen's down-fjord position relative to the Stølsvatnet outlet, the latter of which would still have been dammed when the ice retreated past the former. If Espedalen was still dammed at the time of the outwash fan deposition in Nedre Espedalen, then the ice-dammed lake, and thus the ice dam, must have had a surface elevation lower than 120 m a.s.l., given that the glaciofluvial terrace underlying the fan indicates subaerial conditions at 120 m a.s.l. (Figure 7.2).

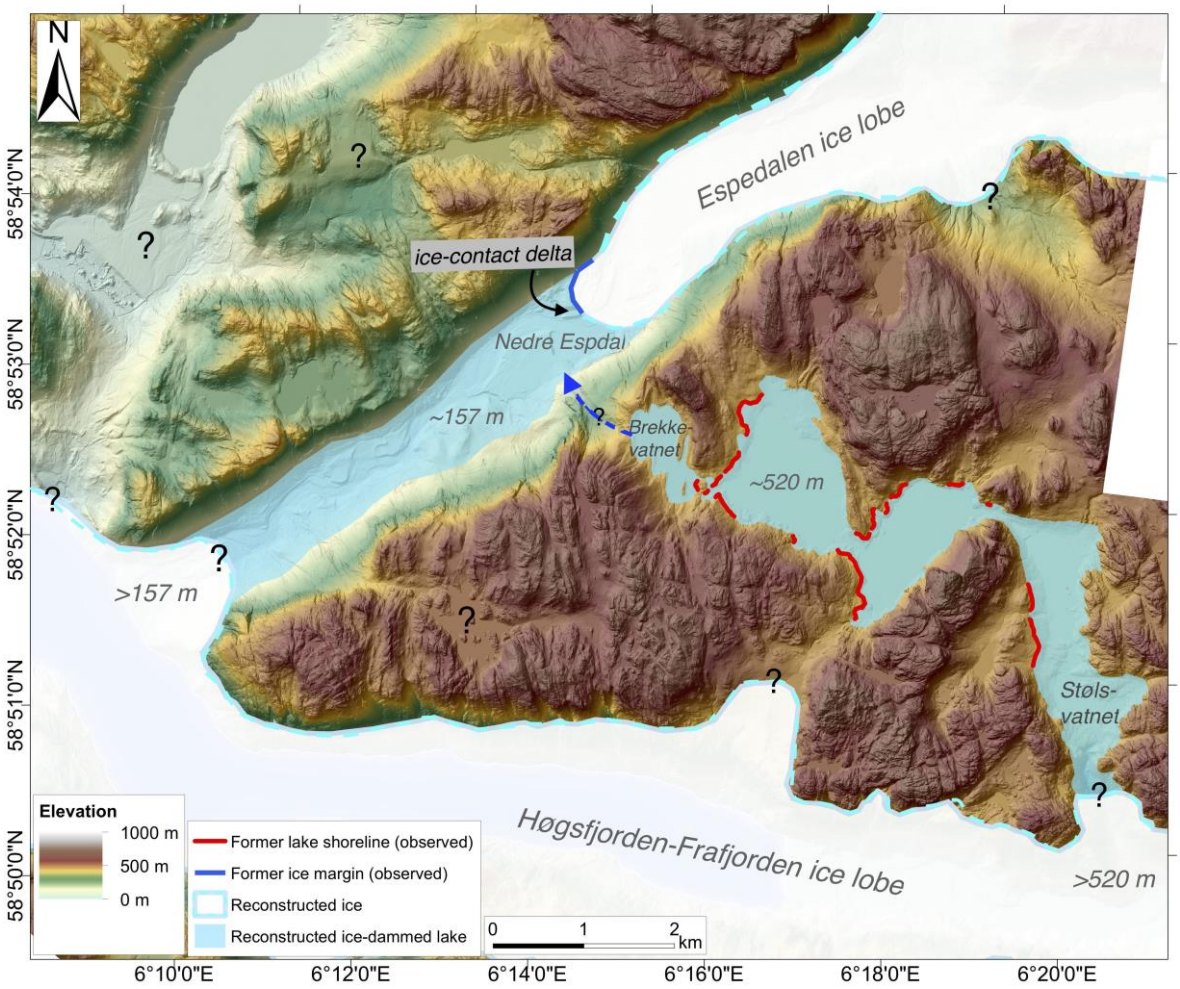

Figure 7.1. Reconstruction of the oldest ice-dammed lake phase in Espedalen dammed by an ice lobe in Høgsfjorden-Frafjorden that has a >157 m a.s.l. surface elevation across the mouth of Espedalen. A higher elevation ice-dammed lake southeast of Espedalen is reconstructed based on the mapped shoreline elevations and it likely existed contemporaneously to lake in Espedalen, dammed by the upfjord extension of the Høgsfjorden-Frafjorden ice lobe with a surface elevation >520 m a.s.l in inner Frafjorden. Discharge from the higher lake into the lower Espedalen lake through the secondary outlet at Brekkevatnet may have occurred (blue-dashed arrow). The reconstructed Høgsfjorden-Frafjorden ice lobe represents only a minimum approximation of ice extent, designated by the two ice-dammed lake elevations. The ice lobe extent in Espedalen is demonstrated by an ice-contact delta in Nedre Espedal. Surrounding areas not shown with lake or ice cover may or may not have been ice-free during this time.

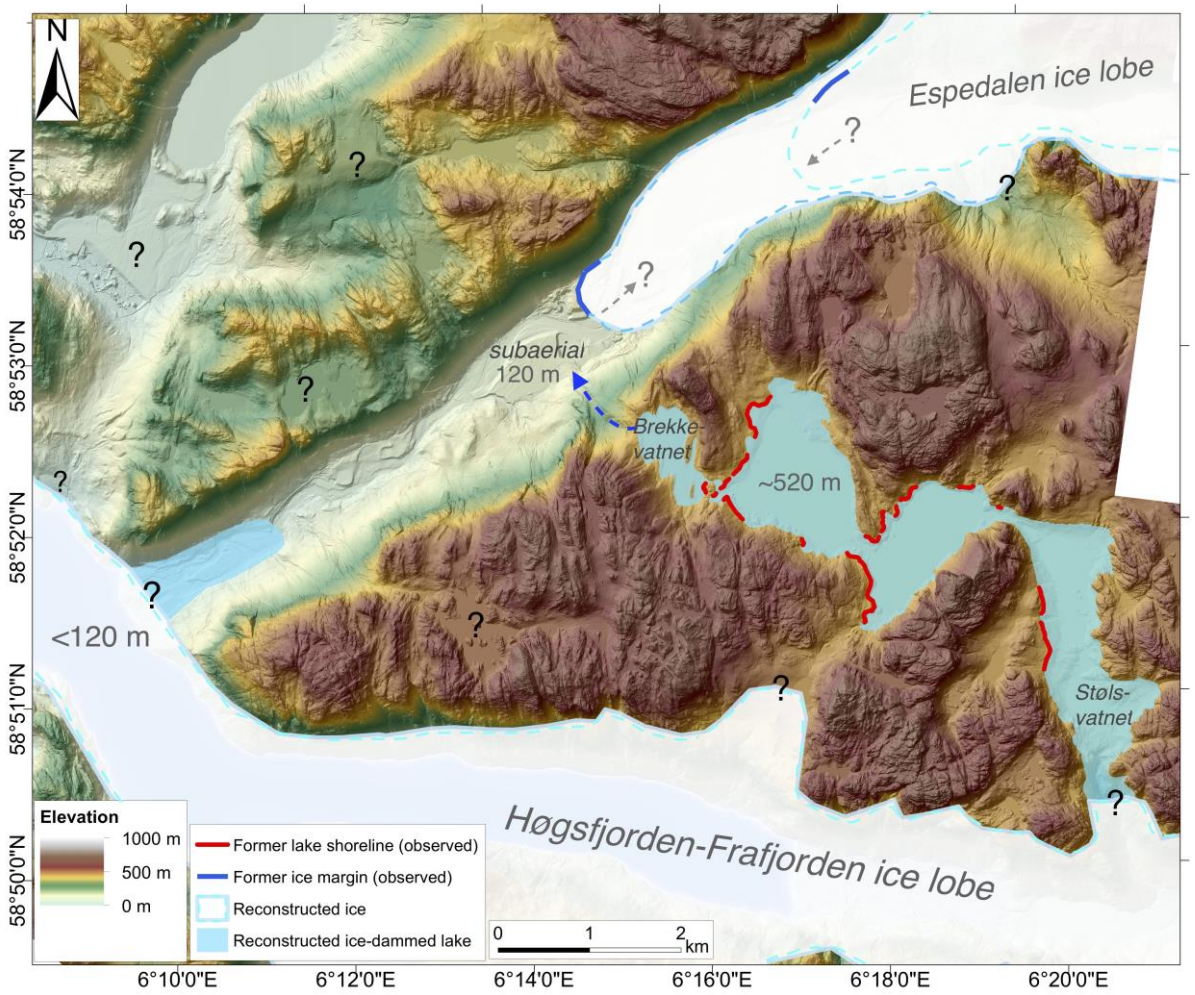

Figure. 7.2. Reconstructed environmental scenario subsequent to the oldest ice-dammed lake phase in Espedalen. Deposition of alluvial fan by Brekkevatnet outlet discharge (blue dashed-arrow) indicates subaerial conditions at 120 m a.s.l. in Nedre Espedalen. Contemporaneous position of the Espedalen ice lobe is unknown. The reconstructed Høgsfjorden-Frafjorden ice lobe at the mouth of Espedalen represents a maximum estimate of ice surface elevation, while the ice surface in inner Frafjorden is a minimum approximation of ice extent, designated by the Brekkevatnet outlet elevation. Surrounding areas not shown with lake or ice cover may or may not have been ice-free.

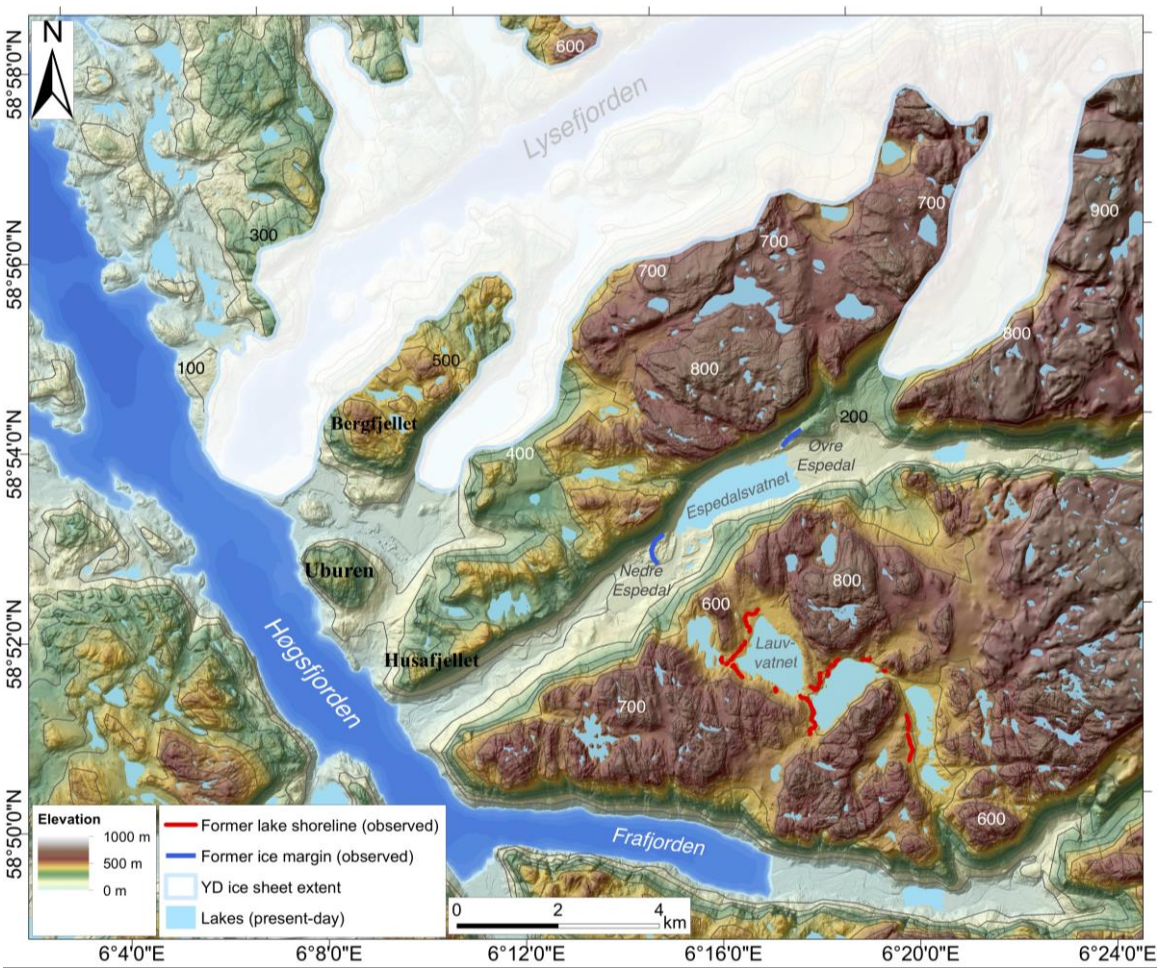

Figure 7.3. Overview map of the Lysefjorden-Høgsfjorden study region showing the ice sheet extent during the Younger Dryas, as mapped by Andersen (1954). 100-meter topographic contour intervals are shown, with particular elevations denoted by the black/white numbers. Older observed ice margins in Espedalen are outlined in blue.

7.3 Development of glaciofluvial/fluvial terraces

Aside from the glaciolacustrine terrace at Løland that corresponds to the oldest ice-dammed lake phase, all the Espedalen terraces would have been formed by fluvial/glaciofluvial processes after Espedalen became a subaerial following the presumed drainage of the lake. Of the several fluvial/glaciofluvial terrace generations observed in Espedalen, the higher lying terraces (> 60 m a.s.l.) seem to grade towards a water-body that is distinctly higher than the lower terraces (<40 m a.s.l.). Interestingly, the down-valley gradations of the higher terrace generations demonstrate a subtle, but evident flattening of surface gradient just prior to abruptly terminating at elevations of about 60, 80, and 120 m a.s.l. The flattening of surface gradients could very well be indicative of a deltaic terrace, but as of now, it cannot be stated with any certainty that the flatter terraces represent deltas based solely on surface gradient. As such, field observations of specific terrace stratigraphy and sedimentology is necessary to provide conclusive evidence of deltaic deposits.

Moving towards the valley mouth, the lower set of terraces that appear at ~40 m.a.s.l grade down to and just below the YD marine limit (~34 m a.s.l.;Anundsen, 1985). The ~34 m a.s.l. marine limit in Forsand is denoted by the elevation of a glaciomarine delta that is believed to correspond to the RSL high-stand reached by the end of Younger Dryas (Anundsen, 1985). The relative sea-level history of southwestern Norway indicates that there was a regional ~10-meter rise in RSL that initiated as early as the mid-Allerød, culminating near the end of the Younger Dryas (Lohne et al., 2007). Thus, the <40 m a.s.l. terraces may be grading towards a sea level within the range of the YD high-stand. Further investigation of terrace stratigraphy is necessary to more precisely determine the contemporaneous sea level. Overall, it is evident that the highest-lying fluvial/glaciofluvial terraces in Espedalen (>60 m a.s.l.) grade down to a significantly higher water body than the younger, lower terraces (40 m a.s.l.).

There are two potential theories that may explain the higher terraces gradation. The first theory proposes that when the ice-dammed lake in Espedalen drained, the valley was infiltrated by a contemporaneous post-glacial relative sea level (RSL) that was higher than that of the subsequent Younger Dryas marine limit. It is generally accepted that the Younger Dryas marine limit is the highest post-glacial relative sea level in southwestern Norway (Anundsen, 1985; Lohne et al., 2007; Vasskog et al., in press). However, the highest Espedalen terraces seem to grade to an even higher relative sea level (> 60 m a.s.l.) prior to the YD high-stand. If this were the case, then correspondingly high shoreline features should exists elsewhere in the region. LiDAR data were accordingly consulted in a search for any evidence of shorelines above the YD marine limit, but ultimately no such evidence was found. It should however be noted that shorelines are not always expressed as easily detectable features on LiDAR like beach ridges or terraces. Thus, a lack of obvious higher shorelines in the Lysefjorden-Høgsfjorden region on LiDAR is not necessarily conclusive evidence that relative sea level was never higher than the YD marine during the deglaciation. Overall, the RSL curves from the Boknafjord region do not show indications of RSL significantly higher than that of the YD high-stand (Figure 7.4). It is worth to note that the RSL shown by the southern Karmøy curve (Figure 7.4a) does show an RSL regressing from a level higher than the YD marine limit, but such a phenomenon occurs simply because Karmøy became ice-free rather early during the deglaciation (Vasskog et al, in press). As a result, it seems rather unlikely that Espedalen anomalously experienced an RSL greater than 60 m a.s.l prior to the YD transgression.

The second theory suggests that the Espedalen fluvial/glaciofluvial terraces are simply grading down to a gradually lowering ice-dammed lake level, which would be explained by the gradual thinning of the Høgsfjord ice lobe damming the valley. This latter theory is proposed as the most likely explanation for the seemingly high ‘sea level’ reflected by the terrace gradations, since it can also account for the abrupt drop in terrace elevation from ~60 to 40 m a.s.l. at ~1.6 km from the valley mouth postulated to reflect the complete draining of the ice-dammed lake in Espedalen.

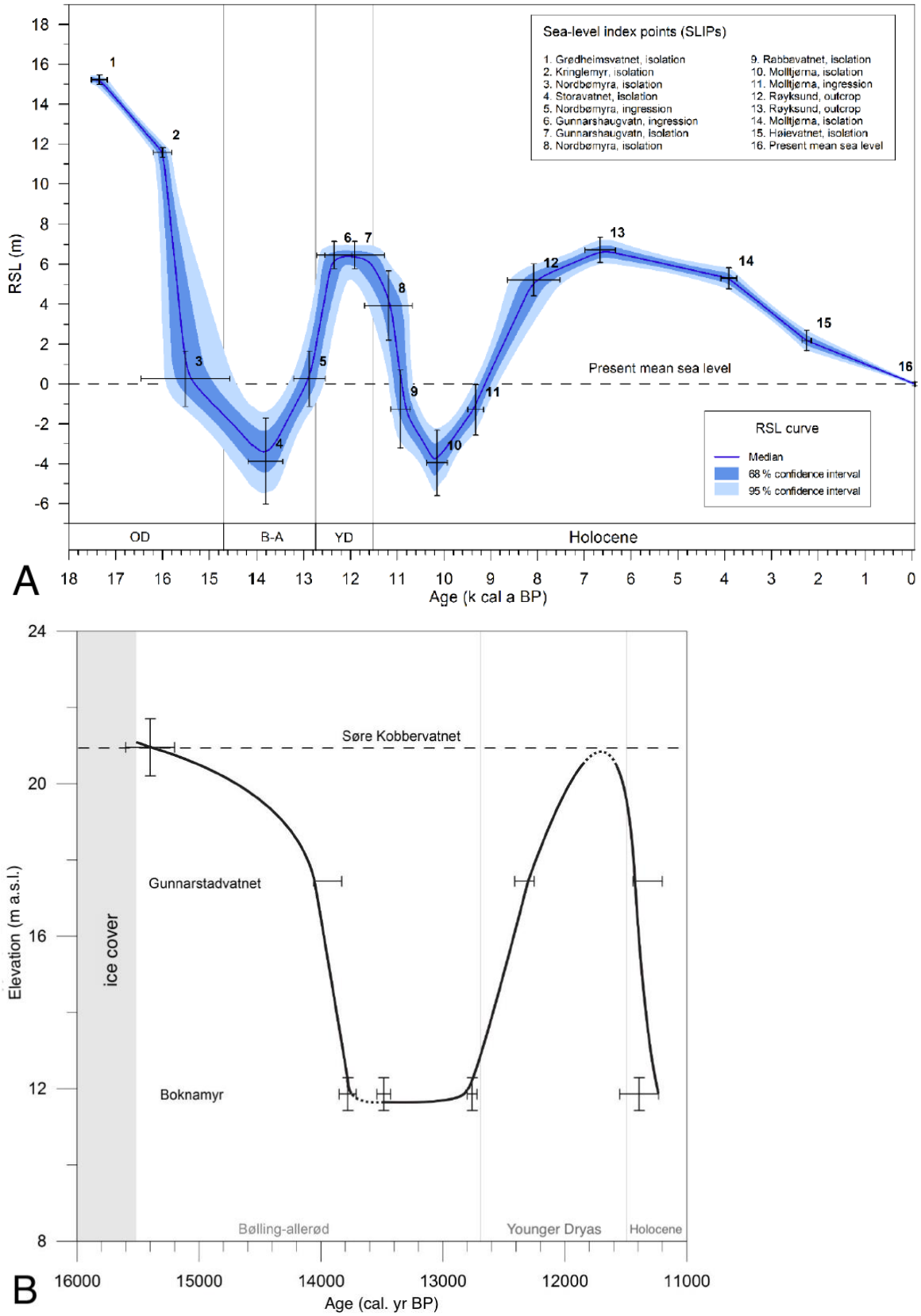

Figure 7.4. Relative sea level curves from (A) southern Karmøy (Vasskog et al., in press) and (B) Bokn (Strømsnes, 2018).

7.4 Environmental development of Espedalen during deglaciation

A simplified deglacial environmental development of Espedalen is presented based on the discussed sedimentological and geomorphological observations (Figure 7.5). During the oldest identified ice-dammed lake phase, an ice-contact delta was formed at an ice-front near Nedre Espedal, reflecting a local standstill in the ice retreat in the valley that presumably occurred sometime between ~15 ka and ~14 ka (Figure 7.5a). Following a subsequent lowering of lake level below 120 m a.s.l., glaciofluvial meltwater flows incised into the relict ice-contact delta, eventually forming the glaciofluvial terrace at Løland (Figure 7.5b). The progressive thinning of the Høgsfjord ice-dam resulted in gradual lake drainage, forming corresponding fluvial/glaciofluvial terraces that grade towards the gradually lowering ice-dammed lake level (Figure 7.5c). With the ultimate retreat of the Høgsfjorden ice lobe from the mouth of the valley, the ice-dammed lake completely drained down to a significantly lower contemporaneous sea level in Høgsfjorden (Figure 7.5d). Consequentially, a lower set of fluvial terraces formed that grade towards the new, relatively lower sea level that was likely transgressing towards or already at the Younger Dryas marine limit (Figure 7.5d). Moving forward to modern-day Espedalen, the river Espedalsåna flows towards the present-day level and a gravel pit has excavated the terraces at Løland (Figure 7.5e)

With the currently presented data and observations, it is not possible conclusively determine the timing of ice retreat from the initial position at Nedre Espedal relative to the drainage of the ice-dammed lake and the development of fluvial/glaciofluvial terraces within the valley. However, it can be stated with reasonable certainty that the Nedre Espedal ice front had retreated from its initial position by the time the lower set of terraces (<40 m a.s.l.) were formed, given that they seem to correspond to a sea level similar to, or just below the YD marine limit (Figure 7.5d). During the Younger Dryas, the ice margin in Espedalen was located further up-valley in Vinddalen (Figure 7.3; Andersen, 1954), after which it ultimately retreated with the onset of the Holocene (Figure 7.9, 7.10).

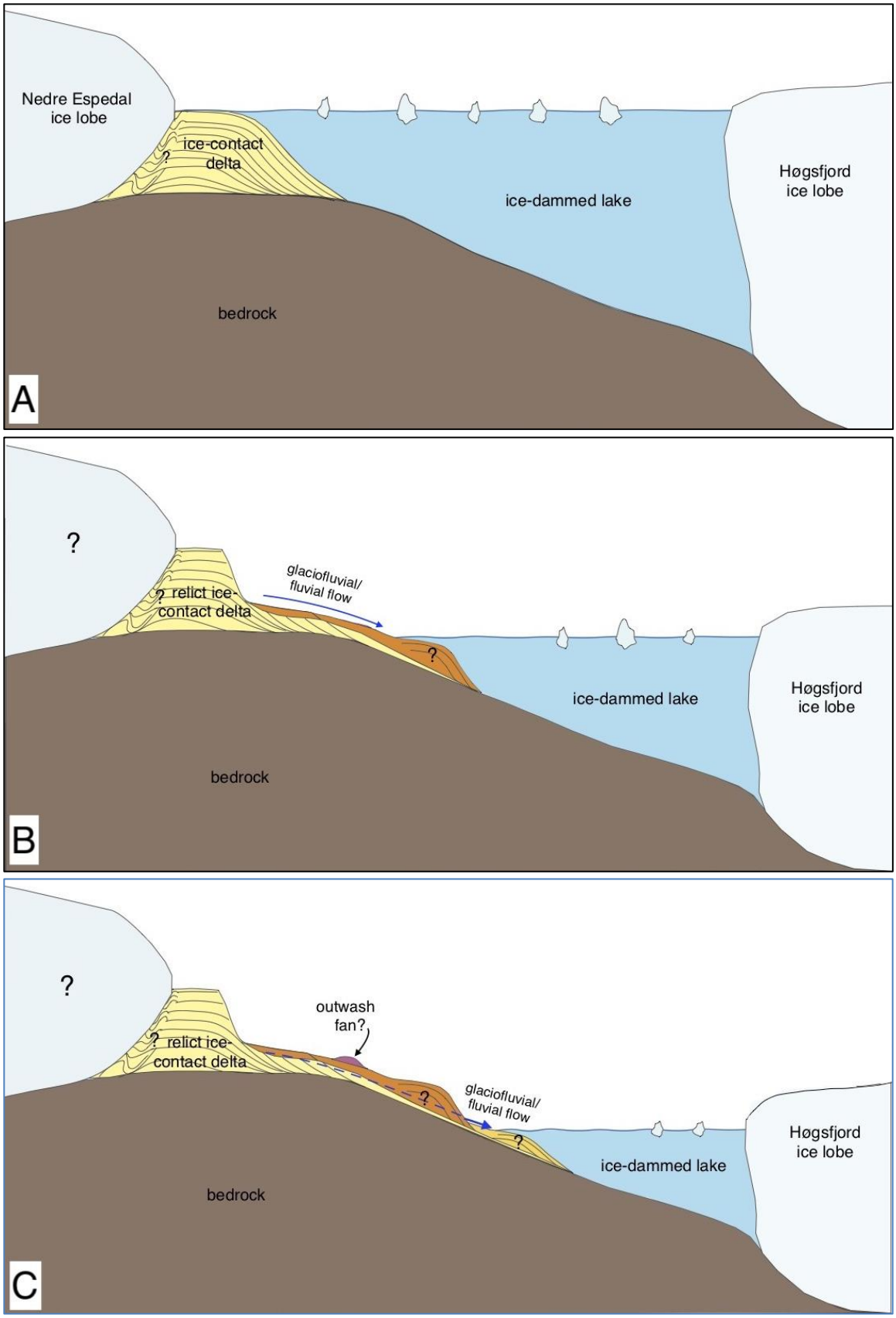
Nedre Espedal
ice lobe
ice-contact
delta
?
ice-dammed lake
Høgsfjord
ice lobe
bedrock
A
?
glaciofluvial/
fluvial flow
? relict ice-
contact delta
?
ice-dammed lake
Høgsfjord
ice lobe
bedrock
B
?
outwash
fan?
? relict ice-
contact delta
glaciofluvial/
fluvial flow
?
?
ice-dammed lake
Høgsfjord
ice lobe
bedrock
C

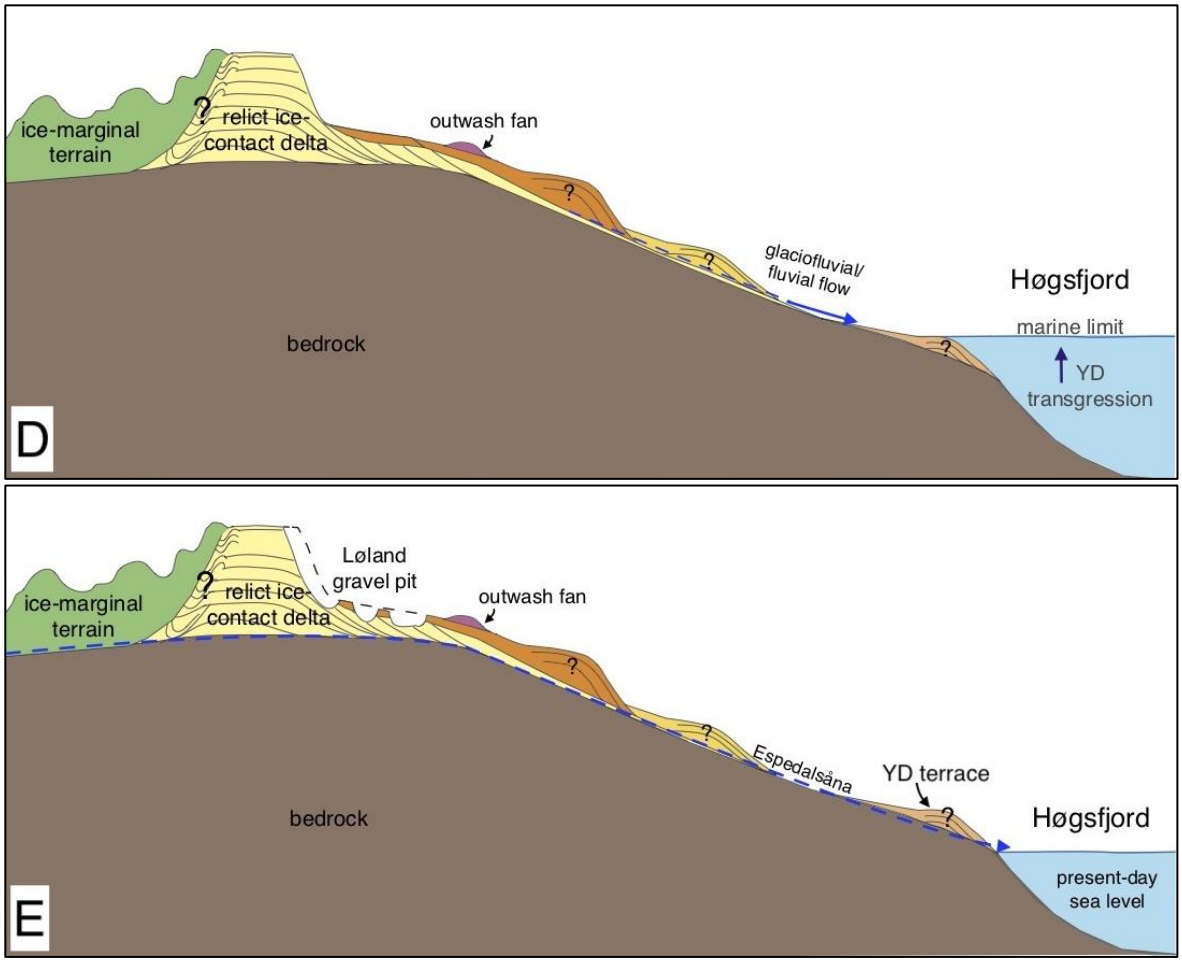

Figure 7.5. Cross-sections of Espedalen showing a simplified overview of its deglacial environmental development. (A) Oldest ice-dammed lake phase in Espedalen during which the ice-contact delta at Løland was formed. (B) Lowering of lake level results in the formation of the glaciofluvial terrace at Løland. (C) Further lowering of lake level caused by thinning ice in Høgsfjorden results in down-valley gradation of glaciofluvial/fluvial flows. Outwash fan has potentially been formed on a glaciofluvial terrace in Nedre Espedal. (D) Collapse of Høgsfjorden ice results in complete drainage of the lake in Espedalen. Outwash fan has been deposited on a glaciofluvial terrace in Nedre Espdal. Glaciofluvial/fluvial flows grade towards a rising relative sea level during the transgression that culminated at the YD marine limit. (F) Present-day Espedalen. Gravel pit excavated at Løland and the modern river Espedalsåna flows towards the present-day sea level in Høgsfjorden. Different terraces colors reflect different terrace generations. Figures are not to scale. Illustrated terrace stratigraphies are speculative, with the exception of the Løland glaciofluvial terrace.

7.5 Ice-margin fluctuations in Espedalen-Vinddalen

After being positioned in Nedre Espedalen, the ice margin ultimately retreated up the valley, leaving behind ice-marginal ridges and hummocky terrain with buried ice blocks at Nedre Espedalen that would eventually melt to form kettle hole lakes. The lateral moraine observed at Øvre Espedal seemingly reflects a younger ice margin than the one contemporaneous to the oldest ice-dammed lake phase at Nedre Espedal. This latter position of the ice margin at Øvre Espedal may represent a halt in ice retreat from its initial position in Nedre Espedal, or may even represent a readvance in the valley after retreating to an unknown degree, given its rather remarkable size. Nonetheless, the ice margin at Øvre Espedal is distal to the YD margin mapped by Andersen (1954), which is also delineated by several marginal moraine ridges in lower Vinddalen (Figure 7.5). Vinddalen is a valley that branches southwards from Lysefjorden, thus Andersen (1954) surmised that the ice that formed the moraines in Vinddalen was a southward extension from ice in Lysefjorden assumed to be of Younger Dryas age (Figure 7.3).

Hence, three distinct ice-front positions have been identified within Espedalen-Vinddalen, which seem to reflect a net ice-retreat through the valleys (Figure 7.5; Andersen, 1954; Holtedahl and Andersen 1960). Although the three identified margins initially seem to form a continuous retreat pattern up the valley, the prominent moraine ridges of the latter/younger two ice-margins are postulated to represent local readvances during the net deglaciation of the region. Compared to the prominent moraines at Øvre Espedal and in Vinddalen, the Nedre Espedal ice margin is markedly lacking in such distinctive moraines that might demonstrate a readvance. Accordingly, the Nedre Espedalen ice front is postulated to represent a halt or standstill in the ice retreat rather than a readvance (Figure 7.9). Although the duration of the standstill is unknown, the ice front would have to have been stable for long enough duration to allow for the formation of an ice-contact delta.

Assuming that the Vinndalen moraines correspond to the maximum extent of the regional YD ice readvance, the lateral moraine at Øvre Espedalen distal to the YD margin may correspond to an older, pre-YD readvance in the valley. Since this ice lobe probably terminated in Espedalsvatnet, a terminal moraine may potentially be found at the lake bottom. Though the bathymetry of Espedalsvatnet does not provide clear evidence of a morainic ridge (Figure 7.6), it is also possible that such a moraine was subsequently buried by substantial sediment accumulation at the lake bottom. Correspondingly, the bathymetry of Espedalsvatnet does reveal a rather flat lake bottom (Figure 7.3), suggesting that there has been significant post-glacial sediment accumulation in the lake.

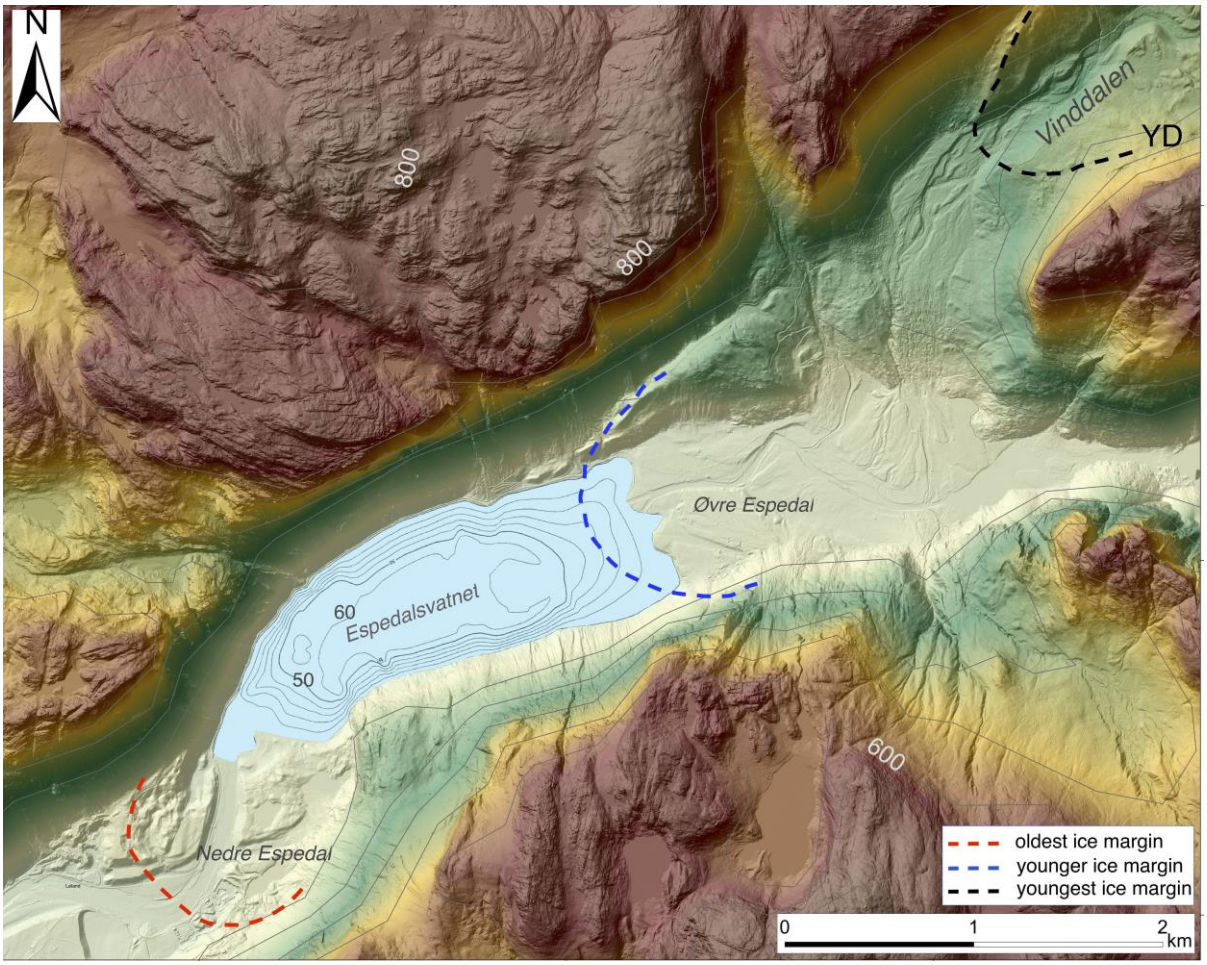

Figure 7.6. Approximate positions of former ice-margin in Espedalen-Vinndalen and their relative ages. Oldest ice margin (red dashed-line) corresponds to the Løland ice-contact delta. The younger margin (blue dashed-line) corresponds to the lateral moraine found along the northern slope of Øvre Espedalen and extends into the northeastern edge of Espedalsvatnet. The youngest margin (black dashed-line) corresponds to the Younger Dryas margin mapped by Andersen (1954). Topographic contour interval: 100 m. Bathymetric contour interval: 10 m. Espedalsvatnet bathymetry mapped by NIVA (1995), accessed through NVE (2015). Topographic contours provided by Kartverket (Norwegian Mapping Authority).

7.6 Evidence of Older Dryas ice advance in the Lysefjord region

Following the Bølling warm period, temperatures evidently underwent a gradual cooling over the course of the Bølling-Allerød (Rasmusen et al., 2014). Subsequently during the mid-Allerød to Younger Dryas, some regions of the Scandinavian ice sheet underwent an advance, particularly in southwestern Norway (Lohne et al., 2007; Mangerud et al., 2016a). However, studies have also found evidence of an Older Dryas (OD) ice advance in some parts of southwestern Norway that occurred within the Bølling-Allerød around 14 ka (Figure 7.10; Blystad and Anundsen, 1983; Briner et al., 2014; Mangerud et al., 2016a). Near the mouth of Hardangerfjorden just north of the Boknafjorden study area, the Older Dryas margin is found just outside the subsequent Younger Dryas margin, corresponding to a readvance around 14 ka (Mangerud et al., 2016a). Slightly to the north in the Bergen region, the Older Dryas ice sheet margin is believed to have been just slightly inland of the Younger Dryas and did not readvance like Hardangerfjorden lobe to the south (Mangerud et al., 2016b).

Further south in the Lysefjord region, Briner et al. (2014) used ^{10}Be dating to yield ages for the outer and inner moraine ridges of the Lysefjord moraine complex, demonstrating that the inner moraine is of Younger Dryas age, while the outer moraine is distinctly older with an age around 14 ka, corresponding instead to the Older Dryas (Figure 2.9). Thus the older outer moraine was separated from the Younger Dryas Lysefjord moraine complex and named the Leiken moraine. Conversely, the younger YD readvance evidently overran the older Leiken moraine at some places, particularly along the mouth of Lysefjorden (Briner et al., 2014). Just outside the YD moraines at the mouth of Lysefjorden, glacial erratics yielded a deglaciation age of ~14 ka, which corresponds to the age of the Leiken moraine (Figure 2.9, 4.34; Briner et al., 2014). Overall, the close proximity of the YD Lysefjord moraines and the OD Leiken moraine demonstrates that the ice extent during the Older Dryas was relatively similar to that of the Younger Dryas in the Lysefjord region (Figure 7.7), notwithstanding some local variations.

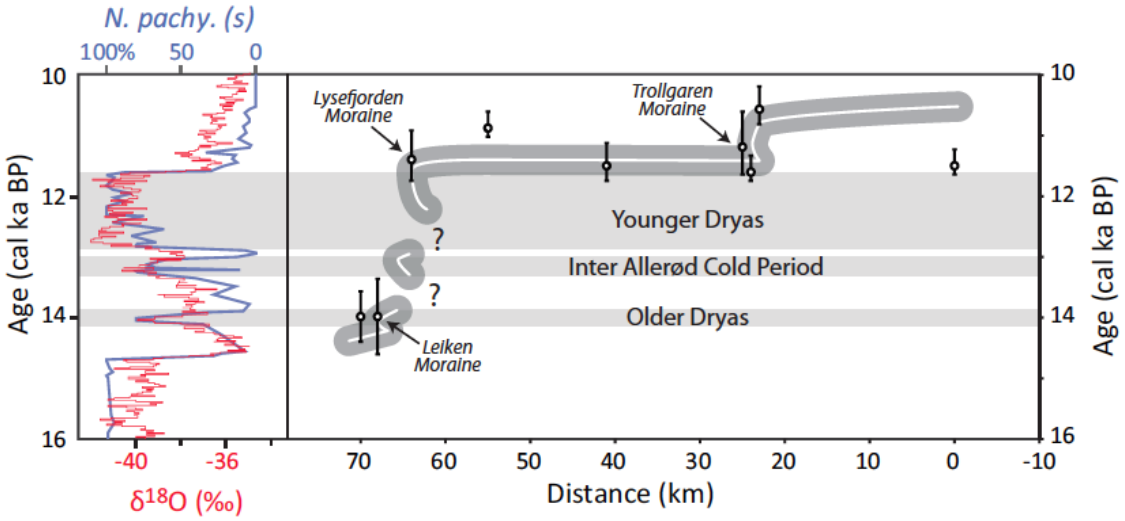

Figure 7.7. Time-distance diagram of the ice sheet retreat over the Lysefjord region correlated with a $\delta^{18}O$ record (NGRIPNgrip Members, 2004) and the *N.patchy.* (s) record (Haflidason et al., 1995; Mangerud et al., 2013). Diagram is based on ^{10}Be ages (Figure 2.9) and shows rapid ice retreat over Lysefjorden in a short span of time after the Younger Dryas (diagram presented by Briner et al., 2014).

Similar ice sheet extent during the OD to that of the YD is also indicated by radiocarbon ages of shells from a raised marine terrace and gyttja from a lake core just distal to the YD moraines near Jøsenfjorden, which place the ice margin within the vicinity of the YD ice extent by ~13.7 cal ka BP (Blystad and Anundsen, 1983). Furthermore, a GPR-based investigation of the sediments underlying the glaciofluvial sandur distal to Esmark's moraine in Forsand (Figure 1.3) also revealed evidence of an ice advance pre-dating the Younger Dryas (Karlsen, 2016). The GPR data revealed glaciofluvial deltaic strata corresponding to a 22 m a.s.l. relative sea level, which is overlain by a till that is deemed to have a similar age as the underlying delta (Karlsen, 2016). The till is overlain by marine sediments, above which are the glaciofluvial deposits associated with the YD Esmark's moraine (Karlsen, 2016). The 22 m a.s.l. glaciofluvial delta is believed to represent the Allerød sea level low-stand, and so a tentative relative sea level curve was constructed for Forsand (Figure 7.8 Karlsen, 2016). Moreover, several low-lying lateral moraines are located in the same area distal to Esmark's moraine, which were correlated with the buried till revealed by GPR (Karlsen, 2016). It was concluded that the till represents a pre-YD ice advance that occurred around the time of the Allerød low-stand, and so it was correlated with the Leiken moraine north of Lysefjorden given their similar ages (Karlsen, 2016).

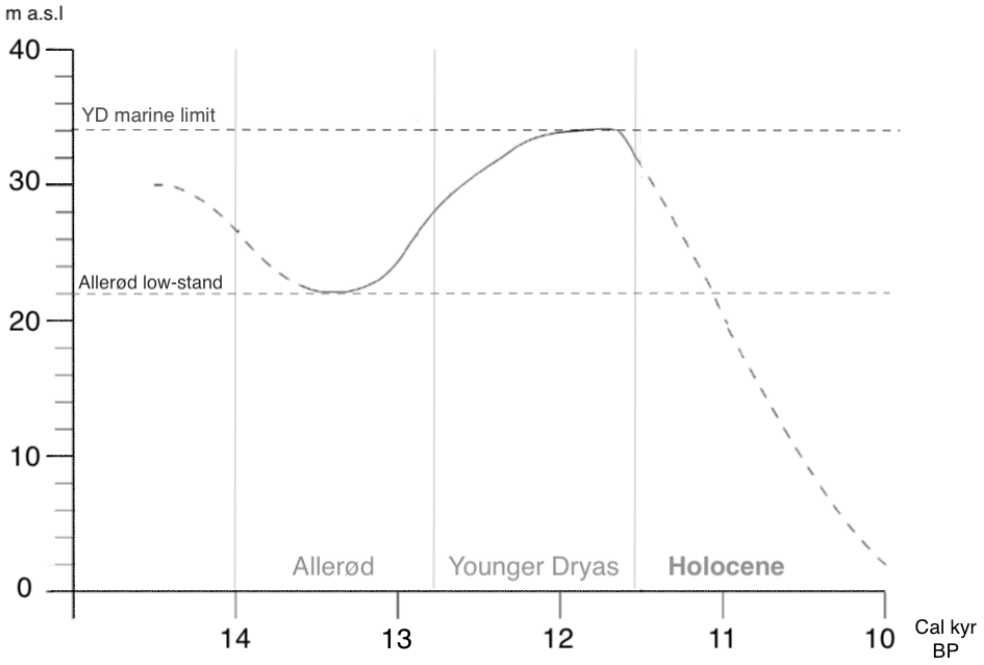

Figure 7.8. Relative sea level curve from Forsand (modified from Karlsen, 2016)

While the timing of the Allerød low-stand is not properly defined by the 22 m a.s.l. glaciofluvial delta at Forsand, a recent RSL curve based on radiocarbon dates from Bokn indicates that RSL reached the Allerød low-stand by ~13.8 cal ka BP (Figure 7.4b; Strømsnes, 2018), which statistically overlaps with the 14.0 ± 0.6 ka ^{10}Be age of the Leiken moraine (Briner et al., 2014). As such, a ~14 ka, Older Dryas age for the pre-YD till at Forsand seems quite conceivable. Once again, the buried till/lateral moraines found just outside Esmark's moraine in Forsand demonstrate that the ice extent during the OD was approximately comparable to that subsequently of the YD.

A similar scenario is observed in the neighboring Espedalen, where a lateral moraine in Øvre Espedal denotes a prominent ice margin distal to, yet relatively proximate to the YD margin in Vinddalen (Andersen, 1954). Thus, the Øvre Espdal ice margin could potentially belong to the same pre-YD regional ice advance identified in Forsand and in the northern Lysefjord area that corresponds to the Older Dryas (Briner et al., 2014; Karlsen, 2017). If the lateral moraine at Øvre Espdal is indeed approximately of Older Dryas age, then the Nedre Espedalen ice-contact delta and the oldest ice-dammed lake phase in Espedalen would have to have existed prior to ~14 ka (Figure 7.9). Finally, a ~15 ka ^{10}Be deglaciation age of mountaintops in Forsand provide a maximum limiting age for the Nedre Espedal ice-contact delta and the corresponding ice-dammed lake phase, since a valley such as Espedalen was likely still occupied by ice when the surrounding mountaintops started to become ice-free as a result of the thinning ice sheet. If the Øvre Espedal lateral moraine can truly be correlated to the Older

Dryas (~14 ka), then the Nedre Espedal ice front could be constrained to a period within ~15 and ~14 ka (Figure 7.9).

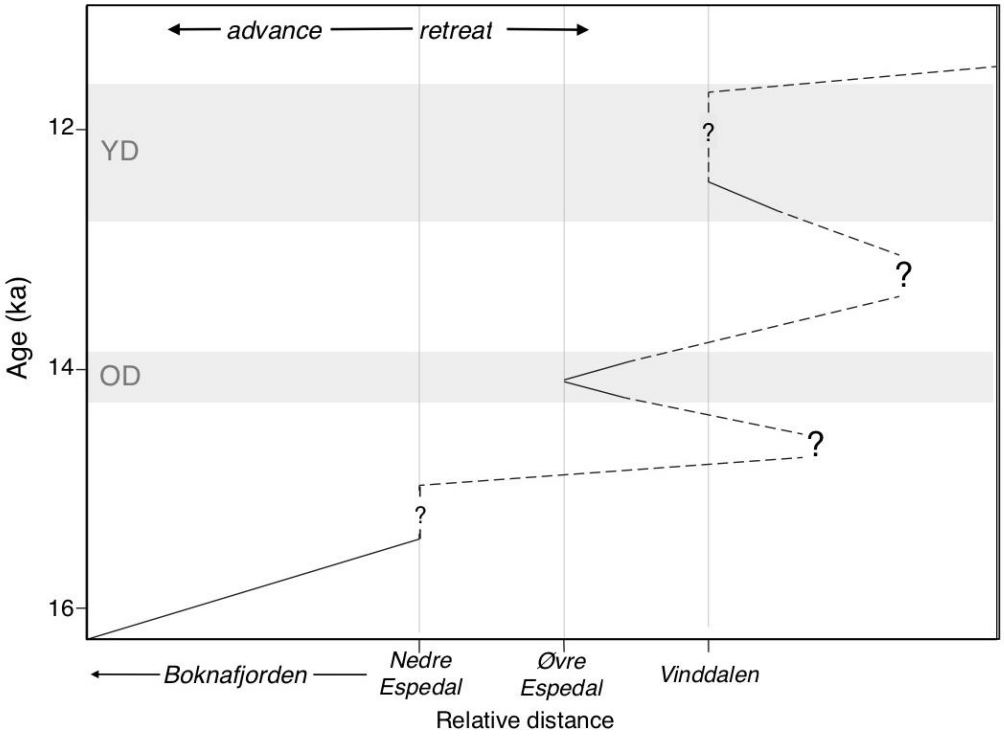

Figure 7.9. A tentative time-distance diagram of the ice sheet margin fluctuations in Espedalen-Vinddalen. The diagram is based on observed ice margins at Nedre Espedal, Øvre Espedal, and the Younger Dryas margin in Vinddalen mapped by Andersen (1954). Timing of the YD and OD ice advances shown in the diagram are adapted after the Lysefjorden/Ryfylke time-distance diagram by Briner et al. (2014) (Figure 7.10). YD, Younger Dryas; OD, Older Dryas. Relative distances are not to scale.

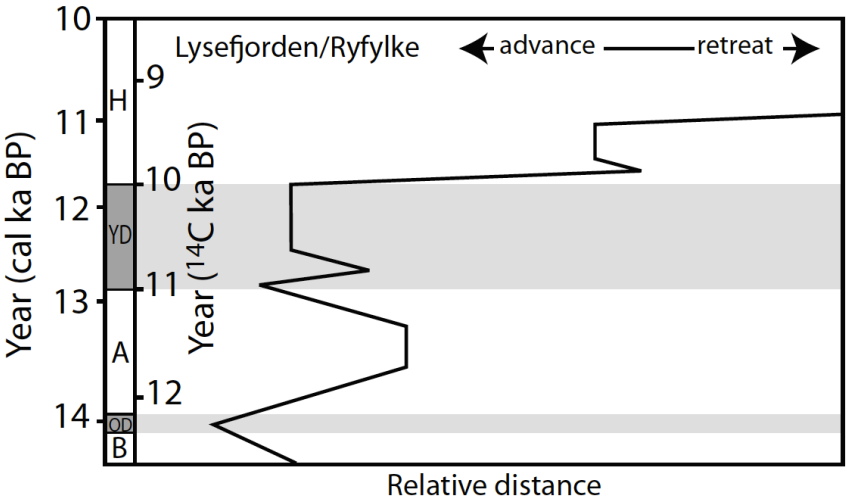

Figure 7.10. Time-distance diagram of the late glacial ice margin fluctuations in the Lysefjord-Ryfylke region. Diagram shows an ice advance during the Older Dryas (OD) as well as the Younger Dryas (YD) (presented by Briner et al., 2014).

8. Conclusions

- The striae assembled from the Boknafjord region demonstrate the changing orientations of the regional ice-flow during the last deglaciation as the ice thinned and retreated. The oldest identified flow is towards the north, which is consistent with the a northerly flow of the Norwegian Channel Ice Stream (NCIS) during the LGM. After the collapse of the NCIS, the inland ice flowed towards the west with an ice margin oriented off the coast of Karmøy while Utsira remained ice-free.
- A subsequent ice flow towards the southwest is expressed by both striae evidence and streamlined terrain around the mouth of Boknafjorden, which may correspond to a period of ice margin stability that potentially occurred sometime between 18 and 16 ka. Finally, a younger southerly flow along the northern Boknafjord region reflects the subsequent development of a calving margin in the fjord.

- ^{10}Be ages from two mountain summits in Forsand yielded largely scattered apparent deglaciation ages between ~18 and ~13 ka. ^{10}Be ages from Bergfjellet overestimate the age of deglaciation likely due to inheritance. Two overlapping ^{10}Be ages from Husafjellet suggest a deglaciation age of around 15 ka, but the overall large scatter in the resulting ages obscures the true age of deglaciation. Nonetheless, taken in conjunction with ^{10}Be ages provided from Uburen, the mountaintops in Forsand seem to have become ice-free around 15 ka.
- Two adjacent ice-dammed lakes existed in the Espedalen region prior to the Younger Dryas. The successive drainage of the ice-dammed lakes reflects the gradual thinning and eventual retreat of the Høgsfjord-Frafjord ice lobe.
- Two ice margins are observed in Espedalen distal to the Younger Dryas margin mapped by Andersen (1954) that could potentially be correlated with late glacial ice-margin fluctuations in the Lysefjord region. Although proper chronology has yet to be established, the Nedre Espedal ice-contact delta and corresponding ice-dammed lake phase may represent a standstill in the ice retreat, while the Øvre Espedal marginal moraine may correspond to a readvance of Older Dryas age.

Further research

The striations database for Rogaland may be applied to a variety of additional investigations into the ice flow patterns of the region, such as a detailed reconstruction of the ice margin geometry during retreat. Additional measurements may also be added to the database, particularly from areas that are currently lacking in measurements for a more comprehensive overview of the regional ice flow and retreat patterns.

Espedalen holds a great deal of potential for further investigation into the deglaciation history of the region. Further examinations of the stratigraphy and sedimentology of the exposed gravel pit sections in Nedre Espedalen may yield a more detailed reconstruction of the depositional environments in the valley. Field-examinations of the numerous terraces observed on LiDAR could also provide more information about the deglacial development of the valley. In the Lauvvatnet region just south of Espedalen, a surface trend model of the ice-dammed lake shorelines could be used to reconstruct the shoreline gradient and the isobases that correspond with the lake. It would also be interesting to sample some of the large boulders from the outwash fan at Nedre Espedal for ^{10}Be exposure dating, which could potentially help constrain the ages of the two ice-dammed lakes that existed in the Espedalen region. Finally, a sediment core from Espedalsvatnet may provide chronological constraints for the three identified ice-margins in the valley, in addition to a wealth of additional information concerning the deglacial history of Espedalen.

References

Åkesson, H., Morlighem, M., Nisancioglu, K. H., Svendsen, J. I. & Mangerud, J. 2018. Atmosphere-driven ice sheet mass loss paced by topography: Insights from modeling the south-western Scandinavian Ice Sheet. *Quaternary Science Reviews*, 195, 32-47.

Andersen, B. G. 1954. Randmorener i Sørvest-Norge. *Norsk Geografisk Tidsskrift,* 14, 273-342.

Andersen, B. G., Sejrup, H. P. & Kirkhus, Ø. 1983. Eemian and Weichselian Deposits at Bø on Karmøy, SW Norway: A Preliminary Report. *Norges Geologiske Undersøkelse*, 380, 189–201.

Andersen, B. G., Wangen, O. P. & Østmo, S.R. 1987. Quaternary geology of Jæren and adjacent areas, southwestern Norway. *Norges Geologiske Undersøkelse Bulletin*, 411.

Anundsen, K. 1972. Glacial chronology in parts of southwestern Norway. *Norges Geologiske Undersøkelse*, 280, l-24.

Anundsen, K. 1977. Radiocarbon datings and glacial striae from the inner part of Boknfjord area, South Norway. *Norsk Geografisk Tidrskrift*, 31, 41-54.

Anundsen, K. 1985. Changes in shore-level and ice-front position in Late Weichsel and Holocene, southern Norway. *Norsk Geografisk Tidsskrift*, 39.

Anundsen, K. 1990. Evidence of ice movement over southwest Norway indicating an ice dome over the coastal district of west Norway. *Quaternary Science Reviews*, 9, 99-116.

Balco, G. 2001. *Camelplot MATLAB script*. http://depts.washington.edu/cosmolab/pubs/gb_pubs/camelplot.m. Date accessed: 5 May 2019.

Balco, G. 2011. *What is a camel diagram anyway?* https://cosmognosis.wordpress.com/2011/07/25/what-is-a-camel-diagram-anyway/. Date accessed: 5 May 2019.

Balco, G., Stone, J. O., Lifton, N. A. & Dunai, T. J. 2008. A complete and easily accessible means of calculating surface exposure ages or erosion rates from ^{10}Be and ^{26}Al measurements. *Quaternary Geochronology*, 3, 174–195.

Benn, D. I. & Evans, D. J. A. 2010: *Glaciers and Glaciation*. Hodder Education, London.

Benson, L., Madole, R., Phillips, W., Landis, G., Thomas, T., Kublik, P. 2004. The probable importance of snow and sediment shielding on cosmogenic ages of north-central Colorado Pinedale and pre-Pinedale moraines. *Quaternary Science Reviews*, 23, 193–206.

Bentley, C. R., 1987. Antarctic ice streams: a review. *Journal of Geophysical Research,* 92 (B9), 8843–8858.

Blystad, R. & Anundsen, K. 1983. Late Weichselian stratigraphy at Hielmeland, Southwest Norway. Norsk Geologisk Tidsskrift, 63, 277–287.

Bøe, R., Hovland, M., Instanes, A., Rise, L. & Vasshus, S. 2000. Submarine slide scars and mass movements in Karmsundet and Skudenesfjorden, southwestern Norway: Morphology and evolution. *Marine Geology*, 167, 147-165.

Brække, H. Betydning av postglasial forvitring, glasial erosjon og tektonikk som landskaputviklende agenser i Lyse, Rogaland. MSc thesis. Department of Earth Science, University of Bergen, in prep.

Briner, J. P., Goehring, B. M., Mangerud, J. & Svendsen, J. I. 2016. The deep accumulation of ^{10}Be at Utsira, southwestern Norway: Implications for cosmogenic nuclide exposure dating in peripheral ice sheet landscapes. *Geophysical Research Letters*, 43, 9121-9129.

Briner, J. P., Svendsen, J. I., Mangerud, J., Lohne, Ø. S. & Young, N. E. 2014. A ^{10}Be chronology of south- western Scandinavian Ice Sheet history during the Lateglacial period. *Journal of Quaternary Science*, 29, 370-380.

CERN. 2019. *Cosmic rays: particles from outer space.* Geneva: CERN. https://home.cern/science/physics/cosmic-rays-particles-outer-space. Date accessed: 14 March 2019.

Chamberlin, T. C. 1883. Preliminary paper on the terminal moraine of the second glacial epoch. Gov't print. off.

CRONUS-Earth 2009: *CRONUS-Earth online cosmogenic nuclide calculators*. http://hess.ess.washington.edu/math/. Date accessed: 16 April 2019.

Dorn, R. I. & Phillips, F. M. 1991. Surface exposure dating: review and critical evaluation. *Physical Geography*, 12, 303-333.

Dowman, I. J. 2004. Integration of LiDAR and IFSAR for mapping. *International Archives of Photogrammetry and Remote Sensing*, 35, 90-100.

Egholm, D.L., Jansen, J. D., Pedersen, V. K., Linge, H., Dühnforth, M., Andersen, J. L., Jacobsen, B.H., Skov, D., Knudsen, M.F. 2018. Glacial erosion and relief production on gneiss-granite plateaus. *EGU General Assembly Conference Abstracts*, 20, 17330.

Eilertsen, R. S., Corner, G. D. & Hansen, L., 2015. Using LiDAR data to characterize and distinguish among different types of raised terraces in a fjord-valley setting. *GFF*, 137, 353–361.

Garnes, K. 1976. Stratigraphi og morfogenese av drumliner på Eigerøya, Rogaland, SV-Norge. *Arkeologisk museum i Stavanger*, 1, 5-53.

Glennie, C. L., Carter, W. E., Shrestha, R. L. & Dietrich, W. E. 2013. Geodetic imagine with airborne LiDAR: the Earth's surface revealed. *Reports on Progress in Physics*, 76**,** 086801.

Goehring, B. M., Lohne, O. S., Mangerud, J., Svendsen, J. I., Gyllencreutz, R., Schaefer, J. & Finkel, R. 2012a. Late glacial and Holocene ^{10}Be production rates for western Norway. *Journal of Quaternary Science*, 27, 89–96.

Goehring, B. M., Lohne, O. S., Mangerud, J., Svendsen, J. I., Gyllencreutz, R., Schaefer, J. & Finkel, R. 2012b. Erratum: Late glacial and Holocene ^{10}Be production rates for western Norway. *Journal of Quaternary Science*, 27, 544–544.

Gosse, J. C. & Phillips, F. M. 2001. Terrestrial in situ cosmogenic nuclides: theory and application. *Quaternary Science Reviews*, 20**,** 1475-1560.

Grant, O.R. 2016. The deglaciation of Kongsfjorden, Svalbard – based on surface exposure dating of glacial erratics and Quaternary geological mapping of Blomstranhalvøya. MSc thesis. Department of Earth Science, University of Bergen, 126 pp.

Gump, D., Briner, J. P., Mangerud, J. & Svendsen, J. I. 2016. The deglaciation of Boknafjorden, southwestern Norway. Journal of Quaternary Science, 32 (1), 80-90.

Haflidason, H., Sejrup, H. P., Klitgaard Kristensen, D., Johnsen, S. 1995. Coupled response of the late glacial climatic shifts of northwest Europe reflected in Greenland ice cores: evidence from the northern North Sea. *Geology*, 23, 1059–1062.

Helle, S. K., Rye, N., Stabell, B., Prösch-Danielsen, L., & Hoel, C. 2007. Neotectonic faulting and the Late Weichselian shoreline gradients in SW Norway. *Journal of Geodynamics*, 44, 96-128.

Hernar, M. K. 2017. Deglasiasjon og strandforskyvning på Bokn, Sørvest-Norge. MSc thesis. Department of Earth Science, University of Bergen, 82 pp.

Hestmark, G. 2018. Jens Esmark's mountain glacier traverse 1823 - the key to his discovery of Ice Ages. *Boreas*, 47, 1–10.

Heymman, J., Stroeven, A. P., Johathan, M. H. & Caffee, M. W. 2011. Too young or too old: Evaluating cosmogenic exposure dating based on an analysis of complied boulder exposure ages. *Earth and Planetary Sciences*, 302, 71-80.

Hjelstuen, B. O., Nygård, A., Sejrup, H. P. & Haflidason, H. 2012. Quaternary denudation of southern Fennoscandia - evidence from the marine realm. *Boreas* 41, 379–390.

Holtedahl, O. & Andersen, B.G. 1960. Glacial Map of Norway. *Norges Geologiske Undersøkelse*, 208.

Hoppe, G. 1948. Isrecessionen från Norrbottens kustland i belysning av de glaciala formelementen. *Geographica*, 20, 112 pp.

Hughes, A. L. C., Gyllencreutz, R., Lohne, Ø. S., Mangerud, J. & Svendsen, J. I. 2016. The last Eurasian ice sheets–a chronological database and time‐slice reconstruction, DATED‐1. *Boreas 45*, 1-45.

Imbrie J., Boyle E.A., Clemens S.C., Duffy A., Howard W.R., Kukla G., Kutzbach J., Martinson D.G., McIntyre A., Mix A.C., Molfino B., Morley J.J., Peterson L.C., Pisias N. G., Prell W.L., Raymo M.E., Shackleton N.J., Toggweiler J.R. 1992. On the Structure and Origin of Major Glaciation Cycles 1. Linear Responses to Milankovitch Forcing. *Paleooceanography*, 7, 701-738.

Imbrie, J., Berger, A., Boyle, E.A., Clemens, S.C., Duffy, A., Howard, W.R., Kukla, G., Kutzbach, J., Martinson, D.G., McIntyre, A., Mix, A.C., Molfino, B., Morley, J.J., Peterson, Larry C, Pisias, N.G., Prell, W.L., Raymo, M.E., Shackleton, N.J., Toggweiler, J.R. 1993. On the structure and origin of major glaciation cycles 2. The 100,000‐year cycle. *Paleooceanography*, 8, 699-735.

Iverson, N.R. 1991. Morphology of glacial striae - implications for abrasion of glacier beds and fault surfaces. *Geological Society of America Bulletin*, 103, 1308-1316.

Ivy-Ochs, S. & Florian, K. 2008. Surface exposure dating with cosmogenic nuclides. *Eiszeitalter und Gegenwart Quaternary Science Journal*, 57(1-2), 179-209.

Ivy-Ochs, S., Kerschner, H., & Schluchter, C. 2007. Cosmogenic nuclides and the dating of Lateglacial and Early Holocene glacier variations: The Alpine perspective. *Quaternary International*, 164-165**,** 53-63.

Jansson, K. N., Kleman, J. & Marchant, D. R. 2002. The succession of ice-flow patterns in north-central Quebec-Labrador, Canada. *Quaternary Science Reviews*, 21, 503-523.

Johnsen, I. S. 2017. Strandforskyvning på Bokn og deglasiasjonen av Boknafjorden, Rogaland. MSc thesis. Department of Earth Science, University of Bergen, 113 pp.
Johnson, M. D., Fredin, O., Ojala, A.E.K. & Peterson, G. 2015. Unraveling Scandinavian geomorphology: the LiDAR revolution. *GFF*, 137**,** 245-251.
Jonsdottir, H. E., Sejrup, H. P., Larsen, E. & Stalsberg, K. 1999. Late Weichselian ice-flow directions in Jæren, SW Norway: clast fabric and clast lithology evidence in the uppermost till. *Norsk Geografisk Tidsskrift*, 53, 177–189.
Karlsen, F. H. 2016. Geofysiske og sedimentologiske undersøkelser av israndavsetningene fremfor Esmarkmorenen, Rogaland. MSc thesis. Department of Earth Science, University of Bergen, 94 pp.
Karlsen, L. C. 2009. Lateglacial vegetation and environment at the mouth of Hardangerfjorden, western Norway. *Boreas*, 38, 315–334.
Kartverket. 2019. *Høydedata*. Norwegian Mapping Authority. https://hoydedata.no/LaserInnsyn/. Date accessed: 21 February 2019.
Kleman, J. 1990. On the use of glacial striae for reconstruction of paleoicesheet flow patterns. *Geografiska Annaler Series A-Physical Geography*, 72, 217-236.
Knudsen, C.G. 2006. Glacier dynamics and Lateglacial environmental changes – evidences from SW Norway and Iceland. PhD Thesis, University of Bergen.
Lal, D. & Peters, B. 1967. Cosmic ray produced radioactivity on the Earth. *Handbuch der Physik*, 551-612.
Lal, D. 1991. Cosmic ray labeling of erosion surfaces: in-situ nuclide production rates and erosion models. *Earth and Planetary Science Letters*, 104**,** 424-439.
Lambeck, K., Rouby, H., Purcell, A., Sun, Y. & Sambridge, M. 2014 . Sea level and global ice volumes from the Last Glacial Maximum to the Holocene. *Proceedings of the National Academy of Sciences*, 111, 15296-15303.
Lang, J., Sievers, J., Loewer, M., Igel, J., Winsemann, J. 2017. 3D architecture of cyclic-step and antidune deposits in glacigenic subaqueous fan and delta settings: Integrating outcrop and ground-penetrating radar data. *Sedimentary Geology*, 262, 83-100.
Larsen, E., Sejrup, H. P., Janocko, J., Landvik, J. Y., Stalsberg, K. & Steinsund, P. I. 2000. Recurrent interaction between the Norwegian Channel Ice stream and terrestrial-based ice across southwest Norway. *Boreas*, 29, 185-203.
Lohne, Ø. S., Bondevik, S., Mangerud, J. & Svendsen, J. I. 2007. Sea-level fluctuations imply that the Younger Dryas ice-sheet expansion in western Norway commenced during the Allerød. *Quaternary Science Reviews*, 26, 2128-2151.
Lohne, Ø. S., Mangerud, J. & Birks, H. H. 2013. Precise ^{14}C ages of the Vedde and Saksunarvatn ashes and the Younger Dryas boundaries from western Norway and their comparison with the Greenland Ice Core (GICC 05) chronology. *Journal of Quaternary Science*, 28, 490-500.
Lohne, Ø. S., Mangerud, J. & Birks, H. H. 2014. IntCal13 calibrated ages of the Vedde and Saksunarvatn ashes and the Younger Dryas boundaries from Kråkenes, western Norway. *Journal of Quaternary Science*, 29(5), 506-507.
Lønne, I. 1993. Physical signatures of ice advance in a Younger Dryas ice-contact delta, Troms, northern Norway: implications for glacier-terminus history. *Boreas*, 22, 59-70.
Mangerud, J., Aarseth, I., Hughes, A. L. C., Lohne, Ø. S., Skår, K., Sønstegaard, E. &

Svendsen, J. I. 2016a. A major re-growth of the Scandinavian Ice Sheet in western Norway during Allerød-Younger Dryas. *Quaternary Science Reviews*, 132, 175-205.

Mangerud, J., Briner, J. P., Goslar, T. & Svendsen, J. I. 2016b. The Bølling-age Blomvåg Beds, western Norway: implications for the Older Dryas glacial re-advance and the age of the deglaciation. *Boreas*, 46, 162-184.

Mangerud, J., Goehring, B. M., Lohne, Ø.S., Svendsen, J. I. & Gyllencreutz, R. 2013. Collapse of marine-based outlet glaciers from the Scandinavian Ice Sheet. *Quaternary Science Reviews*, 67, 8–16.

Mangerud, J., Gulliksen, S. & Larsen, E. 2010. ^{14}C-dated fluctuations of the western flank of the Scandinavian Ice Sheet 45–25 kyr BP compared with Bølling–Younger Dryas fluctuations and Dansgaard–Oeschger events in Greenland. *Boreas*, 39, 328–342.

Mangerud, J., Gyllencreutz, R., Lohne, Ø. & Svendsen, J. I. 2011. Glacial History of Norway.

Mangerud, J., Hughes, A. L. C., Sæle, T. H. & Svendsen, J. I. 2019. Ice-flow patterns and precise timing of ice sheet retreat across a dissected fjord landscape in western Norway. *Quaternary Science Reviews*, 214, 139-163.

Mangerud, J., Sønstegaard, E., Sejrup, H. P., Haldorsen, S., 1981. A continuous Eemian-Early Weichselian sequence containing pollen and marine fossils at Fjøsanger, western Norway. *Boreas*, 10, 137-208.

McCabe, A. M. & Eyles, N. 1988. Sedimentology of an ice-contact glaciomarine delta, Carey Valley, Northern Ireland. *Sedimentary Geology*, 59, 1-14.

Menzies, J. 1979. A review of the literature on the formation and location of drumlins. *Earth Science Reviews,* 14, 315-359.

Miller, G. H., Sejrup, H. P., Mangerud, J. & Andersen, B. G. 1983. Amino acid ratios in Quaternary molluscs and foraminifera from western Norway: correlation, geochronology and paleotemperature estimates. *Boreas*, 12, 107-124.

Möller, P. & Dowling T. P. F. 2015. The importance of thermal boundary transitions on glacial geomorphology, mapping of ribbed/hummocky moraine and streamlined terrain from LiDAR, over Småland, South Sweden. *GFF,* 137**,** 252-283.

Morén, B. M., Sejrup, H.P., Hjelstuen, B. O., Borge, M. V. & Schäuble, C. 2018. The last deglaciation of the Norwegian Channel – geomorphology, stratigraphy and radiocarbon dating. *Boreas*, 47, 347-366.

NGRIP Project Members. 2004. High-resolution record of Northern Hemisphere climate extending into the last interglacial period. *Nature,* 431, 147–151.

NGU 2019. *Berggrunn: National bedrock database for bedrock.* Geological Survey of Norway. http://geo.ngu.no/kart/berggrunn/?lang=English. Date accessed: 24 April 2019.

Nishiizumi, K., Imamura, M., Caffee, M. W., Southon, J. R., Finkel, R. C. & McAninch, J. 2007. Absolute calibration of ^{10}Be AMS standards. *Nuclear Instruments and Methods*, 258, 403–413.

Nishiizumi, K., Kohl, C. P., Arnold, J.R., Dorn, R., Klein, J., Fink, D., Middleton, R. & Lal, D. 1993. Role of *in situ* cosmogenic nuclides ^{10}Be and ^{26}Al in the study of diverse geomorphic processes. *Earth Surface Processes and Landforms,* 18**,** 407-425.

NVE 2015. *Innsjødatabase*. Norwegian Water Resources and Energy Directorate. https://gis3.nve.no/dybdekart/dk1661.pdf. Date accessed: 21 May 2019.

Nygård, A., Sejrup, H. P., Haflidason, H. & Bryn, P. 2005. The glacial North Sea Fan, southern Norwegian Margin: architecture and evolution from the upper continental slope to the deep-sea basin. *Marine and Petroleum Geology*, 22, 71–84.

Nygård, A., Sejrup, H. P., Haflidason, H., Lekens, W. A. H., Clark, C. D. & Bigg, G. R. 2007. Extreme sediment and ice discharge from marine based ice streams: new evidence from the North Sea. *Geology*, 35, 395–398.

Ojala, A. E. K., Palmu, J. P., Åberg, A., Åberg, S. & Virkki, H. 2013. Development of an ancient shoreline database to reconstruct the Litorina Sea maximum extension and the highest shoreline of the Baltic Sea basin in Finland. *Bulletin of the Geological Society of Finland*, 85**,** 127-144.

Ojala, A. E. K., Putkinen, N., Palmu, J. P. & Nenonen, K. 2015. Characterization of De Geer moraines in Finland based on LiDAR DEM mapping. *GFF*, 137**,** 204-318.

Økland, S. 1947. En undersøkelse av skuringsstripenes retning på ytre og mellomste del av Haugesunds-halvøya. Unpublished cand. real. thesis, Department of Geology, University of Oslo.

Ottesen, D., Dowdeswell, J. A. & Rise L. 2005. Submarine landforms and the reconstruction of fast-flowing ice streams within a large Quaternary ice sheet: the 2500-km-long Norwegian-Svalbard margin (57°–80°N). *Geological Society of America Bulletin*, 117, 1033–1050.

Ottesen, D., Stokes, C. R., Bøe, R., Rise, L., Longva, O., Thorsnes, T., Olesen, O., Bugge, T., Lepland, A. & Hestvik, O. B. 2016. Landform assemblages and sedimentary processes along the Norwegian Channel Ice Stream. *Sedimentary Geology*, 338, 115-137.

Paterson, W. S. B. 1994. The physics of glaciers, Oxford, Butterworth/Heinemann.

Patterson, C.J. & Hooke, R. Le B. 1996. Physical environment of drumlin formation. *Journal of Glaciology*, 41, 30-38.

Paus, A. 1988. Late Weichselian vegetation, climate, and floral migration at Sandvikvatn, North-Rogaland, Southwestern Norway. *Boreas*, 17, 113-139.

Powell, R. D. 1990. Glacimarine processes at grounding-line fans and their growth to ice-contact deltas. In: Dowdeswell, J.A., Scourse, J.D. (Eds.), Glacimarine Environments: Processes and Sediments. *Geological Society of London, Special Publication*, 53, 53–73.

Rasmussen, S. O., Andersen, K. K., Svensson, A. M., Steffensen, J.P., Vinther, B. M., Clausen, H. B., Siggaard-Andersen, M. L., Johnsen, S. J., Larsen, L. B., Dahl-Jensen, D., Bigler, M., Röthlisberger, R., Fischer, H., Goto-Azuma, K., Hansson, M. E. & Ruth, U. 2006. A new Greenland ice core chronology for the last glacial termination. *Journal of Geophysical Research*, 111, D06102.

Rasmussen, S. O., Bigler, M., Blockley, S. P., Blunier, T., Buchardt, S. L., Clausen, H. B., Cvijanovic, I., Dahl-Jensen, D., Johnsen, S. J., Fischer, H., Gkinis, V., Guillevic, M., Hoek, W. Z., Lowe, J. J., Pedro, J. B., Popp, T., Seierstad, I. K., Steffensen, J. P., Svensson, A.M., Vallelonga, P., Vinther, B. M., Walker, M. J. C., Wheatley, J. J., Winstrup, M., 2014. A stratigraphic framework for abrupt climatic changes during the Last Glacial period based on three synchronized Greenland ice-core records: refining and extending the INTIMATE event stratigraphy. *Quaternary Science Reviews*, 106, 14-28.

Raunholm, S., Larsen, E. and Sejrup, H. P. 2004. Weichselian interstadial sediments on Jæren (SW Norway) – paleo environments and implications for ice sheet configuration. *Norwegian Journal of Geology*, 84, 91–106.

Raunholm, S., Sejrup, H. P. & Larsen, E. 2003. Lateglacial landform associations at Jæren (SW Norway) and their glaci-dynamic implications. *Boreas*, 32, 462–475.

Ringen, E. 1964. Om drumliner og Skagerakmorene på Karmøy. *Norsk Geografisk Tidsskrift*, 19, 205-228.

Rønnevik, H. C. 1971. Kvartærgeologi på ytre del av Haugesundshalvøya. MSc thesis. Department of Earth Science, University of Bergen.

Rønning, J. S., Dalsegg, E., Dehls, J. F., Haase, C.,Nordgulen, Ø., Olesen, O., Saintot, A. & Solli, A. 2006. *Geological and geophysical investigations for the ROGFAST project*. 2006.076. Trondheim: Norges Geologiske Undersøklese. https://www.ngu.no/filearchive/235/2006_076.pdf. Date accessed: 10 April 2019.

Sæle, T.H. 2017. Skuringsstriper og isbevegelse for Hordaland. MSc thesis. Department of Earth Science, University of Bergen, 110 pp.

Sarala, P., Räisänen, J., Johansson, P. & Eskola, K. O. 2015. Aerial LiDAR analysis in geomorphological mapping and geochronological determination of surficial deposits in the Sodankylä region, northern Finland. *GFF*, 137**,** 293-303.

Sejrup, H.P. 1987. Molluscan and foraminiferal biostratigraphy of an Eemian – Early Weichselian section on Karmøy, southwestern Norway. *Boreas*, 16, 27–42.

Sejrup, H. P., Clark, C. D. & Hjelstuen, B. O. 2016. Rapid ice sheet retreat triggered by ice stream debuttressing: Evidence from the North Sea. *Geology*, 44, 355-358.

Sejrup, H. P., Haflidason, H., Aarseth, I., King, E., Forsberg, C. F., Long, D. & Rokoengen, K. 1994. Late Weichselian glaciation history of the northern North Sea. *Boreas*, 23, 1-13.

Sejrup, H.P., Hjelstuen, B.O., Dahlgren, K.I.T., Haflidason, H., Kuijpers, A., Nygård, A., Praeg, D., Stoker, M.S. & Vorren, T.O. 2005. Pleistocene glacial history of the NW European continental margin. *Marine and Petroleum Geology*, 22, 1111–1129.

Sejrup, H.P., Landvik, J., Larsen, E., Eiriksson, J., Janocko, J. & King, E. 1998. The Jæren Area, a Border Zone of the Norwegian Channel Ice Stream. *Quaternary Science Reviews*, 17, 801–812.

Sejrup, H.P., Larsen, E., Haflidason, H., Berstad, I.M., Hjelstuen, B., Jonsdottir, H., King, E.L., Landvik, J., Longva, O., Nygård, A., Ottesen, D., Raunholm, S., Rise, L. & Stalsberg, K. 2003. Configuration, history and impact of the Norwegian Channel Ice Stream. *Boreas*, 32, 18–36.

Sejrup, H.P., Larsen, E., Landvik, J., King, E. L., Haflidason, H. & Nesje, A. 2000. Quaternary glaciations in southern Fennoscandia: evidence from southwestern Norway and the northern North Sea region. *Quaternary Science Reviews*, 19, 667–685.

Sejrup, H.P., Nygård, A., Hall, A.M. & Haflidason, H. 2009. Middle and Late Weichselian (Devensian) glaciation history of south-western Norway, North Sea and eastern UK. *Quaternary Science Reviews*, *28*(3-4), 370-380.

Smith, M.J. & Knight, J. 2011. Paleoglaciology of the last Irish ice sheet reconstructed from striae evidence. *Quaternary Science Reviews,* 30**,** 147-160.

Staiger, J., Gosse, J., Toracinta, R., Oglesby, B., Fastook, J. & Johnson, J. V. 2007. Atmospheric scaling of cosmogenic nuclide production: climate effect. *Journal of Geophysical Research*, 112, B02205.

Stokes, C. R. & Clark, C. D. 2001. Palaeo-ice streams. *Quaternary Science Reviews*, 20, 1437-1457.

Stone, J. O. 2000. Air pressure and cosmogenic isotope production. *Journal of Geophysical Research*, *105*, 23753–23759.

Stroeven, A. P., Heyman, J., Fabel, D., Björck, S., Caffee, M. W., Fredin, O. & Harbor, J. M. 2015. A new Scandinavian reference ^{10}Be production rate. *Quaternary Geochronology*, 29, 104-115.

Strömberg, B. 1981. Calving bays, striae and moraines at Gysinge-Hedesunda, central Sweden. *Geografiska Annaler. Series A. Physical Geography*, 149-154.

Strømsnes, K. 2018. Isavsmelting og senglasial strandforskyvning på Bokn i Rogaland. MSc thesis. Department of Earth Science, Univeristy of Bergen, 69 pp.

Svean, A. 2016. *Glasiasjonshistorie og strandforskyvning i Boknafjordsområdet i Rogaland.* MSc thesis. Department of Earth Science, University of Bergen.

Svendsen, J. I., Alexanderson, H., Astakhov, V. I., Demidov, I., Dowdeswell, J. A., Funder, S., Gataullin, V., Henriksen, M., Hjort, C., Houmark-Nielsen, M., Hubberten, H. W., Ingolfsson, O., Jakobsson, M., Kjaer, K. H., Larsen, E., Lokrantz, H., Lunkka, J. P., Lysa, A., Mangerud, J., Matiouchkov, A., Murray, A., Moller, P., Niessen, F., Nikolskaya, O., Polyak, L., Saarnisto, M., Siegert, C., Siegert, M. J., Spielhagen, R. F. & Stein, R. 2004: Late Quaternary ice sheet history of northern Eurasia. *Quaternary Science Reviews*, 23, 1229-1271.

Svendsen, J. I., Briner, J. P., Mangerud, J. & Young, N. E. 2015. Early break-up of the Norwegian Channel Ice Stream during the last glacial maximum. *Quaternary Science Reviews*, 107, 231-242.

Thomas, G. S. P. and Connell, R. J. 1985. Iceberg drop, dump and grounding structures from Pleistocene glaciolacustrine sediments, Scotland. *Journal of Sedimentary Research*, 55, 243–249.

Undås, I. 1948. Trekk fra Utsiras natur og den siste Skageraksbre. *Stavangers Museums Årbok*, 59-71.

Vasskog, K., Svendsen, J. I., Mangerud, J., Haaga, K. A., Svean, A. & Lunnan, E. M. (in press). Evidence of early deglaciation (18,000 cal a BP) and a postglacial relative sea-level curve from southern Karmøy, southwest Norway. *Journal of Quaternary Science.*

Wehr, A. & Lohr, U. 1999. Airborne laser scanning—an introduction and overview. *ISPRS Journal of Photogrammetry & Remote Sensing*, 54, 68-82.

Winsemann, J., Hornung, J.J., Meinsen, J., Asprion, U., Polom, U., Brandes, C., Bubmann, M. & Weber, C. 2009. Anatomy of a subaqueous ice-contact fan and delta complex, Middle Pleistocene, North-west Germany. *Sedimentology*, 56, 1041-1076.

Appendix

Appendix A displays the striations database in a table format.

Appendix B is a zip-file that holds a shapefile version of the database that can be opened in ArcMap. The striations table is provided as an excel file as well that includes explanations of the contents and structure of the database.

Striae No	Loc. No	County	Placename	Lat_N	Long_E	Precision	m a.s.l.	Mid pt.	Plus_ Minus	Youngest	Older	Even Older	Even Older 2	Oldest	Undet. rel. age	Quality	Source	Code symbol	All orientations	Comments	Erosional marks
1	R1	Rogaland	Moslifjellet, Strand	58.99350	6.1482	1	531	-	-	252	-	-	-	-	-	3	Tuestad, 2019	211	252	weathered bedrock,	
2	R2	Rogaland	Moslifjellet, Strand	58.99340	6.1484	1	528	-	-	260	-	-	-	-	-	2	Tuestad, 2019	211	260		
3	R3	Rogaland	Moslifjellet, Strand	58.99340	6.1480	1	528	-	-	300	-	-	-	-	-	2	Tuestad, 2019	211	300		Crescentic gouge
4	R4	Rogaland	Moslifjellet, Strand	59.00060	6.1551	1	663	-	-	302	-	-	-	-	-	3	Tuestad, 2019	211	302	very eroded bedrock	
5	R5	Rogaland	Moslifjellet, Strand	58.99560	6.1544	1	516	-	-	300	-	-	-	-	-	3	Tuestad, 2019	211	300		
6	R6	Rogaland	Moslifjellet, Strand	58.99490	6.1537	1	474	-	-	254	-	-	-	-	-	2	Tuestad, 2019	211	254		
7	R7	Rogaland	Preikestolen, Forsand	58.98830	6.1749	1	557	-	-	164	-	-	-	-	-	3	Tuestad, 2019	211	164		Crescentic gouge
8	R8	Rogaland	Preikestolen, Forsand	58.98870	6.1753	1	547	-	-	264	-	-	-	-	-	3	Tuestad, 2019	211	264	very faint striation	Crescentic gouge
9	R9	Rogaland	Preikestolen, Forsand	58.98870	6.1780	1	536	-	-	244	-	-	-	-	-	1	Tuestad, 2019	211	244		Crescentic gouge
10	R10	Rogaland	Preikestolen, Forsand	58.98840	6.1894	1	547	-	-	158	-	-	-	-	-	2	Tuestad, 2019	212	158		
11	R11	Rogaland	Preikestolen, Forsand	58.98820	6.1894	1	578	-	-	302	-	-	-	-	-	3	Tuestad, 2019	212	302		
12	R12	Rogaland	Preikestolen, Forsand	58.98830	6.1786	1	546	-	-	250	-	-	-	-	-	3	Tuestad, 2019	211	250		
13	R13	Rogaland	Preikestolen, Forsand	58.98900	6.1795	1	544	-	-	240	-	-	-	-	-	3	Tuestad, 2019	211	240		Crescentic gouge
14	R14	Rogaland	Erevika, Forsand	58.92160	6.0613	1	32	-	-	286	-	-	-	-	-	3	Tuestad, 2019	211	286		
15	R15	Rogaland	Erevika, Forsand	58.92150	6.0612	1	36	-	-	276	-	-	-	-	-	3	Tuestad, 2019	211	276		
16	R16	Rogaland	Erevika, Forsand	58.92160	6.0613	1	34	-	-	286	-	-	-	-	-	3	Tuestad, 2019	211	286		
17	R17	Rogaland	Oanes, Forsand	58.91060	6.0770	1	5	-	-	147	-	-	-	-	-	2	Tuestad, 2019	211	147		
18	R18	Rogaland	Oanes, Forsand	58.91129	6.0774	1	4	-	-	225	-	-	-	-	-	3	Tuestad, 2019	211	225		
19	R19	Rogaland	Oanes, Forsand	58.91050	6.0776	1	2	163	15	-	-	-	-	-	-	3	Tuestad, 2019	214	163		
20	R20	Rogaland	Oanes, Forsand	58.91050	6.0774	1	3	190	10	190	-	-	-	-	-	3	Tuestad, 2019	214	190		
21	R21	Rogaland	Levik, Forsand	58.91296	6.0773	1	16	-	-	160	-	-	-	-	-	1	Tuestad, 2019	211	160		
22	R22	Rogaland	Levik, Forsand	58.91310	6.0771	1	18	220	5	-	-	-	-	-	-	2	Tuestad, 2019	214	220		
23	R23	Rogaland	Levik, Forsand	58.91320	6.0771	1	19	240	10	-	-	-	-	-	-	2	Tuestad, 2019	214	240		
24	R24	Rogaland	Levik, Forsand	58.91310	6.0769	1	22	-	-	200	-	-	-	-	-	2	Tuestad, 2019	211	200		
25	R25	Rogaland	Levik, Forsand	58.91300	6.0768	1	26	217	7	-	-	-	-	-	-	2	Tuestad, 2019	214	217		
26	R26	Rogaland	Levik, Forsand	58.91280	6.0770	1	27	-	-	202	-	-	-	-	-	2	Tuestad, 2019	211	202		
27	R26	Rogaland	Levik, Forsand	58.91280	6.0768	1	27	-	-	221	-	-	-	-	-	2	Tuestad, 2019	211	221		
28	R27	Rogaland	Levik, Forsand	58.91280	6.0769	1	25	-	-	195	-	-	-	-	-	2	Tuestad, 2019	211	195		

Striae No	Loc. No	County	Placename	Lat_N	Long_E	Precision	m a.s.l.	Mid pt.	Plus_ Minus	Youngest	Older	Even Older	Even Older 2	Oldest	Undet. rel. age	Quality	Source	Code symbol	All orientations	Comments	Erosional marks
29	R28	Rogaland	Levik, Forsand	58.91290	6.0768	1	26	-	-	190	-	-	-	-	-	2	Tuestad, 2019	215	190		
30	R28	Rogaland	Levik, Forsand	58.91290	6.0768	1	26	-	-	-	284	-	-	-	-	1	Tuestad, 2019	216	284		
31	R29	Rogaland	Levik, Forsand	58.91290	6.0767	1	27	-	-	225	-	-	-	-	-	1	Tuestad, 2019	215	225		
32	R29	Rogaland	Levik, Forsand	58.91290	6.0767	1	27	-	-	-	285	-	-	-	-	2	Tuestad, 2019	216	285		
33	R30	Rogaland	Levik, Forsand	58.92160	6.0813	1	28	-	-	224	-	-	-	-	-	2	Tuestad, 2019	211	224		
34	R31	Rogaland	Levik, Forsand	58.92140	6.0811	1	30	-	-	243	-	-	-	-	-	2	Tuestad, 2019	211	243		
35	R32	Rogaland	Levik, Forsand	58.92150	6.0813	1	28	-	-	222	-	-	-	-	-	2	Tuestad, 2019	211	222		
36	R33	Rogaland	Stemtjørna, Forsand	58.94950	6.1048	1	170	-	-	320	-	-	-	-	-	3	Tuestad, 2019	211	320	faint striation	
37	R34	Rogaland	Stemtjørna, Forsand	58.94960	6.1043	1	166	-	-	204	-	-	-	-	-	3	Tuestad, 2019	211	204	faint striation	
38	R35	Rogaland	Stemtjørna, Forsand	58.94940	6.1053	1	178	-	-	315	-	-	-	-	-	3	Tuestad, 2019	211	315	faint striation	
39	R36	Rogaland	Stemtjørna, Forsand	58.94960	6.1054	1	178	279	9	-	-	-	-	-	-	3	Tuestad, 2019	214	279	faint striation	
40	R37	Rogaland	Stemtjørna, Forsand	58.94960	6.1057	1	180	-	-	320	-	-	-	-	-	3	Tuestad, 2019	211	320	faint striation	
41	R38	Rogaland	Stemtjørna, Forsand	58.94960	6.1053	1	177	-	-	300	-	-	-	-	-	3	Tuestad, 2019	211	300	faint striation	
42	R39	Rogaland	Kvernaviga, Forsand	58.91450	6.1033	1	36	211	5	-	-	-	-	-	-	2	Tuestad, 2019	214	211		Crescentic gouge, crescentic fracture
43	R40	Rogaland	Storeknut, Forsand	58.88410	6.1526	1	272	-	-	-	-	-	-	-	195	3	Tuestad, 2019	211	195	faint striation	
44	R41	Rogaland	Storeknut, Forsand	58.88540	6.1539	1	270	-	-	190	-	-	-	-	-	3	Tuestad, 2019	211	190	faint striation	
45	R42	Rogaland	Sirevåg, Hå	58.50975	5.7921	1	5	-	-	270	-	-	-	-	-	2	Tuestad, 2019	211	270		
46	R43	Rogaland	Sirevåg, Hå	58.50975	5.7942	1	4.5	-	-	250	-	-	-	-	-	2	Tuestad, 2019	211	250		
47	R44	Rogaland	Sirevåg, Hå	58.50986	5.7944	1	1.4	-	-	290	-	-	-	-	-	2	Tuestad, 2019	211	290		
48	R45	Rogaland	Sirevåg, Hå	58.51831	5.7939	1	10	-	-	345	-	-	-	-	-	3	Tuestad, 2019	211	345		
49	R46	Rogaland	Tungeneset, Tysvær	59.27148	5.4957	3	2.3	-	-	319	-	-	-	-	-	3	Anundsen 1977	211	315		
50	R47	Rogaland	Skjenet, Tysvær	59.27706	5.5308	3	2.5	-	-	179	-	-	-	-	-	3	Anundsen 1977	211	194		
51	R48	Rogaland	Sandholmen, Tysvær	59.27436	5.5378	3	5.1	-	-	254	-	-	-	-	-	3	Anundsen 1977	211	254		
52	R49	Rogaland	Slettabekk, Tysvær	59.28411	5.5591	3	74	-	-	250	-	-	-	-	-	3	Anundsen 1977	211	250		
53	R50	Rogaland	Bjørklund, Tysvær	59.28579	5.5636	3	45	-	-	212	-	-	-	-	-	3	Anundsen 1977	211	212		
54	R51	Rogaland	Årvikafjell, Tysvær	59.29706	5.5588	3	223	-	-	262	-	-	-	-	-	3	Anundsen 1977	211	262		
55	R52	Rogaland	Litlafjellet, Tysvær	59.29262	5.5398	3	70	-	-	182	-	-	-	-	-	3	Anundsen 1977	211	182		
56	R53	Rogaland	Klov, Tysvær	59.29492	5.4972	3	56	-	-	238	-	-	-	-	-	3	Anundsen 1977	211	238		

Striae No	Loc. No	County	Placename	Lat_N	Long_E	Precision	m a.s.l.	Mid pt.	Plus_ Minus	Youngest	Older	Even Older	Even Older 2	Oldest	Undet. rel. age	Quality	Source	Code symbol	All orientations	Comments	Erosional marks
57	R54	Rogaland	Rehaugane, Tysvær	59.31796	5.4991	3	25	-	-	203	-	-	-	-	-	3	Anundsen 1977	211	203		
58	R55	Rogaland	Kråkelifjellet, Tysvær	59.31031	5.5672	3	213	-	-	162	-	-	-	-	-	3	Anundsen 1977	211	162		
59	R56	Rogaland	Nibba, Tysvær	59.31659	5.5926	3	77	-	-	182	-	-	-	-	-	3	Anundsen 1977	211	164		
60	R57	Rogaland	Tysværheia, Tysvær	59.33887	5.4963	3	74	-	-	221	-	-	-	-	-	3	Anundsen 1977	211	221		
61	R58	Rogaland	Heggelifjellet, Tysvær	59.35753	5.5212	3	150	-	-	248	-	-	-	-	-	3	Anundsen 1977	211	248		
62	R59	Rogaland	Solberget, Tysvær	59.35748	5.5522	3	30	-	-	192	-	-	-	-	-	3	Anundsen 1977	211	192		
63	R60	Rogaland	Narravik, Tysvær	59.34897	5.6139	3	23	-	-	174	-	-	-	-	-	3	Anundsen 1977	211	174		
64	R61	Rogaland	Slupsadalen, Tysvær	59.37561	5.5716	3	58	-	-	241	-	-	-	-	-	3	Anundsen 1977	211	241		
65	R62	Rogaland	Store Sagåsen, Tysvær	59.40098	5.5911	3	34	-	-	250	-	-	-	-	-	3	Anundsen 1977	211	250		
66	R63	Rogaland	Sandvika, Tysvær	59.39425	5.5782	3	13	-	-	214	-	-	-	-	-	3	Anundsen 1977	211	214		
67	R64	Rogaland	Ronningshammaren, Tysvær	59.39038	5.5107	3	54	-	-	242	-	-	-	-	-	3	Anundsen 1977	211	242		
68	R65	Rogaland	Padletjørna, Tysvær	59.38011	5.4829	3	40	-	-	200	-	-	-	-	-	3	Anundsen 1977	211	200		
69	R66	Rogaland	Sygardshaugen, Tysvær	59.38862	5.4821	3	26	-	-	234	-	-	-	-	-	3	Anundsen 1977	211	234		
70	R67	Rogaland	Høganipa, Tysvær	59.40612	5.4878	3	86	-	-	230	-	-	-	-	-	3	Anundsen 1977	211	230		
71	R68	Rogaland	Midtfjellet, Tysvær	59.40414	5.5182	3	140	-	-	256	-	-	-	-	-	3	Anundsen 1977	211	256		
72	R69	Rogaland	Makrellholmen, Tysvær	59.41274	5.5892	3	12	-	-	226	-	-	-	-	-	3	Anundsen 1977	211	226		
73	R70	Rogaland	Straum, Tysvær	59.42654	5.6146	3	34	-	-	160	-	-	-	-	-	3	Anundsen 1977	211	160		
74	R71	Rogaland	Sauahøgda, Tysvær	59.42419	5.5881	3	110	-	-	252	-	-	-	-	-	3	Anundsen 1977	211	252		
75	R72	Rogaland	Auklandstjørna, Tysvær	59.43524	5.5527	3	53	-	-	240	-	-	-	-	-	3	Anundsen 1977	211	240		
76	R73	Rogaland	Nonshaugen, Tysvær	59.42481	5.4782	3	47	-	-	235	-	-	-	-	-	3	Anundsen 1977	211	235		
77	R74	Rogaland	Tjuasteinen, Tysvær	59.45656	5.4841	3	62	-	-	223	-	-	-	-	-	3	Anundsen 1977	211	223		
78	R75	Rogaland	Erlandsvarden, Vindafjord	59.48418	5.5148	3	48	-	-	233	-	-	-	-	-	3	Anundsen 1977	211	233		
79	R76	Rogaland	Hedlehaugen, Vindafjord	59.47605	5.5272	3	81	-	-	225	-	-	-	-	-	3	Anundsen 1977	211	225		
80	R77	Rogaland	Mortveittjørna, Vindafjord	59.49118	5.5232	3	96	-	-	244	-	-	-	-	-	3	Anundsen 1977	211	244		
81	R78	Rogaland	Håvåsen, Vindafjord	59.50522	5.4903	3	101	-	-	274	-	-	-	-	-	3	Anundsen 1977	211	274		
82	R79	Rogaland	Varen, Vindafjord	59.51011	5.5455	3	122	-	-	244	-	-	-	-	-	3	Anundsen 1977	211	244		
83	R80	Rogaland	Svartenakken, Vindafjord	59.52921	5.5546	3	40	-	-	224	-	-	-	-	-	3	Anundsen 1977	211	224		
84	R81	Rogaland	Svensbøelva, Vindafjord	59.54064	5.5721	3	55	-	-	269	-	-	-	-	-	3	Anundsen 1977	211	269		

Striae No	Loc. No	County	Placename	Lat_N	Long_E	Precision	m a.s.l.	Mid pt.	Plus_ Minus	Youngest	Older	Even Older	Even Older 2	Oldest	Undet. rel. age	Quality	Source	Code symbol	All orientations	Comments	Erosional marks
85	R82	Rogaland	Store Timbåsen, Vindafjord	59.53991	5.6058	3	217	-	-	265	-	-	-	-	-	3	Anundsen 1977	211	265		
86	R83	Rogaland	Trondskår, Sveio	59.55232	5.4906	3	94	-	-	290	-	-	-	-	-	3	Anundsen 1977	211	290		
87	R84	Rogaland	Ervesvågen, Sveio	59.55801	5.4883	3	30	-	-	296	-	-	-	-	-	3	Anundsen 1977	211	296		
88	R85	Rogaland	Oahamn, Sveio	59.55296	5.5047	3	29	-	-	237	-	-	-	-	-	3	Anundsen 1977	211	237		
89	R86	Rogaland	Ervesvågen, Sveio	59.56215	5.4773	3	18	-	-	280	-	-	-	-	-	3	Anundsen 1977	211	280		
90	R87	Rogaland	Ramnabørtjørna, Sveio	59.57036	5.4906	3	100	-	-	268	-	-	-	-	-	3	Anundsen 1977	211	268		
91	R88	Rogaland	Vardafjellet, Sveio	59.56551	5.1171	3	154	-	-	222	-	-	-	-	-	3	Anundsen 1977	211	222		
92	R89	Rogaland	Kalhaugen, Sveio	59.57125	5.5224	3	39	-	-	230	-	-	-	-	-	3	Anundsen 1977	211	230		
93	R90	Rogaland	Rabben, Sveio	59.57773	5.2420	3	38	-	-	-	-	-	-	-	234	3	Anundsen 1977	213	234		
94	R90	Rogaland	Rabben, Sveio	59.57773	5.2420	3	38	-	-	-	-	-	-	-	262	3	Anundsen 1977	213	262		
95	R91	Rogaland	Dyråsen, Sveio	59.58161	5.4991	3	83	-	-	242	-	-	-	-	-	3	Anundsen 1977	211	242		
96	R92	Rogaland	Selabakken, Sveio	59.59933	5.4932	3	51	-	-	310	-	-	-	-	-	3	Anundsen 1977	211	310		
97	R93	Rogaland	Nesjaneset, Sveio	59.59308	5.5246	3	20	-	-	-	-	-	-	-	231	3	Anundsen 1977	213	231		
98	R93	Rogaland	Nesjaneset, Sveio	59.59308	5.5246	3	20	-	-	-	-	-	-	-	263	3	Anundsen 1977	213	263		
99	R94	Rogaland	Kobba, Sveio	59.62426	5.5194	3	48	-	-	296	-	-	-	-	-	3	Anundsen 1977	211	296		
100	R95	Rogaland	Austvik, Sveio	59.62456	5.4854	3	59	-	-	284	-	-	-	-	-	3	Anundsen 1977	211	284		
101	R96	Rogaland	Brattestø, Sveio	59.63366	5.5081	3	96	-	-	257	-	-	-	-	-	3	Anundsen 1977	211	257		
102	R97	Rogaland	Øspenes, Sveio	59.64047	5.5098	3	89	-	-	258	-	-	-	-	-	3	Anundsen 1977	211	258		
103	R98	Rogaland	Maradalsfjellet, Sveio	59.64005	5.5018	3	108	-	-	240	-	-	-	-	-	3	Anundsen 1977	211	240		
104	R99	Rogaland	Maradalen, Sveio	59.64293	5.4959	3	92	-	-	260	-	-	-	-	-	3	Anundsen 1977	211	260		
105	R100	Rogaland	Staupefjellet, Sveio	59.65097	5.4941	3	244	-	-	291	-	-	-	-	-	3	Anundsen 1977	211	291		
106	R101	Rogaland	Utbjoa, Vindafjord	59.67662	5.6164	3	17	-	-	-	-	-	-	-	345	3	Anundsen 1977	212	345		
107	R101	Rogaland	Utbjoa, Vindafjord	59.67662	5.6164	3	17	-	-	-	-	-	-	-	262	3	Anundsen 1977	213	262		
108	R101	Rogaland	Utbjoa, Vindafjord	59.67662	5.6164	3	17	-	-	-	-	-	-	-	317	3	Anundsen 1977	213	317		
109	R102	Rogaland	Leirholo, Vindafjord	59.66347	5.6675	3	6	-	-	290	-	-	-	-	-	3	Anundsen 1977	211	290		
110	R103	Rogaland	Brandøyvika, Vindafjord	59.66151	5.6991	3	27	-	-	223	-	-	-	-	-	3	Anundsen 1977	211	223		
111	R104	Rogaland	Rådalstjørna, Vindafjord	59.63941	5.5865	3	49	-	-	225	-	-	-	-	-	3	Anundsen 1977	211	225		
112	R105	Rogaland	Sørehamn, Vindafjord	59.62742	5.5581	3	1	-	-	-	-	-	-	-	239	3	Anundsen 1977	213	239		

Striae No	Loc. No	County	Placename	Lat_N	Long_E	Precision	m a.s.l.	Mid pt.	Plus_ Minus	Youngest	Older	Even Older	Even Older 2	Oldest	Undet. rel. age	Quality	Source	Code symbol	All orientations	Comments	Erosional marks
113	R105	Rogaland	Sørehamn, Vindafjord	59.62742	5.5581	3	1	-	-	-	-	-	-	-	254	3	Anundsen 1977	213	254		
114	R106	Rogaland	Taklidalen, Vindafjord	59.63442	5.6082	3	142	-	-	287	-	-	-	-	-	3	Anundsen 1977	211	287		
115	R107	Rogaland	Kvame, Vindafjord	59.61342	5.5758	3	74	-	-	238	-	-	-	-	-	3	Anundsen 1977	211	238		
116	R108	Rogaland	Slættafjellet, Vindafjord	59.62885	5.6992	3	663	-	-	294	-	-	-	-	-	3	Anundsen 1977	211	294		
117	R109	Rogaland	Rindalen, Vindafjord	59.61986	5.6964	3	330	-	-	292	-	-	-	-	-	3	Anundsen 1977	211	292		
118	R110	Rogaland	Bukkanibba, Vindafjord	59.59871	5.6912	3	464	-	-	250	-	-	-	-	-	3	Anundsen 1977	211	250		
119	R111	Rogaland	Vikastølen, Vindafjord	59.60134	5.6611	3	370	-	-	251	-	-	-	-	-	3	Anundsen 1977	211	251		
120	R112	Rogaland	Feiensbrekka, Vindafjord	59.59486	5.6534	3	347	-	-	256	-	-	-	-	-	3	Anundsen 1977	211	256		
121	R113	Rogaland	Rolegelia, Vindafjord	59.59811	5.6503	3	427	-	-	288	-	-	-	-	-	3	Anundsen 1977	211	288		
122	R114	Rogaland	Vøbrekkefjell, Vindafjord	59.59062	5.6409	3	512	-	-	285	-	-	-	-	-	3	Anundsen 1977	211	285		
123	R115	Rogaland	Våbrekkerinda, Vindafjord	59.58858	5.6010	3	234	-	-	256	-	-	-	-	-	3	Anundsen 1977	211	256		
124	R116	Rogaland	Vikebygd kyrkje, Vindafjord	59.59125	5.5852	3	9	-	-	268	-	-	-	-	-	3	Anundsen 1977	215	268		
125	R116	Rogaland	Vikebygd kyrkje, Vindafjord	59.59125	5.5852	3	9	-	-	-	238	-	-	-	-	3	Anundsen 1977	216	238		
126	R117	Rogaland	Storemyra, Vindafjord	59.57694	5.5717	3	39	-	-	-	-	-	-	-	226	3	Anundsen 1977	213	226		
127	R117	Rogaland	Storemyra, Vindafjord	59.57694	5.5717	3	39	-	-	-	-	-	-	-	268	3	Anundsen 1977	213	268		
128	R118	Rogaland	Skjelkavikshaugane,Vindafjord	59.57028	5.5708	3	29	-	-	223	-	-	-	-	-	3	Anundsen 1977	211	223		
129	R119	Rogaland	Vikelva, Vindafjord	59.58690	5.6131	3	218	-	-	290	-	-	-	-	-	3	Anundsen 1977	211	290		
130	R120	Rogaland	Mørkadalsvatnet, Vindafjord	59.56984	5.6157	3	495	-	-	242	-	-	-	-	-	3	Anundsen 1977	211	242		
131	R121	Rogaland	Moldbrekka, Vindafjord	59.57661	5.6462	3	507	-	-	251	-	-	-	-	-	3	Anundsen 1977	211	251		
132	R122	Rogaland	Moldbrekka, Vindafjord	59.57425	5.6491	3	574	-	-	269	-	-	-	-	-	3	Anundsen 1977	211	269		
133	R123	Rogaland	Storalia, Vindafjord	59.57925	5.6963	3	188	-	-	218	-	-	-	-	-	3	Anundsen 1977	211	218		
134	R124	Rogaland	Skjenet, Vindafjord	59.55535	5.6889	3	72	-	-	197	-	-	-	-	-	3	Anundsen 1977	211	197		
135	R125	Rogaland	Landabekken, Vindafjord	59.53905	5.7152	3	25	-	-	174	-	-	-	-	-	3	Anundsen 1977	211	174		
136	R126	Rogaland	Knapphus, Vindafjord	59.53192	5.6861	3	104	-	-	-	-	-	-	-	246	3	Anundsen 1977	213	246		
137	R126	Rogaland	Knapphus, Vindafjord	59.53192	5.6861	3	104	-	-	-	-	-	-	-	273	3	Anundsen 1977	213	273		
138	R127	Rogaland	Røyrvika, Vindafjord	59.52195	5.6969	3	25	-	-	231	-	-	-	-	-	3	Anundsen 1977	211	231		
139	R128	Rogaland	Eggja, Vindafjord	59.51072	5.6209	3	89	-	-	236	-	-	-	-	-	3	Anundsen 1977	211	236		
140	R129	Rogaland	Tverrliance, Vindafjord	59.55796	5.6303	3	524	-	-	248	-	-	-	-	-	3	Anundsen 1977	211	248		

Striae No	Loc. No	County	Placename	Lat_N	Long_E	Precision	m a.s.l.	Mid pt.	Plus_ Minus	Youngest	Older	Even Older	Even Older 2	Oldest	Undet. rel. age	Quality	Source	Code symbol	All orientations	Comments	Erosional marks
141	R130	Rogaland	Bergahaugen, Vindafjord	59.54091	5.6453	3	376	-	-	257	-	-	-	-	-	3	Anundsen 1977	211	257		
142	R131	Rogaland	Svanavatnet, Vindafjord	59.49764	5.6376	3	26	-	-	250	-	-	-	-	-	3	Anundsen 1977	211	250		
143	R132	Rogaland	Kjorkjeteigen, Vindefjord	59.49155	5.6361	3	34	-	-	240	-	-	-	-	-	3	Anundsen 1977	211	240		
144	R133	Rogaland	Tjørnalimyra, Vindafjord	59.48391	5.6491	3	186	-	-	334	-	-	-	-	-	3	Anundsen 1977	212	334		
145	R134	Rogaland	Storefjellnibba, Vindafjord	59.46255	5.6476	3	498	-	-	268	-	-	-	-	-	3	Anundsen 1977	211	268		
146	R135	Rogaland	Storefjellnibba, Vindafjord	59.46161	5.6485	3	495	-	-	282	-	-	-	-	-	3	Anundsen 1977	211	282		
147	R136	Rogaland	Søre Almen, Vindafjord	59.45045	5.6791	3	252	-	-	252	-	-	-	-	-	3	Anundsen 1977	211	252		
148	R137	Rogaland	Vestalilfjellet, Vindafjord	59.44008	5.6962	3	406	-	-	253	-	-	-	-	-	3	Anundsen 1977	211	253		
149	R138	Rogaland	Strandfjellet, Tysvær	59.42709	5.6908	3	491	-	-	250	-	-	-	-	-	3	Anundsen 1977	211	250		
150	R139	Rogaland	Barnavika, Tysvær	59.40661	5.7256	3	67	-	-	212	-	-	-	-	-	3	Anundsen 1977	211	212		
151	R140	Rogaland	Fossadalen, Tysvær	59.42773	5.6694	3	347	-	-	291	-	-	-	-	-	3	Anundsen 1977	211	291		
152	R141	Rogaland	Hålandsåsen, Tysvær	59.42565	5.6501	3	217	-	-	236	-	-	-	-	-	3	Anundsen 1977	211	236		
153	R142	Rogaland	Haber, Tysvær	59.42873	5.6425	3	98	-	-	272	-	-	-	-	-	3	Anundsen 1977	211	272		
154	R143	Rogaland	Meåsen, Tysvær	59.40689	5.6591	3	97.7	-	-	168	-	-	-	-	-	3	Anundsen 1977	211	168		
155	R144	Rogaland	Bjørkåsen, Tysvær	59.40888	5.6536	3	134	-	-	200	-	-	-	-	-	3	Anundsen 1977	211	200		
156	R145	Rogaland	Løkjen, Tysvær	59.40142	5.6699	3	54	-	-	234	-	-	-	-	-	3	Anundsen 1977	211	234		
157	R146	Rogaland	Yrkjeskaret, Tysvær	59.39627	5.6674	3	71	-	-	260	-	-	-	-	-	3	Anundsen 1977	211	260		
158	R147	Rogaland	Svartatjørna, Tysvær	59.37376	5.6599	3	105	-	-	176	-	-	-	-	-	3	Anundsen 1977	211	176		
159	R148	Rogaland	Sandviktjørna, Tysvær	59.36831	5.6649	3	108	-	-	194	-	-	-	-	-	3	Anundsen 1977	211	194		
160	R149	Rogaland	Skrubbevika, Tysvær	59.35736	5.6597	3	38	-	-	178	-	-	-	-	-	3	Anundsen 1977	211	178		
161	R150	Rogaland	Ballhammaren, Tysvær	59.34585	5.6608	3	187	-	-	157	-	-	-	-	-	3	Anundsen 1977	211	157		
162	R151	Rogaland	Nibbesundet, Tysvær	59.33486	5.6788	3	20	-	-	-	-	-	-	-	166	3	Anundsen 1977	213	166		
163	R151	Rogaland	Nibbesundet, Tysvær	59.33486	5.6788	3	20	-	-	-	-	-	-	-	210	3	Anundsen 1977	213	210		
164	R151	Rogaland	Nibbesundet, Tysvær	59.33486	5.6788	3	20	-	-	-	-	-	-	-	230	3	Anundsen 1977	213	230		
165	R151	Rogaland	Nibbesundet, Tysvær	59.33486	5.6788	3	20	-	-	-	-	-	-	-	292	3	Anundsen 1977	213	292		
166	R151	Rogaland	Nibbesundet, Tysvær	59.33486	5.6788	3	20	-	-	-	-	-	-	-	180	3	Anundsen 1977	213	180		
167	R152	Rogaland	Såta, Tysvær	59.34588	5.6725	3	221	-	-	269	-	-	-	-	-	3	Anundsen 1977	211	269		
168	R153	Rogaland	Espevik, Tysvær	59.33967	5.6794	3	66	-	-	236	-	-	-	-	-	3	Anundsen 1977	211	236		

Striae No	Loc. No	County	Placename	Lat_N	Long_E	Precision	m a.s.l.	Mid pt.	Plus_ Minus	Youngest	Older	Even Older	Even Older 2	Oldest	Undet. rel. age	Quality	Source	Code symbol	All orientations	Comments	Erosional marks
169	R154	Rogaland	Høgehaugen, Tysvær	59.34161	5.6965	3	33	-	-	266	-	-	-	-	-	3	Anundsen 1977	211	266		
170	R155	Rogaland	Hustopt, Tysvær	59.34611	5.7064	3	117	-	-	244	-	-	-	-	-	3	Anundsen 1977	215	244		
171	R155	Rogaland	Hustopt, Tysvær	59.34611	5.7064	3	117	-	-	-	210	-	-	-	-	3	Anundsen 1977	216	210		
172	R156	Rogaland	Fløyen, Tysvær	59.34011	5.7304	3	146	-	-	220	-	-	-	-	-	3	Anundsen 1977	211	220		
173	R157	Rogaland	Varhaug, Tysvær	59.33205	5.7426	3	1.6	-	-	172	-	-	-	-	-	3	Anundsen 1977	215	172		
174	R157	Rogaland	Varhaug, Tysvær	59.33205	5.7426	3	1.6	-	-	-	248	-	-	-	-	3	Anundsen 1977	216	248		
175	R158	Rogaland	Vågsåna, Tysvær	59.34723	5.7469	3	12	-	-	220	-	-	-	-	-	3	Anundsen 1977	211	220		
176	R159	Rogaland	Vatland, Tysvær	59.35605	5.7639	3	53	-	-	274	-	-	-	-	-	3	Anundsen 1977	211	274		
177	R160	Rogaland	Torbjørnsåsen, Tysvær	59.35875	5.7619	3	127	-	-	190	-	-	-	-	-	3	Anundsen 1977	211	190		
178	R161	Rogaland	Trodlaskaret, Tysvær	59.37419	5.7657	3	275	-	-	210	-	-	-	-	-	3	Anundsen 1977	211	210		
179	R162	Rogaland	Skvamplane, Tysvær	59.31823	5.7274	3	64	-	-	-	-	-	-	-	156	3	Anundsen 1977	213	156		
180	R162	Rogaland	Skvamplane, Tysvær	59.31823	5.7274	3	64	-	-	-	-	-	-	-	236	3	Anundsen 1977	213	236		
181	R163	Rogaland	Rabbaneset, Tysvær	59.31238	5.7203	3	7	-	-	166	-	-	-	-	-	3	Anundsen 1977	211	166		
182	R164	Rogaland	Skipsholmen, Tysvær	59.29833	5.6768	3	12	-	-	238	-	-	-	-	-	3	Anundsen 1977	211	238		
183	R165	Rogaland	Varden, Tysvær	59.29055	5.6559	3	120	-	-	290	-	-	-	-	-	3	Anundsen 1977	211	290		
184	R166	Rogaland	Liarvåg, Tysvær	59.28725	5.6553	3	17	-	-	238	-	-	-	-	-	3	Anundsen 1977	211	238		
185	R167	Rogaland	Amdal, Tysvær	59.30991	5.6528	3	40	-	-	264	-	-	-	-	-	3	Anundsen 1977	211	264		
186	R168	Rogaland	Skjeljavika, Tysvær	59.32071	5.6535	3	6	-	-	207	-	-	-	-	-	3	Anundsen 1977	211	207		
187	R169	Rogaland	Narravik, Tysvær	59.31373	5.6512	3	28	-	-	-	-	-	-	-	180	3	Anundsen 1977	213	180		
188	R169	Rogaland	Narravik, Tysvær	59.31373	5.6512	3	28	-	-	-	-	-	-	-	228	3	Anundsen 1977	213	228		
189	R170	Hordaland	Horsnes, Etne	59.68554	6.0104	3	51	-	-	216	-	-	-	-	-	3	Anundsen 1977	211	216		
190	R171	Hordaland	Vassenden, Etne	59.67755	6.0073	3	66	-	-	213	-	-	-	-	-	3	Anundsen 1977	211	213		
191	R172	Hordaland	Takhaug, Etne	59.70881	5.9832	3	620	-	-	306	-	-	-	-	-	3	Anundsen 1977	211	306		
192	R173	Hordaland	Hegelihaugen, Etne	59.69929	5.9335	3	670	-	-	308	-	-	-	-	-	3	Anundsen 1977	211	308		
193	R174	Hordaland	Fitjalia, Etne	59.67521	5.9254	3	7	-	-	228	-	-	-	-	-	3	Anundsen 1977	215	228		
194	R174	Hordaland	Fitjalia, Etne	59.67521	5.9254	3	7	-	-	-	265	-	-	-	-	3	Anundsen 1977	216	265		
195	R175	Hordaland	Brøllom, Etne	59.67174	5.8917	3	100	-	-	223	-	-	-	-	-	3	Anundsen 1977	211	223		
196	R176	Hordaland	Galthaug, Etne	59.65079	5.9069	3	56	-	-	238	-	-	-	-	-	3	Anundsen 1977	211	238		

Striae No	Loc. No	County	Placename	Lat_N	Long_E	Precision	m a.s.l.	Mid pt.	Plus_ Minus	Youngest	Older	Even Older	Even Older 2	Oldest	Undet. rel. age	Quality	Source	Code symbol	All orientations	Comments	Erosional marks
197	R177	Hordaland	Melandsstølen, Etne	59.63541	5.9005	3	87	-	-	240	-	-	-	-	-	3	Anundsen 1977	211	240		
198	R178	Hordaland	Melandsstølen, Etne	59.63275	5.8987	3	121	-	-	265	-	-	-	-	-	3	Anundsen 1977	211	265		
199	R179	Hordaland	Kvammen, Etne	59.62915	5.8979	3	195	-	-	283	-	-	-	-	-	3	Anundsen 1977	211	283		
200	R180	Hordaland	Holmaseid, Etne	59.65561	5.8341	3	39	-	-	243	-	-	-	-	-	3	Anundsen 1977	211	243		
201	R181	Hordaland	Seldalsvika, Etne	59.65252	5.8244	3	67	-	-	255	-	-	-	-	-	3	Anundsen 1977	211	255		
202	R182	Hordaland	Hamnehagen, Etne	59.65383	5.8133	3	142	-	-	280	-	-	-	-	-	3	Anundsen 1977	211	280		
203	R183	Hordaland	Børkjenesklubben, Etne	59.64946	5.7958	3	33	-	-	279	-	-	-	-	-	3	Anundsen 1977	211	279		
204	R184	Rogaland	Dreganes, Vindafjord	59.64290	5.7977	3	114	-	-	-	-	-	-	-	279	3	Anundsen 1977	213	279		
205	R184	Rogaland	Dreganes, Vindafjord	59.64290	5.7977	3	114	-	-	-	-	-	-	-	298	3	Anundsen 1977	213	298		
206	R185	Rogaland	Skarvaberg, Vindafjord	59.66304	5.7522	3	26	-	-	290	-	-	-	-	-	3	Anundsen 1977	211	290		
207	R186	Rogaland	Stavanes, Vindafjord	59.64794	5.7712	3	3.5	-	-	170	-	-	-	-	-	3	Anundsen 1977	211	170		
208	R187	Rogaland	Flatbø, Vindafjord	59.64171	5.7648	3	220	-	-	176	-	-	-	-	-	3	Anundsen 1977	211	176		
209	R188	Rogaland	Mækjevik, Vindafjord	59.65018	5.7507	3	17	-	-	310	-	-	-	-	-	3	Anundsen 1977	211	310		
210	R189	Rogaland	Hallgilje, Vindafjord	59.65417	5.7353	3	20	-	-	315	-	-	-	-	-	3	Anundsen 1977	211	315		
211	R190	Rogaland	Berge, Vindafjord	59.60678	5.7548	3	61	-	-	241	-	-	-	-	-	3	Anundsen 1977	211	241		
212	R191	Rogaland	Bergsneset, Vindafjord	59.60599	5.7628	3	16	-	-	230	-	-	-	-	-	3	Anundsen 1977	211	230		
213	R192	Rogaland	Færåsen, Vindafjord	59.59034	5.7397	3	121	-	-	220	-	-	-	-	-	3	Anundsen 1977	211	220		
214	R193	Rogaland	Gjerdevika, Vindafjord	59.59818	5.7471	3	9	-	-	254	-	-	-	-	-	3	Anundsen 1977	211	254		
215	R194	Rogaland	Saltberget, Vindafjord	59.59961	5.7699	3	29	-	-	250	-	-	-	-	-	3	Anundsen 1977	211	250		
216	R195	Rogaland	Litle Nerheim, Vindafjord	59.60056	5.7780	3	22	-	-	214	-	-	-	-	-	3	Anundsen 1977	211	214		
217	R196	Rogaland	Litle Nerheim, Vindafjord	59.60213	5.7883	3	8	-	-	183	-	-	-	-	-	3	Anundsen 1977	211	183		
218	R197	Rogaland	Vindafjord Kommune, Vindafjord	59.60638	5.8102	3	1	-	-	152	-	-	-	-	-	3	Anundsen 1977	211	152		
219	R198	Rogaland	Skarhaug, Vindafjord	59.58793	5.7997	3	143	-	-	178	-	-	-	-	-	3	Anundsen 1977	211	178		
220	R199	Rogaland	Eiaberget, Vindafjord	59.59788	5.8257	3	186	-	-	216	-	-	-	-	-	3	Anundsen 1977	211	216		
221	R200	Rogaland	Hushaugtjørna, Vindafjord	59.59723	5.8303	3	277	-	-	251	-	-	-	-	-	3	Anundsen 1977	211	251		
222	R201	Rogaland	Dørheim, Vindafjord	59.60178	5.8379	3	96	-	-	286	-	-	-	-	-	3	Anundsen 1977	211	286		
223	R202	Rogaland	Lia, Vindafjord	59.61177	5.8611	3	72	-	-	266	-	-	-	-	-	3	Anundsen 1977	211	266		
224	R203	Rogaland	Sørlia, Vindafjord	59.60815	5.8808	3	301	-	-	198	-	-	-	-	-	3	Anundsen 1977	211	198		

Striae No	Loc. No	County	Placename	Lat_N	Long_E	Precision	m a.s.l.	Mid pt.	Plus_ Minus	Youngest	Older	Even Older	Even Older 2	Oldest	Undet. rel. age	Quality	Source	Code symbol	All orientations	Comments	Erosional marks
225	R204	Rogaland	Fikse, Vindafjord	59.62339	5.8862	3	194	-	-	220	-	-	-	-	-	3	Anundsen 1977	211	220		
226	R205	Rogaland	Svartatjønnsnuten, Vindafjord	59.58833	5.8412	3	457	-	-	226	-	-	-	-	-	3	Anundsen 1977	211	226		
227	R206	Rogaland	Steinsland, Vindafjord	59.57327	5.8040	3	88	-	-	186	-	-	-	-	-	3	Anundsen 1977	211	186		
228	R207	Rogaland	Gamleskarbekken, Vindafjord	59.56905	5.7897	3	259	-	-	256	-	-	-	-	-	3	Anundsen 1977	211	256		
229	R208	Rogaland	Lærdal, Vindafjord	59.55783	5.8206	3	98	-	-	154	-	-	-	-	-	3	Anundsen 1977	211	154		
230	R209	Rogaland	Frøland, Vindafjord	59.57660	5.8530	3	385	-	-	248	-	-	-	-	-	3	Anundsen 1977	211	248		
231	R210	Rogaland	Frøland, Vindafjord	59.57327	5.8553	3	313	-	-	-	-	-	-	-	162	3	Anundsen 1977	213	162		
232	R210	Rogaland	Frøland, Vindafjord	59.57327	5.8553	3	313	-	-	-	-	-	-	-	293	3	Anundsen 1977	213	293		
233	R210	Rogaland	Frøland, Vindafjord	59.57327	5.8553	3	313	-	-	-	-	-	-	-	324	3	Anundsen 1977	213	324		
234	R211	Rogaland	Øklandsdalen, Vindafjord	59.56957	5.8381	3	327	-	-	174	-	-	-	-	-	3	Anundsen 1977	211	174		
235	R212	Rogaland	Øvstabøelva, Vindafjord	59.56121	5.8643	3	66	-	-	188	-	-	-	-	-	3	Anundsen 1977	211	188		
236	R213	Rogaland	Fjellstølbekken, Vindafjord	59.57709	5.8857	3	309	-	-	196	-	-	-	-	-	3	Anundsen 1977	211	196		
237	R214	Rogaland	Rødneelva, Vindafjord	59.57274	5.8865	3	334	-	-	220	-	-	-	-	-	3	Anundsen 1977	211	220		
238	R215	Rogaland	Skillingsfossen, Vindafjord	59.57944	5.9194	3	386	-	-	252	-	-	-	-	-	3	Anundsen 1977	211	252		
239	R216	Rogaland	Fjellstølbekken, Vindafjord	59.57410	5.8750	3	162	-	-	154	-	-	-	-	-	3	Anundsen 1977	215	154		
240	R216	Rogaland	Fjellstølbekken, Vindafjord	59.57410	5.8750	3	162	-	-	-	315	-	-	-	-	3	Anundsen 1977	216	315		
241	R217	Rogaland	Ramnafjellet, Vindafjord	59.56627	5.8941	3	379	-	-	242	-	-	-	-	-	3	Anundsen 1977	211	242		
242	R218	Rogaland	Sauatonå, Vindafjord	59.55720	5.9047	3	320	-	-	211	-	-	-	-	-	3	Anundsen 1977	211	211		
243	R219	Rogaland	Haukakvam, Vindafjord	59.55057	5.8994	3	192	-	-	268	-	-	-	-	-	3	Anundsen 1977	211	268		
244	R220	Rogaland	Steinflotene, Vindafjord	59.53694	5.8775	3	154	-	-	215	-	-	-	-	-	3	Anundsen 1977	211	215		
245	R221	Rogaland	Skeie, Vindafjell	59.55411	5.8402	3	151	-	-	282	-	-	-	-	-	3	Anundsen 1977	211	282		
246	R222	Rogaland	Vestbøholmen, Vindafjord	59.54373	5.8521	3	1	-	-	15	-	-	-	-	-	3	Anundsen 1977	215	15		
247	R222	Rogaland	Vestbøholmen, Vindafjord	59.54373	5.8521	3	1	-	-	-	140	-	-	-	-	3	Anundsen 1977	216	140		
248	R223	Rogaland	Oterberg, Vindafjord	59.53665	5.8387	3	164	-	-	196	-	-	-	-	-	3	Anundsen 1977	211	196		
249	R224	Rogaland	Hadlebakkane, Vindafjord	59.52531	5.8371	3	31	-	-	178	-	-	-	-	-	3	Anundsen 1977	211	178		
250	R225	Rogaland	Juvbekken, Vindafjord	59.52777	5.8211	3	76	-	-	-	-	-	-	-	204	3	Anundsen 1977	213	204		
251	R225	Rogaland	Juvbekken, Vindafjord	59.52777	5.8211	3	76	-	-	-	-	-	-	-	352	3	Anundsen 1977	213	352		
252	R226	Rogaland	Døldarheia, Vindafjord	59.53802	5.7861	3	694	-	-	261	-	-	-	-	-	3	Anundsen 1977	211	261		

Striae No	Loc. No	County	Placename	Lat_N	Long_E	Precision	m a.s.l.	Mid pt.	Plus_ Minus	Youngest	Older	Even Older	Even Older 2	Oldest	Undet. rel. age	Quality	Source	Code symbol	All orientations	Comments	Erosional marks
253	R227	Rogaland	Årakbekken, Vindafjord	59.52453	5.8162	3	55	-	-	291	-	-	-	-	-	3	Anundsen 1977	211	291		
254	R228	Rogaland	Kalvatræsteinen, Vindafjord	59.51647	5.8134	3	23	-	-	-	-	-	-	-	200	3	Anundsen 1977	213	200		
255	R228	Rogaland	Kalvatræsteinen, Vindafjord	59.51647	5.8134	3	23	-	-	-	-	-	-	-	261	3	Anundsen 1977	213	261		
256	R229	Rogaland	Legdene, Vindafjord	59.51993	5.8018	3	186	-	-	257	-	-	-	-	-	3	Anundsen 1977	211	257		
257	R230	Rogaland	Friarsteinen, Vindafjord	59.51606	5.7487	3	353	-	-	290	-	-	-	-	-	3	Anundsen 1977	211	290		
258	R231	Rogaland	Guirines, Vindafjord	59.49912	5.7331	3	46	-	-	158	-	-	-	-	-	3	Anundsen 1977	211	158		
259	R232	Rogaland	Haugen, Vindafjord	59.48937	5.7530	3	52	-	-	212	-	-	-	-	-	3	Anundsen 1977	211	212		
260	R233	Rogaland	Forerinda, Vindafjord	59.48535	5.7577	3	101	-	-	235	-	-	-	-	-	3	Anundsen 1977	211	235		
261	R234	Rogaland	Torvskardet, Vindafjord	59.47811	5.7703	3	386	-	-	232	-	-	-	-	-	3	Anundsen 1977	211	232		
262	R235	Rogaland	Kjort, Vindafjord	59.48261	5.7768	3	604	-	-	322	-	-	-	-	-	3	Anundsen 1977	211	322		
263	R236	Rogaland	Åmselva, Vindafjord	59.47645	5.7394	3	2.7	-	-	184	-	-	-	-	-	3	Anundsen 1977	211	184		
264	R237	Rogaland	Skjervheim, Vindafjord	59.46791	5.7434	3	5	-	-	153	-	-	-	-	-	3	Anundsen 1977	215	153		
265	R238	Rogaland	Skjervheim, Vindafjord	59.46791	5.7434	3	5	-	-	-	264	-	-	-	-	3	Anundsen 1977	216	264		
266	R239	Rogaland	Eikanes, Vindafjord	59.45954	5.7393	3	1	-	-	170	-	-	-	-	-	3	Anundsen 1977	215	170		
267	R240	Rogaland	Eikanes, Vindafjord	59.45954	5.7393	3	1	-	-	-	213	-	-	-	-	3	Anundsen 1977	216	213		
268	R241	Rogaland	Dyna, Vindafjord	59.45292	5.7579	3	1	-	-	160	-	-	-	-	-	3	Anundsen 1977	211	160		
269	R242	Rogaland	Kvamstjørna, Vindafjord	59.46521	5.7757	3	132	-	-	261	-	-	-	-	-	3	Anundsen 1977	211	261		
270	R243	Rogaland	Veikjamyra, Vindafjord	59.48009	5.7969	3	206	-	-	195	-	-	-	-	-	3	Anundsen 1977	211	195		
271	R244	Rogaland	Lauvvika, Vindafjord	59.48412	5.8488	3	57	-	-	172	-	-	-	-	-	3	Anundsen 1977	211	172		
272	R245	Rogaland	Kloppamyr, Vindafjord	59.48160	5.8443	3	94	-	-	256	-	-	-	-	-	3	Anundsen 1977	211	256		
273	R246	Rogaland	Raudnesvika, Vindafjord	59.44013	5.7470	3	3	-	-	135	-	-	-	-	-	3	Anundsen 1977	215	135		
274	R246	Rogaland	Raudnesvika, Vindafjord	59.44013	5.7470	3	3	-	-	-	146	-	-	-	-	3	Anundsen 1977	216	146		
275	R247	Rogaland	Kattrauva, Vindafjord	59.43522	5.7684	3	16	-	-	-	-	-	-	-	293	3	Anundsen 1977	213	293		
276	R247	Rogaland	Kattrauva, Vindafjord	59.43522	5.7684	3	16	-	-	-	-	-	-	-	315	3	Anundsen 1977	213	315		
277	R248	Rogaland	Elfarvika, Tysvær	59.42504	5.7810	3	2	-	-	-	-	-	-	-	190	3	Anundsen 1977	213	190		
278	R248	Rogaland	Elfarvika, Tysvær	59.42504	5.7810	3	2	-	-	-	-	-	-	-	210	3	Anundsen 1977	213	210		
279	R248	Rogaland	Elfarvika, Tysvær	59.42504	5.7810	3	2	-	-	-	-	-	-	-	230	3	Anundsen 1977	213	230		
280	R249	Rogaland	Aplaflota, Tysvær	59.43344	5.8232	3	27	-	-	-	-	-	-	-	228	3	Anundsen 1977	213	228		

Striae No	Loc. No	County	Placename	Lat_N	Long_E	Precision	m a.s.l.	Mid pt.	Plus_ Minus	Youngest	Older	Even Older	Even Older 2	Oldest	Undet. rel. age	Quality	Source	Code symbol	All orientations	Comments	Erosional marks
281	R249	Rogaland	Aplaflota, Tysvær	59.43344	5.8232	3	27	-	-	-	-	-	-	-	255	3	Anundsen 1977	213	255		
282	R249	Rogaland	Aplaflota, Tysvær	59.43344	5.8232	3	27	-	-	-	195	-	-	-	-	3	Anundsen 1977	216	195		
283	R250	Rogaland	Metteneset, Tysvær	59.43707	5.8427	3	8	-	-	214	-	-	-	-	-	3	Anundsen 1977	215	214		
284	R250	Rogaland	Metteneset, Tysvær	59.43707	5.8427	3	8	-	-	-	178	-	-	-	-	3	Anundsen 1977	216	178		
285	R251	Rogaland	Sølvberget, Tysvær	59.37445	5.7839	3	23	-	-	304	-	-	-	-	-	3	Anundsen 1977	211	304		
286	R252	Rogaland	Nypedalen, Tysvær	59.35113	5.7996	3	32	-	-	195	-	-	-	-	-	3	Anundsen 1977	211	195		
287	R253	Rogaland	Hindaråvåg, Tysvær	59.34821	5.7997	3	13	-	-	202	-	-	-	-	-	3	Anundsen 1977	211	202		
288	R254	Rogaland	Flatå, Tysvær	59.34551	5.8188	3	50	-	-	288	-	-	-	-	-	3	Anundsen 1977	211	288		
289	R255	Rogaland	Plasset, Tysvær	59.34988	5.8221	3	124	-	-	-	-	-	-	-	320	3	Anundsen 1977	213	320		
290	R255	Rogaland	Plasset, Tysvær	59.34988	5.8221	3	124	-	-	-	-	-	-	-	288	3	Anundsen 1977	213	288		
291	R255	Rogaland	Plasset, Tysvær	59.34988	5.8221	3	124	-	-	-	-	-	-	-	222	3	Anundsen 1977	213	222		
292	R256	Rogaland	Hetland, Tysvær	59.35409	5.8201	3	191	-	-	-	218	-	-	-	-	3	Anundsen 1977	216	218		
293	R256	Rogaland	Hetland, Tysvær	59.35409	5.8201	3	191	-	-	-	-	-	-	-	161	3	Anundsen 1977	213	161		
294	R256	Rogaland	Hetland, Tysvær	59.35409	5.8201	3	191	-	-	-	-	-	-	-	285	3	Anundsen 1977	213	285		
295	R257	Rogaland	Litla Badnavatnet, Tysvær	59.36635	5.8220	3	447	-	-	177	-	-	-	-	-	3	Anundsen 1977	211	177		
296	R258	Rogaland	Stølanuten, Tysvær	59.36825	5.8165	3	550	-	-	158	-	-	-	-	-	3	Anundsen 1977	211	158		
297	R259	Rogaland	Rossafjellet, Tysvær	59.37648	5.8218	3	544	-	-	180	-	-	-	-	-	3	Anundsen 1977	211	180		
298	R260	Rogaland	Skrubburdnuten, Tysvær	59.38220	5.8322	3	587	-	-	172	-	-	-	-	-	3	Anundsen 1977	211	172		
299	R261	Rogaland	Tverrheia, Tysvær	59.38517	5.8430	3	503	-	-	203	-	-	-	-	-	3	Anundsen 1977	211	203		
300	R262	Rogaland	Skoråsen, Tysvær	59.38782	5.8529	3	419	-	-	205	-	-	-	-	-	3	Anundsen 1977	211	205		
301	R263	Rogaland	Dalvanuten, Tysvær	59.37372	5.8481	3	518	-	-	204	-	-	-	-	-	3	Anundsen 1977	211	204		
302	R264	Rogaland	Aksland, Tysvær	59.35492	5.8320	3	148	-	-	172	-	-	-	-	-	3	Anundsen 1977	215	172		
303	R264	Rogaland	Aksland, Tysvær	59.35492	5.8320	3	148	-	-	-	215	-	-	-	-	3	Anundsen 1977	216	215		
304	R265	Rogaland	Plasset, Tysvær	59.34945	5.8251	3	74	-	-	262	-	-	-	-	-	3	Anundsen 1977	211	262		
305	R266	Rogaland	Stuvvikneset, Tysvær	59.34103	5.8515	3	6	-	-	236	-	-	-	-	-	3	Anundsen 1977	211	236		
306	R267	Rogaland	Stuvvika, Tysvær	59.34567	5.8530	3	22	-	-	288	-	-	-	-	-	3	Anundsen 1977	211	288		
307	R268	Rogaland	Kleiberg, Tysvær	59.35204	5.8550	3	159	-	-	217	-	-	-	-	-	3	Anundsen 1977	211	217		
308	R269	Rogaland	Øredalen, Tysvær	59.34899	5.8664	3	55	-	-	172	-	-	-	-	-	3	Anundsen 1977	211	172		

Striae No	Loc. No	County	Placename	Lat_N	Long_E	Precision	m a.s.l.	Mid pt.	Plus_ Minus	Youngest	Older	Even Older	Even Older 2	Oldest	Undet. rel. age	Quality	Source	Code symbol	All orientations	Comments	Erosional marks
309	R270	Rogaland	Fredheim, Tysvær	59.34468	5.8744	3	4	-	-	210	-	-	-	-	-	3	Anundsen 1977	211	210		
310	R271	Rogaland	Dalshamna, Tysvær	59.33874	5.8761	3	8	-	-	187	-	-	-	-	-	3	Anundsen 1977	215	187		
311	R271	Rogaland	Dalshamna, Tysvær	59.33874	5.8761	3	8	-	-	-	290	-	-	-	-	3	Anundsen 1977	216	290		
312	R272	Rogaland	Kuneset, Tysvær	59.35111	5.8901	3	1	-	-	-	-	-	-	-	214	3	Anundsen 1977	213	214		
313	R272	Rogaland	Kuneset, Tysvær	59.35111	5.8901	3	1	-	-	-	-	-	-	-	309	3	Anundsen 1977	213	309		
314	R273	Rogaland	Iglemyra, Tysvær	59.35794	5.8747	3	99	-	-	212	-	-	-	-	-	3	Anundsen 1977	215	212		
315	R273	Rogaland	Iglemyra, Tysvær	59.35794	5.8747	3	99	-	-	-	284	-	-	-	-	3	Anundsen 1977	216	284		
316	R274	Rogaland	Foråsen, Tysvær	59.36439	5.8675	3	193	-	-	181	-	-	-	-	-	3	Anundsen 1977	211	181		
317	R275	Rogaland	Sjoarberget, Tysvær	59.37415	5.8934	3	15	-	-	170	-	-	-	-	-	3	Anundsen 1977	211	170		
318	R276	Rogaland	Vikaneset, Tysvær	59.37478	5.8971	3	13	-	-	304	-	-	-	-	-	3	Anundsen 1977	211	304		
319	R277	Rogaland	Frøvikneset, Tysvær	59.38157	5.8959	3	29	-	-	-	-	-	-	-	306	3	Anundsen 1977	212	306		
320	R277	Rogaland	Frøvikneset, Tysvær	59.38157	5.8959	3	29	-	-	-	-	-	-	-	224	3	Anundsen 1977	213	224		
321	R277	Rogaland	Frøvikneset, Tysvær	59.38157	5.8959	3	29	-	-	-	-	-	-	-	208	3	Anundsen 1977	213	208		
322	R277	Rogaland	Frøvikneset, Tysvær	59.38157	5.8959	3	29	-	-	-	-	-	-	-	188	3	Anundsen 1977	213	188		
323	R277	Rogaland	Frøvikneset, Tysvær	59.38157	5.8959	3	29	-	-	-	-	-	-	-	172	3	Anundsen 1977	213	172		
324	R277	Rogaland	Frøvikneset, Tysvær	59.38157	5.8959	3	29	-	-	-	-	-	-	-	149	3	Anundsen 1977	213	149		
325	R278	Rogaland	Gauk, Tysvær	59.38060	5.8782	3	195	-	-	165	-	-	-	-	-	3	Anundsen 1977	211	165		
326	R279	Rogaland	Ytra Straumastølstjørna, Tysvær	59.38266	5.8718	3	255	-	-	146	-	-	-	-	-	3	Anundsen 1977	211	146		
327	R280	Rogaland	Rogaland fylke, Tysvær	59.38530	5.8748	3	250	-	-	225	-	-	-	-	-	3	Anundsen 1977	211	225		
328	R281	Rogaland	Ringjastølen, Tysvær	59.39316	5.8545	3	277	-	-	252	-	-	-	-	-	3	Anundsen 1977	211	252		
329	R282	Rogaland	Ringjastølen, Tysvær	59.39728	5.8514	3	322	-	-	145	-	-	-	-	-	3	Anundsen 1977	211	145		
330	R283	Rogaland	Flintavika, Suldal	59.33707	5.9531	3	10	-	-	220	-	-	-	-	-	3	Anundsen 1977	211	220		
331	R284	Rogaland	Båteholet, Suldal	59.33432	5.9792	3	3	-	-	-	-	-	-	-	159	3	Anundsen 1977	213	159		
332	R284	Rogaland	Båteholet, Suldal	59.33432	5.9792	3	3	-	-	-	-	-	-	-	265	3	Anundsen 1977	213	265		
333	R284	Rogaland	Båteholet, Suldal	59.33432	5.9792	3	3	-	-	-	-	-	-	-	300	3	Anundsen 1977	213	300		
334	R284	Rogaland	Båteholet, Suldal	59.33432	5.9792	3	3	-	-	-	-	-	-	-	319	3	Anundsen 1977	213	319		
335	R285	Rogaland	Frøkenhaugen, Suldal	59.33977	5.9801	3	3	-	-	-	253	-	-	-	-	3	Anundsen 1977	216	253		
336	R285	Rogaland	Frøkenhaugen, Suldal	59.33977	5.9801	3	3	-	-	-	-	-	-	-	226	3	Anundsen 1977	213	226		

Striae No	Loc. No	County	Placename	Lat_N	Long_E	Precision	m a.s.l.	Mid pt.	Plus_ Minus	Youngest	Older	Even Older	Even Older 2	Oldest	Undet. rel. age	Quality	Source	Code symbol	All orientations	Comments	Erosional marks
337	R285	Rogaland	Frøkenhaugen, Suldal	59.33977	5.9801	3	3	-	-	-	-	-	-	-	183	3	Anundsen 1977	213	183		
338	R286	Rogaland	Holeneset, Suldal	59.33823	6.0222	3	3	-	-	203	-	-	-	-	-	3	Anundsen 1977	215	203		
339	R286	Rogaland	Holeneset, Suldal	59.33823	6.0222	3	3	-	-	-	299	-	-	-	-	3	Anundsen 1977	216	299		
340	R287	Rogaland	Kaldveta, Suldal	59.32793	6.0844	3	1	-	-	192	-	-	-	-	-	3	Anundsen 1977	215	192		
341	R287	Rogaland	Kaldveta, Suldal	59.32793	6.0844	3	1	-	-	-	213	-	-	-	-	3	Anundsen 1977	216	213		
342	R287	Rogaland	Kaldveta, Suldal	59.32793	6.0844	3	1	-	-	-	-	236	-	-	-	3	Anundsen 1977	217	236		
343	R287	Rogaland	Kaldveta, Suldal	59.32793	6.0844	3	1	-	-	-	-	266	-	-	-	3	Anundsen 1977	217	266		
344	R287	Rogaland	Kaldveta, Suldal	59.32793	6.0844	3	1	-	-	-	-	-	296	-	-	3	Anundsen 1977	218	296		
345	R288	Rogaland	Grønnevik, Suldal	59.34435	6.0860	3	4	-	-	208	-	-	-	-	-	3	Anundsen 1977	211	208		
346	R289	Rogaland	Brennevika, Suldal	59.35914	6.0402	3	12	-	-	215	-	-	-	-	-	3	Anundsen 1977	211	215		
347	R290	Rogaland	Tjørnaneset, Suldal	59.36674	6.0403	3	5	-	-	214	-	-	-	-	-	3	Anundsen 1977	215	214		
348	R290	Rogaland	Tjørnaneset, Suldal	59.36674	6.0403	3	5	-	-	-	248	-	-	-	-	3	Anundsen 1977	216	248		
349	R291	Rogaland	Lomatjørna, Suldal	59.36758	6.0723	3	448	-	-	222	-	-	-	-	-	3	Anundsen 1977	211	222		
350	R292	Rogaland	Østabøflota, Suldal	59.38753	6.0818	3	37	-	-	237	-	-	-	-	-	3	Anundsen 1977	215	237		
351	R292	Rogaland	Østabøflota, Suldal	59.38753	6.0818	3	37	-	-	-	302	-	-	-	-	3	Anundsen 1977	216	302		
352	R293	Rogaland	Lauvdalstunnelen, Suldal	59.40395	6.1409	3	104	-	-	280	-	-	-	-	-	3	Anundsen 1977	211	280		
353	R294	Rogaland	Tysingvatnet, Suldal	59.39683	6.1557	3	202	-	-	212	-	-	-	-	-	3	Anundsen 1977	211	212		
354	R295	Rogaland	Kleivane, Suldal	59.37796	6.1836	3	54	-	-	200	-	-	-	-	-	3	Anundsen 1977	211	200		
355	R296	Rogaland	Kvednavika, Suldal	59.34899	6.1013	3	9	-	-	224	-	-	-	-	-	3	Anundsen 1977	215	224		
356	R296	Rogaland	Kvednavika, Suldal	59.34899	6.1013	3	9	-	-	-	268	-	-	-	-	3	Anundsen 1977	216	268		
357	R297	Rogaland	Bogstjørna, Suldal	59.33533	6.1776	3	123	-	-	214	-	-	-	-	-	3	Anundsen 1977	211	214		
358	R298	Rogaland	Hagen, Suldal	59.32577	6.1797	3	108	-	-	180	-	-	-	-	-	3	Anundsen 1977	211	180		
359	R299	Rogaland	Bogsund, Suldal	59.32488	6.1860	3	15	-	-	202	-	-	-	-	-	3	Anundsen 1977	211	202		
360	R300	Rogaland	Lysåsen, Suldal	59.32292	6.1581	3	284	-	-	253	-	-	-	-	-	3	Anundsen 1977	211	253		
361	R301	Rogaland	Landsnes, Suldal	59.31844	6.1227	3	3	-	-	268	-	-	-	-	-	3	Anundsen 1977	215	268		
362	R301	Rogaland	Landsnes, Suldal	59.31844	6.1227	3	3	-	-	-	221	-	-	-	-	3	Anundsen 1977	216	221		
363	R302	Rogaland	Fuglastein, Suldal	59.32574	6.1120	3	64	-	-	238	-	-	-	-	-	3	Anundsen 1977	211	238		
364	R303	Rogaland	Husafjellet, Suldal	59.32818	6.1084	3	160	-	-	177	-	-	-	-	-	3	Anundsen 1977	211	177		

Striae No	Loc. No	County	Placename	Lat_N	Long_E	Precision	m a.s.l.	Mid pt.	Plus_ Minus	Youngest	Older	Even Older	Even Older 2	Oldest	Undet. rel. age	Quality	Source	Code symbol	All orientations	Comments	Erosional marks
365	R304	Rogaland	Sørvika, Suldal	59.33626	6.1037	3	1	-	-	225	-	-	-	-	-	3	Anundsen 1977	211	225		
366	R305	Rogaland	Mallastova, Suldal	59.35638	5.9612	3	1	-	-	199	-	-	-	-	-	3	Anundsen 1977	211	199		
367	R306	Rogaland	Leirvika, Suldal	59.35878	5.9689	3	23	-	-	198	-	-	-	-	-	3	Anundsen 1977	215	198		
368	R306	Rogaland	Leirvika, Suldal	59.35878	5.9689	3	23	-	-	-	150	-	-	-	-	3	Anundsen 1977	216	150		
369	R306	Rogaland	Leirvika, Suldal	59.35878	5.9689	3	23	-	-	-	-	243	-	-	-	3	Anundsen 1977	217	243		
370	R306	Rogaland	Leirvika, Suldal	59.35878	5.9689	3	23	-	-	-	-	-	291	-	-	3	Anundsen 1977	218	291		
371	R307	Rogaland	Ostvikstanga, Suldal	59.37427	5.9372	3	5	-	-	304	-	-	-	-	-	3	Anundsen 1977	211	304		
372	R308	Rogaland	Hildravika, Suldal	59.37883	6.0005	3	13	-	-	187	-	-	-	-	-	3	Anundsen 1977	211	187		
373	R309	Rogaland	Jektavika, Suldal	59.38508	6.0188	3	2	-	-	293	-	-	-	-	-	3	Anundsen 1977	211	293		
374	R310	Rogaland	Kviteholmen, Suldal	59.38024	6.0420	3	7	-	-	218	-	-	-	-	-	3	Anundsen 1977	211	218		
375	R311	Rogaland	Rauneholmen, Suldal	59.40756	6.0160	3	2	-	-	206	-	-	-	-	-	3	Anundsen 1977	215	206		
376	R311	Rogaland	Rauneholmen, Suldal	59.40756	6.0160	3	2	-	-	-	315	-	-	-	-	3	Anundsen 1977	216	315		
377	R312	Rogaland	Stemnes, Suldal	59.41836	6.0200	3	43	-	-	180	-	-	-	-	-	3	Anundsen 1977	215	180		
378	R312	Rogaland	Stemnes, Suldal	59.41836	6.0200	3	43	-	-	-	154	-	-	-	-	3	Anundsen 1977	216	154		
379	R313	Rogaland	Otradalen, Suldal	59.41956	6.0144	3	31	-	-	198	-	-	-	-	-	3	Anundsen 1977	211	198		
380	R314	Rogaland	Smalafjellet, Suldal	59.43173	5.9999	3	400	-	-	264	-	-	-	-	-	3	Anundsen 1977	211	264		
381	R315	Rogaland	Skatjørna, Suldal	59.43173	5.9825	3	643	-	-	266	-	-	-	-	-	3	Anundsen 1977	211	266		
382	R316	Rogaland	Grytenuten, Suldal	59.43012	5.9647	3	850	-	-	244	-	-	-	-	-	3	Anundsen 1977	211	244		
383	R317	Rogaland	Rødnejuvet, Suldal	59.43433	5.9779	3	509	-	-	236	-	-	-	-	-	3	Anundsen 1977	211	236		
384	R318	Rogaland	Terneholmen, Suldal	59.44494	5.9617	3	7	-	-	275	-	-	-	-	-	3	Anundsen 1977	211	275		
385	R319	Rogaland	Båsen, Suldal	59.45296	5.9288	3	6	-	-	274	-	-	-	-	-	3	Anundsen 1977	215	274		
386	R319	Rogaland	Båsen, Suldal	59.45296	5.9288	3	6	-	-	-	184	-	-	-	-	3	Anundsen 1977	216	184		
387	R320	Rogaland	Hamnen, Suldal	59.43890	5.9224	3	26	-	-	-	-	-	-	-	204	3	Anundsen 1977	213	204		
388	R320	Rogaland	Hamnen, Suldal	59.43890	5.9224	3	26	-	-	-	-	-	-	-	250	3	Anundsen 1977	213	250		
389	R321	Rogaland	Helland, Suldal	59.42977	5.9167	3	22	-	-	182	-	-	-	-	-	3	Anundsen 1977	211	182		
390	R322	Rogaland	Nautadalsneset, Suldal	59.44763	5.9943	3	40	-	-	200	-	-	-	-	-	3	Anundsen 1977	215	200		
391	R322	Rogaland	Nautadalsneset, Suldal	59.44763	5.9943	3	40	-	-	-	252	-	-	-	-	3	Anundsen 1977	216	252		
392	R322	Rogaland	Nautadalsneset, Suldal	59.44763	5.9943	3	40	-	-	-	-	271	-	-	-	3	Anundsen 1977	217	271		

Striae No	Loc. No	County	Placename	Lat_N	Long_E	Precision	m a.s.l.	Mid pt.	Plus_ Minus	Youngest	Older	Even Older	Even Older 2	Oldest	Undet. rel. age	Quality	Source	Code symbol	All orientations	Comments	Erosional marks
393	R322	Rogaland	Nautadalsneset, Suldal	59.44763	5.9943	3	40	-	-	-	-	-	295	-	-	3	Anundsen 1977	218	295		
394	R322	Rogaland	Nautadalsneset, Suldal	59.44763	5.9943	3	40	-	-	-	-	-	-	326	-	3	Anundsen 1977	219	326		
395	R323	Rogaland	Rosseid, Suldal	59.44447	6.0192	3	58	-	-	190	-	-	-	-	-	3	Anundsen 1977	211	190		
396	R324	Rogaland	Finnvik, Suldal	59.45030	6.0307	3	8	-	-	265	-	-	-	-	-	3	Anundsen 1977	215	265		
397	R324	Rogaland	Finnvik, Suldal	59.45030	6.0307	3	8	-	-	-	294	-	-	-	-	3	Anundsen 1977	216	294		
398	R325	Rogaland	Torsteinbøneset, Sudal	59.45655	6.0527	3	11	-	-	265	-	-	-	-	-	3	Anundsen 1977	211	265		
399	R326	Rogaland	Senganeset, Suldal	59.45928	6.0713	3	8	-	-	240	-	-	-	-	-	3	Anundsen 1977	211	240		
400	R327	Rogaland	Såteheia, Suldal	59.44427	6.0821	3	604	-	-	217	-	-	-	-	-	3	Anundsen 1977	211	217		
401	R328	Rogaland	Fjetland, Suldal	59.43150	6.0645	3	254	-	-	212	-	-	-	-	-	3	Anundsen 1977	211	212		
402	R329	Rogaland	Indre Hedleberheia, Suldal	59.44631	6.1044	3	600	-	-	236	-	-	-	-	-	3	Anundsen 1977	211	236		
403	R330	Rogaland	Kalvhagneset, Suldal	59.46744	6.1348	3	127	-	-	275	-	-	-	-	-	3	Anundsen 1977	215	275		
404	R330	Rogaland	Kalvhagneset, Suldal	59.46744	6.1348	3	127	-	-	-	260	-	-	-	-	3	Anundsen 1977	216	260		
405	R331	Rogaland	Drengstivika, Suldal	59.47171	6.1717	3	69	-	-	-	293	-	-	-	-	3	Anundsen 1977	216	293		
406	R331	Rogaland	Drengstivika, Suldal	59.47171	6.1717	3	69	-	-	-	-	-	-	-	260	3	Anundsen 1977	213	260		
407	R331	Rogaland	Drengstivika, Suldal	59.47171	6.1717	3	69	-	-	-	-	-	-	-	293	3	Anundsen 1977	213	293		
408	R332	Rogaland	Oynatangen, Suldal	59.43095	6.1819	3	15	-	-	216	-	-	-	-	-	3	Anundsen 1977	211	216		
409	R333	Rogaland	Inda Åsarøy, Suldal	59.42253	6.1307	3	6	-	-	221	-	-	-	-	-	3	Anundsen 1977	211	221		
410	R334	Rogaland	Ytra Åsarøy, Suldal	59.41267	6.1218	3	4	-	-	294	-	-	-	-	-	3	Anundsen 1977	211	294		
411	R335	Rogaland	Gjertruholmen, Suldal	59.40458	6.1087	3	9	-	-	278	-	-	-	-	-	3	Anundsen 1977	215	278		
412	R335	Rogaland	Gjertruholmen, Suldal	59.40458	6.1087	3	9	-	-	-	302	-	-	-	-	3	Anundsen 1977	216	302		
413	R336	Rogaland	Holmen, Suldal	59.41585	6.0844	3	65	-	-	211	-	-	-	-	-	3	Anundsen 1977	211	211		
414	R337	Rogaland	Martahaugen, Suldal	59.41290	6.0731	3	26	-	-	310	-	-	-	-	-	3	Anundsen 1977	211	310		
415	R338	Rogaland	Strand, Vindafjord	59.52499	5.8703	3	18	-	-	181	-	-	-	-	-	3	Anundsen 1977	211	181		
416	R338	Rogaland	Strand, Vindafjord	59.52273	5.8748	3	120	-	-	205	-	-	-	-	-	3	Anundsen 1977	211	205		
417	R339	Rogaland	Lysenuten, Vindafjord	59.52770	5.9026	3	794	-	-	224	-	-	-	-	-	3	Anundsen 1977	211	224		
418	R340	Rogaland	Vestergård, Vindafjord	59.49770	5.8953	3	32	-	-	-	-	-	-	-	190	3	Anundsen 1977	213	190		
419	R340	Rogaland	Vestergård, Vindafjord	59.49770	5.8953	3	32	-	-	-	-	-	-	-	220	3	Anundsen 1977	213	220		
420	R341	Rogaland	Brenneset, Vindafjord	59.47820	5.8932	3	14	-	-	-	320	-	-	-	-	3	Anundsen 1977	216	320		

Striae No	Loc. No	County	Placename	Lat_N	Long_E	Precision	m a.s.l.	Mid pt.	Plus_ Minus	Youngest	Older	Even Older	Even Older 2	Oldest	Undet. rel. age	Quality	Source	Code symbol	All orientations	Comments	Erosional marks
421	R341	Rogaland	Brenneset, Vindafjord	59.47820	5.8932	3	14	-	-	-	-	-	-	-	240	3	Anundsen 1977	213	240		
422	R341	Rogaland	Brenneset, Vindafjord	59.47820	5.8932	3	14	-	-	-	-	-	-	-	216	3	Anundsen 1977	213	216		
423	R341	Rogaland	Brenneset, Vindafjord	59.47820	5.8932	3	14	-	-	-	-	-	-	-	178	3	Anundsen 1977	213	178		
424	R342	Rogaland	Holmen, Vindafjord	59.47689	5.9044	3	4	-	-	-	187	-	-	-	-	3	Anundsen 1977	216	187		
425	R342	Rogaland	Holmen, Vindafjord	59.47689	5.9044	3	4	-	-	-	-	332	-	-	-	3	Anundsen 1977	217	332		
426	R342	Rogaland	Holmen, Vindafjord	59.47689	5.9044	3	4	-	-	-	-	-	-	-	302	3	Anundsen 1977	213	302		
427	R342	Rogaland	Holmen, Vindafjord	59.47689	5.9044	3	4	-	-	-	-	-	-	-	205	3	Anundsen 1977	213	205		
428	R343	Rogaland	Haugen, Vindafjord	59.47547	5.9141	3	48	-	-	259	-	-	-	-	-	3	Anundsen 1977	215	259		
429	R343	Rogaland	Haugen, Vindafjord	59.47547	5.9141	3	48	-	-	-	312	-	-	-	-	3	Anundsen 1977	216	312		
430	R343	Rogaland	Haugen, Vindafjord	59.47547	5.9141	3	48	-	-	-	344	-	-	-	-	3	Anundsen 1977	216	344		
431	R344	Rogaland	Svalefjellet, Vindafjord	59.48178	5.9296	3	71	-	-	178	-	-	-	-	-	3	Anundsen 1977	211	178		
432	R345	Rogaland	Rødstegane, Vindafjord	59.48653	5.9506	3	256	-	-	251	-	-	-	-	-	3	Anundsen 1977	211	251		
433	R346	Rogaland	Kjellarhaugane, Vindafjord	59.49508	5.9372	3	300	-	-	202	-	-	-	-	-	3	Anundsen 1977	211	202		
434	R347	Rogaland	Svartops, Vindafjord	59.51094	5.9374	3	305	-	-	243	-	-	-	-	-	3	Anundsen 1977	211	243		
435	R348	Rogaland	Ørnes, Vindafjord	59.51531	5.9265	3	57	-	-	-	-	-	-	-	206	3	Anundsen 1977	213	206		
436	R348	Rogaland	Ørnes, Vindafjord	59.51531	5.9265	3	57	-	-	-	-	-	-	-	242	3	Anundsen 1977	213	242		
437	R349	Rogaland	Geitaberget, Vindafjord	59.51618	5.9109	3	267	-	-	205	-	-	-	-	-	3	Anundsen 1977	211	205		
438	R350	Rogaland	Imslandsjøen, Vindafjord	59.47870	5.9925	3	41	-	-	254	-	-	-	-	-	3	Anundsen 1977	215	254		
439	R350	Rogaland	Imslandsjøen, Vindafjord	59.47870	5.9925	3	41	-	-	-	315	-	-	-	-	3	Anundsen 1977	216	315		
440	R350	Rogaland	Imslandsjøen, Vindafjord	59.47870	5.9925	3	41	-	-	-	339	-	-	-	-	3	Anundsen 1977	216	339		
441	R351	Rogaland	Rindanuten, Vindafjord	59.48157	5.9949	3	202	-	-	183	-	-	-	-	-	3	Anundsen 1977	211	183		
442	R352	Rogaland	Stemmyrhaugen, Vindafjord	59.47998	6.0233	3	114	-	-	290	-	-	-	-	-	3	Anundsen 1977	211	290		
443	R353	Rogaland	Torkjelsurene, Vindafjord	59.48627	6.0443	3	294	-	-	298	-	-	-	-	-	3	Anundsen 1977	211	298		
444	R354	Rogaland	Kråkedal, Vindafjord	59.48341	6.1012	3	125	-	-	242	-	-	-	-	-	3	Anundsen 1977	211	242		
445	R355	Rogaland	Frøvikneset, Vindafjord	59.47662	6.0956	3	13	-	-	-	-	-	-	-	228	3	Anundsen 1977	213	228		
446	R355	Rogaland	Frøvikneset, Vindafjord	59.47662	6.0956	3	13	-	-	-	-	-	-	-	242	3	Anundsen 1977	213	242		
447	R355	Rogaland	Frøvikneset, Vindafjord	59.47662	6.0956	3	13	-	-	-	-	-	-	-	278	3	Anundsen 1977	213	278		
448	R355	Rogaland	Frøvikneset, Vindafjord	59.47662	6.0956	3	13	-	-	-	303	-	-	-	-	3	Anundsen 1977	216	303		

Striae No	Loc. No	County	Placename	Lat_N	Long_E	Precision	m a.s.l.	Mid pt.	Plus_ Minus	Youngest	Older	Even Older	Even Older 2	Oldest	Undet. rel. age	Quality	Source	Code symbol	All orientations	Comments	Erosional marks
449	R356	Rogaland	Hårborvika, Vindafjord	59.48343	6.1572	3	17	-	-	218	-	-	-	-	-	3	Anundsen 1977	211	218		
450	R357	Rogaland	Studatal, Suldal	59.49244	6.1920	3	182	-	-	258	-	-	-	-	-	3	Anundsen 1977	211	258		
451	R358	Rogaland	Tysselandsstølen, Suldal	59.53007	6.1965	3	375	-	-	212	-	-	-	-	-	3	Anundsen 1977	211	212		
452	R359	Rogaland	Skansen, Suldal	59.55173	6.1648	3	757	-	-	190	-	-	-	-	-	3	Anundsen 1977	211	190		
453	R360	Rogaland	Nonshei,Vindafjord	59.56665	6.1170	3	587	-	-	275	-	-	-	-	-	3	Anundsen 1977	211	275		
454	R361	Rogaland	Sjurdsstølen, Vindafjord	59.56507	6.0997	3	365	-	-	281	-	-	-	-	-	3	Anundsen 1977	211	281		
455	R362	Rogaland	Stegatjørn, Vindafjord	59.55239	6.0974	3	577	-	-	228	-	-	-	-	-	3	Anundsen 1977	211	228		
456	R363	Rogaland	Søtetjørn, Vindafjord	59.54469	6.0822	3	662	-	-	250	-	-	-	-	-	3	Anundsen 1977	211	250		
457	R364	Rogaland	Horganuten, Vindafjord	59.53820	6.0588	3	617	-	-	279	-	-	-	-	-	3	Anundsen 1977	211	279		
458	R365	Rogaland	Horganuten, Vindafjord	59.53261	6.0532	3	712	-	-	233	-	-	-	-	-	3	Anundsen 1977	211	233		
459	R366	Rogaland	Fevatnet, Vindafjord	59.52345	6.0481	3	787	-	-	250	-	-	-	-	-	3	Anundsen 1977	211	250		
460	R367	Rogaland	Flatet, Vindafjord	59.50629	6.0556	3	540	-	-	238	-	-	-	-	-	3	Anundsen 1977	211	238		
461	R368	Rogaland	Dyråna, Vindafjord	59.53091	6.0247	3	545	-	-	230	-	-	-	-	-	3	Anundsen 1977	211	230		
462	R369	Rogaland	Ulvavoll, Vindafjord	59.53464	6.0042	3	358	-	-	210	-	-	-	-	-	3	Anundsen 1977	211	210		
463	R370	Rogaland	Rødne, Vindafjord	59.51172	5.9946	3	315	-	-	170	-	-	-	-	-	3	Anundsen 1977	211	170		
464	R371	Rogaland	Lokafoss, Vindafjord	59.53539	5.9787	3	122	-	-	226	-	-	-	-	-	3	Anundsen 1977	211	226		
465	R372	Rogaland	Eikjelandskaret, Vindafjord	59.54230	5.9476	3	305	-	-	210	-	-	-	-	-	3	Anundsen 1977	211	210		
466	R373	Rogaland	Trodalselva, Vindafjord	59.54444	5.9444	3	385	-	-	258	-	-	-	-	-	3	Anundsen 1977	211	258		
467	R374	Rogaland	Mørkstjørna, Vindafjord	59.56044	5.9503	3	593	-	-	210	-	-	-	-	-	3	Anundsen 1977	211	210		
468	R375	Rogaland	Hetlelia, Vindafjord	59.54897	6.0195	3	269	-	-	166	-	-	-	-	-	3	Anundsen 1977	211	166		
469	R376	Rogaland	Tverrlia, Vindafjord	59.55072	6.0476	3	383	-	-	260	-	-	-	-	-	3	Anundsen 1977	211	260		
470	H1	Hordaland	Brudnaklampane, Etne	59.59624	5.9711	3	506	-	-	267	-	-	-	-	-	3	Anundsen 1977	211	267		
471	R377	Rogaland	Lysevatnet, Tysvær	59.59768	6.0236	3	650	-	-	280	-	-	-	-	-	3	Anundsen 1977	211	280		
472	R378	Rogaland	Dyråsen, Vindafjord	59.57479	6.0272	3	652	-	-	226	-	-	-	-	-	3	Anundsen 1977	211	226		
473	R379	Rogaland	Ørekjerven, Vindafjord	59.57308	6.0622	3	228	-	-	261	-	-	-	-	-	3	Anundsen 1977	211	261		
474	R380	Rogaland	Barlundbekken, Vindafjord	59.57826	6.0786	3	513	-	-	290	-	-	-	-	-	3	Anundsen 1977	211	290		
475	R381	Rogaland	Flåtavassnutane, Vindafjord	59.58044	6.0849	3	576	-	-	252	-	-	-	-	-	3	Anundsen 1977	211	252		
476	R382	Rogaland	Flåtavassnutane, Vindafjord	59.58305	6.0865	3	633	-	-	239	-	-	-	-	-	3	Anundsen 1977	211	239		

Striae No	Loc. No	County	Placename	Lat_N	Long_E	Precision	m a.s.l.	Mid pt.	Plus_ Minus	Youngest	Older	Even Older	Even Older 2	Oldest	Undet. rel. age	Quality	Source	Code symbol	All orientations	Comments	Erosional marks
477	R383	Rogaland	Flåtavassnutane, Vindafjord	59.58703	6.0798	3	671	-	-	215	-	-	-	-	-	3	Anundsen 1977	211	215		
478	R384	Rogaland	Flåtevasstølen, Vindafjord	59.58569	6.0717	3	630	-	-	189	-	-	-	-	-	3	Anundsen 1977	211	189		
479	R385	Rogaland	Midtnuten, Vindafjord	59.58398	6.0513	3	664	-	-	232	-	-	-	-	-	3	Anundsen 1977	211	232		
480	R386	Rogaland	Lysevassnuten, Vindafjord	59.59354	6.0551	3	817	-	-	236	-	-	-	-	-	3	Anundsen 1977	211	236		
481	H2	Hordaland	Veradalstjørnene, Etne	59.61274	6.0366	3	791	-	-	269	-	-	-	-	-	3	Anundsen 1977	211	269		
482	H3	Hordaland	Høylandsvatnet, Etne	59.61911	6.0313	3	743	-	-	280	-	-	-	-	-	3	Anundsen 1977	211	280		
483	H4	Hordaland	Auastadstølen, Etne	59.61253	6.0684	3	659	-	-	202	-	-	-	-	-	3	Anundsen 1977	211	202		
484	H5	Hordaland	Kaldeimshovda, Etne	59.61084	6.0854	3	622	-	-	340	-	-	-	-	-	3	Anundsen 1977	212	340		
485	R387	Rogaland	Djupatjørn, Vindafjord	59.58944	6.1078	3	476	-	-	236	-	-	-	-	-	3	Anundsen 1977	211	236		
486	R388	Rogaland	Djupatjørn, Vindafjord	59.58413	6.1148	3	434	-	-	200	-	-	-	-	-	3	Anundsen 1977	211	200		
487	R389	Rogaland	Djupatjørn, Vindafjord	59.57575	6.1137	3	460	-	-	240	-	-	-	-	-	3	Anundsen 1977	211	240		
488	R390	Rogaland	Botnavatnet, Vindafjord	59.59245	6.1284	3	485	-	-	230	-	-	-	-	-	3	Anundsen 1977	211	230		
489	H6	Hordaland	Kvannenuten, Etne	59.61383	6.1472	3	841	-	-	287	-	-	-	-	-	3	Anundsen 1977	211	287		
490	H7	Hordaland	Reinsfossen, Etne	59.61152	6.1619	3	739	-	-	219	-	-	-	-	-	3	Anundsen 1977	211	219		
491	H8	Hordaland	Indra Jordavatnet, Etne	59.62018	6.1550	3	759	-	-	266	-	-	-	-	-	3	Anundsen 1977	211	266		
492	H9	Hordaland	Krokavatnet, Etne	59.62555	6.1597	3	800	-	-	265	-	-	-	-	-	3	Anundsen 1977	211	265		
493	H10	Hordaland	Krokavassnuten, Etne	59.63559	6.1762	3	853	-	-	324	-	-	-	-	-	3	Anundsen 1977	211	324		
494	H11	Hordaland	Fiskedalen, Etne	59.63689	6.1523	3	800	-	-	300	-	-	-	-	-	3	Anundsen 1977	211	300		
495	H12	Hordaland	Nedre Jordavatnet, Etne	59.62431	6.1328	3	680	-	-	177	-	-	-	-	-	3	Anundsen 1977	212	177		
496	H13	Hordaland	Grindheimsstølen, Etne	59.63347	6.1187	3	590	-	-	305	-	-	-	-	-	3	Anundsen 1977	211	305		
497	H14	Hordaland	Bordfjellet, Etne	59.63678	6.1414	3	858	-	-	244	-	-	-	-	-	3	Anundsen 1977	211	244		
498	H15	Hordaland	Bordfjellet, Etne	59.63924	6.1321	3	900	-	-	324	-	-	-	-	-	3	Anundsen 1977	211	324		
499	H16	Hordaland	Raunevika, Etne	59.64470	6.1357	3	850	-	-	172	-	-	-	-	-	3	Anundsen 1977	211	172		
500	H17	Hordaland	Fiskedalen, Etne	59.64884	6.1469	3	717	-	-	309	-	-	-	-	-	3	Anundsen 1977	211	309		
501	H18	Hordaland	Raunevika, Etne	59.64348	6.1229	3	724	-	-	250	-	-	-	-	-	3	Anundsen 1977	211	250		
502	H19	Hordaland	Raunevika, Etne	59.65055	6.1174	3	680	-	-	265	-	-	-	-	-	3	Anundsen 1977	211	265		
503	H20	Hordaland	Hårlandselva, Etne	59.66244	6.1007	3	455	-	-	291	-	-	-	-	-	3	Anundsen 1977	211	291		
504	H21	Hordaland	Suila, Etne	59.66234	6.0844	3	220	-	-	307	-	-	-	-	-	3	Anundsen 1977	211	307		

Striae No	Loc. No	County	Placename	Lat_N	Long_E	Precision	m a.s.l.	Mid pt.	Plus_ Minus	Youngest	Older	Even Older	Even Older 2	Oldest	Undet. rel. age	Quality	Source	Code symbol	All orientations	Comments	Erosional marks
505	H22	Hordaland	Strypeheiane, Etne	59.65390	6.0735	3	604	-	-	304	-	-	-	-	-	3	Anundsen 1977	211	304		
506	H23	Hordaland	Heimrestølen, Etne	59.63702	6.0611	3	581	-	-	307	-	-	-	-	-	3	Anundsen 1977	211	307		
507	H24	Hordaland	Haugalia, Etne	59.64665	6.0913	3	528	-	-	307	-	-	-	-	-	3	Anundsen 1977	211	307		
508	H25	Hordaland	Basurdevatnet, Etne	59.63032	6.0837	3	597	-	-	202	-	-	-	-	-	3	Anundsen 1977	211	202		
509	H26	Hordaland	Nalthaug, Etne	59.63826	6.1011	3	560	-	-	330	-	-	-	-	-	3	Anundsen 1977	211	330		
510	H27	Hordaland	Åborebotn, Etne	59.66736	6.1787	3	714	-	-	278	-	-	-	-	-	3	Anundsen 1977	211	278		
511	H28	Hordaland	Frettestølen, Etne	59.70736	6.1795	3	580	-	-	274	-	-	-	-	-	3	Anundsen 1977	211	274		
512	H29	Hordaland	Fretteskar, Etne	59.71127	6.1851	3	622	-	-	295	-	-	-	-	-	3	Anundsen 1977	211	295		
513	R391	Rogaland	Håbakken, Randaberg	59.03231	5.5851	3	5	-	-	242	-	-	-	-	-	3	Andersen et al. 1987	211	242		
514	R392	Rogaland	Bergsagelvarden, Randaberg	59.00097	5.6264	3	29	-	-	246	-	-	-	-	-	3	Andersen et al. 1987	211	246		
515	R392	Rogaland	Bergsagelvarden, Randaberg	59.00097	5.6264	3	29	-	-	262	-	-	-	-	-	3	Andersen et al. 1987	211	262		
516	R393	Rogaland	Sotrabakken, Randaberg	58.99534	5.6776	3	21	-	-	247	-	-	-	-	-	3	Andersen et al. 1987	211	247		
517	R394	Rogaland	Dalen, Randaberg	58.98784	5.6278	3	33	-	-	248	-	-	-	-	-	3	Andersen et al. 1987	211	248		
518	R395	Rogaland	Måkeberget, Stavanger	58.96982	5.5938	3	6	-	-	242	-	-	-	-	-	3	Andersen et al. 1987	211	242		
519	R396	Rogaland	Myklabust, Sola	58.94627	5.5821	3	34	-	-	239	-	-	-	-	-	3	Andersen et al. 1987	211	239		
520	R397	Rogaland	Håstein, Sola	58.94988	5.4398	2	45	-	-	237	-	-	-	-	-	3	Andersen et al. 1987	211	237		
521	R398	Rogaland	Storetjør, Sola	58.88661	5.4404	3	6	-	-	242	-	-	-	-	-	3	Andersen et al. 1987	211	242		
522	R399	Rogaland	Nadaskjeret, Sola	58.84414	5.5631	3	7	-	-	250	-	-	-	-	-	3	Andersen et al. 1987	215	250		
523	R399	Rogaland	Nadaskjeret, Sola	58.84414	5.5631	3	7	-	-	-	270	-	-	-	-	3	Andersen et al. 1987	216	270		
524	R400	Rogaland	Hundvåg, Stavanger	58.99334	5.7261	3	5	-	-	243	-	-	-	-	-	3	Andersen et al. 1987	211	243		
525	R400	Rogaland	Hundvåg, Stavanger	58.99334	5.7261	3	5	-	-	228	-	-	-	-	-	3	Andersen et al. 1987	211	228		
526	R401	Rogaland	Tastagata, Stavanger	58.97915	5.7156	3	26	-	-	213	-	-	-	-	-	3	Andersen et al. 1987	211	213		
527	R402	Rogaland	Ledaalsgata, Stavanger	58.96887	5.7256	3	33	-	-	184	-	-	-	-	-	3	Andersen et al. 1987	211	184		
528	R402	Rogaland	Ledaalsgata, Stavanger	58.96887	5.7256	3	33	-	-	198	-	-	-	-	-	3	Andersen et al. 1987	211	198		
529	R403	Rogaland	Orrestien, Stavanger	58.95691	5.6907	3	36	-	-	225	-	-	-	-	-	3	Andersen et al. 1987	211	225		
530	R404	Rogaland	Madlalia, Stavanger	58.93480	5.6823	3	4	-	-	236	-	-	-	-	-	3	Andersen et al. 1987	211	236		
531	R405	Rogaland	Veslefrikkveien, Stavanger	58.94483	5.7096	3	89	-	-	220	-	-	-	-	-	3	Andersen et al. 1987	211	220		
532	R406	Rogaland	Solhøgda, Stavanger	58.94052	5.7534	3	25	-	-	195	-	-	-	-	-	3	Andersen et al. 1987	211	195		

Striae No	Loc. No	County	Placename	Lat_N	Long_E	Precision	m a.s.l.	Mid pt.	Plus_ Minus	Youngest	Older	Even Older	Even Older 2	Oldest	Undet. rel. age	Quality	Source	Code symbol	All orientations	Comments	Erosional marks
533	R407	Rogaland	Vaulen, Stavanger	58.92514	5.7484	3	4	-	-	187	-	-	-	-	-	3	Andersen et al. 1987	211	187		
534	R408	Rogaland	Midtgårdveien, Stavanger	58.89618	5.7445	3	13	-	-	239	-	-	-	-	-	3	Andersen et al. 1987	211	239		
535	R409	Rogaland	Fjogstad, Sandnes	58.89027	5.8112	3	279	-	-	250	-	-	-	-	-	3	Andersen et al. 1987	211	250		
536	R409	Rogaland	Fjogstad, Sandes	58.89027	5.8112	3	279	-	-	282	-	-	-	-	-	3	Andersen et al. 1987	211	282		
537	R410	Rogaland	Dalevika, Sandes	58.89887	5.7757	3	4	-	-	240	-	-	-	-	-	3	Andersen et al. 1987	211	240		
538	R411	Rogaland	Lihesthammaren, Sandnes	58.91583	5.8119	3	136	-	-	235	-	-	-	-	-	3	Andersen et al. 1987	211	235		
539	R411	Rogaland	Lihesthammaren, Sandnes	58.91583	5.8119	3	136	-	-	248	-	-	-	-	-	3	Andersen et al. 1987	211	248		
540	R412	Rogaland	Storhaug, Sandnes	58.91545	5.8473	3	71	-	-	230	-	-	-	-	-	3	Andersen et al. 1987	211	230		
541	R412	Rogaland	Storhaug, Sandnes	58.91545	5.8473	3	71	-	-	250	-	-	-	-	-	3	Andersen et al. 1987	211	250		
542	R413	Rogaland	Ulsneset, Sandnes	58.93200	5.8430	3	17	-	-	256	-	-	-	-	-	3	Andersen et al. 1987	211	256		
543	R414	Rogaland	Heståvatn, Sandnes	58.93658	5.8538	3	29	-	-	248	-	-	-	-	-	3	Andersen et al. 1987	211	248		
544	R415	Rogaland	Vardhaug, Sandnes	58.94500	5.8292	3	55	-	-	252	-	-	-	-	-	3	Andersen et al. 1987	211	252		
545	R416	Rogaland	Viervågen, Sandnes	58.96346	5.8974	3	3	-	-	278	-	-	-	-	-	3	Andersen et al. 1987	211	278		
546	R417	Rogaland	Holmatjørna, Sandnes	58.95511	5.8929	3	81	-	-	266	-	-	-	-	-	3	Andersen et al. 1987	215	266		
547	R417	Rogaland	Holmatjørna, Sandnes	58.95511	5.8929	3	81	-	-	-	224	-	-	-	-	3	Andersen et al. 1987	216	224		
548	R418	Rogaland	Klåberget, Sandnes	58.95057	5.8979	3	60	-	-	239	-	-	-	-	-	3	Andersen et al. 1987	211	239		
549	R419	Rogaland	Hammarsdalen, Sandnes	58.93595	5.9460	3	78	-	-	307	-	-	-	-	-	3	Andersen et al. 1987	211	307		
550	R420	Rogaland	Landpåsane, Sandnes	58.93155	5.9776	3	50	-	-	308	-	-	-	-	-	3	Andersen et al. 1987	211	308		
551	R421	Rogaland	Eikelivatnet, Sandnes	58.90625	5.9410	3	31	-	-	250	-	-	-	-	-	3	Andersen et al. 1987	211	250		
552	R422	Rogaland	Ims, Sandnes	58.90508	5.9628	3	9	-	-	236	-	-	-	-	-	3	Andersen et al. 1987	211	236		
553	R423	Rogaland	Krusafjellet, Sandnes	58.88743	6.0283	3	279	-	-	261	-	-	-	-	-	3	Andersen et al. 1987	211	261		
554	R424	Rogaland	Høle, Sandnes	58.88220	6.0275	3	171	-	-	253	-	-	-	-	-	3	Andersen et al. 1987	211	253		
555	R425	Rogaland	Vassbotnlia, Sandnes	58.87646	6.0367	3	278	-	-	225	-	-	-	-	-	3	Andersen et al. 1987	211	225		
556	R426	Rogaland	Gloppefjellet, Sandnes	58.87518	6.0214	3	227	-	-	-	-	-	-	-	243	3	Andersen et al. 1987	213	243		
557	R426	Rogaland	Gloppefjellet, Sandnes	58.87518	6.0214	3	227	-	-	-	-	-	-	-	145	3	Andersen et al. 1987	213	145		
558	R427	Rogaland	Erlonsbakken, Sandnes	58.88245	6.0193	3	100	-	-	181	-	-	-	-	-	3	Andersen et al. 1987	211	181		
559	R428	Rogaland	Bukkaknuten, Sandnes	58.87441	5.9922	3	350	-	-	245	-	-	-	-	-	3	Andersen et al. 1987	211	245		
560	R429	Rogaland	Undeknuten, Sandnes	58.85556	5.9907	3	425	-	-	256	-	-	-	-	-	3	Andersen et al. 1987	211	256		

Striae No	Loc. No	County	Placename	Lat_N	Long_E	Precision	m a.s.l.	Mid pt.	Plus_ Minus	Youngest	Older	Even Older	Even Older 2	Oldest	Undet. rel. age	Quality	Source	Code symbol	All orientations	Comments	Erosional marks
561	R430	Rogaland	Alsnes, Sandnes	58.86304	5.8417	3	67	-	-	264	-	-	-	-	-	3	Andersen et al. 1987	215	264		
562	R430	Rogaland	Alsnes, Sandnes	58.86304	5.8417	3	67	-	-	-	198	-	-	-	-	3	Andersen et al. 1987	216	198		
563	R431	Rogaland	Auestadkanalen, Sandnes	58.84988	5.7855	3	34	-	-	269	-	-	-	-	-	3	Andersen et al. 1987	211	269		
564	R432	Rogaland	Torsteinfjellet, Sandnes	58.84138	5.8206	3	119	-	-	242	-	-	-	-	-	3	Andersen et al. 1987	211	242		
565	R433	Rogaland	Svilandsåna, Sandnes	58.83194	5.8232	3	28	-	-	226	-	-	-	-	-	3	Andersen et al. 1987	211	226		
566	R434	Rogaland	Skrusseikjeland, Sandnes	58.84101	5.8574	3	107	-	-	255	-	-	-	-	-	3	Andersen et al. 1987	215	255		
567	R434	Rogaland	Skrusseikjeland, Sandnes	58.84101	5.8574	3	107	-	-	-	163	-	-	-	-	3	Andersen et al. 1987	216	163		
568	R435	Rogaland	Grasdalen, Sandnes	58.84367	5.9089	3	302	-	-	253	-	-	-	-	-	3	Andersen et al. 1987	211	253		
569	R436	Rogaland	Vaulaberget, Sandnes	58.82755	5.8612	3	105	-	-	269	-	-	-	-	-	3	Andersen et al. 1987	215	269		
570	R436	Rogaland	Vaulaberget, Sandnes	58.82755	5.8612	3	105	-	-	-	251	-	-	-	-	3	Andersen et al. 1987	216	251		
571	R437	Rogaland	Buktahagen, Sandnes	58.81880	5.9323	3	210	-	-	244	-	-	-	-	-	3	Andersen et al. 1987	211	244		
572	R438	Rogaland	Figgjo, Time	58.79444	5.7604	3	118	-	-	238	-	-	-	-	-	3	Andersen et al. 1987	211	238		
573	R439	Rogaland	Litle Blegafjell, Sandnes	58.78893	5.8498	3	195	-	-	248	-	-	-	-	-	3	Andersen et al. 1987	211	248		
574	R439	Rogaland	Litle Blegafjell, Sandnes	58.78893	5.8498	3	195	-	-	261	-	-	-	-	-	3	Andersen et al. 1987	211	261		
575	R440	Rogaland	Langsolen, Time	58.76578	5.8001	3	144	-	-	250	-	-	-	-	-	3	Andersen et al. 1987	211	250		
576	R441	Rogaland	Trollkirken, Gjesdal	58.75541	5.8073	3	166	-	-	242	-	-	-	-	-	3	Andersen et al. 1987	211	242		
577	R442	Rogaland	Vordefjell, Time	58.75170	5.8089	3	185	-	-	248	-	-	-	-	-	3	Andersen et al. 1987	211	248		
578	R443	Rogaland	Høylandsvatnet, Time	58.72996	5.7538	3	106	-	-	255	-	-	-	-	-	3	Andersen et al. 1987	211	255		
579	R444	Rogaland	Floen, Time	58.72431	5.7954	3	124	-	-	244	-	-	-	-	-	3	Andersen et al. 1987	211	244		
580	R445	Rogaland	Høga Håland, Time	58.74348	5.8315	3	192	-	-	232	-	-	-	-	-	3	Andersen et al. 1987	211	232		
581	R446	Rogaland	Bursfjellet, Time	58.73177	5.8419	3	234	-	-	257	-	-	-	-	-	3	Andersen et al. 1987	211	257		
582	R447	Rogaland	Skurvenuten, Gjesdal	58.75027	5.9121	3	255	-	-	254	-	-	-	-	-	3	Andersen et al. 1987	211	254		
583	R448	Rogaland	Skiftesmyra, Gjesdal	58.74892	5.9201	3	204	-	-	239	-	-	-	-	-	3	Andersen et al. 1987	211	239		
584	R449	Rogaland	Orrenfjellet, Gjesdal	58.75022	5.9702	3	283	-	-	257	-	-	-	-	-	3	Andersen et al. 1987	211	257		
585	R450	Rogaland	Errevatnet, Gjesdal	58.72341	5.9384	3	231	-	-	259	-	-	-	-	-	3	Andersen et al. 1987	215	259		
586	R450	Rogaland	Errevatnet, Gjesdal	58.72341	5.9384	3	231	-	-	-	307	-	-	-	-	3	Andersen et al. 1987	216	307		
587	R451	Rogaland	Moldtjørn, Time	58.71815	5.8513	3	259	-	-	252	-	-	-	-	-	3	Andersen et al. 1987	211	252		
588	R452	Rogaland	Sikvalandskula, Gjesdal	58.69912	5.8701	3	408	-	-	261	-	-	-	-	-	3	Andersen et al. 1987	211	261		

Striae No	Loc. No	County	Placename	Lat_N	Long_E	Precision	m a.s.l.	Mid pt.	Plus_ Minus	Youngest	Older	Even Older	Even Older 2	Oldest	Undet. rel. age	Quality	Source	Code symbol	All orientations	Comments	Erosional marks
589	R453	Rogaland	Tjensvollbakkance, Time	58.68861	5.7185	3	56	-	-	257	-	-	-	-	-	3	Andersen et al. 1987	211	257		
590	R454	Rogaland	Midtholen, Hå	58.67743	5.6413	3	20	-	-	260	-	-	-	-	-	3	Andersen et al. 1987	211	260		
591	R455	Rogaland	Tjåland, Time	58.67321	5.8198	3	206	-	-	272	-	-	-	-	-	3	Andersen et al. 1987	211	272		
592	R456	Rogaland	Heddance, Time	58.68287	5.9134	3	312	-	-	256	-	-	-	-	-	3	Andersen et al. 1987	211	256		
593	R457	Rogaland	Lauvholsbekken, Gjesdal	58.67882	5.9608	3	324	-	-	260	-	-	-	-	-	3	Andersen et al. 1987	211	260		
594	R458	Rogaland	Tangen, Bjerkreim	58.65432	5.8991	3	261	-	-	257	-	-	-	-	-	3	Andersen et al. 1987	211	257		
595	R459	Rogaland	Mauratuva, Bjerkreim	58.64109	5.9396	3	457	-	-	265	-	-	-	-	-	3	Andersen et al. 1987	211	265		
596	R460	Rogaland	Brusaknuden, Time	58.62934	5.8799	3	404	-	-	259	-	-	-	-	-	3	Andersen et al. 1987	211	259		
597	R461	Rogaland	Kartavoll, Time	58.63894	5.8268	3	260	-	-	262	-	-	-	-	-	3	Andersen et al. 1987	211	262		
598	R462	Rogaland	Synesvarden, Time	58.61892	5.8171	3	332	-	-	255	-	-	-	-	-	3	Andersen et al. 1987	211	255		
599	R463	Rogaland	Orrtua, Bjerkreim	58.56621	5.9404	3	136	-	-	251	-	-	-	-	-	3	Andersen et al. 1987	211	251		
600	R464	Rogaland	Nevlandsveien, Hå	58.53130	5.9134	3	102	-	-	242	-	-	-	-	-	3	Andersen et al. 1987	211	242		
601	R465	Rogaland	Hyljafjellet, Hå	58.57537	5.8025	3	150	-	-	-	-	-	-	-	246	3	Andersen et al. 1987	213	246		
602	R465	Rogaland	Hyljafjellet, Hå	58.57537	5.8025	3	150	-	-	-	-	-	-	-	258	3	Andersen et al. 1987	213	258		
603	R466	Rogaland	Stokkaland, Hå	58.55092	5.7303	3	9	-	-	260	-	-	-	-	-	3	Andersen et al. 1987	211	260		
604	R467	Rogaland	Store Kvittjørna, Hå	58.55268	5.7993	3	56	-	-	254	-	-	-	-	-	3	Andersen et al. 1987	211	254		
605	R468	Rogaland	Hestafjellet, Hå	58.55181	5.7940	3	29	-	-	248	-	-	-	-	-	3	Andersen et al. 1987	211	248		
606	R469	Rogaland	Varden, Hå	58.52776	5.7826	3	6	-	-	-	-	-	-	-	252	3	Andersen et al. 1987	213	252		
607	R469	Rogaland	Varden, Hå	58.52776	5.7826	3	6	-	-	-	-	-	-	-	268	3	Andersen et al. 1987	213	268		
608	R470	Rogaland	Sirevåg, Hå	58.50630	5.7906	3	2	-	-	-	-	-	-	-	250	3	Andersen et al. 1987	213	250		
609	R470	Rogaland	Sirevåg, Hå	58.50630	5.7906	3	2	-	-	-	-	-	-	-	265	3	Andersen et al. 1987	213	265		
610	R471	Rogaland	Revurstjørna, Hå	58.49523	5.8084	3	14	-	-	-	-	-	-	-	252	3	Andersen et al. 1987	213	252		
611	R471	Rogaland	Revurstjørna, Hå	58.49523	5.8084	3	14	-	-	-	-	-	-	-	241	3	Andersen et al. 1987	213	241		
612	R472	Rogaland	Kinnarvåg, Hå	58.49314	5.8091	3	7	-	-	238	-	-	-	-	-	3	Andersen et al. 1987	211	238		
613	R473	Rogaland	Holmavågen, Hå	58.48594	5.8174	3	5	-	-	238	-	-	-	-	-	3	Andersen et al. 1987	211	238		
614	R474	Rogaland	Nesheim, Eigersund	58.47418	5.8808	3	20	-	-	235	-	-	-	-	-	3	Andersen et al. 1987	211	235		
615	R475	Rogaland	Øksnadø, Eigersund	58.49512	5.9556	3	99	-	-	243	-	-	-	-	-	3	Andersen et al. 1987	211	243		
616	R476	Rogaland	Ryssebakken, Eigersund	58.43920	5.8929	3	24	-	-	213	-	-	-	-	-	3	Andersen et al. 1987	211	213		

Striae No	Loc. No	County	Placename	Lat_N	Long_E	Precision	m a.s.l.	Mid pt.	Plus_ Minus	Youngest	Older	Even Older	Even Older 2	Oldest	Undet. rel. age	Quality	Source	Code symbol	All orientations	Comments	Erosional marks
617	R477	Rogaland	Midbrød, Eigersund	58.44260	5.8993	3	17	-	-	222	-	-	-	-	-	3	Andersen et al. 1987	211	222		
618	R478	Rogaland	Tyskerbrygga, Eigersund	58.44720	5.9897	3	9	-	-	236	-	-	-	-	-	3	Andersen et al. 1987	211	236		
619	R479	Rogaland	Husavatnet, Sveio	59.50833	5.3335	3	30	-	-	280	-	-	-	-	-	3	Rønnevik, 1971	211	280		
620	R480	Rogaland	Ervesvågen, Sveio	59.55678	5.4899	3	30	-	-	270	-	-	-	-	-	3	Rønnevik, 1971	211	270		
621	R481	Rogaland	Ervesvågen, Sveio	59.56070	5.4754	3	5	288	-	-	-	-	-	-	-	3	Rønnevik, 1971	214	288		
622	R482	Rogaland	Ervesvåg, Sveio	59.56637	5.4748	3	60	-	-	300	-	-	-	-	-	3	Rønnevik, 1971	211	300		
623	R483	Rogaland	Tveit, Sveio	59.54450	5.4972	3	80	-	-	258	-	-	-	-	-	3	Rønnevik, 1971	211	258		
624	R484	Rogaland	Tveitefjellet, Sveio	59.54229	5.4928	3	150	-	-	291	-	-	-	-	-	3	Rønnevik, 1971	211	291		
625	R485	Rogaland	Buaviktjørna, Sveio	59.52825	5.4961	3	38	-	-	257	-	-	-	-	-	3	Rønnevik, 1971	211	257		
626	R486	Rogaland	Hovda, Sveio	59.55011	5.4769	3	50	-	-	286	-	-	-	-	-	3	Rønnevik, 1971	211	286		
627	R487	Rogaland	Hovda, Sveio	59.55071	5.4765	3	50	-	-	259	-	-	-	-	-	3	Rønnevik, 1971	211	259		
628	R488	Rogaland	Hovda, Sveio	59.54815	5.4739	3	40	-	-	280	-	-	-	-	-	3	Rønnevik, 1971	211	280		
629	R489	Rogaland	Austvik-Rabben, Sveio	59.62874	5.4924	3	60	-	-	271	-	-	-	-	-	3	Rønnevik, 1971	211	271		
630	R490	Rogaland	Rødspollen, Sveio	59.58535	5.4447	3	20	-	-	325	-	-	-	-	-	3	Rønnevik, 1971	211	325		
631	R491	Rogaland	Tidno, Sveio	59.51008	5.4505	3	50	-	-	278	-	-	-	-	-	3	Rønnevik, 1971	211	278		
632	R492	Rogaland	Kvalvågneset, Sveio	59.51932	5.4515	3	30	-	-	274	-	-	-	-	-	3	Rønnevik, 1971	211	274		
633	R493	Rogaland	Søre Dalshaug, Haugesund	59.45554	5.2856	3	50	-	-	261	-	-	-	-	-	3	Rønnevik, 1971	211	261		
634	R494	Rogaland	Saltveit, Haugesund	59.47027	5.2876	3	40	-	-	261	-	-	-	-	-	3	Rønnevik, 1971	211	261		
635	R495	Rogaland	Bleivik, Haugesund	59.47864	5.2431	3	0	-	-	275	-	-	-	-	-	3	Rønnevik, 1971	211	275		
636	R496	Rogaland	Mannabergstjørn, Haugesund	59.46487	5.3632	3	50	-	-	264	-	-	-	-	-	3	Rønnevik, 1971	211	264		
637	R497	Rogaland	Skastad, Haugesund	59.46125	5.3675	3	30	-	-	258	-	-	-	-	-	3	Rønnevik, 1971	211	258		
638	R498	Rogaland	Hamrane, Haugesund	59.46057	5.3710	3	20	-	-	261	-	-	-	-	-	3	Rønnevik, 1971	211	261		
639	R499	Rogaland	Hamrane, Haugesund	59.46238	5.3721	3	40	-	-	265	-	-	-	-	-	3	Rønnevik, 1971	211	265		
640	R500	Rogaland	Eileråsa, Haugesund	59.49544	5.3975	3	20	-	-	264	-	-	-	-	-	3	Rønnevik, 1971	211	264		
641	R501	Rogaland	Tveita, Sveio	59.57077	5.4103	3	60	-	-	267	-	-	-	-	-	3	Rønnevik, 1971	211	267		
642	R502	Rogaland	Sunnfør,Tysvær	59.47781	5.4520	3	100	-	-	264	-	-	-	-	-	3	Rønnevik, 1971	211	264		
643	R503	Rogaland	Grinde, Tysvær	59.43279	5.4629	3	10	-	-	227	-	-	-	-	-	3	Rønnevik, 1971	211	227		
644	R504	Rogaland	Eikjehaugen, Tysvær	59.42017	5.4674	3	50	-	-	243	-	-	-	-	-	3	Rønnevik, 1971	211	243		

Striae No	Loc. No	County	Placename	Lat_N	Long_E	Precision	m a.s.l.	Mid pt.	Plus_ Minus	Youngest	Older	Even Older	Even Older 2	Oldest	Undet. rel. age	Quality	Source	Code symbol	All orientations	Comments	Erosional marks
645	R505	Rogaland	Grindaneset, Tysvær	59.43699	5.4769	3	30	-	-	268	-	-	-	-	-	3	Rønnevik, 1971	211	268		
646	R506	Rogaland	Aksdalselva, Tysvær	59.42210	5.4683	3	30	-	-	245	-	-	-	-	-	3	Rønnevik, 1971	211	245		
647	R507	Rogaland	Steinbryvetnet, Tysvær	59.45065	5.5591	3	0	-	-	215	-	-	-	-	-	3	Rønnevik, 1971	211	215		
648	R508	Rogaland	Svinakleiv, Tysvær	59.46209	5.5122	3	70	-	-	240	-	-	-	-	-	3	Rønnevik, 1971	211	240		
649	R509	Rogaland	Lielva, Tysvær	59.47753	5.5303	3	50	-	-	219	-	-	-	-	-	3	Rønnevik, 1971	211	219		
650	R510	Rogaland	Mæland, Tysvær	59.48896	5.5454	3	60	-	-	246	-	-	-	-	-	3	Rønnevik, 1971	211	246		
651	R511	Rogaland	Haugen, Tysvær	59.50726	5.5244	3	60	-	-	256	-	-	-	-	-	3	Rønnevik, 1971	211	256		
652	R512	Rogaland	Dagsland, Tysvær	59.49848	5.5301	3	70	-	-	295	-	-	-	-	-	3	Rønnevik, 1971	211	295		
653	R513	Rogaland	Volder, Tysvær	59.50186	5.5529	3	120	-	-	266	-	-	-	-	-	3	Rønnevik, 1971	211	266		
654	R514	Rogaland	Bjordal, Vindafjord	59.54247	5.5932	3	200	-	-	266	-	-	-	-	-	3	Rønnevik, 1971	211	266		
655	R515	Rogaland	Nutadalen, Vindafjord	59.54257	5.5804	3	120	-	-	290	-	-	-	-	-	3	Rønnevik, 1971	211	290		
656	R516	Rogaland	Vikebygd, Vindafjord	59.59204	5.5833	3	0	-	-	284	-	-	-	-	-	3	Rønnevik, 1971	211	284		
657	R517	Rogaland	Røyrvik, Tysvær	59.41740	5.5990	3	20	-	-	198	-	-	-	-	-	3	Rønnevik, 1971	211	198		
658	R518	Rogaland	Vassmyr, Tysvær	59.40375	5.4706	3	30	-	-	210	-	-	-	-	-	3	Rønnevik, 1971	215	210		
659	R518	Rogaland	Vassmyr, Tysvær	59.40375	5.4706	3	30	-	-	-	235	-	-	-	-	3	Rønnevik, 1971	216	235		
660	R519	Rogaland	Nipane, Tysvær	59.40647	5.4787	3	50	-	-	209	-	-	-	-	-	3	Rønnevik, 1971	215	209		
661	R519	Rogaland	Nipane, Tysvær	59.40647	5.4787	3	50	-	-	-	221	-	-	-	-	3	Rønnevik, 1971	216	221		
662	R520	Rogaland	Nipane, Tysvær	59.40952	5.4773	3	80	-	-	234	-	-	-	-	-	3	Rønnevik, 1971	211	234		
663	R521	Rogaland	Kvithaugen, Tysvær	59.41716	5.4696	3	30	-	-	228	-	-	-	-	-	3	Rønnevik, 1971	211	228		
664	R522	Rogaland	Eikjehaugen, Tysvær	59.42162	5.4685	3	30	225	10	-	-	-	-	-	-	3	Rønnevik, 1971	214	225		
665	R523	Rogaland	Amdalsløkjen, Tysvær	59.40578	5.5044	3	60	-	-	222	-	-	-	-	-	3	Rønnevik, 1971	211	222		
666	R524	Rogaland	Førrestjørna, Tysvær	59.42230	5.3938	3	50	-	-	242	-	-	-	-	-	3	Rønnevik, 1971	211	242		
667	R525	Rogaland	Førrestjørna, Tysvær	59.42322	5.3939	3	80	-	-	251	-	-	-	-	-	3	Rønnevik, 1971	211	251		
668	R526	Rogaland	Førrestjørna, Tysvær	59.42137	5.3903	3	40	-	-	233	-	-	-	-	-	3	Rønnevik, 1971	211	233		
669	R527	Rogaland	Steinsfjellet, Tysvær	59.42249	5.3347	3	200	-	-	259	-	-	-	-	-	3	Rønnevik, 1971	211	259		
670	R528	Rogaland	Såt, Tysvær	59.42412	5.3564	3	210	-	-	269	-	-	-	-	-	3	Rønnevik, 1971	211	269		
671	R529	Rogaland	Frakkagjerd, Tysvær	59.41902	5.4149	3	50	-	-	259	-	-	-	-	-	3	Rønnevik, 1971	211	259		
672	R530	Rogaland	Søylå, Tysvær	59.31826	5.3984	3	0	-	-	221	-	-	-	-	-	3	Rønnevik, 1971	211	221		

Striae No	Loc. No	County	Placename	Lat_N	Long_E	Precision	m a.s.l.	Mid pt.	Plus_ Minus	Youngest	Older	Even Older	Even Older 2	Oldest	Undet. rel. age	Quality	Source	Code symbol	All orientations	Comments	Erosional marks
673	R531	Rogaland	Tømmerdal, Tysvær	59.42055	5.3246	3	120	-	-	252	-	-	-	-	-	3	Rønnevik, 1971	211	252		
674	R532	Rogaland	Kvednåsen, Tysvær	59.34545	5.5012	3	120	-	-	191	-	-	-	-	-	3	Rønnevik, 1971	211	191		
675	R533	Rogaland	Hamnarholmen, Tysvær	59.30081	5.4597	3	0	-	-	216	-	-	-	-	-	3	Rønnevik, 1971	211	216		
676	R534	Rogaland	Nibba, Tysvær	59.31470	5.5920	3	130	-	-	155	-	-	-	-	-	3	Rønnevik, 1971	211	155		
677	R535	Rogaland	Nibba, Tysvær	59.31475	5.5915	3	150	-	-	151	-	-	-	-	-	3	Rønnevik, 1971	211	151		
678	R536	Rogaland	Rossadal, Tysvær	59.31858	5.5622	3	120	-	-	155	-	-	-	-	-	3	Rønnevik, 1971	211	155		
679	R537	Rogaland	Storemyra, Tysvær	59.32965	5.5640	3	80	-	-	163	-	-	-	-	-	3	Rønnevik, 1971	211	163		
680	R538	Rogaland	Leirviksfjellet, Tysvær	59.28577	5.4814	3	120	-	-	194	-	-	-	-	-	3	Rønnevik, 1971	215	194		
681	R538	Rogaland	Leirviksfjellet, Tysvær	59.28577	5.4814	3	120	-	-	-	240	-	-	-	-	3	Rønnevik, 1971	216	240		
682	R539	Rogaland	Haukaberget, Tysvær	59.28588	5.4824	3	130	-	-	327	-	-	-	-	-	3	Rønnevik, 1971	211	327		
683	R540	Rogaland	Sandvikvatnet, Tysvær	59.28591	5.4912	3	130	-	-	182	-	-	-	-	-	3	Rønnevik, 1971	211	182		
684	R541	Rogaland	Sandvikvatnet, Tysvær	59.28693	5.4909	3	130	-	-	193	-	-	-	-	-	3	Rønnevik, 1971	211	193		
685	R542	Rogaland	Leirviksfjellet, Tysvær	59.28788	5.4826	3	130	224	10	-	-	-	-	-	-	3	Rønnevik, 1971	214	224		
686	R543	Rogaland	Brattabø, Tysvær	59.28061	5.5631	3	10	-	-	128	-	-	-	-	-	3	Rønnevik, 1971	211	128		
687	R544	Rogaland	Røyksund, Karmøy	59.33322	5.3603	3	0	-	-	231	-	-	-	-	-	3	Rønnevik, 1971	211	231		
688	R545	Rogaland	Uglesmog, Karmøy	59.32464	5.3702	3	20	-	-	218	-	-	-	-	-	3	Rønnevik, 1971	211	218		
689	R546	Rogaland	Vormedalsvatnet, Karmøy	59.35906	5.3278	3	40	-	-	259	-	-	-	-	-	3	Rønnevik, 1971	211	259		
690	R547	Rogaland	Helgalandsvatnet, Karmøy	59.36944	5.3327	3	70	-	-	242	-	-	-	-	-	3	Rønnevik, 1971	211	242		
691	R548	Rogaland	Spannavatnet, Karmøy	59.38072	5.3258	3	70	-	-	258	-	-	-	-	-	3	Rønnevik, 1971	211	258		
692	R549	Rogaland	Spannavegen, Haugesund	59.40311	5.2974	3	40	-	-	256	-	-	-	-	-	3	Rønnevik, 1971	211	256		
693	R550	Rogaland	Karmsundgata, Haugesund	59.39912	5.2938	3	30	-	-	272	-	-	-	-	-	3	Rønnevik, 1971	211	272		
694	R551	Rogaland	Snik, Karmøy	59.34179	5.3310	3	30	-	-	249	-	-	-	-	-	3	Rønnevik, 1971	211	249		
695	R552	Rogaland	Vormedalsvatnet, Karmøy	59.35346	5.3309	3	40	-	-	250	-	-	-	-	-	3	Rønnevik, 1971	211	250		
696	R553	Rogaland	Kjøtrot, Karmøy	59.40920	5.2255	3	7	-	-	297	-	-	-	-	-	3	Ringen, 1974	211	297		
697	R554	Rogaland	Stangemyrane, Karmøy	59.38171	5.2602	3	25	-	-	263	-	-	-	-	-	3	Ringen, 1974	211	263		
698	R555	Rogaland	Bøkrossen, Karmøy	59.36416	5.2815	3	3	-	-	263	-	-	-	-	-	3	Ringen, 1974	211	263		
699	R556	Rogaland	Nygård, Karmøy	59.33524	5.2722	3	22	-	-	268	-	-	-	-	-	3	Ringen, 1974	211	268		
700	R557	Rogaland	Austreimneset, Karmøy	59.29006	5.3109	3	23	-	-	233	-	-	-	-	-	3	Ringen, 1974	211	233		

Striae No	Loc. No	County	Placename	Lat_N	Long_E	Precision	m a.s.l.	Mid pt.	Plus_ Minus	Youngest	Older	Even Older	Even Older 2	Oldest	Undet. rel. age	Quality	Source	Code symbol	All orientations	Comments	Erosional marks
701	R558	Rogaland	Kopar, Karmøy	59.28006	5.3084	3	13	-	-	196	-	-	-	-	-	3	Ringen, 1974	211	196		
702	R559	Rogaland	Haringstad, Karmøy	59.27298	5.2392	3	40	-	-	266	-	-	-	-	-	3	Ringen, 1974	211	266		
703	R560	Rogaland	Rindå, Karmøy	59.26511	5.3168	3	33	-	-	263	-	-	-	-	-	3	Ringen, 1974	211	263		
704	R561	Rogaland	Karmøy, Karmøy	59.23502	5.2625	3	82	-	-	266	-	-	-	-	-	3	Ringen, 1974	211	266		
705	R562	Rogaland	Stemmen, Karmøy	59.19575	5.2012	3	35	-	-	272	-	-	-	-	-	3	Ringen, 1974	211	272		
706	R563	Rogaland	Mjølhus, Karmøy	59.16679	5.2062	3	30	-	-	280	-	-	-	-	-	3	Ringen, 1974	211	280		
707	R564	Rogaland	Stokkavika, Karmøy	59.14802	5.2172	3	3	-	-	282	-	-	-	-	-	3	Ringen, 1974	211	282		
708	R565	Rogaland	Fladaberg, Karmøy	59.15230	5.2681	3	30	-	-	272	-	-	-	-	-	3	Ringen, 1974	211	272		
709	R566	Rogaland	Moksheim, Karmø¥	59.36945	5.3095	3	24	-	-	240	-	-	-	-	-	3	Økland, 1947	211	240		
710	R567	Rogaland	Storøya, Haugesund	59.41333	5.2285	3	4	-	-	280	-	-	-	-	-	3	Økland, 1947	211	280		
711	R568	Rogaland	Jøtnafjell, Haugesund	59.43449	5.3215	3	183	-	-	259	-	-	-	-	-	3	Økland, 1947	211	259		
712	R569	Rogaland	Steinsfjellet, Haugesund	59.42177	5.3354	3	210	-	-	259	-	-	-	-	-	3	Økland, 1947	211	259		
713	R570	Rogaland	Spannsvarden, Karmøy	59.37648	5.3416	3	222	-	-	266	-	-	-	-	-	3	Økland, 1947	211	266		
714	R571	Rogaland	Tronfjell, Karmøy	59.37091	5.3437	3	139	-	-	266	-	-	-	-	-	3	Økland, 1947	211	266		
715	R572	Rogaland	Hola, Tysvær	59.31894	5.4014	3	23	-	-	226	-	-	-	-	-	3	Økland, 1947	211	226		
716	R573	Rogaland	Nordtveit, Tysvær	59.36127	5.3881	3	5	-	-	-	-	-	-	-	245	3	Økland, 1947	213	245		
717	R573	Rogaland	Nordtveit, Tysvær	59.36127	5.3881	3	5	-	-	-	-	-	-	-	239	3	Økland, 1947	213	239		
718	R574	Rogaland	Krabbatveit, Tysvær	59.39424	5.4637	3	78	-	-	206	-	-	-	-	-	3	Økland, 1947	211	206		
719	R575	Rogaland	Haukås, Tysvær	59.34095	5.4502	3	33	-	-	-	-	-	-	-	190	3	Økland, 1947	213	190		
720	R575	Rogaland	Haukås, Tysvær	59.34095	5.4502	3	33	-	-	-	-	-	-	-	175	3	Økland, 1947	213	175		
721	R576	Rogaland	Nes, Tysvær	59.38621	5.4698	3	29	-	-	238	-	-	-	-	-	3	Økland, 1947	211	238		
722	R577	Rogaland	Slåttevik, Tysvær	59.31463	5.4623	3	18	-	-	190	-	-	-	-	-	3	Økland, 1947	211	190		
723	R578	Rogaland	Hesthammar, Tysvær	59.29805	5.5286	3	30	-	-	185	-	-	-	-	-	3	Økland, 1947	211	185		
724	R579	Rogaland	Djupdal, Tysvær	59.31373	5.4965	3	35	-	-	199	-	-	-	-	-	3	Økland, 1947	211	199		
725	R580	Rogaland	Årvikafjell, Tysvær	59.29663	5.5600	3	217	-	-	262	-	-	-	-	-	3	Økland, 1947	211	262		
726	R581	Rogaland	Årvikafjell, Tysvær	59.29751	5.5605	3	213	-	-	257	-	-	-	-	-	3	Økland, 1947	211	257		
727	R582	Rogaland	Emberlandsnipen, Sveio	59.59986	5.3963	3	246	-	-	271	-	-	-	-	-	3	Økland, 1947	211	271		
728	R583	Rogaland	Staupefjellet, Sveio	59.65837	5.4958	3	201	-	-	278	-	-	-	-	-	3	Økland, 1947	211	278		

Striae No	Loc. No	County	Placename	Lat_N	Long_E	Precision	m a.s.l.	Mid pt.	Plus_ Minus	Youngest	Older	Even Older	Even Older 2	Oldest	Undet. rel. age	Quality	Source	Code symbol	All orientations	Comments	Erosional marks
729	R584	Rogaland	Trollevassnibba, Sveio	59.68769	5.5070	3	366	-	-	272	-	-	-	-	-	3	Økland, 1947	211	272		
730	R585	Rogaland	Klubben, Randaberg	58.99430	5.5686	4	4	-	-	240	-	-	-	-	-	3	Anundsen, 1990	215	240		
731	R585	Rogaland	Klubben, Randaberg	58.99430	5.5686	4	4	-	-	-	252	-	-	-	-	3	Anundsen, 1990	216	252		
732	R585	Rogaland	Klubben, Randaberg	58.99430	5.5686	4	4	-	-	-	297	-	-	-	-	3	Anundsen, 1990	216	297		
733	R585	Rogaland	Klubben, Randaberg	58.99430	5.5686	4	4	-	-	-	320	-	-	-	-	3	Anundsen, 1990	216	320		
734	R586	Rogaland	Ringaberg, Randaberg	58.99001	5.6178	4	13	-	-	244	-	-	-	-	-	3	Anundsen, 1990	211	244		
735	R587	Rogaland	Skjelbreidveien, Stavanger	58.97545	5.6144	4	5	-	-	242	-	-	-	-	-	3	Anundsen, 1990	211	242		
736	R588	Rogaland	Prestaskjerslia, Sola	58.95401	5.6052	4	9	-	-	-	-	-	-	-	225	3	Anundsen, 1990	213	225		
737	R588	Rogaland	Prestaskjerslia, Sola	58.95401	5.6052	4	9	-	-	-	-	-	-	-	272	3	Anundsen, 1990	213	272		
738	R589	Rogaland	Tennisveien, Stavanger	58.95281	5.7010	4	60	-	-	210	-	-	-	-	-	3	Anundsen, 1990	215	210		
739	R589	Rogaland	Tennisveien, Stavanger	58.95281	5.7010	4	60	-	-	220	-	-	-	-	-	3	Anundsen, 1990	215	220		
740	R589	Rogaland	Tennisveien, Stavanger	58.95281	5.7010	4	60	-	-	-	310	-	-	-	-	3	Anundsen, 1990	216	310		
741	R590	Rogaland	Tungevika, Randaberg	59.03288	5.5897	4	19	-	-	260	-	-	-	-	-	3	Anundsen, 1990	211	260		
742	R591	Rogaland	Galtasteinen, Randaberg	59.02865	5.5992	4	7	-	-	270	-	-	-	-	-	3	Anundsen, 1990	211	270		
743	R592	Rogaland	Sandviga, Rennesøy	59.09206	5.6137	4	8	-	-	-	-	-	-	-	238	3	Anundsen, 1990	213	238		
744	R592	Rogaland	Sandviga, Rennesøy	59.09206	5.6137	4	8	-	-	-	-	-	-	-	170	3	Anundsen, 1990	213	170		
745	R592	Rogaland	Sandviga, Rennesøy	59.09206	5.6137	4	8	-	-	-	-	-	-	-	260	3	Anundsen, 1990	213	260		
746	R593	Rogaland	Skipanes, Rennesøy	59.08976	5.5928	4	12	-	-	210	-	-	-	-	-	3	Anundsen, 1990	211	210		
747	R594	Rogaland	Gråttnes, Rennsøy	59.09463	5.6422	4	14	-	-	270	-	-	-	-	-	3	Anundsen, 1990	211	270		
748	R595	Rogaland	Rinnå, Rennesøy	59.05530	5.6691	4	8	-	-	270	-	-	-	-	-	3	Anundsen, 1990	211	270		
749	R596	Rogaland	Litlevåg, Stavanger	59.03715	5.7502	4	24	-	-	260	-	-	-	-	-	3	Anundsen, 1990	215	260		
750	R596	Rogaland	Litlevåg, Stavanger	59.03715	5.7502	4	24	-	-	-	165	-	-	-	-	3	Anundsen, 1990	216	165		
751	R597	Rogaland	Eigerøya, Stavanger	59.01713	5.7810	4	8	-	-	250	-	-	-	-	-	3	Anundsen, 1990	215	250		
752	R597	Rogaland	Eigerøya, Stavanger	59.01713	5.7810	4	8	-	-	-	180	-	-	-	-	3	Anundsen, 1990	216	180		
753	R598	Rogaland	Lindøysund, Stavanger	58.99300	5.8076	4	12	-	-	250	-	-	-	-	-	3	Anundsen, 1990	215	250		
754	R598	Rogaland	Lindøysund, Stavanger	58.99300	5.8076	4	12	-	-	-	178	-	-	-	-	3	Anundsen, 1990	216	178		
755	R599	Rogaland	Blindå, Rennesøy	59.07214	5.7672	4	7	-	-	244	-	-	-	-	-	3	Anundsen, 1990	211	244		
756	R600	Rogaland	Gongenes, Rennesøy	59.08052	5.7827	4	20	-	-	175	-	-	-	-	-	3	Anundsen, 1990	211	175		

Striae No	Loc. No	County	Placename	Lat_N	Long_E	Precision	m a.s.l.	Mid pt.	Plus_ Minus	Youngest	Older	Even Older	Even Older 2	Oldest	Undet. rel. age	Quality	Source	Code symbol	All orientations	Comments	Erosional marks
757	R601	Rogaland	Dravika, Rennesøy	59.11600	5.7727	4	11	-	-	-	-	-	-	-	208	3	Anundsen, 1990	213	208		
758	R601	Rogaland	Dravika, Rennesøy	59.11600	5.7727	4	11	-	-	-	-	-	-	-	252	3	Anundsen, 1990	213	252		
759	R602	Rogaland	Gongstø, Rennesøy	59.10747	5.8573	4	26	-	-	178	-	-	-	-	-	3	Anundsen, 1990	215	178		
760	R603	Rogaland	Navarnes, Finnøy	59.13896	5.7974	4	20	-	-	-	180	-	-	-	-	3	Anundsen, 1990	216	180		
761	R603	Rogaland	Navarnes, Finnøy	59.13896	5.7974	4	20	-	-	260	-	-	-	-	-	3	Anundsen, 1990	211	260		
762	R604	Rogaland	Lasteinen, Finnøy	59.14185	5.8084	4	9	-	-	250	-	-	-	-	-	3	Anundsen, 1990	211	250		
763	R605	Rogaland	Klubben, Finnøy	59.16064	5.8626	4	12	-	-	200	-	-	-	-	-	3	Anundsen, 1990	211	200		
764	R606	Rogaland	Bøneset, Finnøy	59.15148	5.9033	4	24	-	-	180	-	-	-	-	-	3	Anundsen, 1990	212	180		
765	R606	Rogaland	Bøneset, Finnøy	59.15148	5.9033	4	24	-	-	240	-	-	-	-	-	3	Anundsen, 1990	211	240		
766	R607	Rogaland	Vedaberget, Finnøy	59.15073	5.9359	4	11	-	-	280	-	-	-	-	-	3	Anundsen, 1990	211	280		
767	R608	Rogaland	Engjavika, Hjelmeland	59.15986	6.0368	4	23	-	-	-	-	-	-	-	195	3	Anundsen, 1990	213	195		
768	R608	Rogaland	Engjavika, Hjelmeland	59.15986	6.0368	4	23	-	-	-	-	-	-	-	238	3	Anundsen, 1990	213	238		
769	R608	Rogaland	Engjavika, Hjelmeland	59.15986	6.0368	4	23	-	-	-	-	-	-	-	294	3	Anundsen, 1990	213	294		
770	R609	Rogaland	Fisterhammaren, Hjelmeland	59.17890	6.0568	4	14	-	-	240	-	-	-	-	-	3	Anundsen, 1990	211	240		
771	R610	Rogaland	Hegrefjellet, Hjelmeland	59.18703	6.0684	4	58	-	-	235	-	-	-	-	-	3	Anundsen, 1990	211	235		
772	R611	Rogaland	Hilsavika, Hjelmeland	59.20671	6.0891	4	20	-	-	233	-	-	-	-	-	3	Anundsen, 1990	211	233		
773	R612	Rogaland	Viganeset, Hjelmeland	59.21728	6.1027	4	25	-	-	240	-	-	-	-	-	3	Anundsen, 1990	211	240		
774	R613	Rogaland	Hundsnes, Hjelmeland	59.21929	6.1199	4	3	-	-	220	-	-	-	-	-	3	Anundsen, 1990	211	220		
775	R614	Rogaland	Kleppa, Hjelmeland	59.22958	6.1414	4	44	-	-	242	-	-	-	-	-	3	Anundsen, 1990	211	242		
776	R615	Rogaland	Puntsnes, Hjelmeland	59.23258	6.1589	4	24	-	-	238	-	-	-	-	-	3	Anundsen, 1990	211	238		
777	R616	Rogaland	Hagebyen, Hjelmeland	59.23396	6.1735	4	6	-	-	298	-	-	-	-	-	3	Anundsen, 1990	211	298		
778	R617	Rogaland	Saltkil, Finnøy	59.16262	5.9863	4	12	-	-	200	-	-	-	-	-	3	Anundsen, 1990	211	200		
779	R617	Rogaland	Saltkil, Finnøy	59.16262	5.9863	4	12	-	-	180	-	-	-	-	-	3	Anundsen, 1990	211	180		
780	R618	Rogaland	Røytevågen, Finnøy	59.22921	5.7977	4	8	-	-	-	176	-	-	-	-	3	Anundsen, 1990	216	176		
781	R618	Rogaland	Røytevågen, Finnøy	59.22921	5.7977	4	8	-	-	312	-	-	-	-	-	3	Anundsen, 1990	215	312		
782	R619	Rogaland	Storskog, Finnøy	59.23048	5.8064	4	8	-	-	176	-	-	-	-	-	3	Anundsen, 1990	211	176		
783	R619	Rogaland	Storskog, Finnøy	59.23048	5.8064	4	8	-	-	267	-	-	-	-	-	3	Anundsen, 1990	211	267		
784	R620	Rogaland	Skadfluneset, Finnøy	59.22537	5.8054	4	19	-	-	270	-	-	-	-	-	3	Anundsen, 1990	211	270		

Striae No	Loc. No	County	Placename	Lat_N	Long_E	Precision	m a.s.l.	Mid pt.	Plus_ Minus	Youngest	Older	Even Older	Even Older 2	Oldest	Undet. rel. age	Quality	Source	Code symbol	All orientations	Comments	Erosional marks
785	R621	Rogaland	Kjipeneset, Finnøy	59.23268	5.8431	4	15	-	-	310	-	-	-	-	-	3	Anundsen, 1990	211	310		
786	R622	Rogaland	Langenes, Finnøy	59.23691	5.8239	4	17	-	-	248	-	-	-	-	-	3	Anundsen, 1990	211	248		
787	R623	Rogaland	Tandravoll, Finnøy	59.24405	5.8107	4	17	-	-	250	-	-	-	-	-	3	Anundsen, 1990	211	250		
788	R624	Rogaland	Norheimsbøen, Finnøy	59.25687	5.8328	4	10	-	-	180	-	-	-	-	-	3	Anundsen, 1990	211	180		
789	R625	Rogaland	Øye, Hjelmeland	59.23139	6.0872	4	15	-	-	-	-	-	-	-	181	3	Anundsen, 1990	213	181		
790	R625	Rogaland	Øye, Hjelmeland	59.23139	6.0872	4	15	-	-	-	-	-	-	-	270	3	Anundsen, 1990	213	270		
791	R626	Rogaland	Øyeman, Hjelmeland	59.23057	6.0756	4	18	-	-	265	-	-	-	-	-	3	Anundsen, 1990	211	265		
792	R627	Rogaland	Ytra Holå, Hjelmeland	59.21772	6.0160	4	19	-	-	-	-	-	-	-	180	3	Anundsen, 1990	213	180		
793	R627	Rogaland	Ytra Holå, Hjelmeland	59.21772	6.0160	4	19	-	-	-	-	-	-	-	275	3	Anundsen, 1990	213	275		
794	R628	Rogaland	Tapptongjen, Hjelmeland	59.21715	5.9997	4	18	-	-	182	-	-	-	-	-	3	Anundsen, 1990	211	182		
795	R629	Rogaland	Kunes, Hjelmeland	59.20257	5.9974	4	6	-	-	-	-	-	-	-	176	3	Anundsen, 1990	213	176		
796	R629	Rogaland	Kunes, Hjelmeland	59.20257	5.9974	4	6	-	-	-	-	-	-	-	236	3	Anundsen, 1990	213	236		
797	R629	Rogaland	Kunes, Hjelmeland	59.20257	5.9974	4	6	-	-	-	-	-	-	-	248	3	Anundsen, 1990	213	248		
798	R629	Rogaland	Kunes, Hjelmeland	59.20257	5.9974	4	6	-	-	-	-	-	-	-	290	3	Anundsen, 1990	213	290		
799	R630	Rogaland	Randa, Hjelmeland	59.20628	6.0001	4	38	-	-	215	-	-	-	-	-	3	Anundsen, 1990	211	215		
800	R631	Rogaland	Austrevik, Hjelmeland	59.18815	6.0265	4	16	-	-	177	-	-	-	-	-	3	Anundsen, 1990	211	177		
801	R632	Rogaland	Honkaberget, Hjelmeland	59.18349	6.0360	4	11	-	-	-	-	-	-	-	178	3	Anundsen, 1990	213	178		
802	R633	Rogaland	Honkaberget, Hjelmeland	59.18349	6.0360	4	11	-	-	-	-	-	-	-	232	3	Anundsen, 1990	213	232		
803	R634	Rogaland	Smalaholmane, Hjelmeland	59.21190	5.9800	4	6	-	-	-	-	-	-	-	176	3	Anundsen, 1990	213	176		
804	R634	Rogaland	Smalaholmane, Hjelmeland	59.21190	5.9800	4	6	-	-	-	-	-	-	-	220	3	Anundsen, 1990	213	220		
805	R634	Rogaland	Smalaholmane, Hjelmeland	59.21190	5.9800	4	6	-	-	-	-	-	-	-	256	3	Anundsen, 1990	213	256		
806	R635	Rogaland	Kunes, Finnøy	59.20844	5.9494	4	14	-	-	-	-	-	-	-	178	3	Anundsen, 1990	213	178		
807	R635	Rogaland	Kunes, Finnøy	59.20844	5.9494	4	14	-	-	-	-	-	-	-	212	3	Anundsen, 1990	213	212		
808	R635	Rogaland	Kunes, Finnøy	59.20844	5.9494	4	14	-	-	-	-	-	-	-	271	3	Anundsen, 1990	213	271		
809	R636	Rogaland	Hellevik, Finnøy	59.19342	5.9667	4	7	-	-	-	240	-	-	-	-	3	Anundsen, 1990	216	240		
810	R636	Rogaland	Hellevik, Finnøy	59.19342	5.9667	4	7	-	-	175	-	-	-	-	-	3	Anundsen, 1990	215	175		
811	R637	Rogaland	Djupasund, Hjelmeland	59.17710	6.0083	4	17	-	-	165	-	-	-	-	-	3	Anundsen, 1990	211	165		
812	R638	Rogaland	Jiljavika, Hjelmeland	59.18084	6.0050	4	9	-	-	205	-	-	-	-	-	3	Anundsen, 1990	211	205		

Striae No	Loc. No	County	Placename	Lat_N	Long_E	Precision	m a.s.l.	Mid pt.	Plus_ Minus	Youngest	Older	Even Older	Even Older 2	Oldest	Undet. rel. age	Quality	Source	Code symbol	All orientations	Comments	Erosional marks
813	R639	Rogaland	Korgavågen, Hjelmeland	59.18302	5.9908	4	1	-	-	270	-	-	-	-	-	3	Anundsen, 1990	211	270		
814	R640	Rogaland	Forøya, Finnøy	59.17448	5.9824	4	30	-	-	-	-	-	-	-	163	3	Anundsen, 1990	213	163		
815	R640	Rogaland	Forøya, Finnøy	59.17448	5.9824	4	30	-	-	-	-	-	-	-	260	3	Anundsen, 1990	213	260		
816	R641	Rogaland	Sauøya, Finnøy	59.17063	5.9683	4	8	-	-	180	-	-	-	-	-	3	Anundsen, 1990	211	180		
817	R642	Rogaland	Øksneset, Finnøy	59.23300	5.9926	4	130	-	-	-	-	-	-	-	175	3	Anundsen, 1990	213	175		
818	R642	Rogaland	Øksneset, Finnøy	59.23300	5.9926	4	130	-	-	-	-	-	-	-	260	3	Anundsen, 1990	213	260		
819	R643	Rogaland	Garavika, Finnøy	59.22837	5.9476	4	12	-	-	180	-	-	-	-	-	3	Anundsen, 1990	211	180		
820	R644	Rogaland	Neset, Finnøy	59.28502	5.9482	4	5	-	-	-	-	-	-	-	178	3	Anundsen, 1990	213	178		
821	R644	Rogaland	Neset, Finnøy	59.28502	5.9482	4	5	-	-	-	-	-	-	-	270	3	Anundsen, 1990	213	270		
822	R645	Rogaland	Låvaberga, Finnøy	59.29184	5.9773	4	14	-	-	-	-	-	-	-	175	3	Anundsen, 1990	213	175		
823	R645	Rogaland	Låvaberga, Finnøy	59.29184	5.9773	4	14	-	-	-	-	-	-	-	270	3	Anundsen, 1990	213	270		
824	R646	Rogaland	Hagen, Finnøy	59.29023	5.9935	4	3	-	-	208	-	-	-	-	-	3	Anundsen, 1990	211	208		
825	R647	Rogaland	Klområ, Finnøy	59.29184	6.0078	4	12	-	-	-	-	-	-	-	210	3	Anundsen, 1990	213	210		
826	R647	Rogaland	Klområ, Finnøy	59.29184	6.0078	4	12	-	-	-	-	-	-	-	261	3	Anundsen, 1990	213	261		
827	R648	Rogaland	Røykjanes, Finnøy	59.29617	6.0568	4	23	-	-	-	-	-	-	-	175	3	Anundsen, 1990	213	175		
828	R648	Rogaland	Røykjanes, Finnøy	59.29617	6.0568	4	23	-	-	-	-	-	-	-	220	3	Anundsen, 1990	213	220		
829	R648	Rogaland	Røykjanes, Finnøy	59.29617	6.0568	4	23	-	-	-	-	-	-	-	295	3	Anundsen, 1990	213	295		
830	R649	Rogaland	Buervika, Finnøy	59.28204	6.0825	4	31	-	-	308	-	-	-	-	-	3	Anundsen, 1990	211	308		
831	R650	Rogaland	Tjueneset, Finnøy	59.26318	6.1032	4	33	-	-	174	-	-	-	-	-	3	Anundsen, 1990	211	174		
832	R651	Rogaland	Porsberg, Finnøy	59.26158	6.1569	4	20	-	-	238	-	-	-	-	-	3	Anundsen, 1990	211	238		
833	R652	Rogaland	Apalviga, Hjelmeland	59.27066	6.1488	4	10	-	-	238	-	-	-	-	-	3	Anundsen, 1990	215	238		
834	R652	Rogaland	Apalviga, Hjelmeland	59.27066	6.1488	4	10	-	-	-	288	-	-	-	-	3	Anundsen, 1990	216	288		
835	R653	Rogaland	Kjerhammar, Hjelmeland	59.27695	6.1368	4	3	-	-	-	-	-	-	-	180	3	Anundsen, 1990	213	180		
836	R653	Rogaland	Kjerhammar, Hjelmeland	59.27695	6.1368	4	3	-	-	-	-	-	-	-	152	3	Anundsen, 1990	213	152		
837	R653	Rogaland	Kjerhammar, Hjelmeland	59.27695	6.1368	4	3	-	-	-	-	-	-	-	220	3	Anundsen, 1990	213	220		
838	R654	Rogaland	Håneset, Hjelmeland	59.28176	6.1295	4	17	-	-	260	-	-	-	-	-	3	Anundsen, 1990	211	260		
839	R655	Rogaland	Knutsvika, Hjelmeland	59.28406	6.1267	4	15	-	-	244	-	-	-	-	-	3	Anundsen, 1990	211	244		
840	R656	Rogaland	Skarvaneset, Hjelmeland	59.29232	6.1180	4	8	-	-	180	-	-	-	-	-	3	Anundsen, 1990	211	180		

Striae No	Loc. No	County	Placename	Lat_N	Long_E	Precision	m a.s.l.	Mid pt.	Plus_ Minus	Youngest	Older	Even Older	Even Older 2	Oldest	Undet. rel. age	Quality	Source	Code symbol	All orientations	Comments	Erosional marks
841	R657	Rogaland	Øygarden, Hjelmeland	59.29892	6.1160	4	9	-	-	315	-	-	-	-	-	3	Anundsen, 1990	215	315		
842	R657	Rogaland	Øygarden, Hjelmeland	59.29892	6.1160	4	9	-	-	-	270	-	-	-	-	3	Anundsen, 1990	216	270		
843	R657	Rogaland	Øygarden, Hjelmeland	59.29892	6.1160	4	9	-	-	-	175	-	-	-	-	3	Anundsen, 1990	216	175		
844	R658	Rogaland	Eidadalen, Hjelmeland	59.31326	6.3218	4	325	-	-	298	-	-	-	-	-	3	Anundsen, 1990	211	298		
845	R659	Rogaland	Skiftesvika, Suldal	59.32201	6.2690	4	16	-	-	240	-	-	-	-	-	3	Anundsen, 1990	211	240		
846	R660	Rogaland	Falkås, Suldal	59.33184	6.2515	4	40	-	-	180	-	-	-	-	-	3	Anundsen, 1990	211	180		
847	R661	Rogaland	Åsen, Suldal	59.33285	6.2495	4	8	-	-	165	-	-	-	-	-	3	Anundsen, 1990	211	165		
848	R662	Rogaland	Skipet, Suldal	59.37369	6.2501	4	264	-	-	230	-	-	-	-	-	3	Anundsen, 1990	211	230		
849	R663	Rogaland	Skipet, Suldal	59.37916	6.2527	4	611	-	-	245	-	-	-	-	-	3	Anundsen, 1990	211	245		
850	R664	Rogaland	Kro, Suldal	59.40793	6.3036	4	722	-	-	315	-	-	-	-	-	3	Anundsen, 1990	215	315		
851	R664	Rogaland	Kro, Suldal	59.40793	6.3036	4	722	-	-	-	255	-	-	-	-	3	Anundsen, 1990	216	255		
852	R665	Rogaland	Kaldåtjørnane, Suldal	59.42738	6.3018	4	840	-	-	200	-	-	-	-	-	3	Anundsen, 1990	211	200		
853	R666	Rogaland	Båsabuhaugen, Suldal	59.42778	6.3257	4	866	-	-	200	-	-	-	-	-	3	Anundsen, 1990	211	200		
854	R667	Rogaland	Middagheia, Suldal	59.37633	6.3446	4	705	-	-	228	-	-	-	-	-	3	Anundsen, 1990	211	228		
855	R668	Rogaland	Skåradn, Suldal	59.38666	6.3602	4	748	-	-	245	-	-	-	-	-	3	Anundsen, 1990	211	245		
856	R669	Rogaland	Ersdalen, Suldal	59.44301	6.2328	4	36	-	-	212	-	-	-	-	-	3	Anundsen, 1990	211	212		
857	R670	Rogaland	Illasteinen, Suldal	59.45503	6.2388	4	28	-	-	-	-	-	-	-	251	3	Anundsen, 1990	213	251		
858	R670	Rogaland	Illasteinen, Suldal	59.45503	6.2388	4	28	-	-	-	-	-	-	-	215	3	Anundsen, 1990	213	215		
859	R671	Rogaland	Berge, Suldal	59.47400	6.2836	4	44	-	-	241	-	-	-	-	-	3	Anundsen, 1990	211	241		
860	R672	Rogaland	Einersneset, Suldal	59.48560	6.2473	4	15	-	-	285	-	-	-	-	-	3	Anundsen, 1990	215	285		
861	R672	Rogaland	Einersneset, Suldal	59.48560	6.2473	4	15	-	-	-	224	-	-	-	-	3	Anundsen, 1990	216	224		
862	R673	Rogaland	Maleniusåsen, Suldal	59.48606	6.2620	4	66	-	-	152	-	-	-	-	-	3	Anundsen, 1990	211	152		
863	R674	Rogaland	Garlagheia, Suldal	59.50281	6.3057	4	528	-	-	248	-	-	-	-	-	3	Anundsen, 1990	211	248		
864	R675	Rogaland	Garlagheia, Suldal	59.49925	6.3088	4	585	-	-	246	-	-	-	-	-	3	Anundsen, 1990	211	246		
865	R676	Rogaland	Månastøllio, Suldal	59.51245	6.3576	4	498	-	-	308	-	-	-	-	-	3	Anundsen, 1990	211	308		
866	R677	Rogaland	Månastøllio, Suldal	59.50702	6.3547	4	720	-	-	286	-	-	-	-	-	3	Anundsen, 1990	211	286		
867	R678	Rogaland	Søthei, Suldal	59.48773	6.3659	4	818	-	-	314	-	-	-	-	-	3	Anundsen, 1990	211	314		
868	R679	Rogaland	Høyskorheio, Suldal	59.49005	6.3791	4	657	-	-	252	-	-	-	-	-	3	Anundsen, 1990	211	252		

Striae No	Loc. No	County	Placename	Lat_N	Long_E	Precision	m a.s.l.	Mid pt.	Plus_ Minus	Youngest	Older	Even Older	Even Older 2	Oldest	Undet. rel. age	Quality	Source	Code symbol	All orientations	Comments	Erosional marks
869	R680	Rogaland	Holmabu, Suldal	59.49827	6.3696	4	514	-	-	305	-	-	-	-	-	3	Anundsen, 1990	211	305		
870	R681	Rogaland	Augnastølvatnet, Suldal	59.50299	6.3758	4	440	-	-	317	-	-	-	-	-	3	Anundsen, 1990	211	317		
871	R682	Rogaland	Mork, Suldal	59.50267	6.3936	4	421	-	-	314	-	-	-	-	-	3	Anundsen, 1990	215	314		
872	R682	Rogaland	Mork, Suldal	59.50267	6.3936	4	421	-	-	-	284	-	-	-	-	3	Anundsen, 1990	216	284		
873	R683	Rogaland	Markosvatnet, Suldal	59.50277	6.3990	4	384	-	-	260	-	-	-	-	-	3	Anundsen, 1990	211	260		
874	R684	Rogaland	Smidjebekken, Suldal	59.48832	6.4047	4	270	-	-	205	-	-	-	-	-	3	Anundsen, 1990	211	205		
875	R685	Rogaland	Lendingstranda, Hjelmeland	59.28461	6.3937	4	409	-	-	270	-	-	-	-	-	3	Anundsen, 1990	211	270		
876	R686	Rogaland	Raudlende, Hjelmeland	59.28869	6.4284	4	352	-	-	268	-	-	-	-	-	3	Anundsen, 1990	211	268		
877	R687	Rogaland	Subbelihallene, Hjelmeland	59.27640	6.4024	4	454	-	-	270	-	-	-	-	-	3	Anundsen, 1990	211	270		
878	R688	Rogaland	Subbilheia, Hjelmeland	59.27535	6.4194	4	571	-	-	252	-	-	-	-	-	3	Anundsen, 1990	215	252		
879	R688	Rogaland	Subbilheia, Hjelmeland	59.27535	6.4194	4	571	-	-	-	282	-	-	-	-	3	Anundsen, 1990	216	282		
880	R689	Rogaland	Takliane, Hjelmeland	59.28837	6.4991	4	595	-	-	291	-	-	-	-	-	3	Anundsen, 1990	211	291		
881	R690	Rogaland	Øyestølen, Hjelmeland	59.29577	6.5312	4	770	-	-	258	-	-	-	-	-	3	Anundsen, 1990	211	258		
882	R691	Rogaland	Verkvelvheia, Hjelmeland	59.30231	6.5209	4	812	-	-	270	-	-	-	-	-	3	Anundsen, 1990	211	270		
883	R692	Rogaland	Brendeknutåna, Hjelmeland	59.28952	6.5786	4	800	-	-	260	-	-	-	-	-	3	Anundsen, 1990	211	260		
884	R693	Rogaland	Brendeknutvatnet, Hjelmeland	59.28013	6.5974	4	945	-	-	260	-	-	-	-	-	3	Anundsen, 1990	211	260		
885	R694	Rogaland	Kvivatnet, Hjelmeland	59.31122	6.5727	4	750	-	-	284	-	-	-	-	-	3	Anundsen, 1990	211	284		
886	R695	Rogaland	Kvivassheia, Hjelmeland	59.31445	6.5803	4	747	-	-	274	-	-	-	-	-	3	Anundsen, 1990	211	274		
887	R696	Rogaland	Kvivassheia, Hjelmeland	59.31717	6.5903	4	737	-	-	280	-	-	-	-	-	3	Anundsen, 1990	211	280		
888	R697	Rogaland	Kvivassheia, Hjelmeland	59.32091	6.5985	4	557	-	-	315	-	-	-	-	-	3	Anundsen, 1990	211	315		
889	R698	Rogaland	Stølsdalen, Hjelmeland	59.30382	6.6118	4	685	-	-	-	-	-	-	-	292	3	Anundsen, 1990	213	292		
890	R698	Rogaland	Stølsdalen, Hjelmeland	59.30382	6.6118	4	685	-	-	-	-	-	-	-	320	3	Anundsen, 1990	213	320		
891	R699	Rogaland	Stølsdalen, Hjelmeland	59.30122	6.6153	4	652	-	-	308	-	-	-	-	-	3	Anundsen, 1990	211	308		
892	R700	Rogaland	Vassbottvatnet, Hjelmeland	59.29702	6.6226	4	584	-	-	358	-	-	-	-	-	3	Anundsen, 1990	211	358		
893	R701	Rogaland	Glommedalsfossen, Hjelmeland	59.29272	6.6271	4	586	-	-	350	-	-	-	-	-	3	Anundsen, 1990	211	350		
894	R702	Rogaland	Glommedalen, Hjelmeland	59.28964	6.6427	4	976	-	-	301	-	-	-	-	-	3	Anundsen, 1990	211	301		
895	R703	Rogaland	Ryfylkeheiane, Hjelmeland	59.32478	6.6569	4	908	-	-	283	-	-	-	-	-	3	Anundsen, 1990	211	283		
896	R704	Rogaland	Ryfylkeheiane, Hjelmeland	59.33170	6.6597	4	843	-	-	286	-	-	-	-	-	3	Anundsen, 1990	211	286		

Striae No	Loc. No	County	Placename	Lat_N	Long_E	Precision	m a.s.l.	Mid pt.	Plus_ Minus	Youngest	Older	Even Older	Even Older 2	Oldest	Undet. rel. age	Quality	Source	Code symbol	All orientations	Comments	Erosional marks
897	R705	Rogaland	Litla Blåfjellvatnet, Hjelmeland	59.33407	6.6792	4	933	-	-	254	-	-	-	-	-	3	Anundsen, 1990	211	254		
898	R706	Rogaland	Litla Blåfjell, Hjelmeland	59.33110	6.7001	4	1006	-	-	280	-	-	-	-	-	3	Anundsen, 1990	211	280		
899	R707	Rogaland	Stora Blåfjellvatnet, Hjelmeland	59.33794	6.7065	4	1100	-	-	280	-	-	-	-	-	3	Anundsen, 1990	211	280		
900	R708	Rogaland	Stora Gilavatnet, Hjelmeland	59.34581	6.7356	4	1100	-	-	280	-	-	-	-	-	3	Anundsen, 1990	211	280		
901	R709	Rogaland	Stora Gilavatnet, Hjelmeland	59.35444	6.7416	4	1074	-	-	266	-	-	-	-	-	3	Anundsen, 1990	211	266		
902	R710	Rogaland	Førrevassdammen, Hjelmeland	59.36194	6.7482	4	1080	-	-	250	-	-	-	-	-	3	Anundsen, 1990	211	250		
903	R711	Rogaland	Førrevassdammen, Hjelmeland	59.36438	6.7415	4	1060	-	-	260	-	-	-	-	-	3	Anundsen, 1990	211	260		
904	R712	Rogaland	Førrevassdammen, Hjelmeland	59.36877	6.7453	4	1040	-	-	273	-	-	-	-	-	3	Anundsen, 1990	211	273		
905	R713	Rogaland	Førrevassdammen, Hjelmeland	59.36921	6.7335	4	960	-	-	292	-	-	-	-	-	3	Anundsen, 1990	211	292		
906	R714	Rogaland	Kvæstadåsen, Suldal	59.45015	6.3994	4	306	-	-	-	-	-	-	-	220	3	Anundsen, 1990	213	220		
907	R714	Rogaland	Kvæstadåsen, Suldal	59.45015	6.3994	4	306	-	-	-	-	-	-	-	277	3	Anundsen, 1990	213	277		
908	R714	Rogaland	Kvæstadåsen, Suldal	59.45015	6.3994	4	306	-	-	-	-	-	-	-	155	3	Anundsen, 1990	212	155		
909	R715	Rogaland	Kvæstadbekken, Suldal	59.44104	6.3930	4	571	-	-	205	-	-	-	-	-	3	Anundsen, 1990	211	205		
910	R716	Rogaland	Nonsskar, Suldal	59.45180	6.4783	4	718	-	-	198	-	-	-	-	-	3	Anundsen, 1990	211	198		
911	R717	Rogaland	Froastøllio, Suldal	59.41338	6.4491	4	614	-	-	242	-	-	-	-	-	3	Anundsen, 1990	215	242		
912	R717	Rogaland	Froastøllio, Suldal	59.41338	6.4491	4	614	-	-	-	224	-	-	-	-	3	Anundsen, 1990	216	224		
913	R718	Rogaland	Såto, Suldal	59.38464	6.4289	4	571	-	-	223	-	-	-	-	-	3	Anundsen, 1990	211	223		
914	R719	Rogaland	Gullingshammaren, Suldal	59.38693	6.4627	4	691	-	-	182	-	-	-	-	-	3	Anundsen, 1990	211	182		
915	R720	Rogaland	Langeli, Suldal	59.38302	6.4753	4	684	-	-	181	-	-	-	-	-	3	Anundsen, 1990	211	181		
916	R721	Rogaland	Nebbtjørna, Suldal	59.38738	6.4867	4	709	-	-	192	-	-	-	-	-	3	Anundsen, 1990	211	192		
917	R722	Rogaland	Finnadalsheia	59.40308	6.4704	4	785	-	-	218	-	-	-	-	-	3	Anundsen, 1990	211	218		
918	R723	Rogaland	Litla Heiavatnet, Suldal	59.42404	6.4946	4	843	-	-	288	-	-	-	-	-	3	Anundsen, 1990	211	288		
919	R724	Rogaland	Ørekvamsbakkane, Suldal	59.39814	6.4991	4	622	-	-	230	-	-	-	-	-	3	Anundsen, 1990	211	230		
920	R725	Rogaland	Kvelvanuten, Suldal	59.39805	6.5210	4	602	-	-	225	-	-	-	-	-	3	Anundsen, 1990	211	225		
921	R726	Rogaland	Sandvatnet, Suldal	59.40970	6.5192	4	800	-	-	282	-	-	-	-	-	3	Anundsen, 1990	211	282		
922	R727	Rogaland	Ytre Djupadal, Suldal	59.42769	6.5108	4	1072	-	-	331	-	-	-	-	-	3	Anundsen, 1990	211	331		
923	R728	Rogaland	Bøljanuten, Suldal	59.44350	6.5058	4	985	-	-	326	-	-	-	-	-	3	Anundsen, 1990	211	326		
924	R729	Rogaland	Furedalen, Suldal	59.45433	6.5130	4	665	-	-	224	-	-	-	-	-	3	Anundsen, 1990	211	224		

Striae No	Loc. No	County	Placename	Lat_N	Long_E	Precision	m a.s.l.	Mid pt.	Plus_ Minus	Youngest	Older	Even Older	Even Older 2	Oldest	Undet. rel. age	Quality	Source	Code symbol	All orientations	Comments	Erosional marks
925	R730	Rogaland	Sandsaskard, Suldal	59.44111	6.5233	4	940	-	-	283	-	-	-	-	-	3	Anundsen, 1990	215	283		
926	R730	Rogaland	Sandsaskard, Suldal	59.44111	6.5233	4	940	-	-	-	259	-	-	-	-	3	Anundsen, 1990	216	259		
927	R731	Rogaland	Tytesbekken, Suldal	59.40081	6.5647	4	648	-	-	245	-	-	-	-	-	3	Anundsen, 1990	211	245		
928	R732	Rogaland	Langanes, Suldal	59.41401	6.5795	4	655	-	-	213	-	-	-	-	-	3	Anundsen, 1990	211	213		
929	R733	Rogaland	Uføreberget, Suldal	59.42169	6.6136	4	682	-	-	-	-	-	-	-	228	3	Anundsen, 1990	213	228		
930	R733	Rogaland	Uføreberget, Suldal	59.42169	6.6136	4	682	-	-	-	-	-	-	-	253	3	Anundsen, 1990	213	253		
931	R734	Rogaland	Månastølen, Suldal	59.44251	6.6689	4	731	-	-	-	-	-	-	-	274	3	Anundsen, 1990	213	274		
932	R734	Rogaland	Månastølen, Suldal	59.44251	6.6689	4	731	-	-	-	-	-	-	-	161	3	Anundsen, 1990	212	161		
933	R735	Rogaland	Grovene, Suldal	59.44570	6.5768	4	956	-	-	256	-	-	-	-	-	3	Anundsen, 1990	211	256		
934	R736	Rogaland	Skarstøldalen, Suldal	59.46260	6.5506	4	794	-	-	220	-	-	-	-	-	3	Anundsen, 1990	215	220		
935	R736	Rogaland	Skarstøldalen, Suldal	59.46260	6.5506	4	794	-	-	-	294	-	-	-	-	3	Anundsen, 1990	216	294		
936	R737	Rogaland	Rishaugtjørnane, Suldal	59.46342	6.5319	4	828	-	-	186	-	-	-	-	-	3	Anundsen, 1990	211	186		
937	R738	Rogaland	Vikebakkane, Suldal	59.48917	6.5409	4	335	-	-	265	-	-	-	-	-	3	Anundsen, 1990	211	265		
938	R739	Rogaland	Røyrdalen, Suldal	59.49778	6.5629	4	233	-	-	170	-	-	-	-	-	3	Anundsen, 1990	211	170		
939	R740	Rogaland	Tveitanåna, Suldal	59.50800	6.5602	4	185	-	-	238	-	-	-	-	-	3	Anundsen, 1990	211	238		
940	R741	Rogaland	Helganes, Suldal	59.48315	6.5864	4	524	-	-	288	-	-	-	-	-	3	Anundsen, 1990	211	288		
941	R742	Rogaland	Vætekleiv, Suldal	59.47506	6.5852	4	598	-	-	220	-	-	-	-	-	3	Anundsen, 1990	211	220		
942	R743	Rogaland	Nyastølen, Suldal	59.47824	6.5744	4	515	-	-	220	-	-	-	-	-	3	Anundsen, 1990	211	220		
943	R744	Rogaland	Tverrdalsåsen, Suldal	59.48293	6.5614	4	451	-	-	218	-	-	-	-	-	3	Anundsen, 1990	211	218		
944	R745	Rogaland	Skarstølknattane, Suldal	59.47348	6.5590	4	708	-	-	166	-	-	-	-	-	3	Anundsen, 1990	211	166		
945	R746	Rogaland	Skithei, Suldal	59.42883	6.6217	4	888	-	-	266	-	-	-	-	-	3	Anundsen, 1990	211	266		
946	R747	Rogaland	Steinsstølen, Suldal	59.42482	6.6337	4	724	-	-	260	-	-	-	-	-	3	Anundsen, 1990	211	260		
947	R748	Rogaland	Steinsstølen, Suldal	59.43278	6.6315	4	809	-	-	211	-	-	-	-	-	3	Anundsen, 1990	211	211		
948	R749	Rogaland	Grunnavatnet, Suldal	59.43634	6.6337	4	752	-	-	190	-	-	-	-	-	3	Anundsen, 1990	211	190		
949	R750	Rogaland	Kviavatnet, Suldal	59.44051	6.6336	4	782	-	-	182	-	-	-	-	-	3	Anundsen, 1990	211	182		
950	R751	Rogaland	Svinstølen, Suldal	59.44573	6.6335	4	785	-	-	219	-	-	-	-	-	3	Anundsen, 1990	211	219		
951	R752	Rogaland	Stølstjørna, Suldal	59.45567	6.6265	4	895	-	-	305	-	-	-	-	-	3	Anundsen, 1990	211	305		
952	R753	Rogaland	Litletjørn, Suldal	59.45291	6.6424	4	734	-	-	270	-	-	-	-	-	3	Anundsen, 1990	211	270		

Striae No	Loc. No	County	Placename	Lat_N	Long_E	Precision	m a.s.l.	Mid pt.	Plus_ Minus	Youngest	Older	Even Older	Even Older 2	Oldest	Undet. rel. age	Quality	Source	Code symbol	All orientations	Comments	Erosional marks
953	R754	Rogaland	Løkjahaugen, Suldal	59.48707	6.6509	4	603	-	-	250	-	-	-	-	-	3	Anundsen, 1990	211	250		
954	R755	Rogaland	Holmaliåno, Suldal	59.48659	6.6533	4	592	-	-	310	-	-	-	-	-	3	Anundsen, 1990	211	310		
955	R756	Rogaland	Kjetilstad, Sudal	59.48195	6.6762	4	694	-	-	350	-	-	-	-	-	3	Anundsen, 1990	211	350		
956	R757	Rogaland	Kjetilstaddalen, Sudal	59.46875	6.6840	4	692	-	-	300	-	-	-	-	-	3	Anundsen, 1990	211	300		
957	R758	Rogaland	Svartavatnet, Suldal	59.45981	6.6901	4	759	-	-	282	-	-	-	-	-	3	Anundsen, 1990	211	282		
958	R759	Rogaland	Landavatnet, Suldal	59.45516	6.7016	4	803	-	-	295	-	-	-	-	-	3	Anundsen, 1990	211	295		
959	R760	Rogaland	Øykjaheia, Suldal	59.45073	6.6961	4	902	-	-	280	-	-	-	-	-	3	Anundsen, 1990	211	280		
960	R761	Rogaland	Grønenuten, Suldal	59.44093	6.6878	4	940	-	-	240	-	-	-	-	-	3	Anundsen, 1990	211	240		
961	R762	Rogaland	Øykjaheia, Suldal	59.44667	6.6920	4	874	-	-	280	-	-	-	-	-	3	Anundsen, 1990	211	280		
962	R763	Rogaland	Øvrestølen, Suldal	59.51306	6.4664	4	750	-	-	286	-	-	-	-	-	3	Anundsen, 1990	211	286		
963	R764	Rogaland	Glompedalen, Suldal	59.50709	6.5058	4	739	-	-	220	-	-	-	-	-	3	Anundsen, 1990	215	220		
964	R764	Rogaland	Glompedalen, Suldal	59.50709	6.5058	4	739	-	-	-	264	-	-	-	-	3	Anundsen, 1990	216	264		
965	R765	Rogaland	Glompedalen, Suldal	59.50955	6.4971	4	934	-	-	216	-	-	-	-	-	3	Anundsen, 1990	211	216		
966	R766	Rogaland	Smaladalsvatnet, Suldal	59.52438	6.4976	4	840	-	-	320	-	-	-	-	-	3	Anundsen, 1990	211	320		
967	R767	Rogaland	Hestakvelven, Suldal	59.53445	6.4977	4	836	-	-	293	-	-	-	-	-	3	Anundsen, 1990	211	293		
968	R768	Rogaland	Vatndalsnuten, Suldal	59.54141	6.5243	4	626	-	-	325	-	-	-	-	-	3	Anundsen, 1990	211	325		
969	R769	Rogaland	Lomåstjørna, Suldal	59.54430	6.5316	4	585	-	-	268	-	-	-	-	-	3	Anundsen, 1990	211	268		
970	R770	Rogaland	Liastøl, Suldal	59.54249	6.5144	4	574	-	-	274	-	-	-	-	-	3	Anundsen, 1990	211	274		
971	R771	Rogaland	Plomreidnuten, Suldal	59.54403	6.5613	4	852	-	-	138	-	-	-	-	-	3	Anundsen, 1990	212	138		
972	R772	Rogaland	Fantaskåro, Suldal	59.54724	6.5768	4	703	-	-	146	-	-	-	-	-	3	Anundsen, 1990	212	146		
973	R773	Rogaland	Fantaskåro, Suldal	59.54724	6.5768	4	703	-	-	-	268	-	-	-	-	3	Anundsen, 1990	216	268		
974	R774	Rogaland	Dalakleivtjørn, Suldal	59.54918	6.5896	4	468	-	-	151	-	-	-	-	-	3	Anundsen, 1990	212	151		
975	R774	Rogaland	Dalakleivtjørn, Suldal	59.54918	6.5896	4	468	-	-	-	298	-	-	-	-	3	Anundsen, 1990	216	298		
976	R775	Rogaland	Rundesteinheia, Suldal	59.54734	6.6273	4	615	-	-	240	-	-	-	-	-	3	Anundsen, 1990	211	240		
977	R776	Rogaland	Åsane, Suldal	59.50025	6.5644	4	222	-	-	-	-	-	-	-	260	3	Anundsen, 1990	213	260		
978	R776	Rogaland	Åsane, Suldal	59.50025	6.5644	4	222	-	-	-	-	-	-	-	236	3	Anundsen, 1990	213	236		
979	R777	Rogaland	Hesjane, Suldal	59.49886	6.5926	4	457	-	-	158	-	-	-	-	-	3	Anundsen, 1990	211	158		
980	R778	Rogaland	Øystad, Suldal	59.51220	6.6184	4	219	-	-	175	-	-	-	-	-	3	Anundsen, 1990	211	175		

Striae No	Loc. No	County	Placename	Lat_N	Long_E	Precision	m a.s.l.	Mid pt.	Plus_ Minus	Youngest	Older	Even Older	Even Older 2	Oldest	Undet. rel. age	Quality	Source	Code symbol	All orientations	Comments	Erosional marks
981	R779	Rogaland	Regahaugen, Suldal	59.50651	6.6388	4	180	-	-	190	-	-	-	-	-	3	Anundsen, 1990	215	190		
982	R779	Rogaland	Regahaugen, Suldal	59.50651	6.6388	4	180	-	-	-	218	-	-	-	-	3	Anundsen, 1990	216	218		
983	R780	Rogaland	Lakvelven, Suldal	59.52507	6.6817	4	867	-	-	228	-	-	-	-	-	3	Anundsen, 1990	211	228		
984	R781	Rogaland	Steinaleitet, Suldal	59.53064	6.6917	4	892	-	-	248	-	-	-	-	-	3	Anundsen, 1990	211	248		
985	R782	Rogaland	Midtheia, Suldal	59.53040	6.7006	4	985	-	-	268	-	-	-	-	-	3	Anundsen, 1990	211	268		
986	R783	Rogaland	Indre Grubbedalen, Suldal	59.63971	6.7381	4	839	-	-	204	-	-	-	-	-	3	Anundsen, 1990	211	204		
987	R784	Rogaland	Trosavikåsen, Sauda	59.64426	6.3275	4	43	-	-	174	-	-	-	-	-	3	Anundsen, 1990	215	174		
988	R784	Rogaland	Trosavikåsen, Sauda	59.64426	6.3275	4	43	-	-	198	-	-	-	-	-	3	Anundsen, 1990	215	198		
989	R784	Rogaland	Trosavikåsen, Sauda	59.64426	6.3275	4	43	-	-	-	215	-	-	-	-	3	Anundsen, 1990	216	215		
990	R784	Rogaland	Trosavikåsen, Sauda	59.64426	6.3275	4	43	-	-	-	265	-	-	-	-	3	Anundsen, 1990	216	265		
991	R785	Rogaland	Træsavika, Sauda	59.64768	6.3378	4	4	-	-	-	-	-	-	-	218	3	Anundsen, 1990	213	218		
992	R785	Rogaland	Træsavika, Sauda	59.64768	6.3378	4	4	-	-	-	-	-	-	-	249	3	Anundsen, 1990	213	249		
993	R785	Rogaland	Træsavika, Sauda	59.64768	6.3378	4	4	-	-	-	-	-	-	-	270	3	Anundsen, 1990	213	270		
994	R786	Rogaland	Eidsvågen, Sveio	59.65336	5.4262	4	14	-	-	236	-	-	-	-	-	3	Anundsen, 1990	215	236		
995	R786	Rogaland	Eidsvågen, Sveio	59.65336	5.4262	4	14	-	-	-	292	-	-	-	-	3	Anundsen, 1990	216	292		
996	R787	Rogaland	Straumøy, Sveio	59.65282	5.4310	4	6	-	-	192	-	-	-	-	-	3	Anundsen, 1990	211	192		
997	R788	Rogaland	Lyngneset, Sveio	59.63990	5.3756	4	2	-	-	309	-	-	-	-	-	3	Anundsen, 1990	211	309		
998	R789	Rogaland	Ørebekken, Sveio	59.60519	5.4030	4	134	-	-	311	-	-	-	-	-	3	Anundsen, 1990	211	311		
999	R790	Rogaland	Førde, Sveio	59.60722	5.4707	4	42	-	-	190	-	-	-	-	-	3	Anundsen, 1990	215	190		
1000	R790	Rogaland	Førde, Sveio	59.60722	5.4707	4	42	-	-	230	-	-	-	-	-	3	Anundsen, 1990	215	230		
1001	R790	Rogaland	Førde, Sveio	59.60722	5.4707	4	42	-	-	-	293	-	-	-	-	3	Anundsen, 1990	216	293		
1002	R791	Rogaland	Leirpollen, Sveio	59.62446	5.3366	4	2	-	-	256	-	-	-	-	-	3	Anundsen, 1990	211	256		
1003	R792	Rogaland	Rotdaltjørna, Sveio	59.60399	5.3365	4	40	-	-	204	-	-	-	-	-	3	Anundsen, 1990	211	204		
1004	R793	Rogaland	Torjulsbekken, Sveio	59.59290	5.3445	4	43	-	-	187	-	-	-	-	-	3	Anundsen, 1990	211	187		
1005	R794	Rogaland	Gjermundshaugen, Sveio	59.54208	5.3385	4	32	-	-	270	-	-	-	-	-	3	Anundsen, 1990	211	270		
1006	R795	Rogaland	Mølstrevåg, Sveio	59.52414	5.2526	4	3	-	-	190	-	-	-	-	-	3	Anundsen, 1990	211	190		
1007	R796	Rogaland	Høgenap, Tysvær	59.41727	5.3884	4	63	-	-	-	-	-	-	-	202	3	Anundsen, 1990	213	202		
1008	R796	Rogaland	Høgenap, Tysvær	59.41727	5.3884	4	63	-	-	-	-	-	-	-	244	3	Anundsen, 1990	213	244		

Striae No	Loc. No	County	Placename	Lat_N	Long_E	Precision	m a.s.l.	Mid pt.	Plus_ Minus	Youngest	Older	Even Older	Even Older 2	Oldest	Undet. rel. age	Quality	Source	Code symbol	All orientations	Comments	Erosional marks
1009	R797	Rogaland	Nuten, Tysvær	59.39918	5.3956	4	37	-	-	-	-	-	-	-	200	3	Anundsen, 1990	213	200		
1010	R797	Rogaland	Nuten, Tysvær	59.39918	5.3956	4	37	-	-	-	-	-	-	-	270	3	Anundsen, 1990	213	270		
1011	R798	Rogaland	Våga, Karmøy	59.28622	5.3652	4	16	-	-	227	-	-	-	-	-	3	Anundsen, 1990	215	227		
1012	R798	Rogaland	Våga, Karmøy	59.28622	5.3652	4	16	-	-	-	145	-	-	-	-	3	Anundsen, 1990	216	145		
1013	R799	Rogaland	Eidsåg, Sveio	59.71481	5.5209	4	12	-	-	310	-	-	-	-	-	3	Anundsen, 1990	215	310		
1014	R799	Rogaland	Eidsåg, Sveio	59.71481	5.5209	4	12	-	-	250	-	-	-	-	-	3	Anundsen, 1990	215	250		
1015	R799	Rogaland	Eidsåg, Sveio	59.71481	5.5209	4	12	-	-	-	225	-	-	-	-	3	Anundsen, 1990	216	225		
1016	R800	Rogaland	Nesjaneset, Sveio	59.71811	5.5143	4	19	-	-	255	-	-	-	-	-	3	Anundsen, 1990	215	255		
1017	R800	Rogaland	Nesjaneset, Sveio	59.71811	5.5143	4	19	-	-	-	216	-	-	-	-	3	Anundsen, 1990	216	216		
1018	R800	Rogaland	Nesjaneset, Sveio	59.71811	5.5143	4	19	-	-	-	185	-	-	-	-	3	Anundsen, 1990	216	185		
1019	R801	Rogaland	Ulla, Suldal	59.40743	6.7107	4	740	-	-	271	-	-	-	-	-	3	Anundsen, 1990	211	271		
1020	R801	Rogaland	Ulla, Suldal	59.41114	6.7266	4	767	-	-	274	-	-	-	-	-	3	Anundsen, 1990	211	274		
1021	R802	Rogaland	Moakvelven, Suldal	59.41221	6.7368	4	803	-	-	301	-	-	-	-	-	3	Anundsen, 1990	211	301		
1022	R802	Rogaland	Moakvelven, Suldal	59.41248	6.7417	4	817	-	-	294	-	-	-	-	-	3	Anundsen, 1990	211	294		
1023	R803	Rogaland	Oddåa, Suldal	59.41112	6.7814	4	880	-	-	318	-	-	-	-	-	3	Anundsen, 1990	211	318		
1024	R804	Rogaland	Oddatjørnhytta, Suldal	59.40475	6.7943	4	948	-	-	278	-	-	-	-	-	3	Anundsen, 1990	211	278		
1025	R805	Rogaland	Oddatjørndammen, Suldal	59.39875	6.7984	4	1081	-	-	272	-	-	-	-	-	3	Anundsen, 1990	211	272		
1026	R806	Rogaland	Helganeset, Utsira	59.30600	4.8565	3	12	-	-	340	-	-	-	-	-	3	Undås, 1943	211	340		
1027	R807	Rogaland	Helganeskrono, Utsira	59.30749	4.8582	3	17	-	-	351	-	-	-	-	-	3	Undås, 1943	211	351		
1028	R808	Rogaland	Kvitagro, Utsira	59.31084	4.8600	3	11	-	-	340	-	-	-	-	-	3	Undås, 1943	211	340		
1029	R809	Rogaland	Breimyr, Utsira	59.30836	4.8617	3	22	-	-	334	-	-	-	-	-	3	Undås, 1943	211	334		
1030	R810	Rogaland	Søra Vågadalsskjeret, Utsira	59.30240	4.8632	3	7	-	-	340	-	-	-	-	-	3	Undås, 1943	211	340		
1031	R811	Rogaland	Koltemyr, Utsira	59.31221	4.9010	3	16	-	-	356	-	-	-	-	-	3	Undås, 1943	211	356		
1032	R812	Rogaland	Tjørekloven, Utsira	59.31423	4.9050	3	15	-	-	358	-	-	-	-	-	3	Undås, 1943	211	358		
1033	R813	Rogaland	Tednevik, Utsira	59.30659	4.9046	3	20	-	-	339	-	-	-	-	-	3	Undås, 1943	211	339		
1034	R814	Rogaland	Segleimstranda, Eigerøy	58.44014	5.890	3	39	226	4	-	-	-	-	-	-	3	Garnes, 1976	214	226		
1035	R815	Rogaland	Tårnesbukta, Eigerøy	58.44924	5.904	3	7	-	-	-	-	-	-	-	210	3	Garnes, 1976	213	210		
1036	R815	Rogaland	Tårnesbukta, Eigerøy	58.44924	5.904	3	7	-	-	-	-	-	-	-	237	3	Garnes, 1976	213	237		

Striae No	Loc. No	County	Placename	Lat_N	Long_E	Precision	m a.s.l.	Mid pt.	Plus_ Minus	Youngest	Older	Even Older	Even Older 2	Oldest	Undet. rel. age	Quality	Source	Code symbol	All orientations	Comments	Erosional marks
1037	R816	Rogaland	Segleimm, Eigerøy	58.45165	5.904	3	6	-	-	220	-	-	-	-	-	3	Garnes, 1976	211	220		
1038	R817	Rogaland	Haugan, Eigerøy	58.45185	5.898	3	12	-	-	253	-	-	-	-	-	3	Garnes, 1976	211	253		
1039	R818	Rogaland	Selvågen, Eigerøy	58.45319	5.896	3	26	-	-	253	-	-	-	-	-	3	Garnes, 1976	211	253		
1040	R819	Rogaland	Selvågen, Eigerøy	58.45232	5.893	3	12	-	-	232	-	-	-	-	-	3	Garnes, 1976	211	232		
1041	R820	Rogaland	Nordre Eigerøy	58.45277	5.892	3	8	-	-	-	-	-	-	-	242	3	Garnes, 1976	213	242		
1042	R820	Rogaland	Nordre Eigerøy	58.45277	5.892	3	8	-	-	-	-	-	-	-	249	3	Garnes, 1976	213	249		
1043	R821	Rogaland	Floget, Eigerøy	58.45488	5.894	3	22	-	-	230	-	-	-	-	-	3	Garnes, 1976	211	230		
1044	R822	Rogaland	Floget, Eigerøy	58.45474	5.894	3	23	-	-	242	-	-	-	-	-	3	Garnes, 1976	211	242		
1045	R823	Rogaland	Bergan, Eigerøy	58.45631	5.904	3	19	-	-	239	-	-	-	-	-	3	Garnes, 1976	211	239		
1046	R824	Rogaland	Bergan, Eigerøy	58.45592	5.904	3	22	-	-	226	-	-	-	-	-	3	Garnes, 1976	211	226		
1047	R825	Rogaland	Bergan, Eigerøy	58.45585	5.904	3	22	-	-	215	-	-	-	-	-	3	Garnes, 1976	211	215		
1048	R826	Rogaland	Grønevigberget, Eigerøy	58.45918	5.910	3	21	-	-	230	-	-	-	-	-	3	Garnes, 1976	211	230		
1049	R827	Rogaland	Skadbergfjellet, Eigerøy	58.45873	5.919	3	47	-	-	231	-	-	-	-	-	3	Garnes, 1976	211	231		
1050	R828	Rogaland	Lundarviga, Eigeøy	58.45689	5.923	3	5	243	7	-	-	-	-	-	-	3	Garnes, 1976	214	243		
1051	R829	Rogaland	Nygård, Eigerøy	58.46106	5.935	3	30	-	-	236	-	-	-	-	-	3	Garnes, 1976	211	236		
1052	R830	Rogaland	Nygård, Eigerøy	58.45927	5.935	3	32	220	4	-	-	-	-	-	-	3	Garnes, 1976	214	220		
1053	R831	Rogaland	Holevigtjørna, Eigerøy	58.44297	5.975	4	38	-	-	231	-	-	-	-	-	3	Garnes, 1976	211	231		
1054	R832	Rogaland	Vestra Holevik, Eigerøy	58.43895	5.975	4	23	-	-	231	-	-	-	-	-	3	Garnes, 1976	211	231		
1055	R833	Rogaland	Sæstadvatnet, Eigerøy	58.42842	5.967	4	36	-	-	234	-	-	-	-	-	3	Garnes, 1976	211	234		
1056	R834	Rogaland	Løyning, Eigerøy	58.42671	5.957	4	52	-	-	245	-	-	-	-	-	3	Garnes, 1976	211	245		
1057	R835	Rogaland	Auglend, Eigerøy	58.42039	5.975	4	15	-	-	220	-	-	-	-	-	3	Garnes, 1976	211	220		
1058	R836	Rogaland	Auglend, Eigerøy	58.41929	5.975	4	24	-	-	256	-	-	-	-	-	3	Garnes, 1976	211	256		
1059	R837	Rogaland	Hydrogenvegen, Utsira	59.30484	4.9087	1	33	-	-	330	-	-	-	-	-	3	Mangerud, 2013	211	330	course striaiton on granite, eroded bedrock surface	
1060	R838	Rogaland	Høga Berget, Utsira	59.30492	4.9111	1	16	-	-	355	-	-	-	-	-	3	Mangerud, 2013	211	355	course striation on horizontal surface	
1061	R838	Rogaland	Høga Berget, Utsira	59.30492	4.9111	1	16	-	-	360	-	-	-	-	-	3	Mangerud, 2013	211	360	course striation on horizontal surface	
1062	R839	Rogaland	Grindabekken, Sveio	59.59464	5.3124	1	30	-	-	300	-	-	-	-	-	1	Mangerud, 2014	211	300	clear striation	
1063	R840	Rogaland	Boknafjellet, Bokn	59.22031	5.4271	1	288	-	-	268	-	-	-	-	-	3	Mangerud, 2014	211	268	clear but coarse striation, on a weathered surface	
1064	R841	Rogaland	Boknafjellet, Bokn	59.21899	5.4283	1	281	-	-	240	-	-	-	-	-	3	Mangerud, 2014	211	240	clear striation	in front of a rundsva

Striae No	Loc. No	County	Placename	Lat_N	Long_E	Precision	m a.s.l.	Mid pt.	Plus_ Minus	Youngest	Older	Even Older	Even Older 2	Oldest	Undet. rel. age	Quality	Source	Code symbol	All orientations	Comments	Erosional marks
1065	R842	Rogaland	Lyngnes, Bokn	59.16656	5.3993	1	1	-	-	250	-	-	-	-	-	2	Mangerud, 2014	211	250	Clear striae, but not many finer striae	
1066	R842	Rogaland	Lyngnes, Bokn	59.16656	5.3993	1	1	-	-	270	-	-	-	-	-	2	Mangerud, 2014	211	270	Clear striae, but not many finer striae	
1067	R843	Rogaland	Laksaberget, Bokn	59.16667	5.4552	1	1	-	-	230	-	-	-	-	-	3	Mangerud, 2014	211	230	one clear, coarse striation. No others were found	
1068	R844	Rogaland	Spakemyra, Tysvær	59.29021	5.5099	1	74	-	-	170	-	-	-	-	-	1	Mangerud, 2014	211	170	clear striation	
1069	R845	Rogaland	Sandvikfjellet, Tysvær	59.28560	5.4980	1	180	-	-	170	-	-	-	-	-	3	Mangerud, 2014	211	170	coarse striation	
1070	R846	Rogaland	Mikkelett, Utsira	59.31440	4.8818	1	22	-	-	10	-	-	-	-	-	1	Mangerud, 2016	211	10		
1071	R847	Rogaland	Lauvvik ferjekai, Sandnes	58.89470	6.0554	1	1	-	-	326	-	-	-	-	-	3	Tuestad, 2019	211	326	clear, but coarse striation, ~0.5 - 1cm grooves, weathered	
1072	R848	Rogaland	Lauvvik ferjekai, Sandnes	58.89501	6.0550	1	1	-	-	318	-	-	-	-	-	3	Tuestad, 2019	212	318	clear, but coarse striation, ~0.5 - 1cm grooves, weathered	
1073	R849	Rogaland	Lauvvik ferjekai, Sandnes	58.89520	6.0547	1	1	-	-	308	-	-	-	-	-	3	Tuestad, 2019	213	308	clear, but coarse striation, ~0.5 - 1cm grooves, weathered	